Site-specific incorporation of synthetic amino acids into functioning ion channels

Thesis by

Gabriel Shaw Brandt

In Partial Fulfillment of the

Requirements for the Degree of

Doctor of Philosophy

California Institute of Technology

Pasadena, California

2003

(Defended October 4, 2002)

in memory of Teresa Hsu and Norman Davidson

Acknowledgments

The life of a man is a dubious experiment.
C. G. Jung

First of all, I'd like to put in a good word for our nation's high school science teachers, who in my case were Linda Bell, Mark Smith, Gary Miller, and Ron McCray. Good teachers make the difference all the way along, and I've benefited from an excellent crop at Reed College and here at Caltech. Dennis is an excellent advisor, a deeply humane individual who invariably reaches for the carrot rather than the stick. He's been a fount of scientific clarity and sound advice from my very first days at Caltech. Henry is a voracious collaborator, who's allowed a generation of Dougherty grad students to travel where chemists usually fear to tread. Through his guidance, along with that of Norman Davidson, I've been able to transcend disciplinary boundaries a little and try to address real biological questions. Doug Rees, John Bercaw, Peter Dervan, and Barbara Imperiali, the past and present members of my committee, have been excellent as teachers and periodic mentors.

Grad school becomes a lifestyle after a while, so it's difficult to distinguish among friends, colleagues, associates, mentors, accomplices. Rather than just jumbling everyone together, I'll divide it up this way. These are people associated with our labs to whom I would owe a debt of gratitude, if I didn't consider most of them to be good friends: Alison McCurdy, for her wise ways; Purnima Deshpande, Cesar Labarca, Mark Nowak, Paolo Kofuji, and Craig Doupnik of the Lester labs, who helped initiate me into the world of ion channels and the frog eggs who love them; Pam England, whose friendship, creativity, and wide-ranging curiosity got me started off right; Jesse Lin, Sarah Ngola, Seth Miller, and Jennifer Ma, whose openness, on-the-ballness, and general

coolness helped persuade me to join this lab; Scott Silverman, Anthony West, and Wenge Zhong, for all the former plus their scientific assistance with all aspects of unnatural amino acid mutagenesis; Yanhe Tong, for identifying a good idea when he saw it, and for sticking it out when things got ugly; Ken Philipson, for his generosity of spirit; Justin Gallivan, for oodles of scientific advice over the years; Marcus Sarofim, for any manner of assistance selflessly proffered; Lintong Li, for her inspiring commitment to learning at every opportunity, whether experimental or linguistic; Bal Khakh, for his enthusiasm for all things purinergic; Don Elmore, for leavening our drab existence with poetry and Midwestern charm; David Dahan, for impeccable scientific logic and admirable devotion to cats; James Petersson, for congenial camaraderie, conversation, and chemical commiseration as needed; Sarah Monahan, who's always ready for a conversation about psychoneuroimmunopharmacology; Darren Beene, for following the True Path; Steve Spronk, whose commitment to the positive is positively infectious; Lisa Turner, whose perspicacity and tenacity were continually tested by the wickedness of receptors; Anita Choi, for her efforts to make everything work out in the end; and to Tingwei Mu, Amanda Cashin, Michael Torrice, and Jordan Benjamin, who have every intention, I'm sure, of rocking on. In a category by themselves are Josh Maurer and Niki Zacharias. Josh probably does himself a disservice by being too helpful. The barrier to figuring something out myself is usually far higher than the barrier to bugging Josh to find out how to do it. Plus, he's a josh-of-all-trades, so practically everything I've done as a grad student has been with his assistance. It's hard to estimate the amount of time, all of it enjoyable, that I've spent with Niki, my friend, colleague, and housemate. My experience here has been inestimably improved by sharing it with her. Insofar as

perseverance and generosity are what makes the world a better place, she's certainly doing her part.

Next on this list, but in no way secondary, are friends who happened not to be in my lab. Mike Johnson took me under his wing when I first arrived in Pasadena. Megan Nuñez and Ben Lane, along with Marcus, welcomed me into their house. Liz Boon and Isaac Carrico have been wonderful housemates and friends. Jason Belitsky provided the example for thesis writing with an impressive closing effort. Michael and Traci Shogren-Knaak have been steadfast companions and have been keeping my life together for years, both scientifically and psychologically. My dear friend Catherine Baker has been an evergreen source of lexicology, phytophilia, racing tips, stories, and general wit and warmth.

Others at Caltech who have been crucial for making the experience tolerable, even enjoyable at times, are the many friends with whom I've played soccer, Frisbee, or music, along with Bill and Delores Bing, Donald Caldwell, and Allen Gross.

Finally, here are select friends outside of Caltech: Kris McNeill and Shana Sturla, Jeff and Saralyn Ang-Olson, Julie Veltman, and Christi Corbett have all improved my quality of life without even being here. Most of all, I'm grateful to my beloved friend Pamela Surkan for waiting for me and for introducing me to peixe-boi filhotes.

Caltech seems to have a knack for hiring incredibly competent and friendly people, from whom I've received a great deal of assistance, particularly Dian Buchness, Chris Smith, Steve Gould, Debbie Miles, Linda Syme, Shannan Boss, and Vanna Santoro.

Lastly, special thanks to my parents for not listening to that Willie Nelson song about letting your kids grow up to be chemists.

Abstract

The ability to introduce a synthetic amino acid into a fully folded protein allows the full power of organic chemistry to be applied to protein biochemistry. Any functionalized amino acid which can be incorporated by the ribosomal machinery may be site-specifically introduced. Through the application of chemical creativity, mimicry of the natural behavior of protein side chains and the introduction of novel function may both be attained.

As a class, integral membrane proteins require advanced biochemical tools for their characterization, since many of the classical methods of biochemistry are not applicable. These molecules represent an opportunity for the acquisition of unique information through the use of unnatural amino acid mutagenesis.

Cell-cell communication is fundamental to neurobiology, and leads ultimately to the phenomenon of consciousness. The receipt of extracellular stimuli relies on integral membrane proteins, and membrane-bound ion channels and receptors are the central proteins of molecular biology. Just as integral membrane proteins are well-suited to investigation by unnatural amino acid mutagenesis, molecular neurobiology is an excellent area for the application of this technology.

In the work presented here, tools for the measurement of physical organic parameters associated with molecular recognition events and conformational changes of proteins are developed and implemented in functioning neuroreceptors. In addition, analytical tools are introduced and deployed to investigate the real-time modulation of ion channel function in living cells.

After the work is introduced in Chapter 1, experiments on the use of fluorinated tryptophan analogs to serially modulate the electrostatics of particular amino acid side chains are presented in Chapter 2. The goal of these investigations is to understand an interaction between nicotine and tryptophan residues in the nicotinic acetylcholine receptor. Nicotine is shown not to experience a cation-π interaction with the side chain that mediates this interaction between the receptor and its natural agonist, acetylcholine. Additional studies on analogs of both nicotine and acetylcholine are presented, along with attempts to extend the fluorinated tryptophan methodology to neuronal receptors of the same class.

A series of dynamic amino acids are presented in Chapter 3. The overarching goal of these studies is to obtain information on ion channel conformation, both *in situ* and subsequent to isolation. A photoactive amino acid which induces proteolysis at the site of its incorporation is shown to have significant effects on the nicotinic acetylcholine receptor. Efforts to extend this methodology to biochemically detect backbone cleavage in the functionally affected receptors are also presented in this chapter. Also, the hydrolysis of an ester linkage introduced by the incorporation of a hydroxy acid in place of a natural amino acid is attempted to identify the disulfide connectivity of rat $P2X_2$ receptors. Finally, attempts to utilize photoreactive amino acid side chains to both crosslink adjacent subunits of the nicotinic acetylcholine receptor and to induce local conformational perturbations in the transmembrane regions of this receptor are detailed.

In Chapter 4, tyrosine containing a photo-removable protecting group is introduced in place of a particular tyrosine residue on which the modulation of Kir2.1 channel function depends. By this means, experimental control is gained over the chemical identity of this

side chain. As introduced, it is neither a substrate for tyrosine kinases nor for protein-protein interactions. However, once photolysis has revealed the wild-type residue, these interactions may occur. Co-injection of the tyrosine kinase v-Src along with the irradiation of cells expressing Kir2.1 containing this caged tyrosine residue at position 242 produces a 50% current reduction over a time course of approximately ten minutes. The roles of phosphorylation and endocytosis in causing this reduction were extensively investigated.

The final chapter presents progress toward controlling the *in situ* phosphorylation state of particular residues in a protein. A general method for synthesis of caged phosphoamino acids is developed and applied to the synthesis of analogs of serine, threonine, and tyrosine. A variety of routes toward caged non-hydrolyzable phosphoamino acid analogs are shown, along with the preparation of important synthetic intermediates.

Table of Contents

List of figures

List of tables

Chapter 1. Unnatural amino acid mutagenesis in molecular neurobiology

1.1 The nature of the interface between chemistry and biology

The smallest meaningful unit of a biological system is probably the molecule. Chemists working in the life sciences thus represent the reductionist extreme of biology. Interestingly, biological molecules appear enormous and complex to chemists, and are closer to the holistic end of our intellectual spectrum. The individual biochemist, then, seeks to publish in an environment where both reductionist and holistic thinking count. The general tenor of biological investigation is less reductionist than our usual work, and the viewpoint of most chemists is more so. Thus, the challenge of biochemistry is often pinpointing the specific interactions that interest us as chemists and yet putting them in the perspective of their effect on organisms as a whole. This increased level of generality in biological chemistry often arises through method development. To take a well-known example, the 1991 Nobel Prize in chemistry rewarded the development of two general methods, site-directed mutagenesis and PCR, which have driven much of the biology of the last two decades.

The work presented in this thesis focuses in detail on a number of different proteins and a variety of scientific questions. Following the strategy suggested above, the common theme is a technique. The general method that unites the disparate elements of this thesis is unnatural amino acid mutagenesis, performed on integral membrane proteins, in living cells.

1.2 Nonsense suppression and molecular neurobiology – a felicitous combination

Actually, there is a common intellectual theme as well. All of the questions addressed in this work, though they may differ from the perspective of biochemistry, are questions about neuroreceptors. Molecular neurobiology is a science which has arisen in the latter half of the 20th century. The seminal predictions of Hodgkin, Huxley, and Katz that ion permeability was responsible for the unique behavior of neurons and that dynamic ion channels must account for electronic excitability, action potentials, and the propagation of nerve signals were made largely from 1930-50. In the latter decades of the century, the molecules responsible for neural excitability began to be characterized at the atomic level.

Ion channels and neuroreceptors are molecules like any other, and the full range of techniques of molecular biology and biochemistry is available for their study. They are integral membrane proteins, however, and are thus refractory to many of the manipulations available to soluble proteins. However, they have a remarkable property unavailable to other biological molecules. Unique to these membrane-bound receptors is the ability to regulate the flow of ions across cellular membranes. This ion flux can be very readily measured, and physiologists have developed sophisticated methodology for studying this phenomenon. In addition to making up in some ways for their challenging biochemistry, the electrophysiological response of neuroreceptors is a very sensitive technique. Chemists are generally unused to being able to measure single-molecule events, but the patch clamp permits the electrophysiology of single channels to be measured. If electrophysiology provides a sensitive means to detect the activity of ion

channels, unnatural amino acid mutagenesis provides a sensitive method for manipulating them.

The introduction of unnatural amino acids into proteins may be accomplished by nonsense suppression.[1-5] The particular codon in a gene which encodes the amino acid to be replaced is changed to a non-coding, or 'nonsense' codon. Typically, this is a stop codon. The conversion of a coding codon to a stop codon normally induces termination of translation and a protein truncated at the position of stop codon introduction. If, however, the cell has also been supplied with tRNA molecules modified to recognize this stop codon and carrying an amino acid at their 3' end, translation continues apace. The suppression of the phenotype arising from the presence of a truncated protein in the cell, caused by a nonsense codon, is what gives this phenomenon its name. Nonsense suppression may easily be achieved in an organism by the simple molecular biological manipulation of mRNA and tRNA.

Nonsense suppression is used to introduce unnatural amino acids by charging the suppressor tRNA with a synthetic amino acid. It has been observed that the ribosome, which is responsible for translating mRNA into proteins, is rather tolerant in its accommodation of amino acid side chains. In addition to the natural 21 amino acids which are genetically encoded, the ribosome will accept quite a large number of unnatural amino acids. Thus, if a cell can be provided with two materials, an mRNA altered to contain a stop codon and a tRNA engineered to recognize the stop codon and carrying a synthetic amino acid at its 3'end, it is possible to introduce an unnatural amino acid into a protein by nonsense suppression. (Figure 1.1) In this work, the nomenclature

of nonsense suppression and unnatural amino acid mutagenesis will be used interchangeably.

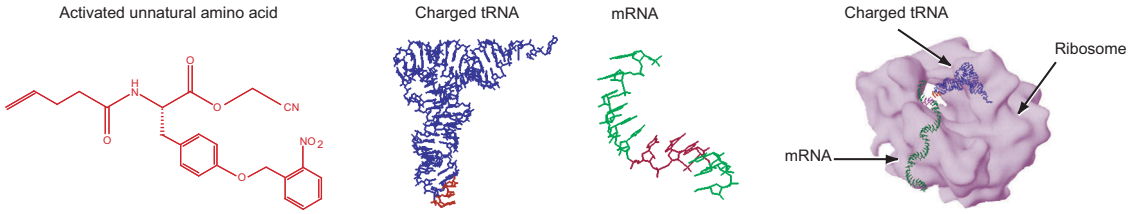

Figure 1.1 Schematic of the components necessary for unnatural amino acid mutagenesis. Left: Unnatural amino acid, C-terminally activated as the cyanomethyl ester for chemical conjugation to tRNA, and N-terminally protected for stability. Center: Suppressor tRNA (anticodon indicated in red) and mRNA containing a stop codon (also red) at the site of desired synthetic amino acid insertion. Right: Ribosomal translation, using the synthetically aminoacylated tRNA (blue) and stop codon-containing mRNA (green) to generate a protein containing an unnatuaral amino acid.

The marriage of ion channel electrophysiology and unnatural amino acid mutagenesis is consummated in the cells of a South African clawed frog. The oocyte of *Xenopus laevis* has been discovered to be an excellent vehicle for the functional expression of a wide variety of molecules fundamental to molecular neurobiology.[6] (Figure 1.2)

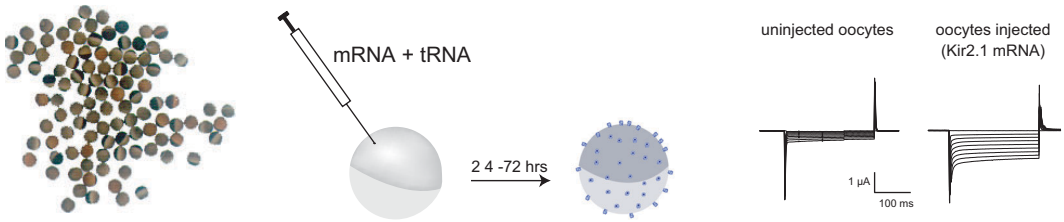

Figure 1.2 *Xenopus* oocytes are utilized in molecular neurobiology for the heterologous expression of ion channel proteins. Left: *Xenopus* oocytes at 1x magnification. Center: Schematic showing the microinjection of mRNA and tRNA into oocytes, followed by the expression of receptors (not to scale) at the cell surface. Right: Example of electrophysiological data obtained by two-electrode voltage clamp from oocytes expressing a potassium channel Kir2.1 arising from nonsense suppression.

Physical injection of mRNA into oocytes (these are very large cells, approximately 1 mm in diameter, which is why they were selected for this purpose) usually results in the expression of functional proteins. In addition, it was demonstrated in our laboratory in 1995 that these cells may accommodate also the co-injection of synthetically charged

suppressor tRNA, which results in the plasma membrane expression of ion channels containing synthetic amino acids.[7] Thus, in living *Xenopus* oocytes, unnatural amino acids are introduced site-specifically into functioning ion channels.[7-10] The behavior of these channels may be measured using electrophysiology.

1.3 Implementation of the suppression method in molecular neurobiology

1.3.1 tRNA synthesis

The organic chemistry required to synthesize amino acids is clearly well-established. However, the requirement to specifically attach a synthetic amino acid to a full-length tRNA is potentially a much bigger synthetic challenge.[11] A fundamental step in the development of the unnatural amino acid mutagenesis methodology was the realization that this synthesis may be largely avoided.[12] The bulk of the tRNA may be prepared using molecular biology. Only a small piece is chemically synthesized, the dinucleotide corresponding to the 3' end of the tRNA. The desired amino acid is chemically coupled to this dCA dinucleotide (the cytosine 2' hydroxyl is not necessary for translation, so dC is used instead of C for ease of specific aminoacylation). Then, the dCA-amino acid is attached to body of the tRNA by enzymatic ligation. The tRNA body itself is prepared by runoff transcription from a plasmid template, a very standard molecular biology procedure.

1.3.2 General considerations

1.3.2.1 Variability in suppression efficiency

The choice of which residue to replace clearly depends on the experiment. This is sometimes complicated by the fact that suppression efficiency is also highly variable from residue to residue. Some amino acids may not be readily replaced, or may be replaceable by some unnatural side chains but not others. In practice, we have identified no reliable guidelines for predicting which sites will work well. There is no substitute for simply attempting incorporation of the desired amino acid at the desired position. Fortunately, trying several different sites is a matter of fairly routine mutagenesis, so trial and error is not terribly time-consuming. There are a number of factors which may account for the observed variability in suppression efficiency.

1.3.2.2 Optimizing translational efficiency

Factors associated with translation include codon context, read-through of the stop codon, and effects from truncated proteins. First, the 5' and 3' nucleotide sequence around a stop codon can govern the efficiency with which it is suppressed by suppressor tRNA's.[13-16] Since some amino acids may be coded for by codons in unfavorable contexts, suppression at these positions may be difficult. It should be mentioned, however, that we have never observed a clear correlation between suppression efficiency and codon context, despite the large body of literature on the subject. It could be that trends are confounded by post-translational effects of incorporating unnatural side chains, some of which are discussed below. In any case, an unfavorable codon context can sometimes be ameliorated via silent mutations around the desired site. Codon bias,

where a heterologous expression system may translate mRNA poorly because their native codons represent rare tRNA's in the heterologous system, may be addressed similarly.[17-20]

A second difficulty which may arise at the translational level is read-through of the stop codon.[21] We use the term generally here to mean any process by which full-length protein is produced which does not contain the desired unnatural amino acid at the appropriate position. This may occur if a) the stop codon is recognized by an endogenous tRNA even without a perfect codon:anticodon match, or b) if the exogenously applied tRNA loses its unnatural amino acid and an endogenous synthetase replaces it with a natural amino acid, or c) if the anticodon is skipped to generate a mutant protein with a deletion at the desired incorporation site. Again, it has proven difficult to generate formal rules for predicting the likelihood of these events. Typically, the amount of injected mRNA or, if applicable, the ratio of subunits to each other can be altered to reach a regime where there is reasonable expression with little evidence of read-through.

Finally, suppression efficiency is far from quantitative, so translation frequently terminates at the introduced stop codon. When this occurs, the truncated protein which forms must be checked for its ability to function, any deleterious effect on cell health, or possible dominant negative effects.[22,23] Particularly with suppression near the C-terminus of polytopic membrane proteins such as receptors, partial-length proteins may be trafficked to the surface and interfere with certain experiments. Again, the best experimental recourse might be to adjust the amounts of mRNA involved.

1.3.2.3 Efficiency of folding and assembly

A second class of complications has to do with folding, assembly, and trafficking of proteins containing mutant side chains subsequent to translation.[24-26] Once again, it is

difficult to predict the side chains and sites at which this will be problematic. Also, it can be difficult to distinguish between improper folding and loss of function as a result of unnatural amino acid incorporation. These two scenarios, and also whether a problem is translational or post-translational, may sometimes be distinguished by SDS-PAGE. Separation of cytosolic from surface proteins followed by PAGE will reveal a) whether or not full-length protein is being produced by the cell, and b) whether or not the receptor is making it to the cell surface.

1.3.3 Essential controls

As a result of the translation and post-translational complications associated with the nonsense suppression methodology, it is absolutely essential to perform the requisite controls. The incorporation of caged side chains has the benefit of conferring chemical reactivity unavailable to the twenty naturally occurring amino acids, so it is usually straightforward to distinguish between proteins containing caged amino acids and those which do not. Nonetheless, the following controls are necessary each time suppression is attempted in a new receptor, at a new residue, or with a new amino acid analog.

1.3.3.1 mRNA only

Injection of the stop codon-containing mRNA without exogenous tRNA is a simple experiment which controls for a number of outcomes. If truncated protein is functional, this control should reveal it. Likewise, if read-through of the stop codon is occurring, it will be evident. The mRNA-only control with ion channels in *Xenopus* oocytes frequently gives rise to measurable currents, for instance. If a dominant negative effect from truncated protein is suspected, it is again a simple matter to co-inject mutant mRNA

with wild-type mRNA to see if the presence of the mutant RNA decreases the expression of functional protein.

1.3.3.2 mRNA with uncharged suppressor tRNA

Even if read-through of the mRNA alone is not occurring, the presence of uncharged exogenous tRNA frequently leads to full-length protein. Presumably, the exogenous tRNA is being recognized by endogenous synthetases or the suppressor tRNA facilitates skipping of the stop codon to generate a deletion mutant. Again, this problem can be addressed by decreasing the amount of mRNA injected into the cell to find a concentration which gives reasonable expression without measurable read-through. In this control, mutant mRNA is injected with 74mer tRNA enzymatically ligated to dCA. Alternatively, mutant mRNA is injected with 74mer tRNA. Eukaryotic cells transcribe tRNA in a truncated form and enzymatically add the final CCA bases to the 3' end. In oocytes, the 74mer often gives rise to greater read-through currents than full-length tRNA generated by ligating dCA to the 74mer. This confirms that oocytes are capable of completing truncated tRNA and suggests that perhaps dC at position 75 is a poorer substrate for endogenous synthetases than C, or that interaction with the ribosome is weaker, resulting in less full-length protein being produced.

1.4 Uses of unnatural amino acid suppression in molecular neurobiology

1.4.1 Structure-function studies

Because of the site-specificity of unnatural amino acid mutagenesis, it is an excellent tool for determining the functional role and structural context of particular side chains.

Since the range of amino acid side chains tolerated by the ribosome is rather generous, a number of functional and structural probes may be introduced.[1-5]

Chapter 2 presents an example of such a use of unnatural amino acids. This work follows the initial observation by Wenge Zhong that nicotine appears to bind the nicotinic acetylcholine receptor (nAChR) differently from either its natural ligand acetylcholine (ACh) or the weak agonist tetramethylammonium (TMA).[27] The chapter is largely based on a *Biochemistry* paper written in collaboration with Darren Beene, who performed an enormous amount of work on the neurotransmitter serotonin (5-hydroxytryptamine, or 5-HT) and its receptor, 5-HT_{3A}R.[28] Valuable synthetic assistance was also provided by Niki Zacharias, who prepared an *N*-alkylated analog of nicotine used in these studies. The second section of this chapter describes attempts to extend the use of our structure-function probe to a class of nAChR found in the central nervous system (CNS). Much of this work was carried out with great persistence and skill by Lisa Turner, during the summers of 1999 and 2000.

1.4.2 Dynamic in situ manipulation of ion channels

In addition to their use as probes, unnatural amino acids may be used to exert control over biological molecules while they are functional and in their native environment. This ability is actually almost without precedent, and could conceivably be used to carry out experiments which have no counterpart outside the realm of unnatural amino acid mutagenesis. Thus, there is undoubtedly information which could be supplied by these techniques which would be of great interest to the biological community. However, experiments of this nature remain technically challenging, as can be seen in Chapters 3-5.

1.4.2.1 Conformational studies

In Chapter 3, a number of experimental approaches to understanding details of the conformation of ion channels are presented. The first deals with attempts to site-specifically cleave the backbone of a functioning ion channel. This work is based on imaginative chemistry developed by Dr. Pam England in this laboratory in 1997.[29] The experiments presented herein were carried out with a great deal of useful assistance from her, and many of the ideas were developed with her guidance. The second area treated in this chapter is site-specific photocrosslinking. This work mirrors conventional photoaffinity labeling with the added benefit that the label may be introduced site-specifically. The experiments described in the section were carried out in collaboration with Justin Gallivan, who prepared the unnatural amino acid used in the studies and performed some of the electrophysiology.[30] Thirdly, a method for determining disulfide connectivity in folded, native proteins is presented. This section is also based on a method developed by Pam England.[31] Experiments to determine the cysteine topology of the ATP receptor $P2X_2$ were carried out with intellectual input from her and both intellectual and material collaboration with the knowledgeable and hard-working Dr. Baljit Khakh. Finally, a technique for dynamically altering the local conformation of a native protein the vicinity of a particular residue is presented. This work was carried out almost entirely by Dr. Ken Philipson, who generously shared authorship on a paper in the *American Journal of Physiology* for my assistance with the early phases of the project.[32]

1.4.2.2 Controlling protein-protein interaction and post-translational modification

The ability to introduce photoreactive amino acid side chains permits some control over the chemical identity of particular residues. Prior to photolysis, one chemical

species is present, while after photoinduced reaction an altogether different compound may be present. In Chapter 4, the photochemical conversion of a tyrosine analog to tyrosine itself is presented as a means of controlling interactions involving a particular Tyr residue. This chapter is based in its entirety on a paper in the *Journal of General Physiology* written in collaboration with Dr. Yanhe Tong, whose dedication in the face of an extremely difficult and complex problem was necessary to shepherd the project to a favorable conclusion.[33] He was responsible for all of the electrophysiology reported in this chapter, with the exception of the single-channel recordings, which were performed by George Shapovalov. Fluorescence assays were carried out with the able assistance of Dr. Ming Li. The introduction includes portions of an invited review in *Methods in Enzymology*.[34] The text is my own, written under the guidance of James Petersson and with additional editorial assistance from Niki Zacharias.

In Chapter 5, a similar strategy of photoreaction is introduced as a means of controlling phosphorylation, arguably the single most important biological regulatory pathway acting at the protein level. Where the work of Chapter 4 is based on revealing wild-type tyrosine, the experiments in this chapter represent progress toward developing a technique to reveal phosphoamino acids and their non-hydrolyzable analogs. The synthesis of these compounds was performed with the valuable help of Anita Choi, who prepared caged threonine and the important synthetic intermediate nitrobenzyl bromodifluorophosphonate, during the summer of 2002. Caged serine and threonine, mentioned in this chapter, were synthesized earlier in this laboratory by Justin Gallivan.[30]

1.5 References

1. Nowak, M. W. et al. *In vivo* incorporation of unnatural amino acids into ion channels in *Xenopus* oocyte expression system. *Meth. Enz.* **293**, 504-529 (1998).
2. Sisido, M. and Hohsaka, T. Extension of protein functions by the incorporation of nonnatural amino acids. *Bull. Chem. Soc. Japan* **72**, 1409-1425 (1999).
3. Steward, L. E. and Chamberlin, A. R. Protein engineering with nonstandard amino acids. *Meth. Mol. Biol.* **77**, 325-354 (1998).
4. Thorson, J. S. et al. A biosynthetic approach for the incorporation of unnatural amino acids into proteins. *Meth. Mol. Biol.* **77**, 43-73 (1998).
5. Gilmore, M. A., Steward, L. E. and Chamberlin, A. R. Incorporation of noncoded amino acids by in vitro protein biosynthesis. *Top. Curr. Chem.* **202**, 77-99 (1999).
6. Soreq, H. and Seidman, S. *Xenopus* oocyte microinjection: from gene to protein. *Meth. Enz.* **207**, 225-265 (1992).
7. Nowak, M. W. et al. Nicotinic receptor binding site probed with unnatural amino acid incorporation in intact cells. *Science* **268**, 439-442. (1995).
8. Turcatti, G. et al. Probing the structure and function of the tachykinin neurokinin-2 receptor through biosynthetic incorporation of fluorescent amino acids at specific sites. *J. Biol. Chem.* **271**, 19991-19998. (1996).
9. Turcatti, G. et al. Fluorescent labeling of NK2 receptor at specific sites *in vivo* and fluorescence energy transfer analysis of NK2 ligand-receptor complexes. *Receptors Channels* **5**, 201-207 (1997).
10. Lu, T. et al. Probing ion permeation and gating in a K^+ channel with backbone mutations in the selectivity filter. *Nat. Neurosci.* **4**, 239-246. (2001).
11. Pitsch, S. Towards a total synthesis of aminoacylated tRNAs. *Chimia* **55**, 60-64 (2001).
12. Payne, R. C., Nichols, B. P. and Hecht, S. M. *Escherichia coli* tryptophan synthase - synthesis of catalytically competent alpha-subunit in a cell-free system containing preacylated transfer-RNAs. *Biochemistry* **26**, 3197-3205 (1987).
13. Harrell, L., Melcher, U. and Atkins, J. F. Predominance of six different hexanucleotide recoding signals 3 ' of read-through stop codons. *Nucl. Acids Res.* **30**, 2011-2017 (2002).
14. Mottagui-Tabar, S., Tuite, M. F. and Isaksson, L. A. The influence of 5 ' codon context on translation termination in *Saccharomyces cerevisiae*. *Eur. J. Biochem.* **257**, 249-254 (1998).
15. Pavlov, M. Y. et al. A direct estimation of the context effect on the efficiency of termination. *J. Mol. Biol.* **284**, 579-590 (1998).
16. Tate, W. P. and Mannering, S. A. Three, four or more: The translational stop signal at length. *Mol. Microbiol.* **21**, 213-219 (1996).
17. Horvath, H. et al. The production of recombinant proteins in transgenic barley grains. *PNAS* **97**, 1914-1919 (2000).
18. Karlin, S. and Mrazek, J. What drives codon choices in human genes? *J. Mol. Biol.* **262**, 459-472 (1996).
19. Karlin, S. and Mrazek, J. Predicted highly expressed genes of diverse prokaryotic genomes. *J. Bacteriol.* **182**, 5238-5250 (2000).
20. Vervoort, E. B. et al. Optimizing heterologous expression in *Dictyostelium*: importance of 5 ' codon adaptation. *Nucl. Acids Res.* **28**, 2069-2074 (2000).
21. Nakamura, Y., Ito, K. and Isaksson, L. A. Emerging understanding of translation termination. *Cell* **87**, 147-150 (1996).
22. Cooper, S. T. and Millar, N. S. Host cell-specific folding and assembly of the neuronal nicotinic acetylcholine receptor alpha 7 subunit. *J. Neurochem.* **68**, 2140-2151 (1997).
23. Buller, A. L. and White, M. M. Control of *Torpedo* acetylcholine-receptor biosynthesis in *Xenopus* oocytes. *PNAS* **85**, 8717-8721 (1988).
24. Green, W. N. *Perspective* - Ion channel assembly: Creating structures that function. *J. Gen. Phys.* **113**, 163-169 (1999).
25. Chang, W., Gelman, M. S. and Prives, J. M. Calnexin-dependent enhancement of nicotinic acetylcholine receptor assembly and surface expression. *J. Biol. Chem.* **272**, 28925-28932 (1997).

26. Lansdell, S. J., Schmitt, B., Betz, H., Sattelle, D. B. and Millar, N. S. Temperature-sensitive expression of *Drosophila* neuronal nicotinic acetylcholine receptors. *J. Neurochem.* **68**, 1812-1819 (1997).
27. Zhong, W. *Ph.D. Thesis*. (California Institute of Technology, Pasadena, CA, 1998).
28. Beene, D. L. et al. Cation-pi interactions in ligand recognition by serotonergic ($5\text{-}HT_{3A}$) and nicotinic acetylcholine receptors: theanomalous binding properties of nicotine. *Biochemistry* **41**, 10262-10269 (2002).
29. England, P. M., Lester, H. A., Davidson, N. and Dougherty, D. A. Site-specific, photochemical proteolysis applied to ion channels in vivo. *PNAS* **94**, 11025-11030. (1997).
30. Gallivan, J. P. *Ph.D. Thesis* (California Institute of Technology, Pasadena, CA, 2000).
31. England, P. M., Lester, H. A. and Dougherty, D. A. Mapping disulfide connectivity using backbone ester hydrolysis. *Biochemistry* **38**, 14409-14415. (1999).
32. Philipson, K. P., Gallivan, J. P., Brandt, G. S., Dougherty, D. A. and Lester, H. A. Incorporation of caged cysteine and caged tyrosine into a transmembrane segment of the nicotinic acetylcholine receptor. *Am. J. Phys. Cell Phys.* **281**, C195-C208 (2001).
33. Tong, Y. *et al.* Tyrosine Decaging Leads to Substantial Membrane Trafficking during Modulation of an Inward Rectifier Potassium Channel. *J. Gen. Phys.* **117**, 103-118. (2001).
34. Petersson, E.J., *et al. Meth. Enz.*, in press (2003).

Chapter 2. Cation-π analysis using fluorinated Trp derivatives

2.1 Introduction

From the perspective of the participating molecules, the lock-and-key analogy for the binding of a neurotransmitter to its receptor is a rather optimistic description. In fact, the small molecule is tumbling, colliding with solvent molecules, spastically sampling different conformations as it diffuses through the medium. Upon entering the electrostatic field of its receptor, it's violently jerked this way and that by the protein's charged residues and hydrophobic cavities. Likewise, the multi-subunit receptor undergoes massive breathing motions on the timescale of the neurotransmitter's approach. Obtaining atomic-scale information about a binding event in the midst of this chaos is not easy. Everything depends on having a probe in the right place at the right time.

Classically, probe introduction has been accomplished in two rather different ways. Affinity labeling places the probe on the ligand and allows the receptor to position it accordingly. Any modification to the ligand which still allows binding may be introduced, including reactive groups for photoaffinity labeling, for example. The second means of obtaining structural information about ligand binding has been site-directed mutagenesis. The desirable aspect of this technique is the ability to precisely target single residues with discrete spatial locations. However, only the chemistry available to the natural amino acids may be utilized, such as disulfide formation using cysteine residues. As mentioned in the previous chapter, the extension of site-directed mutagenesis to accommodate synthetic amino acids has led to entirely new kinds of structural probes. For instance, a series of fluorinated tryptophan analogs has been used

in this laboratory as a sensitive probe of the role of side chain electrostatics in ligand binding.[1]

Ligand binding is a central event in almost every aspect of biology, and molecular neuroscience is no exception. The binding of small molecule neurotransmitters to membrane-bound receptors is the process which drives synaptic transmission. The advent of widespread cloning efforts in the past two decades or so has revealed the primary sequence of a large number of neurotransmitter receptors. Among the first of these was the nicotinic acetylcholine receptor (nAChR).[2] Attempts to understand the principles of molecular recognition by which the nAChR binds its agonist initially centered on attempting to reconcile the known amino acid sequence of the receptor with a variety of biochemical, electrophysiological, and pharmacological experiments, the conclusions of which have been extensively reviewed.[3-9] Muscle preparations and the electroplax organs of electric rays, which contain exceptionally dense clusters of nicotinic receptors, were used to conduct these experiments before advances in molecular biology made heterologous expression of the nAChR routine. Physiological experiments revealed that the nAChR is a cation channel which opens in response to acetylcholine, as well as nicotine. Furthermore, the apparent cooperativity of opening implied the presence of at least two agonist binding sites. Biochemical experiments involving photoaffinity labeling had identified a number of aromatic residues, both tyrosine and tryptophan, in the binding site. The observation that nAChR agonists are uniformly cationic had led to the expectation that anionic residues in the binding site would provide the necessary electrostatic attraction to draw neurotransmitters into the binding site.

However, it was also appreciated, particularly in this laboratory, that the aromatic residues identified by labeling studies could stabilize agonist binding through cation-π interactions.[10] Based on studies of molecular recognition of cationic substrates by synthetic hosts in water, the role of aromatic residues in binding acetylcholine was proposed in 1990.[11] In the absence of structural data on the nAChR, this proposal remained an attractive hypothesis until 1998, when the interaction was demonstrated directly.[1] In this set of experiments, the series of fluorinated Trp analogs alluded to above was introduced into the nAChR binding site by unnatural amino acid mutagenesis in *Xenopus* oocytes. At a single position in the binding site, a strict dependence on the negative electrostatic potential on the surface of the aromatic side chain was observed.[1] This dependence pointed to the role of Trp149 in ACh binding, via a cation-π interaction.

This assessment was subsequently confirmed in 2001 by the crystallization of a soluble acetylcholine-binding protein from the snail *Lymnaea helicalis*.[12] This crystallography represents a watershed event in structural analysis of ligand-gated ion channels, because the ACh binding protein (AChBP) is highly homologous to the extracellular portion of the nAChR. It is widely believed that structural insights gained from the AChBP crystal structure will be transferable to the extracellular domain of the receptor itself. One small detail of the crystal structure was quite gratifying to this laboratory. Cationic HEPES molecules from the crystallization buffer were reported to be bound to the face of the tryptophan homologous to the muscle Trp149 identified by Zhong *et al*. in 1998.[12]

Some of the structural detail revealed by the crystal structure is shown in Figure 2.1. Much of the gross structure had been previously gleaned from the physiological and

biochemical experiments mentioned above, along with primary sequence analysis and electron tomography.[9] The receptor is a pentamer, composed of five subunits around a central pore, which contains the ion channel region.

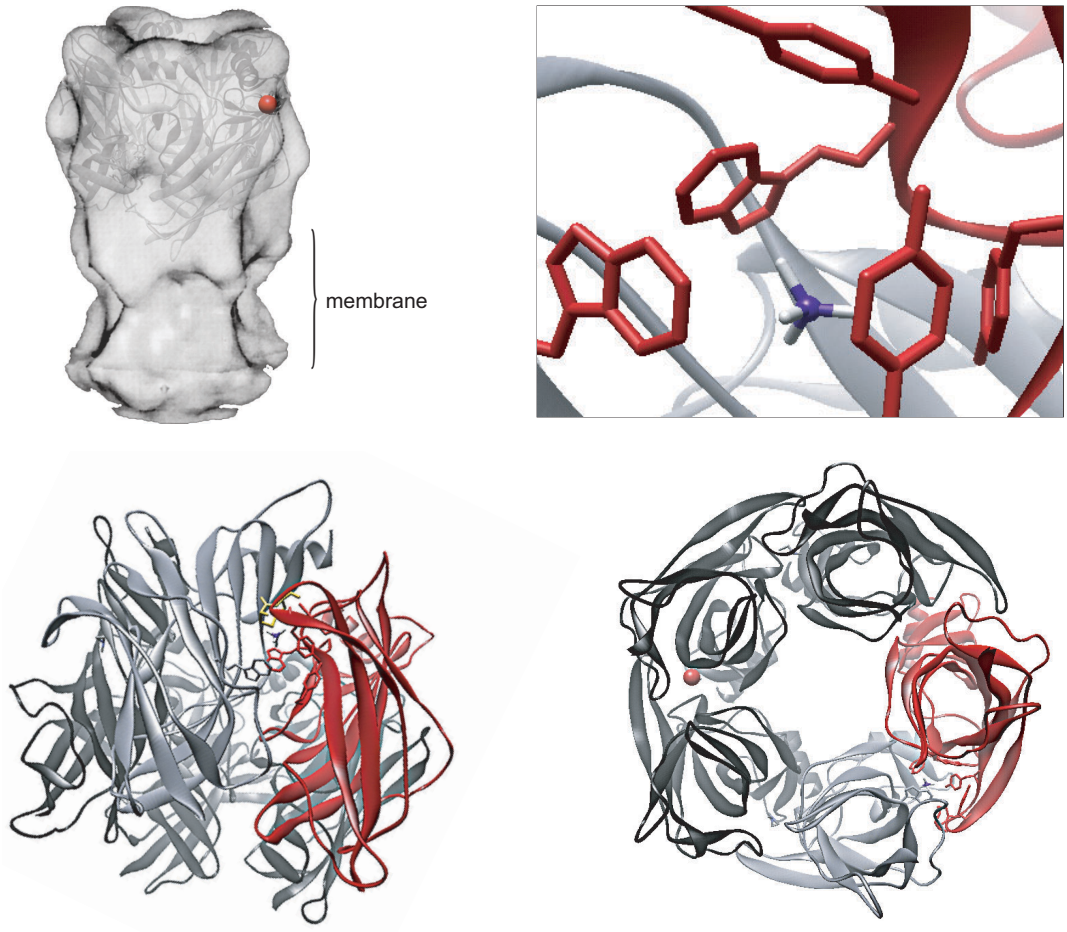

Figure 2.1 Views of the nAChR based on X-ray crystallography of the highly homologous snail acetylcholine binding protein.[12] Top left: Receptor electron density from electron cryomicroscopy,[9] superimposed over a ribbon diagram of AChBP, which corresponds to the extracellular domain of the receptor. Approximate location of bound agonist is indicated by the red sphere. Top right: Detailed view of the binding site, showing the arrangement of aromatic residues around the quaternary ammonium of the agonist. Bottom: Side and top views of the receptor with binding site residues in the subunit highlighted in red rendered as stick diagrams.

The muscle receptor is made up of four different subunits, denoted α, β, γ, and ε. The fetal form of the receptor, however, contains α, β, γ, and δ subunits, and it is this murine embryonic receptor used in the experiments below. In addition to the muscle-type receptor, found at neuromuscular junctions, there are neuronal forms of the receptor.[5,7,8]

Here, the subunit nomenclature differs somewhat. One class of subunits, which are identified by the presence of a vicinal Cys disulfide loop, is known as α. The muscle α is α1, and α2-9 are the neuronal isoforms. All other nicotinic subunits in the CNS are referred to as β, of which there are four known. Again, β1 is the muscle subunit and β2-4 are neuronal subunits.

The pore region of the nAChR is made up primarily of the second transmembrane region, known as M2. The conformational changes accompanying agonist binding are communicated to this transmembrane region, thus opening the channel. Previous work in this and other laboratories has identified mutations in the central region of this domain which confer greater sensitivity to agonists.[13-16] One of these mutations, Leu258Ser (also called L9'S, using commonly accepted nAChR nomenclature), will be utilized in the work below.

The binding domain, for which the structural information obtained from the AChBP applies, is the focus of the work presented below. The same series of fluorinated tryptophan analogs that was used to identify Trp149 as the cation-π binding site of ACh was employed to study the binding of a variety of agonists, revealing varying degrees of interaction with aromatic residues in the binding site. The behavior of nicotine was extensively characterized, along with a number of related nAChR agonist analogs. In addition, the technique was extended to a related serotonin receptor, the neuronal 5-HT_3R.[6,17] Unlike crystallography, this combination of unnatural amino acid mutagenesis and pharmacology is able to give information from only a single residue, so it lacks the scale of a crystal structure. However, it has the advantage over a crystal structure in that

it reports on the structure and function of residues in fully functioning ion channels in the plasma membrane of living cells.

2.2 Results

2.2.1 Nicotine dose-response to F_x-Trp at α149

The response of nAChR to nicotine was measured by two-electrode voltage clamp of oocytes expressing murine embryonic muscle nAChR. These receptors contained a pore mutation in the beta or gamma subunits, in order to reduce the EC_{50} and avoid channel block at higher agonist concentrations. Each L9'S mutation lowers EC_{50} by approximately a factor of ten relative to wild type. The effects of this mutation on EC_{50} are well-characterized, and it is expected not to alter agonist binding.[14,15,18] Dose-response curves for βL9'S receptors were collected by Wenge Zhong.[19] When a L9'S mutation is present in the β subunit, EC_{50} for otherwise wild-type nAChR is 45.3 ± 0.6 μM. If a single fluorine is added to the tryptophan ring by incorporating F-Trp at position 149, the EC_{50} rises to 129.8 ± 4.8 μM. This increase of almost threefold is comparable to the fourfold increase observed with ACh. What is observed, though, is that further fluorination does not lead to a significant further increase the EC_{50}. A small increase is noted for F_2-Trp, as the EC_{50} is 172.3 ± 5.7 μM. However, this is much smaller than the factor of four which characterizes the ACh interaction with Trp analogs at α149. Continuing in this vein, F_3-Trp gives an EC_{50} of 187.8 ± 11.4 μM and F_4-Trp produces a receptor with an EC_{50} of 136.4 ± 5.0 μM. Again, this increase is significantly less than that observed for ACh, implying that nicotine may not interact with Trp149 through a cation-π interaction.

The trend of these results was largely replicated in the receptor containing two L9'S mutations, as seen in Table 2.1. In this βγL9'S receptor, the EC_{50} for nicotine is 1.31 ± 0.45 μM. Introduction of F-Trp at position α149 causes a small increase to 4.19 ± 1.00 μM. However, further fluorination of the ring leads to little significant increase relative to the tenfold increase seen with acetylcholine. For F_2-Trp, the value is 5.43 ± 0.74 μM, increasing slightly to 12.56 ± 2.10 μM for F_3-Trp and to 10.93 for F_4-Trp.

L9'S	**Residue**	**EC_{50} (μM) SEM**	**n_H SEM**
β	Trp	45.3 ± 0.6	
β	F-Trp	129.8 ± 4.8	
β	F_2-Trp	172.3 ±5.7	
β	F_3-Trp	187.8 ± 11.4	
β	F_4-Trp	136.4 ± 5.0	
βγ	Trp	1.31 ± 0.32	2.92 ± 1.47
βγ	F-Trp	4.19 ± 0.71	1.57 ± 0.09
βγ	F_2-Trp	5.43 ± 0.52	1.53 ± 0.08
βγ	F_3-Trp	12.56 ± 1.49	1.13 ± 0.07
βγ	F_4-Trp	10.93	1.28

Table 2.1 Nicotine dose-response data for oocytes expressing β and βγ L9'S nAChR suppressed with the indicated residue at α149.

As an additional test that pore mutations exert their effects independently of binding interactions between agonists and Trp149, the response of ACh to fluorinated Trp analogs was measured in nAChR containing two L9'S mutation, in the beta and gamma subunits. (Table 2.2) These data replicate the trend observed for β L9'S by Zhong *et al.*[1,19]

Residue	**EC_{50} (μM)**	**n_H**
Trp	ND	ND
F-Trp	0.04	1.46
F_2-Trp	0.13	1.49
F_3-Trp	0.45	1.05
F_4-Trp	0.86	1.06

Table 2.2 ACh dose-response data for oocytes expressing βγ L9'S nAChR suppressed with the indicated residue at α149.

2.2.2 Nicotine dose-response to fluorination at other binding site Trp residues

The above results raise the question of how nicotine is binding to the receptor, if it does not rely on a cation-π interaction with Trp149. One possibility is that it retains the interaction, but with an aromatic residue other than Trp149. In order to test this hypothesis, a separate line of experimentation was undertaken involving probing other aromatic residues in the binding site for cation-π interactions. Initially, we focused on tryptophan residues implicated in nicotine binding by mutagenesis and photoaffinity labeling studies from other labs.[3-6] As in previous work with acetylcholine, these residues included αTrp86, αTrp184, γTrp55, and δTrp57. However, while this work was underway, the crystal structure of AChBP was published. From the crystal structure, it appears that of these four residues, only the γ55/δ57 pair are part of the agonist binding site around Trp149.[12] Because of this, only α184 and γ55/δ57 were tested.

The experimental procedure for this test was reported earlier.[1] In brief, 5-CN-Trp or 5-Br-Trp is incorporated into the receptor at the position of interest. Both these substituents withdraw electron density from the tryptophan ring, but the cyano group is much stronger in this regard than bromine, even though the two are similar in size. The calculated cation-π binding energy for 5-CN-Trp is 21.5 kcal/mol, relative to 27.8 kcal/mol for 5-Br-Trp. The expectation is that an agonist binding to the face of an aromatic ring at this position would be dramatically affected by the presence of 5-CN-Trp at this position and less by 5-Br-Trp. In the case of ACh at position 149, for example, there is an approximately 50-fold difference between 5-CN-Trp and 5-Br-Trp.[19] On the other hand, if binding to the face of an aromatic at this position is not important, little

difference between the two will be observed. At position α184, for instance, the ratio between 5-CN-Trp and 5-Br-Trp for ACh is 0.96.

As shown in Figure 2.2, nicotine shows no marked reliance on the aromatic face of side chains at α184 or γ55/δ57. At α184, the EC_{50} of receptors containing 5-CN-Trp is nearly identical to that of those containing 5-Br-Trp, which is no surprise if the AChBP structure reflects the actual structure of the nAChR binding site. At γ55/δ57, there is a slightly larger effect. EC_{50} for 5-CN-Trp is 1.43 ± 0.18 μM and 3.04 ± 0.45 μM for 5-Br-Trp. However, the ratio is approximately 0.5, well below that expected for an agonist relying on the energetics of a cation-π interaction for binding and, in fact, in the opposite direction.

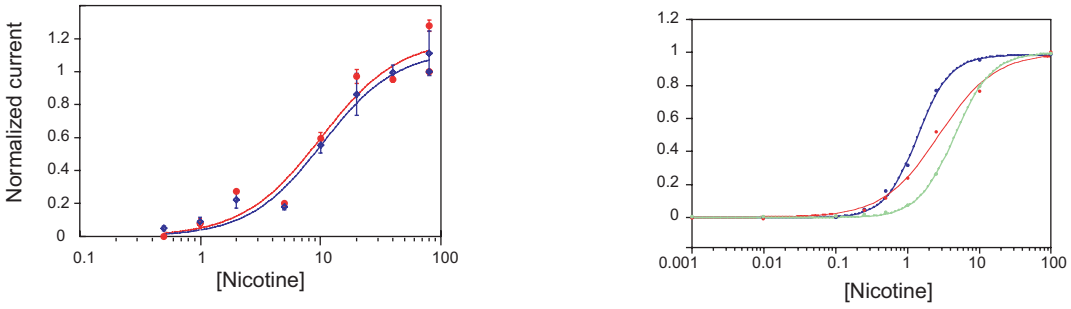

Figure 2.2 Nicotine dose-response for oocytes expressing nAChR suppressed at position α184 (left) and γ55/δ57 (right) with Trp (green), 5-CN-Trp (blue), and 5-Br-Trp (red). Receptors suppressed at α184 contain βγ L9'S mutations, while those suppressed at γ55/δ57 contain α L9'S.

From these data, we conclude that nicotine does not bind nAChR via a cation-π interaction at any of the sites tested. Most surprisingly, there is no apparent interaction with Trp149, at which cation-π interactions were observed for ACh and for serotonin at the homologous residue in the $5\text{-}HT_3R$. In light of photoaffinity labeling of γ55 by nicotine in experiments by Jonathan Cohen's lab, it is perhaps also surprising that the cation of nicotine does not apparently interact with γ55/δ57.[20,21]

2.2.3 N-methyl-nicotinium dose-response

One way in which protonated tertiary cations differ from quaternary cations is in their charge density and ability to benefit from cation-π interaction with aromatic systems. However, an equally important difference is that the protonated tertiary amine may lose its proton and revert to neutrality, presumably resulting in a non-binding form of the agonist. This is in contrast to the quaternary ammonium center, which is permanently charged under normal physiological conditions. In the case of nicotine, the pK_a of the pyrrolidinium nitrogen is 7.8, quite close to physiological pH.[22] Thus, it is quite reasonable to suppose that the microenvironment at the nAChR binding site might be sufficiently basic to induce deprotonation. Further, it is reasonable to suppose that perturbing the electrostatics of the side chain at α149 might alter the electrostatics of the binding site in such a way as to promote or hinder deprotonation. In order to test the hypothesis that fluorination affects not only the cation-π binding ability of the residue at α149 but also the protonation state of nicotine, a quaternary analog of nicotine, *N*-methyl-nicotinium, was prepared by Niki Zacharias.[22]

Sterically, *N*-methyl-nicotinium is bulkier than nicotine, as a result of the additional *N*-methyl group. As discussed, the relatively diffuse charge density decreases the ability of this quaternary cation to interact with the face of an aromatic residue relative to nicotine. Finally, the quaternary analog of nicotine is unable to undergo deprotonation and thus serves as a test for the hypothesis that fluorination at α149 promotes deprotonation and results in an apparent decrease in agonist affinity. As shown in Table 2.3, the EC_{50} for *N*-methyl-nicotinium in βγL9'S nAChR is 0.77 ± 0.14 μM, quite similar to that that of nicotine. (Table 2.1) In response to F-Trp, the EC_{50} increases fivefold to

4.23 ± 0.44 μM. Like nicotine, *N*-methyl-nicotinium does not respond significantly to further increases in fluorination. F_2-Trp gives rise to an EC_{50} of 5.70 ± 0.76 μM, F_3-Trp to 3.27 ± 0.44 μM, and F_4-Trp to 4.56 ± 1.01 μM. Thus, it seems that changes in protonation state do not account for the increased EC_{50} of F_x-Trp. Furthermore, quaternized nicotine does not appear to acquire a cation-π interaction.

Residue	EC_{50} (μM)	SEM	n_H	SEM
Trp	0.77 ± 0.14		1.34	± 0.07
F-Trp	4.23 ± 0.44		1.44	± 0.08
F_2-Trp	5.70 ± 0.76		1.42	± 0.09
F_3-Trp	3.27 ± 0.44		1.33	± 0.07
F_4-Trp	4.56 ± 1.01		1.05	± 0.13

Table 2.3 *N*-methylnicotinium dose-response data for oocytes expressing βγ L9'S nAChR suppressed with the indicated residue at α149.

2.2.4 Noracetylcholine dose-response

A complementary line of experimentation analyzed the behavior of a tertiary analog of ACh. The expectation, strictly on charge-density considerations, is that this agonist should show a steeper slope in the plot of EC_{50} versus cation-π binding ability of α149. However, the data do not conform to this expectation (Table 2.4).

Residue	EC_{50} (μM)	SEM	n_H	SEM
Trp	22.75 ± 6.45		2.62 ± 1.00	
F-Trp	161.03 ± 9.31		1.92 ± 0.26	
F_2-Trp	225.46 ± 27.92		1.62 ± 0.04	
F_3-Trp	326.59 ± 18.16		1.62 ± 0.03	
F_4-Trp	152.24 ± 4.31		1.53 ± 0.03	

Table 2.4 NorACh dose-response data for oocytes expressing βγ L9'S nAChR suppressed with the indicated residue at α149.

Noracetylcholine is vastly inferior to the natural agonist, with an EC_{50} of 22.75 ± 6.45 μM in the βγL9'S receptor. Interestingly, the tertiary analog of ACh shows a trend which is ambiguous as to whether or not it implies a cation-π interaction with α149. The EC_{50} for norACh in receptors containing F-Trp is 161.03 ± 9.31 μM, a sevenfold increase. However, EC_{50} with F_2-Trp at α149 is 225.46 ± 27.92 μM, F_3-Trp is

326.59 ± 18.16 μM, and F_4-Trp is 152.24 ± 4.31 μM. As with nicotine, there is a formal possibility that norACh is being deprotonated in the binding site, although the pK_a of this amine is greater (8.3).[23]

2.2.5 Variation of pH with tertiary ACh

Work by James Petersson in this laboratory has shown that the apparent local pK_a of amine-containing compounds in the muscle receptor binding site differs dramatically from their behavior in bulk solvent.[24] We reasoned that it may be such a distinction which accounts for the marked difference in response to ACh and the very similar compound norACh. To provide an initial test of this hypothesis, the trend of activation by norACh with varying pH was investigated. (Figure 2.3)

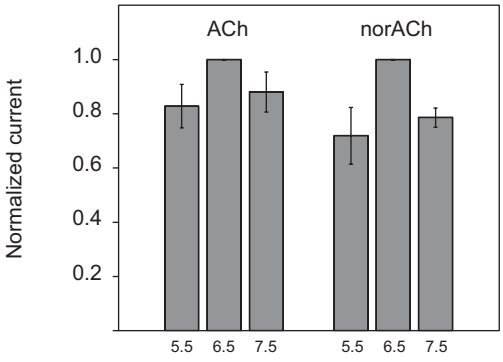

Figure 2.3 ACh and norACh response in αL9'S muscle nAChR measured at varying pH. Mean whole-cell currents were recorded in response to 10 μM ACh and 100 μM norACh, then normalized to the maximal current and are reported as the mean value (±SEM).

The whole-cell current peaked at pH 7.5 for both agonists, and no great difference was observed between the behavior of tertiary and quaternary analogs. It may be that the binding-site environment shields agonists from buffer pH effects, but the lack of overt variation with pH is perhaps suggestive that the potential proton lability of norACh does not account for the difference between its behavior and that of ACh.

2.2.6 TMA dose-response

It also appears that weak agonism does not necessarily correlate with lack of a cation-π interaction with α149, since data for TMA reported by Wenge Zhong show the expected trend for cation-π interactions.[19] Here, the EC_{50} for βδL9'S nAChR is 47.6 ± 1.7 μM, comparable to that of norACh. There is a significant increase with F-Trp, to 155.4 ± 3.5 μM, and additional linear increase to 312.7 ± 8.0 μM for F_2-Trp and 788.6 ± 22.7 μM for F_3-Trp. Thus, the absence of a cation-π interaction between norACh and α149 cannot be explained by the low efficacy of norACh relative to ACh. Nor is it the case that cation-π interactions are only observed with quaternary agonists, as primary and secondary serotonin analogs undergo the interaction with the 5-HT_3 receptor.

2.2.7 Serotonin binding to 5-HT_{3A}R substituted with F_x-Trp series at W183

The position in the 5-HT_{3A}R homologous to α149 in the mouse muscle receptor was substituted with the series of fluorinated Trp analogs. The results for W183 suppression were obtained by Darren Beene and are reported in Table 2.5. As was observed for the nAChR, the other Trp side chain which aligns with the conserved residues of the aromatic box was tested and showed no difference between Trp and F_4-Trp. Thus, it appears that the behavior of residue 183 is unique.

2.2.8 Binding of tertiary and quaternary 5-HT analogs

In an effort to understand whether ammonium centers with differing degrees of alkylation, such as those of nicotine and ACh, interact more or less strongly with aromatic residues, a series of *N*-alkylated serotonin analogs was tested on the 5-HT_{3A}R.

In the usual fashion, the series of fluorinated Trp analogs was incorporated at position 183 and dose-response relations collected. (Table 2.5)

2.2.9 Involvement of hydrogen bonding at W183 investigated

As in the case of the initial studies on the nAChR carried out by Wenge Zhong, we were mindful of the fact that fluorination of the tryptophan side chain changes the hydrogen bond donation ability of the indole nitrogen as well as the electrostatic character of the aromatic portion of the molecule.[1] As before, in order to verify that the observed effects were not due to hydrogen bonding, a series of non-hydrogen bonding analogs of tryptophan with similar calculated cation-π binding energy was tested at position 183 by Darren Beene. The results of these experiments are also reported in Table 2.5.

Residue	EC_{50}±SEM (μM)	Hill coefficient±SEM
5-HT		
Trp	1.21±0.06	2.0±0.16
F-Trp	6.03±0.51	1.4±0.14
F_2-Trp	37.7±2.96	1.9±0.23
F_3-Trp	244±8.4	2.5±0.17
***N*-Me-5-HT**		
Trp	1.82±0.10	2.5±0.13
F-Trp	2.70±0.17	1.9±0.19
F_2-Trp	23.1±2.73	2.6±0.22
F_3-Trp	368±	2.0±0.10
5-HTQ		
Trp	1.07±0.07	2.1±0.25
F-Trp	1.65±0.15	1.65±0.19
F_2-Trp	12.8±0.95	1.8±0.19
F_3-Trp	284±18.7	2.0±0.15
5-HT		
1-Nap-Ala	30.4±1.75	1.6±0.10
2-Nap-Ala	32.0±2.30	1.6±0.12
N-Me-Trp	25.6±1.66	1.8±0.16
Trp 90		
Trp	1.21±0.06	2.0±0.16
F_4-Trp	1.01±0.049	1.6±0.09

Table 2.5 Serotonin and 5-HT analog dose-response data for oocytes expressing $5-HT_{3A}R$ suppressed with the indicated residue at position 183 and, where indicated, 90.

2.2.10 Efficacy

The EC_{50} for a receptor is a composite measurement, comprising multiple elementary steps. Even in the most simplistic two-state model of channel opening, agonist binding to the closed channel is followed by a conformational change to an open channel state. Since the dose-response measurement fails to deconvolute these two steps, experiments were undertaken to determine whether binding or channel gating accounted for the observed alterations in EC_{50} in response to increasing Trp fluorination. The efficacy of a compound on a ligand-gated ion channel is reflected in the maximal current passed at saturating agonist concentration under given electrophysiological conditions.[25,26] Relative efficacies of all nicotinic drugs were determined in ND96 medium in oocytes clamped at a membrane potential of -80 mV at a concentration approximately five times the EC_{50} of the compound. (Figure 2.4)

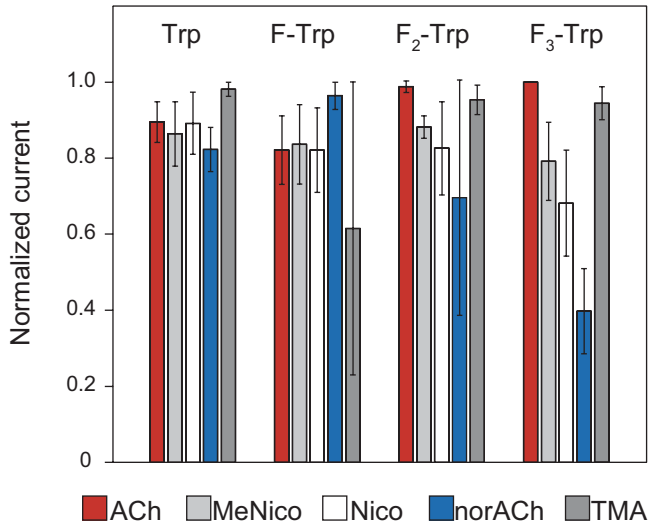

Figure 2.4 Efficacy measurements for oocytes expressing βγ L9'S nAChR suppressed with the indicated residue at α149ACh, in response to saturating concentrations of the indicated agonist. Mean whole-cell currents were obtained and normalized to the maximal signal elicited for each oocyte. Normalized data were averaged and are reported along with SEM. Concentrations of each agonist were ACh, 10 and 100 μM; *N*-Me-nicotinium, 10 and 100 μM; nicotine, 10 and 100 μM; norACh, 100 and 500 μM; and TMA, 250 and 500 μM.

For the nAChR agonists considered here, there was no significant difference in efficacy among them. Nor was the relative efficacy observed to differ in receptors containing fluorinated Trp analogs. There are some small effects, such as the apparent drop in efficacy of TMA with F-Trp and norACh with F_3-Trp, although in both cases the sample size was small and at least one oocyte showed uniform efficacy for all five compounds. Also, the measurements were taken at high concentrations, in order to obtain maximal current. Particularly with fluorinated Trp residues, the potency of certain compounds is sufficiently low that maximally efficacious concentrations begin to overlap with concentrations which induce channel block. Data for TMA and norACh were particularly affected. Additional data were collected at -40 mV, in an attempt to reduce open-channel block by these agonists, although it differed little from that collected at -80 mV.

The process of channel gating is a complicated one and is postulated to involve numerous elementary steps for the nAChR. Thus, it is overly simplistic to conclude from these efficacy experiments that the effects observed are due exclusively to binding.[27] However, the fact that all compounds tested exhibit the same efficacy is somewhat suggestive that the effects we observe are primarily relevant to binding. The ability of these compounds to initiate the conformational changes associated with channel opening is not apparently affected by the presence of variously fluorinated Trp analogs in the binding site. Thus, the large effects that we see on potency probably arise due to effects on agonist binding.

2.2.11 Results from neuronal nAChR

Unlike the muscle-type nAChR, neuronal nicotinic receptors uniformly show higher affinity for nicotine than they do for ACh.[5] It would be quite interesting to know whether these high-affinity nicotine receptors bind nicotine via a cation-π interaction with the Trp149 homolog, which is conserved across all nAChR. However, these receptors proved not to be amenable to unnatural amino acid suppression. Wild-type recovery in the α4β2 receptor was possible, although injection of 25 ng of total mRNA in various subunit ratios gave rise only to several hundred nA of whole-cell current at -80 mV in ND96 under the most optimal circumstances. Fluorinated analogs expressed even more poorly, with less than 100 nA whole-cell current. As a result, dose-response curves could not be collected for α4β2 receptors. Chimeric constructs consisting of the extracellular domain of neuronal nAChR α4, β2, and α7 and the transmembrane domains of the 5-HT_3R have been shown to express better than native nAChR in numerous cell lines.[28-32] These constructs also failed to give substantial currents in wild-type recovery suppression experiments. Work to increase the expression efficiency of neuronal receptors in nonsense suppression experiments in *Xenopus* oocytes is treated in further detail in Section 2.4.

2.3 Discussion

The binding of a neurotransmitter to its receptor is a testament to the organizing power of weak, noncovalent interactions. Determining the impact these low-energy interactions have on a dynamic process such as molecular recognition requires that the analysis, involving physical organic chemistry, be carried out on a functioning integral membrane protein. The technique of introducing synthetic amino acid side chains

through *in vivo* nonsense suppression is one of the few methods available for performing such analyses. In the case of the nicotinic acetylcholine receptor, we have previously proposed a unique role for Trp149 in the alpha subunit in the binding of the natural agonist, acetylcholine.[1] The cation-π binding ability of the side chain at this position was subtly and serially altered by introducing a series of increasingly fluorinated tryptophan derivatives.[33,34] (Figure 2.5)

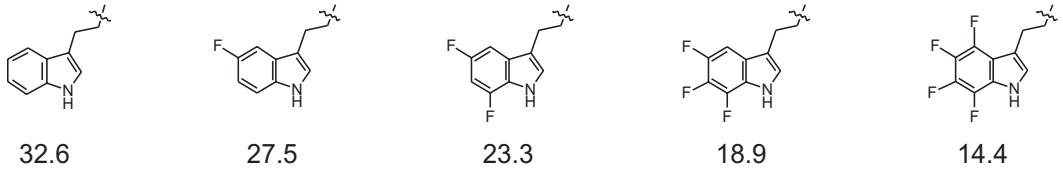

Figure 2.5 The series of fluorinated Trp analogues, with the gas phase cation-π binding energy of fluoroindoles (HF 6-31G**) in kcal/mol.[33,34]

The ability of ACh to trigger receptor opening decreased with decreasing cation-π binding ability of the side chain at this position. From this, we concluded that α149 participated in a direct cation-π interaction with the quaternary ammonium center of ACh. More recent structural work from other labs has confirmed our conclusion and provided much greater detail as to the composition of the binding site.[12] (Figure 2.6 and Figure 2.7)

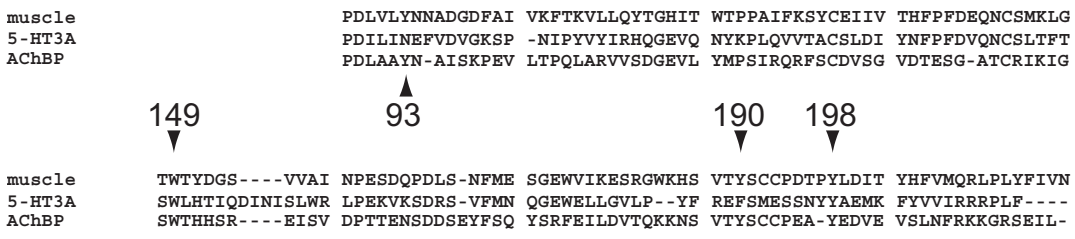

Figure 2.6 Sequence alignment of muscle nAChRα, 5-HT_{3A}R, and AChBP.[12,35,36] The residues which comprise the aromatic box are indicated with arrows, with the exception of the Trp residue contributed by the interfacial subunit, which is conserved among all members of the nAChR receptor family and which is γ55 or δ57 in muscle nAChR.

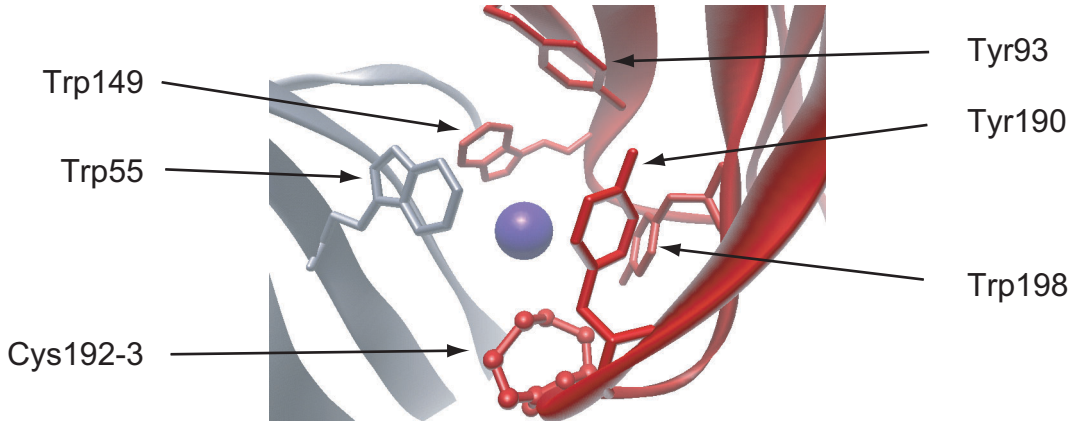

Figure 2.7 Diffraction data from AChBP showing the quaternary ammonium center (blue) of a HEPES molecule from the crystallization buffer bound to the face of Trp143, the homolog of muscle nAChR Trp149 and 5-HT_{3A}R Trp183. The residues of the aromatic box comprising the nAChR active site are numbered according to the nAChR muscle numbering. Trp55 is from the γ subunit.

In the work presented here, we extend this technique to consider the binding of the pharmacologically important nAChR agonist, nicotine. In addition, the approach of altering side chain electrostatics is complemented by modification of the ammonium center of both ACh and nicotine. Finally, related work by Beene on the ligand-gated serotonin receptor, 5-HT_3R, is introduced to support and further the analysis of results obtained on the nAChR.

2.3.1 Anomalous behavior of nicotine

Probing nAChR containing variously fluorinated Trp derivatives with ACh gives a very clear relationship between calculated cation-π binding energy and the measured dose-response.[1] However, this is not true at all with nicotine.[19] As may be appreciated from Figure 2.8, fluorination of Trp149 gives rise to a receptor with diminished responsiveness to nicotine. However, further fluorination does not further impact nicotine's ability to open the channel. Thus, it does not appear that there is a direct electrostatic interaction between the ammonium center of nicotine and Trp149. Nicotine

is a full agonist for the nAChR and would be expected by all conventional pharmacophore models to share roughly the same binding mode as ACh.[37-42]

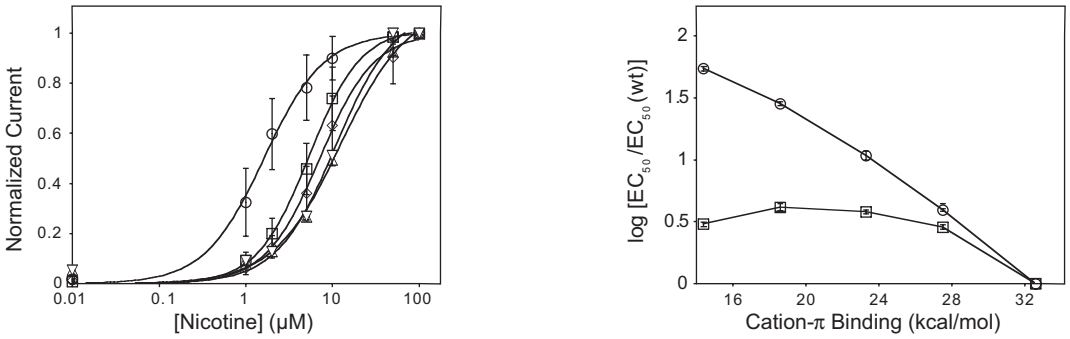

Figure 2.8 Electrophysiological analysis of nicotine. Left panel: Nicotine dose-response relations for βγ L9'S nAChR suppressed with Trp (O), F-Trp (□), F_2-Trp (◊), F_3-Trp (△), and F_4-Trp (▽) at α149. (b) Fluorination plot for ACh (O) and nicotine (□) at the nAChR.

2.3.2 Similarity between ACh and serotonin

The linear response to fluorination seen with ACh is not a property peculiar to the nAChR. The introduction of a series of fluorinated Trp analogs at position 183 of human 5-HT_3R provides clear evidence for a cation-π interaction between this residue and serotonin, as had been suggested by earlier studies from the Lummis laboratory.[43] This interaction appears to be unique to Trp183. Substitution of the fluorinated Trp series at other aromatic residues in the binding site region causes no significant effects. Interestingly, the slope of the plot relating EC_{50} to calculated cation-π binding energy is rather different than for ACh binding to nAChR. Inspection of Figure 2.9 shows that the serotonin slope is markedly steeper. However, the similarity between these two completely different systems is much more striking than the difference, in light of observations on two highly related agonists at the nAChR.

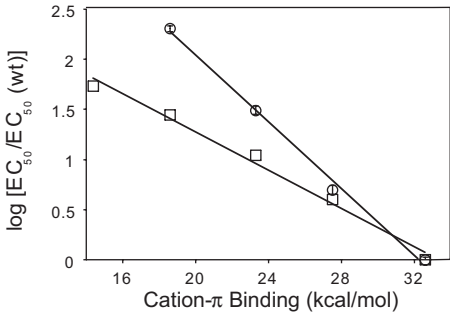

Figure 2.9 Fluorination plots showing dependence of ACh (□) and 5-HT (O) on Trp fluorination at position α149 in βγ L9'S nAChR and 183 in 5-HT_{3A}R. Fluorination plot ($\log[EC_{50}/EC_{50(wt)}]$ versus calculated cation-π binding ability for the series of fluorinated Trp derivatives) for 5-HT data fit the line $y = 5.37 - 0.17x$ and for ACh fit the line $y = 3.2 - 0.096x$. The correlation for both linear fits is $R = 0.99$.

2.3.3 Expected behavior of primary, tertiary, and quaternary ammonium compounds

In comparing ACh, 5-HT, and nicotine, a very evident difference is the nature of the cationic center. ACh contains a quaternary ammonium group, nicotine a tertiary *N*-methyl-pyrrolidinium, and serotonin a primary ammonium. (Figure 2.10) From the standpoint of molecular recognition by aromatic residues, these differences are expected to be significant. The three methyl groups of ACh carry most of the positive charge, and they distribute it relatively diffusely and symmetrically around the nitrogen center. At the opposite extreme, serotonin bears most of the charge of its protonated ammonium on hydrogen atoms close to the nitrogen. The relatively higher charge density of the primary center makes it more attractive to the face of an aromatic amino acid side chain, such as tryptophan. Nicotine occupies a middle ground in terms of cation-π binding ability, but it is important to note as well that the distribution of positive charge around the nitrogen in nicotine is highly asymmetric.

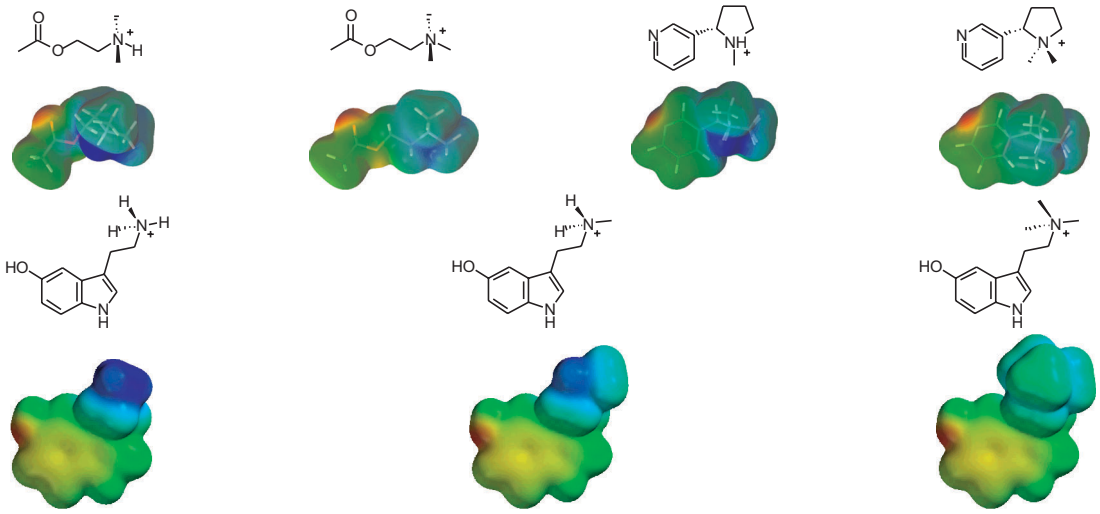

Figure 2.10 Agonists utilized in this study. Top: nAChR agonists with AM1 electrostatic surfaces showing the overall geometrical similarity of the structurally distinct nicotinoid and cholinergic agonists. Bottom: 5-HT_{3A}R agonists, with AM1 electrostatic surfaces showing the varying charge density around the nitrogen center. Electrostatic surfaces were calculated using Spartan and correspond to an energy range of -5 to +160 kcal/mol, where blue is positive and red is negative.

Indeed, all three of these compounds are not modeled at all accurately by considering a spherical distribution of charge, as would be the case for a sodium or potassium atom. As a result, high-level quantum mechanical calculations of the kind performed for fluorinated indoles are not feasible for these cations. The issue of geometry is too important and too difficult to assign to permit any kind of quantitative analysis. However, it is the case that the two molecules which exhibit the hallmark of a cation-π interaction with the Trp homologous to 149 behave as expected from this analysis. In the case of nAChR, the slope of plot of log EC_{50} vs. cation-π binding energy is rather shallow.

Ab initio calculations show that the surface of F_4-Trp is essentially electrostatically neutral.[33,34] Thus, a comparison of F_4-Trp and Trp provides a measure of the *electrostatic component* of the cation-π interaction. The F_4-Trp/Trp ratio reflects the energy cost of removing the attractive electrostatics but maintaining the residue, as if the Trp were

replaced by a hydrophobic residue of the same shape. This new residue maintains most van der Waals and dispersion interactions but cannot experience a cation-interaction. For ACh, the F_4-Trp/Trp ratio is 54. For serotonin, the F_4-Trp EC_{50} value is obtained by extrapolation of the line in Figure 2.9, which leads to a F_4-Trp/Trp ratio of 836. If these are viewed as ratios of binding constants, then the implied energetics of a cation-π interaction are 2.4 and 4.0 kcal/mol, respectively, for ACh and serotonin. These are consistent with other estimates of the magnitude of the cation-π interaction[10] Based on these calculations, it would appear that the primary cation interacts more strongly with the face of tryptophan.

2.3.4 Experimental behavior of primary and substituted ammonium compounds

Examination of the results for a series of substituted serotonin analogs shows that this simple explanation does not do justice to the complexity of the molecular recognition problem. An *N*-trimethyl version of serotonin has a very similar charge distribution to that seen for ACh. However, Figure 2.11 shows clearly that the slope for this compound is more similar to that of serotonin than that of ACh. Indeed, a secondary analog of serotonin behaves even more like the quaternary version than it does like 5-HT, thus ruling out the hypothesis that slope of this plot reports in a simple way on the strength of the interaction. However, all three of these compounds follow the general trend that we associate with an electrostatic interaction with Trp183. As electron density is withdrawn from the face of the aromatic side chain, the drugs are less and less effective agonists. The EC_{50} rises, in fact, in a fairly regular way with decreasing cation-π binding ability of the aromatic.

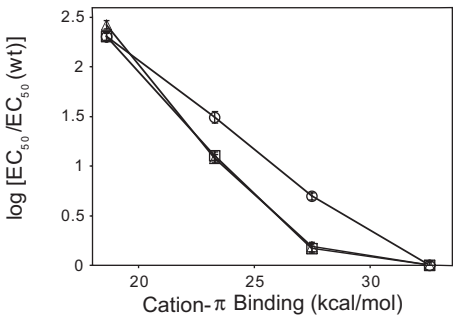

Figure 2.11 Fluorination plots for N-alkylated serotonin analogs showing variation in dependence on Trp fluorination at 5-HT_{3A}R position 183. Agonists are indicated by 5-HT (O), *N*-Me-5-HT ( ), and 5-HTQ (△).

At first glance, these data appear mutually incompatible. On the one hand, EC_{50} can be tuned by varying the attractiveness of the aromatic side chain to the cation. On the other hand, varying the cation-π binding ability of the other partner, the cation, shows no such trend. We interpret this to mean that comparing a series of fluorinated analogs for a given agonist represents the impact of changing electrostatics on a given binding mode, namely, one where the cation is brought within van der Waals contact with the Trp analog. Predictable alteration of the energetics of this interaction gives rise to a predictable trend in EC_{50}. When considering different agonists, however, the comparison is potentially negated by the fact that the binding modes may be different. The distance of the cation from the aromatic face may be different; the geometry may vary, since the highest region of local charge density is probably pointing toward the face of the aromatic; the energetic contribution of other kinds of interactions with other parts of the molecule may differ; and the ability of different agonists to gate the channel may contribute.

2.3.5 Potential acidity of protonated nicotine

Additionally, there is the interesting fact that serotonin analogs differ in a fundamental way from what we have seen with nicotine and ACh. While all the 5-HT analogs show signs of an electrostatic interaction with Trp183, nicotine apparently does not interact in this way with Trp149. Having learned from the 5-HT_3R that cation-π binding ability of the agonist is not a good predictor of dose-response change with increasing fluorination, we considered another hypothesis for nicotine, namely the possibility of deprotonation. Presumably, deprotonation would render the compound unable to bind at all, since no neutral agonists of ligand-gated channels are known. This is a special concern for nicotine, as the pK_a of the pyrrole is decreased to 7.8, almost physiological pH, due to the inductive effect of the pyridyl ring. It is a possibility that the microenvironment of the binding site is such that it buffers the nicotine. This could explain why there is an apparent leveling in the EC_{50} response to increasing fluorination. Rather than reflecting an electrostatic interaction between agonist and receptor, it could be that the assay is reporting on changes in active site basicity as a result of incorporating fluorinated indole side chains. To test this hypothesis, a quaternary derivative of nicotine was analyzed.

2.3.6 Behavior of tertiary and quaternary nAChR agonists

As is readily evident from Figure 2.12, nicotine deprotonation is unable to explain the line shape seen in the plot of log EC_{50} versus cation-π binding ability. *N*-methyl-nicotinium is incapable of being deprotonated, but it gives very similar results to nicotine itself. Certainly, there is no regular increase in EC_{50} with increasing fluorination that characterizes a direct electrostatic interaction with Trp149.

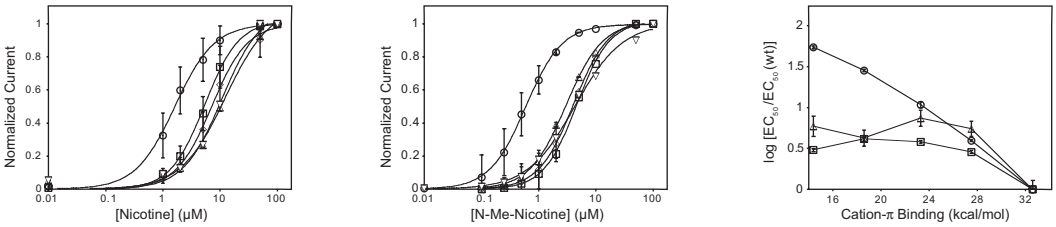

Figure 2.12 Electrophysiological analysis of nicotine and its quaternary analog. Left panel: Nicotine dose-response relations for βγ L9'S nAChR suppressed at α149 with Trp (O), F–Trp (□), F_2-Trp (◊), F_3-Trp (△), and F_4-Trp (▽). Center panel: Dose-response relations for *N*-Me-nicotinium for βγ L9'S receptors suppressed with Trp (O), F–Trp (□), F_2-Trp (◊), F_3-Trp (△), and F_4-Trp (▽) at α149. Right panel: Plot of log [$EC_{50}/EC_{50(wt)}$] for ACh (O), nicotine (□), and *N*-Me-nicotine (△) at the nAChR versus the calculated cation-π binding energy of the series of fluorinated Trp derivatives.

Indeed, nicotine does not experience such an interaction with any of the aromatic amino acids comprising the binding site, as inferred from the AChBP crystal structure. Figure 2.2 shows that substitution of γ55/δ57 with Trp analogs of radically different electrostatic character gives very little difference in EC_{50}. Additionally, earlier studies carried out on Tyr93 and Tyr198 do not show shifts characteristic of nicotine-tyrosine cation-π interactions.[16] Substitution of Tyr190 with even very modestly different unnatural analogs proved impossible, however, so we are unable to rule out the possibility that nicotine interacts with this residue.

Where does this leave us as far as comparing the means of molecular recognition in the two receptors? The expectation for 5-HT_3R was that modulation of the charge density of the cationic center would track with the slope of log EC_{50} versus cation-π binding energy. It stands to reason that the more energetic the interaction between cation and aromatic, the more binding would depend on it. In the simplest case of gas-phase binding of ions to a series of fluorinated Trp's, the slope for Li^+ would be greater than Na^+, which would be greater than K^+, and so on.[10] Clearly, the situation in the binding site is more complicated than this.

Where alkali metal ions are approximately spherical, the charge density of serotonin analogs is highly anisotropic. In fact, shape selection is usually considered to be extremely important in the binding of small molecules in hydrophobic protein active sites.[44] The 5-HT_3R has evolved to bind serotonin, which is a primary amine. Even though 5-HTQ binds and gates with channel with identical potency and efficacy to 5-HT, it is safe to assume that the binding site is optimized for the smaller serotonin cation. The fluoro-Trp-based assay may, in fact, be reporting on extremely subtle differences in positioning, as the electrostatic interaction between cation and π system is strongly distance-dependent. In the case where the natural agonists are being compared, as in 5–HT with 5-HT_3R and ACh with nAChR, it may well be the case that the comparison is significant. Here, the systems are comparable, in that the binding site has been optimized for best fit. The implication that the productive binding mode for 5-HT is more dependent on the electrostatics of Trp183 than is ACh on Trp149 may well be taken to mean that non-cationic interactions with the receptor play a greater role in nAChR.

This interpretation is in some ways consistent with what was observed for TMA by Wenge Zhong.[19] This very simple cation is an agonist of nAChR, but with very low potency. Of all agonists tested, in fact, its potency is the lowest. However, it exhibits a cation-π interaction with Trp149. (Figure 2.13) In other words, productive binding of TMA involves the quaternary ammonium group nestled up against the face of Trp149. From the perspective of the aromatic box, when TMA gets this close, it is quite similar to ACh. The acetyl component of ACh doesn't have room to fit in the box, and probably extends out of the box altogether during productive binding. If TMA looks so similar to ACh at its ammonium head group, then, is it safe to conclude that the additional potency

of ACh comes from interactions between the acetyl group and another part of the binding site? It certainly seems so. This is also in accord with what is observed for nicotine and its *N*-methylated derivative.

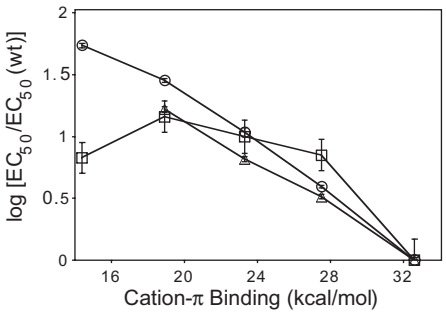

Figure 2.13 Plot of log [$EC_{50}/EC_{50\ (wt)}$] for ACh (O), norACh ( ), and TMA (△) at the nAChR versus the calculated cation-π binding energy of the series of fluorinated Trp derivatives.

Like TMA, these compounds are significantly less potent than ACh. But unlike TMA, they do not appear to come quite so close to the aromatics of the box during their productive binding mode. Indeed, no cation-π interaction is detected with any part of the aromatic box. Nonetheless, the compounds are reasonably efficacious. The conclusion is that the channel can be opened by compounds relying on interactions outside of the aromatic box. The most surprising result of all, *a priori*, is probably the behavior of norACh. (Figure 2.13) The backbone of this compound is identical to ACh. Any non-cationic interaction available to ACh should be equally available to norACh. Indeed, the cationic center of norACh is an even better cation-π binder than the quaternary ammonium of ACh. However, norACh is an agonist of amazingly low potency. It is tempting to conclude that the aromatic box of the nicotinic receptor has evolved to accommodate a quaternary ammonium, and anything smaller is rejected. Until a tertiary compound is discovered which displays an unequivocal cation-π interaction, this argument may even be maintained.

However, it is important to note that nicotine certainly opens the channel without apparently coming in van der Waals contact with the aromatic box. And productive binding is primarily what one is interested in, as far as understanding channel function. The neuronal receptors, for which nicotine is a far more potent agonist than the muscle receptor, will present a very interesting system for study. It is tempting to speculate that these receptors contain aromatic boxes which are more accommodating of nicotine's pyrrolidinium cation and allow it to behave like ACh in all respects. It is also the case that there are hundreds of interesting nicotinic agonists which remain unstudied by this method, including the secondary amine epibatidine. It is highly likely that high-resolution structural data of AChBP may be able to shed further light on the varieties of agonist binding modes.

2.3.7 Conclusions

In conclusion, we have learned several things from these studies. First of all, it is clear that 5-HT experiences a unique cation-π interaction with Trp183. Furthermore, the binding site of 5-HT_3R is such that it can accommodate significant increases in bulk around the ammonium center. Even the quaternary analog retains a direct electrostatic interaction with Trp183 and is an effective agonist for the channel. Second, we have shown that nicotine differs in a dramatic way from ACh in its reliance on direct electrostatic interaction with nAChR Trp149. This finding may prove to be relevant for future generations of nicotinoid drugs. Finally, we have determined that the fluorinated Trp series works well as a general technique. The differences in slope between the EC_{50} vs. cation-π binding energy plots of ACh and serotonin that it reveals may reflect interesting differences in how molecular recognition of neurotransmitters by their

receptors is effected. It remains unwise to generalize too much about the nature of molecular recognition of neurotransmitters by their receptors. The amount of structural information is still too limited. However, elucidation of the atomic-level details of these interactions continues, and the importance of these molecules to biology is so great that we are optimistic that answers will be forthcoming.

2.4 Attempts to introduce unnatural amino acids into neuronal nAChR

2.4.1 Motivation

As indicated above, any serious study of nicotine and its analogs should most properly be carried out on the receptors on which these compounds act. In animals, these receptors are neuronal nAChR.[5,7,8,45] Mice in which either the α4 or β2 nAChR subunits have been genetically knocked out show severely diminished self-administration of nicotine, suggesting that these receptors play a substantive role in the physiological effects of nicotine.[46,47] Additionally, binding studies on brain slices from rats have shown that the majority of nicotine binding in the brain is accounted for by α4β2 and α7 receptors.[48,49]

2.4.2 Expression of α4β2 in oocytes

Literature reports on the expression of α4β2 in oocytes present a variety of EC_{50} values for these receptors.[50-53] Frequently, these differences are attributed to heterogeneity of subunit stoichiometry. This heterogeneity is expected to be a difficult variable to control in a suppression experiment, where the amount of suppressed subunit is difficult to control or predict. In order to assess the behavior of α4β2 receptors in

oocytes, wild-type receptors were expressed prior to the initiation of suppression experiments.

Both α4 and β2 from rat were available in the pAMV subunit, from earlier work in the laboratory by Mark Nowak. In addition to these subunits, mutants containing α L9'S were obtained and expressed. Initially, these receptors gave rather inconsistent results, particularly with regard to dose-response relations. However, it was discovered that changing to pH 6.5 gave much more consistent, and apparently normal behavior. An EC_{50} of 0.99 μM was obtained for ACh from the wild-type receptor, in accord with most published reports.[50-53] (Figure 2.14) The Hill coefficient for this experiment, 0.80, was also in the range of typically reported values.[50-53]

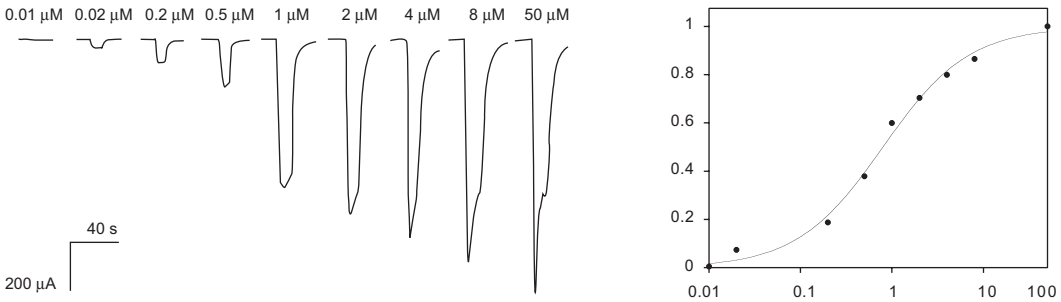

Figure 2.14 ACh dose-response for wild-type rat α4β2 nAChR. Left panel: Individual traces from two-electrode voltage clamp of oocytes treated with the indicated ACh concentrations. Right panel: Dose-response curve for a single oocyte, plotting normalized ACh response against log [ACh] and fitted to the Hill equation.

Because of the presumed stoichiometry of two alpha subunits and three beta subunits, the use of βL9'S subunits was expected to give receptors with a dramatically shifted EC_{50}, so α 9' mutants were used instead. Unfortunately, these receptors proved troublesome to characterize, because of frequent ill effects on oocyte health.

Initial studies attempting to introduce Trp at position α184, homologous to α149 of the muscle receptor, produced absolutely minimal measurable response. Currents were

notably higher for suppression of alpha9' subunits, although these receptors proved difficult to work with, as mentioned above. As the need for optimization became clear, human α4 and β2 subunits were obtained, on the grounds that work on the human receptor would have more direct relevance to the clinical pharmacology of nicotine. Here, the wild-type receptors were obtained from Jon Lindstrom's laboratory in the pSP64 vector. The overall level of expression of both human and rat α4β2 nAChR was noticeably less than that of the mouse muscle receptor, but whole-cell currents of 3-5 μA were routinely obtained.

2.4.3 Initial attempts at wild-type recovery by nonsense suppression

As in the rat receptor, the human α4 W182TAG mutation corresponding to muscle α149TAG was made. Attempts to recover wild-type activity by suppressing with tRNA-Trp were disappointing. The maximum whole-cell currents obtained were on the order of 50 nA, with median values in the range of 20 nA. Co-injection of TAG-containing subunits with wild-type subunits in the absence of suppressor tRNA was performed to test for dominant-negative effects, with no evidence of such an effect. The other residues corresponding the aromatic box of the AChBP were altered to *amber* stop codons and suppressed with Trp. It was observed that the best suppression efficiency was obtained at α182. After many months of optimization, sufficient currents were achieved to collect a dose-response curve for suppressed hα4β2 nAChR. (Figure 2.15) This experiment gave an EC_{50} value of 0.6 ± 0.1 μM, with a Hill coefficient of 1.2 ± 0.1.

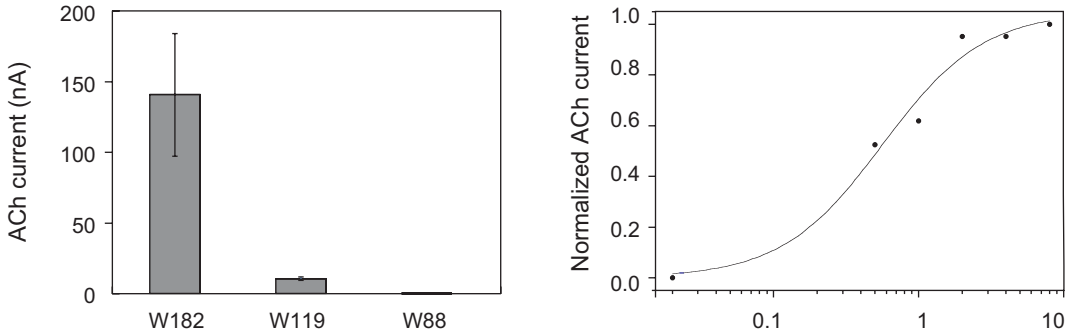

Figure 2.15 Trp suppression of hα4β2 at the indicated position in the alpha subunit. Left panel: Mean whole-cell current (±SEM) in response to 20 μM ACh from oocytes expressing suppressed α4β2 nAChR. Right panel: ACh dose-response curve from a single oocyte suppressed with Trp at position hα4-182. In all cases, 30 ng total mRNA (50:1 hα4-W182TAG:β2) was injected, and recordings made 48 hr post-injection in ND96, pH 6.5.

However, such expression levels were not typical, and even these whole-cell currents were barely adequate for obtaining dose-response relations. It appeared that poor suppression efficiency was characteristic of α4β2 nAChR. Accordingly, a broad-based program to boost expression was undertaken.

2.4.4 Increasing translational efficiency

2.4.4.1 Use of vectors optimized for oocyte expression

One possible reason for low expression is that the suppressed subunits are not being efficiently translated. Given the importance of heterologous expression in *Xenopus* oocytes to ion channel biology, a number of expression vectors have been developed and optimized for expression in this system. A vector developed in the Lester laboratory, pAMV, has typically given good results. This vector contains a 3' UTR from alfalfa mosaic virus, which is thought to confer upon the mRNA the ability to bind relatively well to free ribosomes, thus providing a competitive advantage over endogenous mRNA.[54,55] Another common strategy for vector design has been to flank the desired gene with 5' and 3' UTR from a highly expressed gene, such as β-globin.[56] A vector

containing a multiple-cloning site surrounded by *Xenopus* β-globin UTR was obtained, along with several others which have been reported to produce high levels of expression in oocytes.

Unfortunately, two of these vectors (pBSTAII and pNKS)[56,57] proved difficult to clone the hα4 and hβ2 subunits into, and another gave no expression at all (pSGEM).[58] The complete lack of expression with pSGEM gave reason to believe that the latter constructs were faulty, although restriction digestion and sequencing of the gene region appeared normal. Some favorable results were obtained with pAMV, particularly where expression was measured two days after injection. (Figure 2.16)

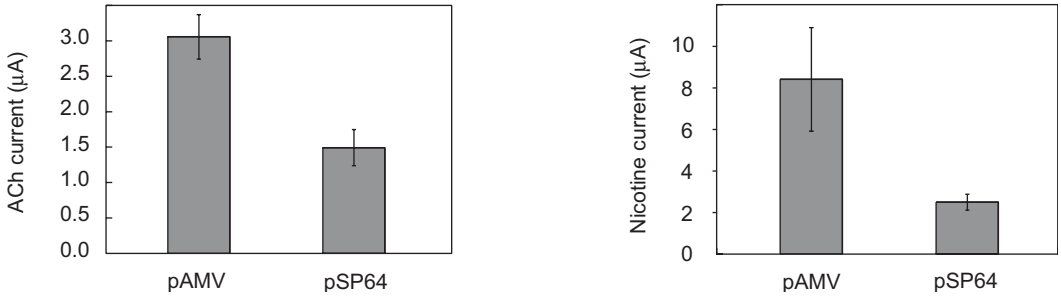

Figure 2.16 Comparison of pAMV and pSP64 vectors for wild-type hα4β2 expression. Left panel: Mean whole-cell currents (±SEM) in response to 20 μM ACh. Right panel: Mean whole-cell currents (±SEM) in response to 20 mM nicotine. In all cases, 27.5 ng total mRNA (10:1 α4:β2) were injected. Recordings were made 48 hr subsequent to injection, at pH 6.5.

Whether or not this advantage is germane to suppression experiments remains to be tested.

2.4.4.2 Overexpression of elongation factors

Another strategy which may increase translation is to boost the level of proteins associated with translation. One translation factor which is considered a promising candidate for such up regulation is EF-1α.[59] This elongation factor binds to aminoacylated tRNA. There is some evidence suggesting that this binding stabilizes the

charged tRNA toward hydrolysis, which would be desirable.[60] In addition, it is the ternary complex of EF-1α, GTP, and aminoacyl tRNA which binds to the A site of the ribosome in translation.[61,62] The oocyte isoform of *Xenopus* EF-1α has been cloned, but repeated requests for these constructs were ignored.[63,64] Adult *Xenopus* EF-1α was available, as the control RNA in the Ambion mMagic mMessage kit routinely used in the laboratory to produce mRNA *in vitro*, and was also obtained from Paul Krieg.[65] The two isoforms are quite similar, so experiments were carried out with the adult isoform.

In a typical experiment, mRNA coding for EF-1α was injected 24 hours prior to the injection of oocytes with nAChR mRNA. Co-injection was also attempted, as well as injection at a variety of intervals prior to nAChR mRNA injection. Both wild-type and suppressed receptors were examined. In no case was a significant difference observed relative to control oocytes.

2.4.5 Promoting folding, assembly, and transport to the plasma membrane

2.4.5.1 Use of epitope tags as a diagnostic

In addition to possible translational inefficiency, it may be that poor expression results from compromised folding of suppressed subunits, assembly of subunits into functional receptors, or transport of receptors to the plasma membrane. Whether folding and assembly or trafficking is the primary problem may be addressed by biochemical analysis. Synthesis of receptor subunits may be detected through Western blotting, a technique which is treated in much greater depth in Chapter 3. In brief, a crude protein isolate from oocytes expressing the desired receptor is prepared and subject to gel electrophoresis. The proteins are thus separated by size. They may be transferred to

nitrocellulose, which is probed by antibodies. The use of antibodies which specifically recognize an antigenic determinant introduced in an epitope tag results in specific labeling of the protein containing the epitope tag. This technique is of value here, because membrane preparations from the plasma membrane of the cell may be compared to those from the cytoplasm. If receptors are being synthesized but improperly trafficked, this will be evident from staining of cellular membranes but not those from the plasma membrane.

The HA epitope tag was introduced into the hα4 subunit, in two places, a region in the M3-M4 loop previously determined not to affect expression of the muscle-type receptor, and at the extreme C-terminus of the subunit. Whole-cell currents from these two constructs were compared to those of oocytes expressing wild-type α4β2. While current was almost completely eliminated in the C-terminal receptor, only a modest diminution was observed for the M3-M4 HA tag. These results were corroborated by Western blots, both with protein produced *in vitro* and from the plasma membrane of oocytes expressing the two different constructs.

Whether or not the HA tag will prove to be a useful diagnostic in following trafficking of suppressed receptors awaits introduction of the epitope tag into TAG-containing subunits.

2.4.5.2 Co-expression of dominant-negative dynamin

The presence of receptors on the cell surface is the result of a dynamic equilibrium between forward trafficking from the ER and removal from the membrane by endocytosis. A dominant-negative dynamin mutant is available which greatly reduces clathrin-mediated endocytosis.[66,67] In certain cases, disruption of dynamin activity in

Xenopus oocytes has been reported to increase ion channel expression severalfold.[68,69] In experiments with α4β2, no increase was observed through co-injection with dominant-negative dynamin, nor was suppression efficiency improved.

2.4.5.3 Overproduction of BiP

The folding of membrane proteins is thought to be assisted by a number of ER-resident chaperones. Probably the best-characterized is BiP, a soluble protein present in the ER lumen. This protein has been expressed in *Xenopus* oocytes by the laboratory of Käthi Geering.[70] The construct was obtained from her laboratory, and experiments similar to those reported above for EF-1α were carried out. As with the elongation factor experiments, co-expression of wild-type and W182-suppressed hα4β2 nAChR with BiP appeared to have little effect.

2.4.5.4 FAYENE insertion

A study on expressing potassium channels in oocytes has suggested that the sequence FCYENE is a forward-trafficking signal for these channels, which increased expression four- to fivefold in heterologous expression in *Xenopus* oocytes.[71] The report also suggested that transferring this sequence to other channels had a similar effect, and that the sequence FAYENE was likewise effective. In order to avoid any complications associated with introducing a cysteine residue, the sequence FAYENE was introduced into hα4 in the same M3-M4 position which had proven successful for the introduction of the HA epitope. Comparison of these modified receptors with wild-type hα4 revealed no apparent benefit of this sequence on whole-cell expression levels.

2.4.6 Alternative strategies for increasing expression

2.4.6.1 Chimeric receptors

An altogether different strategy for circumventing the expression problems of α4β2 is the use of chimeric subunits. The increased expression of 5-HT_3R relative to α7 nAChR has been traced to its transmembrane regions.[72] The discovery by Changeux that a chimera between the extracellular domain of α7 and the TM domains of 5-HT_{3A}R shows the binding properties of the α7 AChR raises the possibility that binding-site studies could be carried out on chimeric receptors.[29] The α4/5-HT_3 and β2/5-HT_3 chimeras have been generated in the laboratory of Neil Millar and have been reported to assemble, although no functional studies have yet been carried out.[31,32] Nonetheless, these constructs were obtained and injected. A 1:1 mRNA ratio was initially employed, as the stoichiometry of this chimera between a heteromeric and homomeric receptors is difficult to predict. This initial experiment gave no observable whole-cell ACh current, nor did any variation of the relative amounts of mRNA improve upon this result. It may be the case that these chimeras are simply non-functional. No binding studies were undertaken, as the ultimate purpose of the experiment was to obtain functional data.

2.4.6.2 Multiple injection

A conceptually simple and usually effective method for increasing expression in *in vivo* nonsense suppression is to multiply inject oocytes, typically at 24-hour intervals. It was this technique coupled with the use of the pAMV vector which gave the best suppression results to date in α4β2 nAChR. (Figure 2.17)

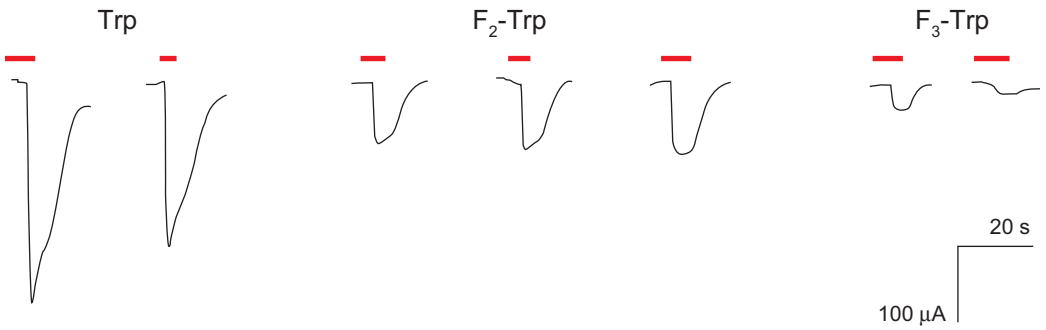

Figure 2.17 Individual traces from two-electrode voltage clamp of oocytes expressing hα4β2 suppressed with the indicated residue at position 182 of the α4 subunit. Oocytes were double-injected (t = 0, and t = 24 hr) with 25 ng total mRNA (1:1 α4:β2) and recorded from 48 hrs after the initial injection. Currents are in response to 50 μM ACh, and red bars indicate the duration of its application.

These whole-cell currents are of sufficient magnitude that dose-response curves could be measured. Disappointingly, however, currents this large were unable to be obtained for any fluorinated Trp residue, precluding the desired characterization of cation-π interactions in neuronal nAChR.

2.4.7 Conventional mutagenesis experiments

A final experiment was undertaken to attempt to shed light on the differing modes of nicotine and ACh binding between muscle and neuronal receptors. The affinity of the muscle-type receptor for ACh is significantly greater than its affinity for nicotine, as noted above. For all neuronal receptors tested, this affinity is reversed.[50-53] In addition, the muscle alpha subunit is alone among all discovered nAChR subunits in having an arginine residue at the 55 position. Every other subunit contains a tryptophan at this position. Even though our results above do not indicate a special relationship between γ55/δ57 and nicotine in the muscle receptor, the photoaffinity experiments of Cohen are suggestive of such a relationship.[20] As a result, this residue was targeted for alteration by

site-directed mutagenesis, and the relative potency of ACh and nicotine were tested on the resulting mutants.

In the muscle receptor, an αR55W mutation was made and in hα4, W88R. The whole-cell currents in response to a variety of ACh and nicotine concentrations were measured, in hopes of observing an alteration of the usual pattern of ACh and nicotine potency. (Figure 2.18) The potency difference between ACh and nicotine at the muscle receptor may be seen from the behavior of the wild-type receptor in response to three concentrations of each agonist, 1 μM, 10 μM, and 100 μM. The αR55W mutant seems to have diminished ACh affinity, but without a corresponding increase in that of nicotine.

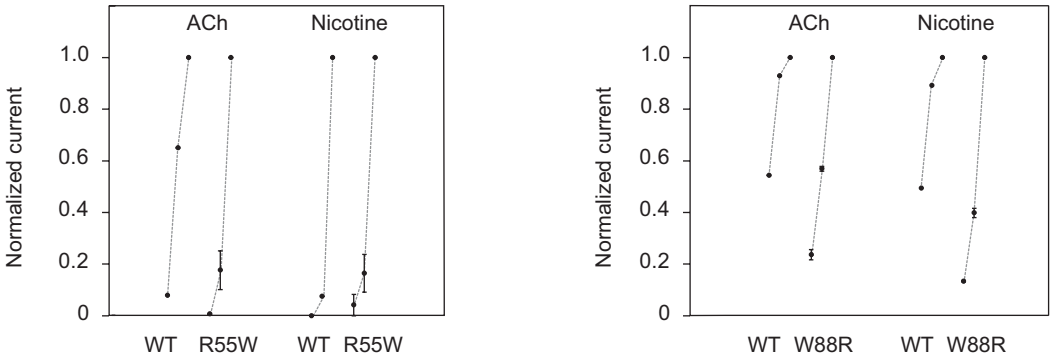

Figure 2.18 Conventional mutagenesis of the position homologous to α55 in muscle nAChR in muscle (R55W) and hα4β2 (W88R). Whole-cell currents in response to 1, 10, and 100 μM ACh and nicotine, as indicated, are shown after normalization to the response to 100 μM agonist. In cases where multiple experiments were performed, SEM is indicated. Dotted line is a guide only, not a fitting of the data. Left panel: Comparison of wild-type and αR55W muscle nAChR response to ACh and nicotine. Right panel: Responses of wild-type and W88R hα4β2 to ACh and nicotine.

The responses of wild-type hα4β2 to both ACh and nicotine were almost identical. Likewise, the response of the mutant W88R receptors to both agonists is very similar. For both, the apparent effectiveness has been decreased in the mutant receptor, but without the predicted switch in potency. It is possible that detailed dose-response studies of these mutants may reveal some interesting trends. This initial study utilized only three

concentrations of agonist, and concentrations that lie in very different regions of the dose-response curve for ACh and nicotine, both of which may mask small effects on potency. However, no dramatic reversal of ACh and nicotine affinities was observed, suggesting that the identity of this residue is not determinative of relative affinity for ACh and nicotine.

2.4.8 Future directions

In order to precisely establish the role of cation-π interactions in agonist binding to neuronal receptors, it is necessary to develop relatively robust methodology for introducing unnatural amino acids. Thus far, the usual methodology applied successfully to so many other receptors in this laboratory has failed to yield sufficiently large whole-cell currents to obtain the necessary dose-response relations for α4β2 nAChR. Through the use of the pAMV vector and multiple injections, useful currents can relatively reproducibly be obtained for suppression of α182 with Trp. Attempts to extend to fluorinated Trp derivative have thus far been unsuccessful. A number of directions could be pursued to perhaps achieve this goal.

First, recent results from the work of Nivalda Rodrigues-Pinguet and Bruce Cohen in the Lester laboratory suggest that a threefold increase in whole-cell current from α4β2-expressing oocytes may be achieved by potentiation with 3 mM Ca^{2+}. Although careful controls would be required to verify that this potentiation is not accompanied by any alteration in agonist affinity, this may be a simple and useful means to obtain usable currents via nonsense suppression. Second, there is reason to believe that the four-base suppression methodology of Sisido *et al*. may give greater suppression efficiency than *amber* suppression.[73] Indeed, generation of the requisite constructs and tRNA's with

four-base anticodons was planned and undertaken, but difficulties in preparing them prevented this methodology from being tested. Third, there is the possibility that alpha7 nAChR, also thought to be an important pharmacological target for nicotine, may be more amenable to nonsense suppression in oocytes. Hong Dang, in the Lester laboratory, has made the TAG mutant homologous to Trp149 in the chimeric construct rα7V201/r5-HT_3-AMV. However, somewhat contrary to expectation, this construct expressed very poorly in his hands. In addition, we have the 'WT' version of this construct as well as rα7 and cα7, both in the pAMV vector. Because of our success with suppression in homomeric 5-HT_3, there is perhaps reason to be optimistic that suppression will work equally well in α7. In addition, there is an interesting observation in the literature that cocaine (a tertiary amine) is not an agonist of α7, while the quaternary cocaine methiodide is a rather good agonist.[74]

In general, identification of the molecular details which account for the difference in potency between nicotine and ACh for muscle and neuronal nAChR is an interesting question. The conclusions from the fluorinated Trp study on the muscle receptor could be augmented by studies on neuronal receptors that do not rely on nonsense suppression. For instance, despite the similarity noted above in the muscle-type receptor's response to nicotine and the perpetually charged *N*-methyl-nicotinium analog, it may be the case that neuronal receptors respond differently to these agonists. In addition to pharmacological studies of this nature, there is the possibility that comparison of the sequence similarities and differences among AChBP, muscle receptors, and neuronal nAChR may provide a guide for future experimentation.

2.5 Experimental methods

2.5.1 Electrophysiology

Stage VI oocytes of *Xenopus laevis* were harvested according to procedures approved by the Institute. Recordings were made 24-72 hours post-injection in standard two-electrode voltage clamp mode. Oocytes were perfused in calcium-free ND96 solution, as previously reported.[1] Nicotinic agonists were either synthesized as described earlier (N-methyl-nicotinium),[22] purchased from Sigma/Adrich/RBI ([-]-nicotine tartrate) or Acros Organics (the tertiary ACh analog, 2-dimethyl aminoethyl acetate). Serotonin and its analogs were purchased from Sigma/Adrich/RBI. All drugs were prepared in sterile ddi water for dilution into calcium-free ND96. Dose-response data were obtained for a minimum of eight concentrations of agonists for a minimum of three different cells. Curves were fit to the Hill equation to determine EC_{50} and Hill coefficient.

2.5.2 Unnatural amino acid suppression in muscle nAChR and 5-HT_{3A}R

Synthetic amino acids were conjugated to the dinucleotide dCA and ligated to truncated 74 nt tRNA as described.[75] Deprotection of charged tRNA was carried out by photolysis immediately prior to co-injection with mRNA, in the manner described.[1,76] Typically, 25 ng tRNA were injected per oocyte along with mRNA in a total volume of 50 nL per cell. mRNA was prepared by *in vitro* runoff transcription using the Ambion mMagic mMessage kit. Mutation to insert the *amber* stop codon at the site of interest was carried out by standard means and was verified by sequencing through both strands. For nAChR suppression, a total of 4.0 ng of mRNA was injected in the subunit ratio of 10:1:1:1 α:β:γ:δ. In many cases, non-α subunits contained a L9'S mutation, as discussed

below. Mouse muscle embryonic nAChR in the pAMV vector was used, as reported previously. For suppression in homomeric 5-HT_3R, 5 ng of mRNA were injected. Experiments involving heteromeric 5-HT_{3A} and 5-HT_{3B} subunits employed a total of 4.0 ng of mRNA in the subunit ratio of 10:1A:B.[77] Mouse 5–HT_{3A}R was used in all cases, in the pAMV vector. Negative and positive controls for suppression were performed in the following way. As a negative control, truncated 74 nt tRNA or truncated tRNA ligated to dCA were co-injected with mRNA in the same manner as fully charged tRNA. At the positions studied here, no current was ever observed from these negative controls. The positive control involved wild-type recovery by co-injection with 74 nt tRNA ligated to dCA-Trp. In all cases, the dose-response was indistinguishable from injection of wild-type mRNA alone.

2.5.3 Molecular biology of α4β2

In the course of attempting to introduce unnatural amino acids into α4β2 nAChR, numerous constructs were made and obtained. They are listed in Table 2.6. All pSP constructs were linearized with *AseI* and then transcribed using the mMagic mMessage SP6 kit. pAMV constructs relied upon *NotI*/T7, in the usual fashion. The pSGEM constructs we made gave no expression at all. Additionally, testing the integrity of individual subunits by co-injection with partners of known integrity (pSGEM-α4 + pAMV-β2 and pAMV-α4 + pSGEM-β2) failed to result in expression. Sequencing of the region of sub-cloning appeared normal. The *SfiI*-linearized pSGEM DNA gave the appropriate UV spectrum. The mRNA produced by the T7 kit was analyzed by agarose gel electrophoresis and appeared very similar in size to α4 and β2 transcribed from pSP

and pAMV constructs. Nonetheless, it is likely that these constructs were faulty in some way. In all of the above experiments, mRNA amounts were not well controlled. The quantities injected were estimated by comparing mRNA band intensity on agarose gels to that of pSP-α4 and pSP-β2 mRNA, and then diluting to give similar band intensities, but this is a rather rough measure.

Construct	Comments	Source
pSP64-hα4		Jon Lindstrom
pSP64-hα5		Jon Lindstrom
pSP64-hβ2		Jon Lindstrom
pAMV-hα4		GSB/LJT
pAMV-hβ2		GSB/LJT
pSP64-hα4/M3-M4HA	contains HA epitope	GSB/LJT
pSP64-hα4/CTHA	contains HA epitope	GSB/LJT
pSP64-hα4/W88TAG	Trp55 homolog	GSB/LJT
pSP64-hα4/W119TAG	Trp86 homolog	GSB/LJT
pSP64-hα4/W182TAG	Trp149 homolog	GSB/LJT
pSGEM-hα4	failed to express	GSB/LJT
pSGEM-hβ2	failed to express	GSB/LJT
BiP		Käthi Geering
EF-1α		Paul Krieg
pSGEM		Andreas Karschin
pBSTAII	difficult to clone into	Ligia Toro
pNKS	difficult to clone into	Gunther Schmalzing
pRK5-rα4/m5-HT_3		Neil Millar
pRK5-rβ2/m5-HT_3		Neil Millar

Table 2.6 List of constructs utilized in α4β2 suppression studies.

The BiP construct was linearized with *BglII* and transcribed using the SP6 kit.[70] With regard to *Xenopus* oocyte EF-1α, Jane Frydenberg never responded to our e-mail request for this clone. Andre Mazabraud and Herman Denis at CNRS, Gif-Sur-Yvette also failed to reply. In the end, Paul Krieg at the University of Texas, sent us a plasmid containing the adult form of *Xenopus* EF-1α.[65] The experiments performed with EF-1α, however, utilized adult Xef1, which is included as a control plasmid in Ambion kits, because of its robustness in *in vitro* translation. The linearized plasmid is included, and was transcribed using the T7 kit. Neil Millar's α4/5-HT_3 and β2/5-HT_3 constructs were linearized with *KpnI* and transcribed using the SP6 kit.[31,32]

Suppression in hα4 was attempted with Trp at positions 88, 119, and 182 (homologous to 55, 86, and 149 in muscle), despite the fact that the TAG mutants were all in the pSP construct. Low, but perhaps usable expression was observed at 182. In some experiments, mean currents of about 250 nA were observed, with individual oocytes giving as much as 500 nA. The very mRNA mixes used in these experiments had consistently given only 20 nA currents over a year previously. It may be that this increase in suppression resulted from improvements that James Petersson made during this time in the arc lamp setup. None of these experiments was rigorously controlled with 74mer, although whenever we did suppress with 74mer, we got no current at all. In addition, a methodical study of subunit amounts and ratios was not carried out.

Since reasonable currents were being obtained with the hα4β2 mRNA mixes, an attempt was made to introduce the 5-CN- and 5-Br-Trp pair at position 182. Both times it was tried, no currents were observed. However, it was also the case that Trp suppression on both days was giving much less than 50 nA whole-cell current. The second time, all three amino acids (Trp, CN-W, and Br-W) were double-injected, but these oocytes failed to express even WT nAChR. In general, there were oocyte problems throughout the laboratory concurrent with these experiments.

Nicotine experiments were performed at pH 6.5, as were most ACh experiments. In general, ACh in pH 6.5 Ca^{2+}-free ND96 gave the same current as it did at pH 7.5, which is the normal pH of recording solution.

2.5.4 Introduction of the HA epitope into hα4

The HA epitope was successfully introduced into pSP-α4, at a position in the M3-M4 loop *[PPQQPLEAE*KASPHP]* homologous to the traditional 347 position (see Chapter

3) in muscle alpha, and also at the C-terminus immediately before the TAA codon *[WLAGMI*]*. By *in vitro* translation, both constructs gave intense staining at about 55 kDa in a Western blot with BAbCo anti-HA antibody, using the usual protocol. Electrophysiologically, we saw absolutely no current with the C-terminal tag construct and about 78% of WT current with the M3-M4 HA construct. mRNA levels were reasonably consistent among the three constructs, but it would be unwise to rely too much on these experiments for quantitative current comparisons, which were not our intent in this study. Membranes manually dissected from the very oocytes used for the electrophysiology showed absolutely no staining for the WT and C-terminal constructs and very clear, intense staining at unusually large molecular weights (doublets at ~100 kDa and ~200 kDa) for the M3 construct. However, all of these experiments were done only once each.

During the course of various experiments, we saw small but measurable currents from an alpha subunit co-injected with non-coding mRNA (in one case, for instance, the mRNA was run off from a β2 construct where we had ordered a faulty primer and inserted a frameshift in the second amino acid). This may be something to be careful of in future experiments.

2.5.5 Planning for four-base codon suppression

The most successful reported four-base suppression in both *E. coli* and rabbit reticulocyte extracts employed the codon *CGGG*.[78] In addition, *AGGT* was reported to work well in *E. coli* extracts.[73] In *Xenopus laevis*, *AGG* is fairly common (12.3 occurrences per thousand), whereas *CGG* is rather uncommonly used (6.0 per thousand).[79] In *E. coli*, these numbers are 1.7 for *AGG* and 5.4 for *CGG*. Least common non-stop codons in *Xenopus* are *UCG* (3.9), *ACG* (4.6), *GCG*

(4.7), and *CCG* (4.8). Comparable numbers for *E. coli* are *UCG* (8.6), *ACG* (13.8), *GCG* (31.8), and *CCG* (22.0).[79] As a result, we chose to emulate the strategy of Sisido in employing *AGGT*, but also in order to minimize competition with endogenous tRNA's, we also chose a codon based on the least-used coding triplet, *UCG*. The fourth base was somewhat arbitrarily made a *G*, giving *TCGG*. The initial experiments were specifically intended to increase the suppression efficiency of hα4-W182 relative to conventional *amber* suppression with TH73G-Trp. Thus, we planned to prepare two mRNA's, namely hα4 W182 *CGGG* and hα4 W182 *TCGG*.

We also chose to utilize two different kinds of tRNA. One followed the strategy of Sisido, and the other was derived from what is known to work for suppression in *Xenopus* oocytes.[73,78,80,81] Sisido's suppressor tRNA is based on yeast Phe, quite similar to our MN3. We planned to use a version where nucleotide 73 has been changed to A, referred to as YF73G. In addition, we designed a modified TH73G to recognize the above four-base codons. In total, we planned to prepare five tRNA's, YF73G *CCCG*, TH73G *CCCG*, YF73G *CCGA*, TH73G *CCGA*, and YF73G *CUA*. Difficulties in preparing the above constructs prevented us from trying four-base suppression, although it may be an interesting strategy for future attempts to suppress in α4β2 nAChR.

2.6 References

1. Zhong, W. G. et al. From ab initio quantum mechanics to molecular neurobiology: A cation-pi binding site in the nicotinic receptor. *PNAS* **95**, 12088-12093 (1998).
2. Mishina, M. et al. Expression of functional acetylcholine-receptor from cloned cDNA. *Nature* **307**, 604-608 (1984).
3. Arias, H. R. Topology of ligand binding sites on the nicotinic acetylcholine receptor. *Brain Res. Rev.* **25**, 133-191 (1997).
4. Arias, H. R. Binding sites for exogenous and endogenous non-competitive inhibitors of the nicotinic acetylcholine receptor. *Biochim. Biophys. Acta* **1376**, 173-220 (1998).
5. Corringer, P. J., Le Novere, N. and Changeux, J. P. Nicotinic receptors at the amino acid level. *Ann. Rev. Pharm.* **40**, 431-458 (2000).
6. Hucho, F. and Weise, C. Ligand-gated ion channels. *Angew. Chem. Int. Ed. Eng.* **40**, 3100-3116 (2001).
7. Jones, S., Sudweeks, S. and Yakel, J. L. Nicotinic receptors in the brain: correlating physiology with function. *Trends Neurosci.* **22**, 555-561 (1999).

8. McGehee, D. S. and Role, L. W. Physiological diversity of nicotinic acetylcholine receptors expressed by vertebrate neurons. *Ann. Rev. Physiol.* **57**, 521-546 (1995).
9. Miyazawa, A., Fujiyoshi, Y., Stowell, M. and Unwin, N. Nicotinic acetylcholine receptor at 4.6 Å resolution: transverse tunnels in the channel wall. *J. Mol. Biol.* **288**, 765-786 (1999).
10. Ma, J. C. and Dougherty, D. A. The cation-pi interaction. *Chem. Rev.* **97**, 1303-1324 (1997).
11. Dougherty, D. A. and Stauffer, D. A. Acetylcholine binding by a synthetic receptor - implications for biological recognition. *Science* **250**, 1558-1560 (1990).
12. Brejc, K. et al. Crystal structure of an ACh-binding protein reveals the ligand-binding domain of nicotinic receptors. *Nature* **411**, 269-276 (2001).
13. Galzi, J. L. et al. Mutations in the channel domain of a neuronal nicotinic receptor convert ion selectivity from cationic to anionic. *Nature* **359**, 500-505 (1992).
14. Labarca, C. et al. Channel gating governed symmetrically by conserved leucine residues in the M2 domain of nicotinic receptors. *Nature* **376**, 514-516 (1995).
15. Kearney, P. C. et al. Interactions of leucine residues at the 9' position of the M2 domain of the AChR probed using unnatural amino acid mutagenesis. *Biophys. J.* **70**, Tuam5-Tuam5 (1996).
16. Kearney, P. C., Zhang, H. Y., Zhong, W., Dougherty, D. A. and Lester, H. A. Determinants of nicotinic receptor gating in natural and unnatural side chain structures at the M2 9' position. *Neuron* **17**, 1221-1229 (1996).
17. Jackson, M. B. and Yakel, J. L. The 5-HT_3 receptor channel. *Ann. Rev. Physiol.* **57**, 447-468 (1995).
18. Kearney, P. C. et al. Dose-response relations for unnatural amino acids at the agonist binding site of the nicotinic acetylcholine receptor: tests with novel side chains and with several agonists. *Mol. Pharm.* **50**, 1401-1412 (1996).
19. Zhong, W. *Ph.D. Thesis* (California Institute of Technology, Pasadena, CA, 1998).
20. Xie, Y. and Cohen, J. B. Contributions of *Torpedo* nicotinic acetylcholine receptor gamma Trp-55 and delta Trp-57 to agonist and competitive antagonist function. *J. Biol. Chem.* **276**, 2417-2426 (2001).
21. Chiara, D. C., Middleton, R. E. and Cohen, J. B. Identification of tryptophan 55 as the primary site of [3H]nicotine photoincorporation in the gamma-subunit of the *Torpedo* nicotinic acetylcholine receptor. *FEBS Lett.* **423**, 223-226 (1998).
22. Seeman, J. I. and Whidby, J. F. The iodomethylation of nicotine. An unusual example of competitive nitrogen alkylation. *J. Org. Chem.* **41**, 3824-3826 (1976).
23. Cho, A. K., Jenden, D. J. and Lamb, S. I. Rates of alkaline hydrolysis and muscarinic activity of some aminoacetates and their quaternary ammonium analogs. *J. Med. Chem.* **15**, 391-399 (1972).
24. Petersson, E.J. *Biochemisry*, in press. (2002).
25. Kenakin, T. Efficacy in drug receptor theory: outdated concept or under-valued tool? *Trends Pharm. Sci.* **20**, 400-405 (1999).
26. Kenakin, T. Inverse, protean, and ligand-selective agonism: matters of receptor conformation. *FASEB J.* **15**, 598-611 (2001).
27. Colquhoun, D. Binding, gating, affinity and efficacy: the interpretation of structure-activity relationships for agonists and of the effects of mutating receptors. *Br. J. Pharm.* **125**, 924-947 (1998).
28. Dineley, K. T. and Patrick, J. W. Amino acid determinants of alpha 7 nicotinic acetylcholine receptor surface expression. *J. Biol. Chem.* **275**, 13974-13985 (2000).
29. Eisele, J. L. et al. Chimeric nicotinic serotonergic receptor combines distinct ligand-binding and channel specificities. *Nature* **366**, 479-483 (1993).
30. Rakhilin, S. et al. alpha-Bungarotoxin receptors contain alpha 7 subunits in two different disulfide-bonded conformations. *J. Cell Biol.* **146**, 203-217 (1999).
31. Harkness, P. C. and Millar, N. S. Inefficient cell-surface expression of hybrid complexes formed by the co-assembly of neuronal nicotinic acetylcholine receptor and serotonin receptor subunits. *Neuropharmacology* **41**, 79-87 (2001).
32. Cooper, S. T., Harkness, P. C., Baker, E. R. and Millar, N. S. Up-regulation of cell-surface alpha 4 beta 2 neuronal nicotinic receptors by lower temperature and expression of chimeric subunits. *J. Biol. Chem.* **274**, 27145-27152 (1999).
33. Mecozzi, S., West, A. P. and Dougherty, D. A. Cation-pi interactions in simple aromatics: Electrostatics provide a predictive tool. *J. Am. Chem. Soc.* **118**, 2307-2308 (1996).

34. Mecozzi, S., West, A. P. and Dougherty, D. A. Cation-pi interactions in aromatics of biological and medicinal interest: Electrostatic potential surfaces as a useful qualitative guide. *PNAS* **93**, 10566-10571 (1996).
35. Maricq, A. V., Peterson, A. S., Brake, A. J., Myers, R. M. and Julius, D. Primary structure and functional expression of the $5HT_3$ receptor, a serotonin-gated ion channel. *Science* **254**, 432-437 (1991).
36. Boess, F. G. et al. Analysis of the ligand binding site of the $5\text{-}HT_3$ receptor using site directed mutagenesis: importance of glutamate 106. *Neuropharmacology* **36**, 637-647 (1997).
37. Curtis, L. et al. A new look at the neuronal nicotinic acetylcholine receptor pharmacophore. *Eur. J. Pharm.* **393**, 155-163 (2000).
38. Schmitt, J. D. Exploring the nature of molecular recognition in nicotinic acetylcholine receptors. *Curr. Med. Chem.* **7**, 749-800 (2000).
39. Schmitt, J. D., Sharples, C. G. and Caldwell, W. S. Molecular recognition in nicotinic acetylcholine receptors: the importance of pi-cation interactions. *J. Med. Chem.* **42**, 3066-3074 (1999).
40. Sheridan, R. P., Nilakantan, R., Dixon, J. S. and Venkataraghavan, R. The ensemble approach to distance geometry: application to the nicotinic pharmacophore. *J. Med. Chem.* **29**, 899-906 (1986).
41. Tonder, J. E. et al. Improving the nicotinic pharmacophore with a series of (isoxazole)methylene-1-azacyclic compounds: synthesis, structure-activity relationship, and molecular modeling. *J. Med. Chem.* **42**, 4970-80 (1999).
42. Tonder, J. E. and Olesen, P. H. Agonists at the alpha4beta2 nicotinic acetylcholine receptors: structure-activity relationships and molecular modelling. *Curr Med Chem* **8**, 651-674 (2001).
43. Spier, A. D. and Lummis, S. C. The role of tryptophan residues in the 5-Hydroxytryptamine(3) receptor ligand binding domain. *J. Biol. Chem.* **275**, 5620-5625 (2000).
44. Davis, A. M. and Teague, S. J. Hydrogen bonding, hydrophobic interactions, and failure of the rigid receptor hypothesis. *Angew. Chem. Int. Ed. Eng.* **38**, 737-749 (1999).
45. Lena, C. and Changeux, J. P. Pathological mutations of nicotinic receptors and nicotine-based therapies for brain disorders. *Curr. Op. Neurobiol.* **7**, 674-682 (1997).
46. Picciotto, M. R. et al. Acetylcholine receptors containing the beta2 subunit are involved in the reinforcing properties of nicotine. *Nature* **391**, 173-177 (1998).
47. Marubio, L. M. et al. Reduced antinociception in mice lacking neuronal nicotinic receptor subunits. *Nature* **398**, 805-810 (1999).
48. Benowitz, N. L. Pharmacology of nicotine: addiction and therapeutics. *Ann. Rev. Pharm.* **36**, 597-613 (1996).
49. Dani, J. A. and Heinemann, S. Molecular and cellular aspects of nicotine abuse. *Neuron* **16**, 905-908 (1996).
50. ChavezNoriega, L. E. et al. Pharmacological characterization of recombinant human neuronal nicotinic acetylcholine receptors h alpha 2 beta 2, h alpha 2 beta 4, h alpha 3 beta 2, h alpha 3 beta 4, h alpha 4 beta 2, h alpha 4 beta 4 and h alpha 7 expressed in *Xenopus* oocytes. *J. Pharm. Exp. Therapeut.* **280**, 346-356 (1997).
51. Papke, R. L. and Heinemann, S. F. Partial Agonist Properties of Cytisine on Neuronal Nicotinic Receptors Containing the Beta-2 Subunit. *Mol. Pharm.* **45**, 142-149 (1994).
52. Spang, J. E. et al. Chemical modification of epibatidine causes a switch from agonist to antagonist and modifies its selectivity for neuronal nicotinic acetylcholine receptors. *Chem. Biol.* **7**, 545-555 (2000).
53. Truong, A. et al. Pharmacological differences between immunoisolated native brain and heterologously expressed rat alpha 4 beta 2 nicotinic receptors. *Mol. Brain Res.* **96**, 68-76 (2001).
54. Gale, M., Tan, S. L. and Katze, M. G. Translational control of viral gene expression in eukaryotes. *Microbiol. Mol. Bio. Rev.* **64**, 239-248 (2000).
55. Hann, L. E., Webb, A. C., Cai, J. M. and Gehrke, L. Identification of a competitive translation determinant in the 3' untranslated region of alfalfa mosaic virus coat protein mRNA. *Mol. Cell. Biol.* **17**, 2005-2013 (1997).
56. Shih, T. M., Smith, R. D., Toro, L. and Goldin, A. L. High-level expression and detection of ion channels in *Xenopus* oocytes. *Meth. Enz.* **293**, 529-556 (1998).
57. Nicke, A. et al. P2X(1) and P2X(3) receptors form stable trimers: a novel structural motif of ligand-gated ion channels. *EMBO J.* **17**, 3016-3028 (1998).

58. Wischmeyer, E., Doring, F. and Karschin, A. Acute suppression of inwardly rectifying Kir2.1 channels by direct tyrosine kinase phosphorylation. *J. Biol. Chem.* **273**, 34063-34068 (1998).
59. Negrutskii, B. S. and El'skaya, A. V. Eukaryotic translation elongation factor 1 alpha: Structure, expression, functions, and possible role in aminoacyl-tRNA channeling. *Prog. Nucl. Acid Res.* **60**, 47-78 (1998).
60. Dreher, T. W., Uhlenbeck, O. C. and Browning, K. S. Quantitative assessment of EF-1 alpha center dot GTP binding to aminoacyl-tRNAs, aminoacyl-viral RNA, and tRNA shows close correspondence to the RNA binding properties of EF-Tu. *J. Biol. Chem.* **274**, 666-672 (1999).
61. Andersen, G. R., Valente, L., Pedersen, L., Kinzy, T. G. and Nyborg, J. Crystal structures of nucleotide exchange intermediates in the eEF1A-eEF1B alpha complex. *Nature Struct. Biol.* **8**, 531-534 (2001).
62. Vitagliano, L., Masullo, M., Sica, F., Zagari, A. and Bocchini, V. The crystal structure of Sulfolobus solfataricus elongation factor 1 alpha in complex with GDP reveals novel features in nucleotide binding and exchange. *EMBO J.* **20**, 5305-5311 (2001).
63. Deschamps, S. et al. 2 Forms of elongation factor-1-alpha (Ef-1-Alpha O and 42sp50), present in oocytes, but absent in somatic cells of *Xenopus laevis*. *J. Cell Biol.* **114**, 1109-1111 (1991).
64. Frydenberg, J., Poulsen, K., Petersen, A. K. B., Lund, A. and Olesen, O. F. Isolation and characterization of the gene encoding Ef-1-Alpha-O, an Elongation-Factor 1-Alpha expressed during early development of *Xenopus laevis*. *Gene* **109**, 185-192 (1991).
65. Johnson, A. D. and Krieg, P. A. A *Xenopus laevis* gene encoding Ef-1-Alpha-S, the somatic form of Elongation-Factor 1-Alpha - sequence, structure, and identification of regulatory elements required for embryonic transcription. *Dev. Gen.* **17**, 280-290 (1995).
66. Damke, H., Baba, T., Warnock, D. E. and Schmid, S. L. Induction of mutant dynamin specifically blocks endocytic coated vesicle formation. *J. Cell Biol.* **127**, 915-34 (1994).
67. van der Bliek, A. M. et al. Mutations in human dynamin block an intermediate stage in coated vesicle formation. *J. Cell Biol.* **122**, 553-563 (1993).
68. Shimkets, R. A., Lifton, R. P. and Canessa, C. M. The activity of the epithelial sodium channel is regulated by clathrin- mediated endocytosis. *J. Biol. Chem.* **272**, 25537-25541 (1997).
69. Hopf, A., Schreiber, R., Mall, M., Greger, R. and Kunzelmann, K. Cystic fibrosis transmembrane conductance regulator inhibits epithelial Na+ channels carrying Liddle's syndrome mutations. *J. Biol. Chem.* **274**, 13894-13899 (1999).
70. Beggah, A. T. and Geering, K. alpha and beta subunits of Na,K-ATPase interact with BiP and calnexin. *Annal. NY Acad. Sci.* **834**, 537-539 (1997).
71. Ma, D. K. et al. Role of ER export signals in controlling surface potassium channel numbers. *Science* **291**, 316-319 (2001).
72. Luetje, C. W., Piattoni, M. and Patrick, J. Mapping of ligand-binding sites of neuronal nicotinic acetylcholine-receptors using chimeric alpha-subunits. *Mol. Pharm.* **44**, 657-666 (1993).
73. Hohsaka, T., Ashizuka, Y., Taira, H., Murakami, H. and Sisido, M. Incorporation of nonnatural amino acids into proteins by using various four-base codons in an *Escherichia coli in vitro* translation system. *Biochemistry* **40**, 11060-11064 (2001).
74. Francis, M. M., Cheng, E. Y., Weiland, G. A. and Oswald, R. E. Specific activation pf the alpha 7 nicotinic acetylcholine receptor by a quaternary analog of cocaine. *Mol. Pharm.* **60**, 71-79 (2001).
75. Nowak, M. W. et al. *In vivo* incorporation of unnatural amino acids into ion channels in *Xenopus* oocyte expression system. *Meth. Enz.* **293**, 504-529 (1998).
76. Li, L. T. et al. The tethered agonist approach to mapping ion channel proteins toward a structural model for the agonist binding site of the nicotinic acetylcholine receptor. *Chem. Biol.* **8**, 47-58 (2001).
77. Davies, P. A. et al. The 5-HT_{3B} subunit is a major determinant of serotonin-receptor function. *Nature* **397**, 359-363 (1999).
78. Sisido, M. and Hohsaka, T. Introduction of specialty functions by the position-specific incorporation of nonnatural amino acids into proteins through four-base codon/anticodon pairs. *App. Microbiol. Biotech.* **57**, 274-281 (2001).
79. Nakamura, Y., Gojobori, T. and Ikemura, T. Codon usage tabulated from international DNA sequence databases: status for the year 2000. *Nuc. Acids Res.* **28**, 292-292 (2000).
80. Saks, M. E. et al. An engineered *Tetrahymena* tRNA(Gln) for in vivo incorporation of unnatural amino acids into proteins by nonsense suppression. *J. Biol. Chem.* **271**, 23169-23175 (1996).

81. Sisido, M. and Hohsaka, T. Extension of protein functions by the incorporation of nonnatural amino acids. *Bull. Chem. Soc. Japan* **72**, 1409-1425 (1999).

Chapter 3. Analysis of protein conformation

3.1 Introduction

In the work presented in the previous chapter, unnatural amino acids were used to make more subtle side chain perturbations than are possible using conventional mutagenesis. However, the range of side chain substitution permitted by the ribosome allows for unnatural amino acids which induce much more radical transformations. In this chapter, nonsense suppression has been used to chemically modify proteins both dynamically and after isolation from the membrane. In the first case, nitrophenylglycine (Npg) was introduced in order to photolytically cleave the polypeptide backbone at the site of the amino acid's introduction.[1] The second set of experiments examined the possibility of site-specific photoinduced cross-linking mediated by the unnatural amino acid benzoylphenylalanine (Bpa).[2] In the third study, hydroxy acids were inserted into the backbone by nonsense suppression.[3-5] The resulting ester linkage is labile to treatment with strong base, which allows for the incorporation of hydroxy acids to be used for mapping protein connectivity.[4] Finally, cysteine and tyrosine residues with bulky photo-removable protecting groups were used to induce conformational changes in a sensitive transmembrane region of the nAChR.[6]

3.2 Site-specific backbone cleavage in nAChR Cys loop using Npg

3.2.1 Site-specific nitrobenzyl-induced photochemical proteolysis (SNIPP)

Site-specific proteolysis is a fundamental step in a wide variety of biological processes.[7] A number of them have become widely publicized because of their role in

human disease.[8] Protease inhibitors for angiotensin-converting enzyme and HIV protease, for example, are highly successful drugs.[9] Targeted proteolysis is typically used at the protein level to activate an enzyme by removing a regulatory domain which holds the proenzyme in check.[10] Among the many examples of this kind of regulation are the caspases, tightly regulated proteases which initiate and carry out the proteolytic steps leading to apoptotic cell death. At the peptide level, potent peptide hormones are synthesized as much larger polypeptides and released by cleavage into their active fragments. As previously mentioned, angiotensin is released this way into the bloodstream. Proteolysis also has a role in certain kinds of pathology. The apparently pathogenic Aβ fragment in Alzheimer's disease is produced by aberrant proteolysis of a precursor protein.[11] A final strategy for proteolytic regulation has been only recently recognized. The protease-activated receptors are thought to be involved in pain pathways, and thus are an increasingly recognized target for clinical intervention.[12] These G-protein-coupled receptors are activated only upon cleavage of an extracellular N-terminal domain.

The ability to site-specifically cleave DNA revolutionized the practice of modern biology. It remains to be seen whether or not site-specific protein cleavage will have such a great effect. The most widespread method of experimental site-specific cleavage is to introduce a protease site into the primary sequence of the protein. This strategy has been used to good effect in structural biology, where proteins may be purified by attached affinity tags, which can then be proteolytically removed to allow characterization of a more native protein.[13] However, *in situ* studies which rely on proteolysis are more difficult, since the proteases responsible for inducing the cleavage can be only under

partial experimental control, at best. Attempts have been made to adapt strategies which have been successful for nucleic acids. Molecules which bind specific DNA sequences have been conjugated to metals or photo-excitable compounds, so that radicals induced by these adducts may cleave the polyphosphate backbone.[14] A similar, though non-specific, strategy has been employed by Daniel Jay to hydrolyze proteins in the vicinity of an irradiated malachite green-conjugated antibody.[15] This technique is known as CALI, or chromophore-assisted laser inactivation.[16] The laboratory of C. V. Kumar has recently introduced a more specific technique for inducing proteolysis this way.[17] Here, dyes are used which bind, under some circumstances, specifically to a given region of a protein. Photolysis of the complex may produce radicals which cleave the backbone.[18,19]

The first general strategy for dynamically cleaving peptide backbones in functioning proteins was only recently introduced. This approach relies on the incorporation of the unnatural amino acid Npg via nonsense suppression. Photolysis induces proton abstraction from the alpha carbon of the amino acid, leading ultimately to hydrolysis.[1] (Figure 3.1)

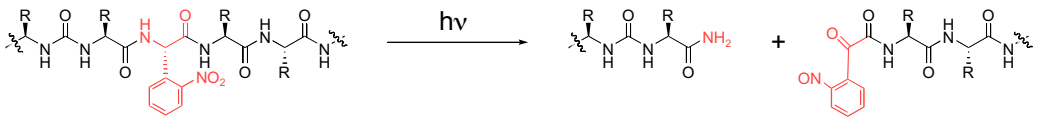

Figure 3.1 Mechanism of SNIPP - backbone cleavage induced by the photolysis of a protein containing a nitrophenylglycine (Npg) residue.[1]

In this initial report, both transmembrane regions and intracellular protein domains were cleaved photolytically in functioning receptors in living cells. A more recent, although less generally useful, derivative of this technique has also been reported, wherein allyl glycine is cleaved by the addition of iodine.[20-22]

The experimental site-specific cleavage of a protein backbone may be used in two general ways. The first involves mimicking a natural process. For example, introducing Npg into the linker region of a protease-activated receptor would place the receptor under direct experimental control. (Figure 3.2) This system would have the additional advantage of generating a signal upon photolysis, whereas the channels examined to date with Npg show reduced current after irradiation.

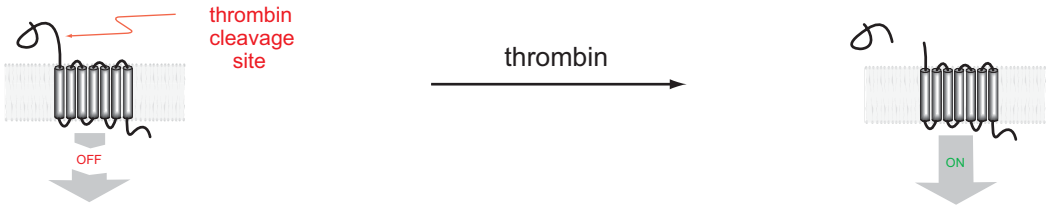

Figure 3.2 Signaling is initiated by proteolysis of the extracellular N-terminal domain of protease-activated receptors.[12]

A second use of *in situ* backbone cleavage is to attempt to map functionally important regions of a protein. This mapping is especially valuable in highly dynamic proteins, such as receptors, where binding of a small molecule induces a conformational change which must be mechanically transduced through the protein. By severing the backbone in a variety of locations, it may be possible to trace the path of conformational changes in the protein. (Figure 3.3)

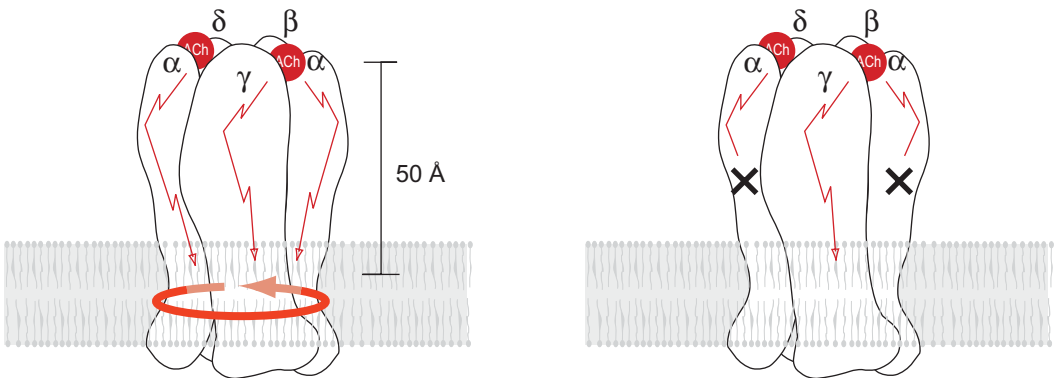

Figure 3.3 Schematic showing how site-specific backbone cleavage may disrupt the pathway of mechanical coupling between binding site conformational change and channel opening.

The ability to target cleavage to a specific residue in a functional protein is obviously of paramount importance to this technique, and this specificity along with the technique's compatibility with living cells represent two of the principal advantages of nonsense suppression.

3.2.2 Previous results with Npg in the nAChR

We have seen in the previous chapter how acetylcholine and nicotine binding may be modulated in the nicotinic acetylcholine receptor. Here, we turn our attention to the biological consequences of agonist binding. The binding of two molecules of agonist to the receptor triggers a conformational change which opens the transmembrane pore of the channel. Relating binding to gating, as this conformational change is called, is fundamental to the process by which a chemical synapse works. The binding of neurotransmitters released by the pre-synaptic cell to ion channels on the post-synaptic cell allows the entry of cations into the post-synaptic cell, thus accomplishing propagation of an action potential from pre- to post-synaptic cell. Understanding, in precise molecule detail, how this conformation change occurs in a protein such as the nAChR could have important consequences, such as the ability to design molecules which affect neurotransmission. However, there are no analytical means available to directly answer such a question. Not only is dynamic crystallography a field in its infancy, but multi-subunit integral membrane proteins such as the nAChR are intrinsically extremely difficult to characterize crystallographically.

Given this experimental context, the ability to introduce unnatural amino acids into functioning nAChR may provide an opportunity for understanding the conformational change associated with gating. In the initial report on Npg, data were shown for

incorporation of this photo-cleavable residue into the Cys loop of the alpha subunit.[1] The Cys loop is a characteristic amino acid sequence which defines the nAChR family of ligand-gated ion channels.[23] (Figure 3.4)

Figure 3.4 Presumed location of Cys loop in the nAChR,[24] based on antibody binding studies and apparent glycosylation of Cys142.

At the time this initial study was undertaken, very little structural information on the positioning of this loop was available. An NMR solution structure of a peptide corresponding to the Cys loop, with and without N-linked glycosylation at Asn142, showed the probable structure of the loop itself.[25] Antibodies which were thought to recognize the Cys loop appeared to bind only after certain maturational processes had taken place, probably dimerization of subunit pairs. However, binding ability was lost in the fully folded receptor, suggesting that the Cys loop was occluded in the pentamer.[26] From these studies, it was surmised that the Cys loop was positioned at inter-subunit interfaces.[24,27] Inter-subunit interfaces were in turn thought to be of critical importance in both making up the agonist binding site, and communicating conformational change from the extracellular binding domain to the transmembrane pore region, some 50 Å away.

Cleavage of the Cys loop in the nAChR alpha subunits had a dramatic effect. Upon photolysis, 90% of the whole-cell current was eliminated. This current reduction was unrecoverable. This experiment appeared to corroborate the prevailing view of the

importance of the Cys loop. An additional experiment in the beta subunit was undertaken to examine the ability of the residue to cleave in a transmembrane domain and also to examine the effects of such cleavage. As with alpha Cys loop cleavage, the effect was expected to be marked. The 9' position of the nAChR is highly conserved, with a leucine residue in all known receptor subunits.[28] It was believed that the Leu residues from all five subunits formed a hydrophobic plug of the pore, which was released during the gating process by subunit movement.[29] In accord with this prediction, photolysis of Npg at the beta9' position led to a 50% decrease in whole-cell current, again in an apparently unrecoverable fashion.

Other than affirming the importance of these two regions to receptor function, it was difficult to know how to interpret the results. Binding studies implied that photolysis of the Cys loop left the receptor able to bind ACh, so the effect appeared to be on gating. However, was it possible to further interpret the result in a mechanistic way? Could the relative amounts of current inactivation be explained? In an attempt to gather more information on these important questions, two lines of experimentation were undertaken.

3.2.3 Experimental design

First, Cys-loop cleavage in all four nAChR subunits was planned. The alpha subunit appears to have a special role in receptor activity. In addition to its stoichiometric double representation, it was thought to largely contain the agonist binding site. Functional receptors may have a variety of subunit compositions and stoichiometries, but alpha subunits are absolutely essential. However, by the time the conformational change associated with binding has been transmitted to the channel pore, each subunit appears to contribute equally. The additive nature of each subunit to the gating process was

established, in part, by previous work from this laboratory involving replacement of the Lue9' residue with unnatural amino acids.[30,31] By analyzing the effects of cleavage in the non-alpha subunits, it was hoped that the results would provide additional information to help delineate the contribution of all five subunits to agonist binding and to help interpret the 90% current reduction observed on alpha Cys-loop photolysis.

Second, attempts were made to extend the analysis of Npg cleavage from electrophysiology to direct biochemical observation of cleavage. The complete scission of a protein should be easily observable by techniques such as gel electrophoresis. However, it was not known whether the small amounts of protein produced by nonsense suppression in oocytes would be detectable. It was hoped, again, that direct confirmation of protein cleavage would assist in the interpretation of results obtained with Npg.

3.2.4 Results

3.2.4.1 Cleavage in non-alpha subunits

The requisite mutations were introduced in the beta, gamma, and delta subunits at the positions homologous to alpha132 and 133, where the initial Npg results were obtained. (Figure 3.5)

α: ^{128}Cys Glu Ile Ile Val Thr His Phe Pro Phe Asp Glu Gln Asn Cys^{142}
β: ^{128}Cys Ser Ile Gln Val Thr Tyr Phe Pro Phe Asp Trp Gln Asn Cys^{142}
γ: ^{128}Cys Ser Ile Ser Val Thr Tyr Phe Pro Phe Asp Trp Gln Asn Cys^{142}
δ: ^{130}Cys Pro Ile Ser Val Thr Tyr Phe Pro Phe Asp Trp Gln Asn Cys^{144}

Figure 3.5 Sequence of the Cys loop in all four subunits of embryonic mouse muscle nAChR.

In these experiments, the expected result was rather difficult to predict. A reasonable presumption would have been that the contribution of different subunits in the extracellular domain would be different. After all, the arrangement of subunits around

the pore calls for different interaction, at the very least, with the important alpha subunits. (Figure 3.4) The gamma subunit, which forms two interfaces with alpha subunits, must have its Cys loop packed against an alpha subunit, if this domain is indeed interfacial. Meanwhile, either the delta or beta subunit must not pack against alpha, because of obvious topological restraints. Upon incorporation of Npg into the receptor, photolysis gave a uniform result. (Figure 3.6)

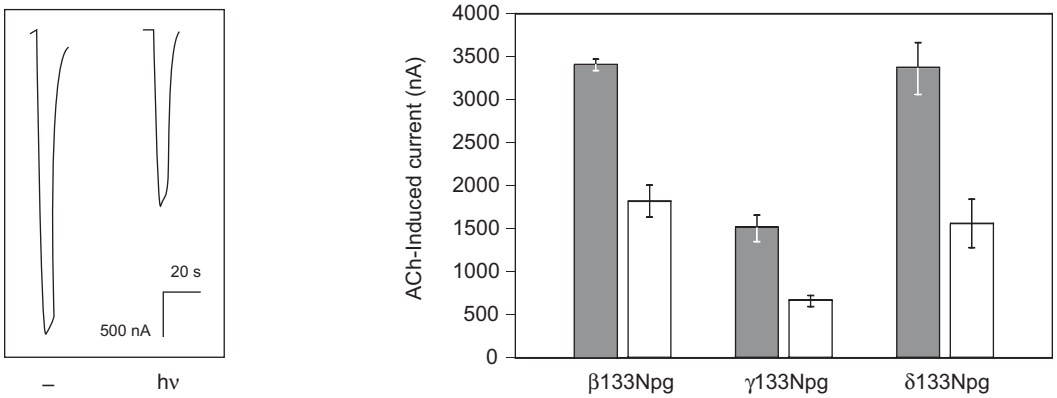

Figure 3.6 Photolysis of nAChR containing Npg in non-alpha Cys loops leads to a consistent 50% reduction in whole-cell current. Left panel: Representative traces from oocytes expressing nAChR with Npg at the γ133 position, without (left) and with (right) photolysis. Right panel: Whole-cell currents from oocytes expressing nAChR suppressed at the indicated position in the presence and absence of irradiation. Filled bars represent mean current (±SEM) in the absence of photolysis. Hollow bars represent mean current (±SEM) from oocytes photolyzed for 4 hr.

In each case, approximately 50% reduction in whole-cell current was observed. The interpretation of this result is by no means straightforward.

One observation which complicates the interpretation of Cys-loop cleavage in non-alpha subunits is the presence of large amounts of background current. Suppression in the alpha subunit of the nAChR typically works very well, with respect to the null control. Co-injection of mRNA and non-aminoacylated tRNA usually produces no observable whole-cell current. In non-alpha subunits, this null control is capable of giving rise to currents of 50% of the maximum suppressed current. (Figure 3.7)

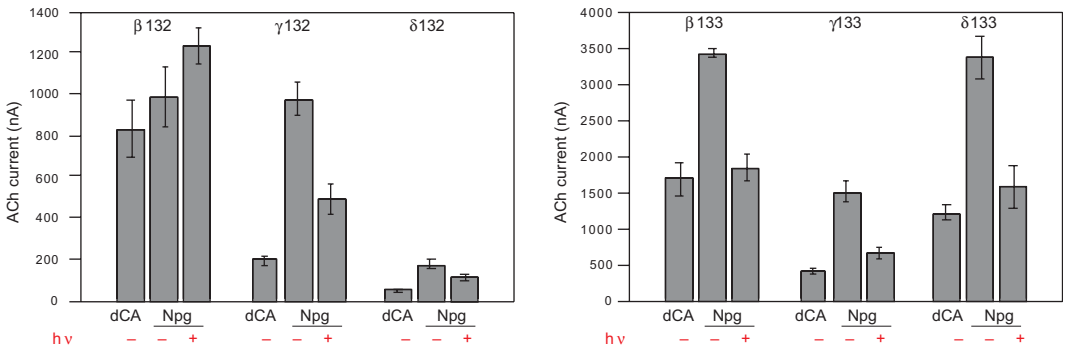

Figure 3.7 Whole-cell currents from oocytes expressing nAChR suppressed with Npg show both the significant background and clear effect of photolysis. Mean currents(±SEM) in response to 200 μM ACh, 24 hr post-injection.

The reason for this difference in behavior is unclear, but there is always concern that receptors with truncated non-alpha subunits or even with non-canonical stoichiometry ($\alpha_2\beta\delta_2$, for example) may be functional.[32] Alternatively, it may be the case that the amounts of read-through (the term is used here to refer to the formation, by any mechanism, of full-length protein which lacks an unnatural amino acid at the desired position) are small, and that the requirement for two alpha subunits means that very little functional protein is formed which has two alphas arising from read-through. In any case, the large currents seen with this control complicate the analysis. Photolysis generally brings the level of whole-cell current down to the level of read-through current. Should photolysis then be scored as 90-100% for all subunits? Or, is it rather the case that the vast majority of functioning receptors on the surface of an oocyte injected with charged tRNA arise from suppression, and that photolysis of non-alpha receptors gives a 50% current decrease? One way to differentiate between these possibilities would be to analyze the products of nonsense suppression with Npg by polyacrylamide gel electrophoresis.

3.2.4.2 Attempts to visualize proteolysis by PAGE

Since electrophoresis separates proteins by mass, photoinduced cleavage should be very evident in PAGE. Since cleavage requires the presence of Npg, it should also be straightforward to distinguish between suppressed protein and full-length protein produced by read-through. Suppressed protein should be cleavable by irradiation, whereas read-through protein will not be. It should be noted that, in the absence of direct evidence for cleavage, there is an additional difficulty in interpreting an experiment with Npg. Has the residue actually cleaved the backbone, or has some conformational change occurred which produces the observed effect? Thus, the ability to directly observe cleavage would simplify analysis by reducing the number of formal possibilities that need to be considered to explain a given result.

The first thing which needs to be established is whether or not protein from suppressed oocytes can be detected by PAGE. The three most common ways of visualizing expressed protein are staining by dyes (Kumasi blue, silver, Ponceau, etc.), detection with antibodies in Western blotting, and by radiolabeling the protein, usually metabolically. These three assays vary in both sensitivity and specificity. Given that oocytes are very large cells with large numbers of membrane proteins, as well as yolk components and vitelline membranes, it was thought that Western blotting might provide an appropriate level of specificity. Sensitivity in a Western blot is largely governed by the affinity of the antibody for its protein target. A number of subunit-specific nAChR antibodies exist which are competent to recognize the denatured protein present in PAGE. However, greater sensitivity may often be gained through the use of epitope tags,

where epitopes for which very high-affinity antibodies exist are introduced into the protein.

Figure 3.8 shows that nAChR from oocytes suppressed with Npg may be detected in Western blotting with anti-nAChRα antibodies. Note also that large amounts of truncated protein are detected in this assay. The domain recognized by Mab 210 is in the extracellular region of the protein, N-terminal to the introduced stop codon.[33] The rather large ratio of truncated to full-length protein illustrates the partial efficiency of the suppression process. In addition, the lack of signal for nAChRα suggests the need for a more sensitive assay.

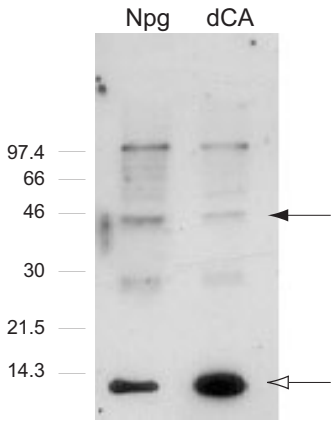

Figure 3.8 Western blot of total membrane preparations from oocytes expressing nAChR suppressed with Npg at position α132, using Mab210 as the primary antibody.[33] Solid arrow indicates full-length alpha subunit. Hollow-headed arrow indicates protein truncated at the 132 position.

Initial attempts to introduce epitope tags into nAChR subunits focused on two widely used tags recognized by the FLAG and HA antibodies. Introduction of an epitope tag potentially constitutes a significant perturbation of the protein's structure. The FLAG epitope is a highly charged sequence of amino acids, optimally DYKDE.[34] The HA sequence is the nine-amino acid YPYDVPDYA.[35,36] In order to determine whether or not introduction of the epitope tag sequence was disruptive to the receptor's function, the

sequences were introduced into a number of regions and the expression of the receptors tested. The FLAG tag had dramatic and negative effects, almost completely eradicating whole-cell nAChR current in all four positions. The HA tag was also highly disruptive at one position in the M3-M4 loop and also at the C-terminus. However, a site with minimal effect on whole-cell current was identified. In addition, it was verified that the HA tag could be introduced at the homologous position in each of the four nAChR subunits. (Figure 3.9) Non-alpha subunits were generally somewhat more tolerant, in that C-terminal HA tags were accepted with little loss of expression. However, for general use the M3-M4 loop position which worked well for alpha was adopted for the other subunits as well. (Figure 3.9) Finally, dose-response relations were found to be unaffected for HA-containing receptors relative to their wild-type counterparts.

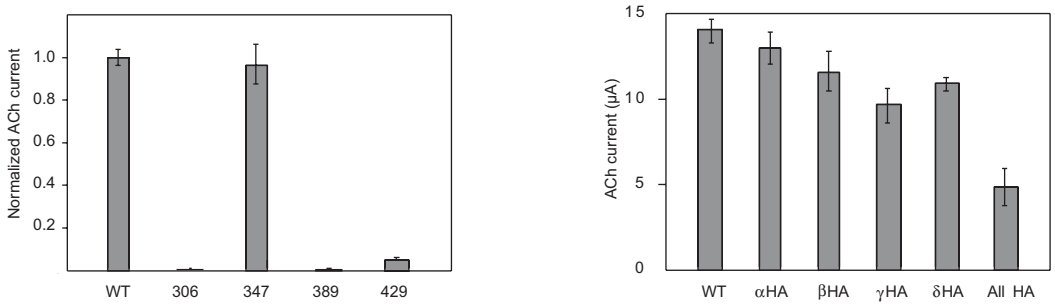

Figure 3.9 Effect of the introduction of the HA epitope tag into nAChR subunits on whole-cell ACh current in response to 200 μM ACh, 24 hr post-injection. Left panel: Mean whole-cell currents (±SEM) resulting from injection of 780 pg mRNA [2:1:1:1] containing an alpha subunit with HA tag inserted at the indicated residue number. Right panel: Mean currents (±SEM) upon injection of nAChR subunit mRNA, where the indicated subunit contains the HA tag at the M3-M4 loop position homologous to α347.

The ability of the epitope tag to render the subunits detectable in Western blots also had to be tested. Isolation of membrane proteins from *Xenopus* oocytes was undertaken in two ways. The first preparation relies on ultracentrifugation of homogenized oocytes, to harvest all of the cell's membranes.[37,38] If sub-cellular fractionation of the various internal membranes is required, this total membrane preparation may be subjected to

sucrose-gradient centrifugation.[39,40] This technique separates the membranes by density, which differs as a result of the varying lipid and protein content of various membrane compartments. Figure 3. shows the results of membrane fractionation. The direct comparison of staining with the anti-HA and Mab210 antibodies shows the superior signal strength of the antibody directed against the epitope tag.

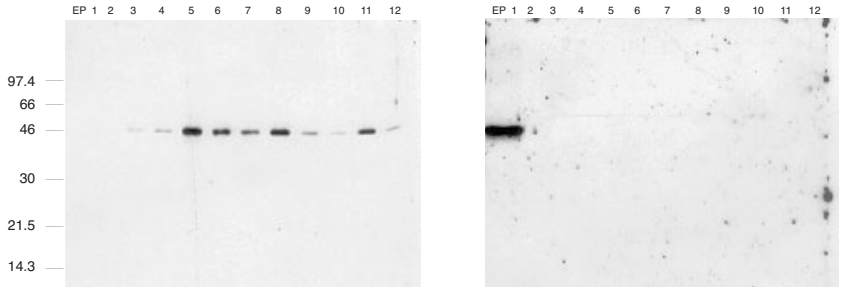

Figure 3.10 Isolation of nAChR from the surface of *Xenopus* oocytes by ultracentrifugation of homogenized oocytes followed by sub-cellular fractionation by sucrose step gradient. Fraction number is indicated above each lane, and molecular weight is indicated to the left. Left panel: Staining with HA.11. Right panel: Staining with Mab210. EP indicates a protein sample from electroplax organs of the *Torpedo* ray (provided by Anthony West).

There are a number of enzyme activity assays which may then be carried out to identify individual membrane fractions. For example, the plasma membrane is the only oocyte membrane to contain a Na^+/K^+ ATPase. Thus, assaying the various fractions for this activity uniquely identifies the plasma membrane.[40] (Figure 3.11)

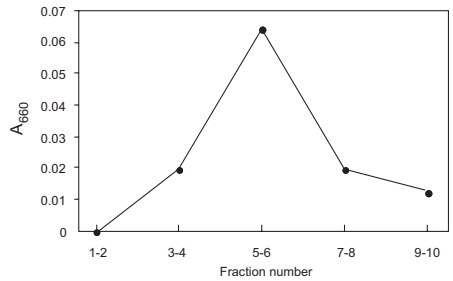

Figure 3.11 Assay for the plasma membrane-resident Na^+/K^+ ATPase, showing that activity is greatest in fractions 5 and 6, which are thus identified as containing the plasma membrane.[40] The assay is based on detection of inorganic phosphate and was carried out by Yan Dang.

A second means of harvesting membrane proteins from oocytes involves physical dissection of the cell.[41] Unlike most cell types, *Xenopus* oocytes have an external glycoprotein membrane known as the vitelline membrane, for its glassy appearance. Unlike a lipid bilayer, this vitelline membrane retains a great degree of structural integrity when isolated from the cell.[42] This rigidity is exploited in a method which fuses the desired plasma membrane with the hardier vitelline membrane. Treatment of the oocytes in a hypotonic solution effects this fusion, as the oocyte swells and the two membranes come in contact.[41] The dissection was found to be facilitated greatly if trace amounts of detergent were present in the hypotonic solution. Figure 3.12 shows membrane proteins isolated from oocytes by physical dissection in the presence and absence of detergents.

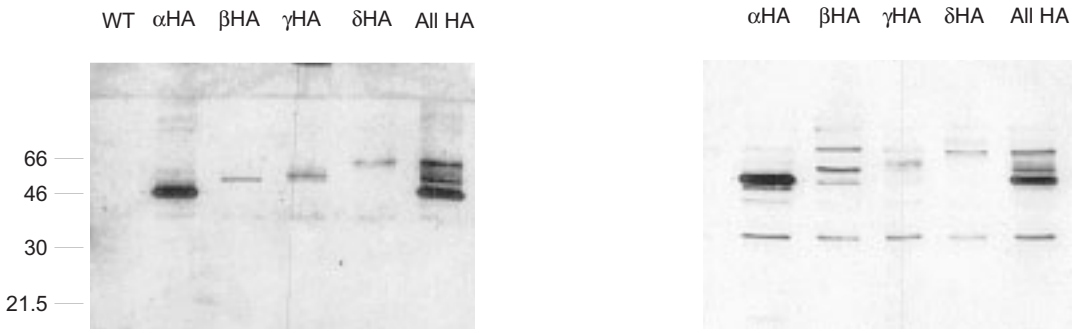

Figure 3.12 Epitope-tagged nAChR subunits isolated from the oocyte membrane and subjected to Western blotting with anti-HA antibody. Subunit which contains the HA tag is indicated above each lane. Note significantly more intense staining of alpha subunits. Left: Fraction 5 from sucrose step gradient subsequent to whole-cell homogenization. Right panel: Protein isolated by physical dissection of oocyte plasma membrane. The non-specific staining in the βHA lane was not typical.

The combination of these techniques to isolate membrane proteins and the use of the HA epitope thus proved satisfactory for visualization of proteins containing unnatural amino acids. It should be noted that staining of non-alpha subunits by the HA.11 antibody is considerably less intense, a phenomenon which is ill-understood but highly

reproducible. Given receptors which may be detected by Western blotting, the analysis of photo-cleavage appeared very straightforward.

Oocytes were irradiated with light of the appropriate wavelength, and whole-cell currents were measured to ascertain whether or not photolysis had occurred. Cells for which current reduction was observed were collected and their membranes harvested for Western blot analysis. In comparison to control oocytes which had not been irradiated, no differences were ever observed. (Figure 3.12)

Figure 3.13 Western blotting of suppressed nAChR βHA L9'TAG and effects of irradiation on Npg-suppressed oocytes. Left panel: Demonstration of suppression at β9'TAG. *Lane 1:* Uninjected. *Lane 2:* mRNA + tRNA-dCA. *Lane 3:* mRNA + tRNA-Val. *Lane 4:* βHA standard. Nine oocytes per lane. Right panel: Effect of irradiation of membrane fraction 3 from oocytes expressing nAChR suppressed with Npg at β9'. *Lane 1:* Irradiated. *Lane 2:* non-irradiated. Four oocytes per lane, whole-cell irradiation for 4 hr at 0 °C.

The explanation for this inability to detect protein fragmentation in response to irradiation remains very unclear. A number of factors complicate the ability to correlate the intensity of bands on the gel to the electrophysiologically observable effect of photolysis.

3.2.4.3 Read-through gives background current and gel bands

It seems evident that there is some read-through of stop codons, as full-length epitope-containing proteins may readily be detected in oocytes co-injected with

uncharged tRNA. The degree to which read-through is observed is rather variable, as may be seen by comparing the relatively light band intensity in Figure 3.13 with the currents observed in oocytes injected with uncharged tRNA in Figure 3.14. Indeed, during the course of these studies, an extremely surprising observation was made. As indicated earlier, the co-injection of mRNA with non-aminoacylated tRNA is a routine null control. These tRNA's are ligated to dCA, so that they are treated in exactly the same way as charged tRNA's. Typically, this 76 nt tRNA-dCA gives much larger currents than mRNA injected alone, but much smaller currents than in cells injected with aminoacylated tRNA carrying a natural or unnatural amino acid. In attempting to identify the source of full-length read-through protein, tRNA which had not been ligated to dCA (i.e. 74 nt tRNA missing the critical CCA motif found at the 3' end of all tRNA) was co-injected with mRNA containing a stop codon. To our great surprise, this 74mer produced larger currents than tRNA-dCA, although still much smaller than those from oocytes injected with charged tRNA. A comparison of a number of tRNA constructs was made. (Figure 3.14)

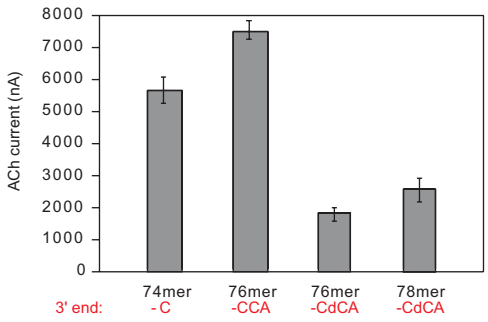

Figure 3.14 Whole-cell currents resulting from the co-injection nAChR mRNA containing β9'TAG with indicated truncated and full-length tRNA.

Eukaryotic tRNA is, in fact, synthesized as a truncated transcript to which the final C, C, and A nucleotides are added by the cytosolic CCA nucleotidyl transferase. The *Xenopus*

isoform has recently been identified.[43] Thus, the 74mer tRNA may well be modified to produce a translationally competent full-length (though uncharged) tRNA. It is presumably this activity which accounts for the ability of the 74mer to produce full-length protein, although it should be noted that no explanation has yet been offered for the exact mechanism of tRNA-mediated read-through.

3.2.4.4 Attempts to eliminate background current by removal of un-ligated 74mer

The fact that 74mer was capable of giving rise to such current led us to the hypothesis that background current in suppression experiments could be eliminated if unreacted 74mer tRNA could be removed after enzymatic ligation of dCA to the 74mer tRNA. The efficiency of this ligation reaction was thought to be on the order of 75%, from the ratio of stained bands corresponding to full-length aminoacylated and 74mer tRNA on sequencing gels. Thus, even when charged tRNA was being injected, a significant amount of 74mer was introduced into the oocyte. Removal of unreacted tRNA was attempted in two ways. First, the vicinal diol of adenine ribose from unreacted dCA was oxidized with periodate. Numerous studies have shown that treating uncharged tRNA with periodate abrogates its ability to function in translation.[44,45] Second, the enzyme polyA polymerase was used in an attempt to add a string of A's to any unreacted tRNA, while charged tRNA would be substitutionally inert.[45,46] It was thought that these polyA tRNA's could then be removed easily using oligo-dT beads, which are traditionally used to capture polyadenylated mRNA from transcriptionally active cells. Neither of these treatments had a significant effect on the electrophysiology of oocytes injected with tRNA subjected to the treatments. One gel showed apparent addition of polyA, although there was little change in the electrophysiology. (Figure 3.) These methods may be

largely irrelevant in light of more recent studies which suggest that the ligation reaction conditions may be modified in such a way as to drive the ligation reaction to completion.[47]

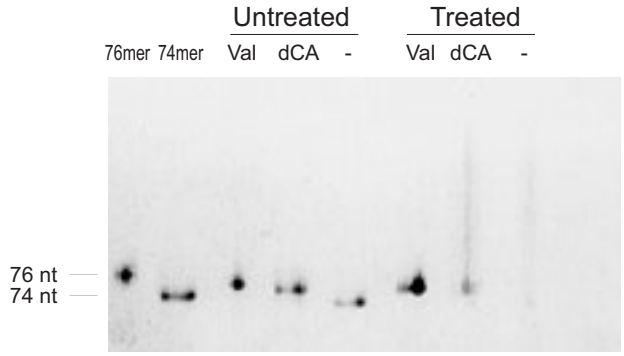

Figure 3.15 SDS-PAGE of ligated and un-ligated tRNA's treated with polyA polymerase subsequent to T4 ligase reaction.

3.2.4.5 Attempts to eliminate background current by tRNA modification

In order for un-ligated tRNA to generate read-through currents, it seems likely that the tRNA must be completed by the nucleotidyl transferase mentioned above. Modifications of the T-loop of tRNA have been reported to compromise the ability of these enzymes to recognize and transfer the final C and A nucleotides to the 3' end of tRNA.[48] TH73G tRNA was accordingly prepared with a G57C mutation. This tRNA was synthetically charged in the usual way by ligation to dCA-Val. Read-through current was indeed dramatically reduced, along with current from suppression. It appears that these mutations may also disrupt ribosome-tRNA interactions, such that the mutant tRNA's are no longer translationally competent.

3.2.4.6 Anomalous subunit trafficking

Another surprising observation which resulted from studies on gel bands resulting from read-through has to do with the fate of nAChR subunits injected alone. The

conventional belief is that single subunits are translated in the ER, but that assembly is required for proper trafficking to the cell surface. Indeed, numerous studies with mammalian cells in culture form the basis for this belief.[49,50] Experiments in oocytes injected with single epitope-tagged subunits suggested that oocytes may be more promiscuous in their trafficking. Harvesting of membranes from such oocytes followed by Western blotting invariably led to detection of the subunits in the membrane fraction. (Figure 3.16)

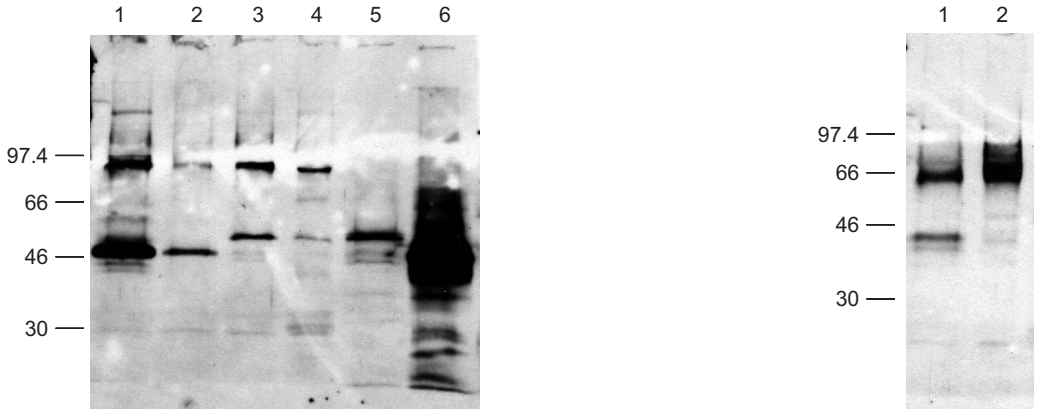

Figure 3.16 Stripped membranes from oocytes expressing HA-tagged subunits either alone or in the full receptor. Left panel: α and β subunits. *Lane 1:* αHA – nAChR. *Lane 2:* αHA only. *Lane 3:* βHA – nAChR. *Lane 4:* βHA only. *Lane 5:* βHA standard. *Lane 6:* αHA standard. Right panel: γ subunit. *Lane 1:* γHA – nAChR. *Lane 2:* γHA only.

It should be noted, of course, that it is extremely difficult to guarantee that a membrane preparation is pure. Interior membranes, scaffolding proteins, and cytoskeletal elements all adhere tightly to the plasma membrane. It is clear during the dissection process that significant amounts of cytosolic tissue are removed along with the fused plasma and vitelline membranes. This difficulty in obtaining pure surface membrane preparations is also a possible confounding variable in attempts to detect photoinduced cleavage of receptors. Although the irradiating light undoubtedly penetrates the oocyte surface to a significant extent (consider the wavelength of 300 nm

light relative to the 3 nm plasma membrane), these sub-surface receptors may not contribute to the observed electrophysiological effects. The apparent cleavage of receptors that is detectable by a loss of whole-cell current may represent only a small fraction of the total receptor protein observed on the gel. Although this does not explain why irradiated sub-surface protein is not photo-cleaved, it does perhaps suggest an explanation for the discrepancy between the electrophysiological result and the result by biochemical analysis.

3.2.4.7 Techniques for harvesting plasma membrane proteins

In an attempt to isolate the surface proteins which were responsible for the measurable electrophysiological change observed upon photolysis, a number of surface-isolation procedures were attempted. The most typical method of this nature is to modify cell-surface proteins with an impermeant reagent, such as an amine-reactive biotin analog. Then, isolation by streptavidin should yield only proteins which were on the surface to be so modified. Indeed, a biotin-based method for detecting oocyte surface expression has been reported.[51] This technique was used apparently successfully, although it gave no better results than manual dissection in terms of visualizing cleavage. (Figure 3.17)

Another surface isolation technique which appeared to be useful was the treatment of the oocytes themselves with antibody, followed by immediate immunoprecipitation.[52] (Figure 3.18) Again, this technique did not allow us to observe fragmentation.

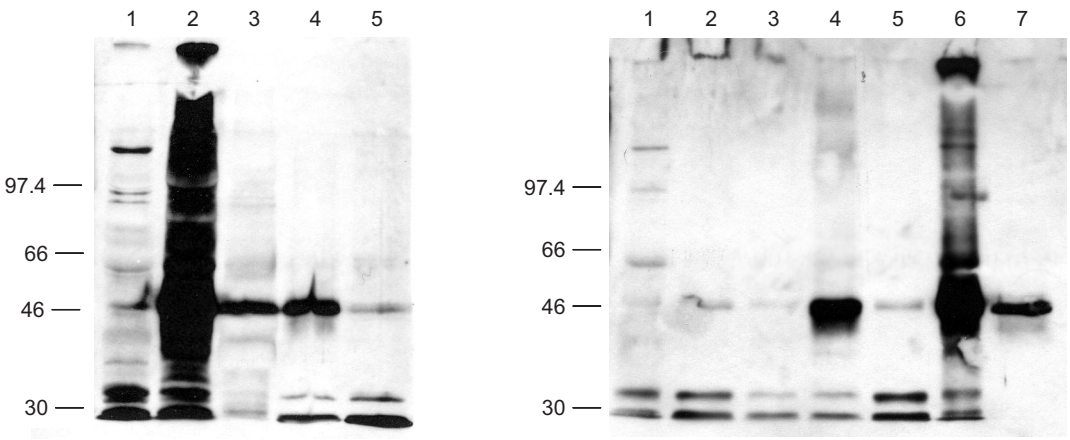

Figure 3.17 Isolation of surface proteins by treatment of oocytes with NHS-biotin followed by streptavidin beads. Left panel: Comparison of whole oocyte, dissected membranes, and streptavidin beads. *Lane 1:* Uninjected – total membranes. *Lane 2:* αHA – total membranes. *Lane 3:* αHA – dissected plasma membrane. *Lane 4:* αHA – streptavidin beads. *Lane 5:* Uninjected – streptavidin beads. Right panel: Capture with streptavidin after surface biotinylation. *Lane 1:* Uninjected – no biotinylation, no beads. *Lane 2:* Uninjected – beads only, no biotinylation. *Lane 3:* Uninjected –biotinylation, beads. *Lane 4:* αHA – biotinylation, beads. *Lane 5:* αHA – beads only, no biotinylation. *Lane 6:* αHA – no biotinylation, no beads. *Lane 7:* αHA standard.

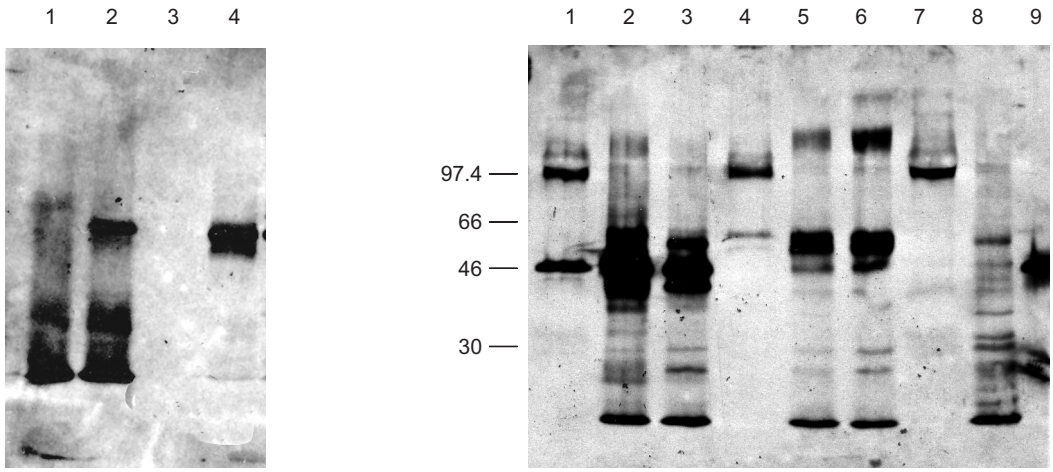

Figure 3.18 Isolation of surface proteins by treatment of whole oocyte with antibodies, followed by recovery with Protein G-sepharose beads. Left panel: Establishing methodology. *Lane 1:* Oocyte homogenate treated with PGS beads. *Lane 2:* Antibody-treated homogenate treated with PGS beads. *Lane 3:* Mab210 and beads only (no oocyte homogenate). Right panel: Testing surface antibody treatment with intra- and extracellular epitope tags. *Lane 1:* αHA – dissected membranes. *Lane 2:* αHA – surface recovery with Mab210. *Lane 3:* αHA – surface recovery with HA.11. *Lane 4:* γ497HA – dissected membranes. *Lane 5:* γ497HA – surface recovery with Mab210. *Lane 6:* γ497HA – surface recovery with HA.11. *Lane 7:* Uninjected – dissected membranes. *Lane 8:* Uninjected – surface recovery with HA.11. *Lane 9:* αHA standard.

3.2.4.8 Use of immunoprecipitation to increase signal strength

Various immunoprecipitation protocols were used and/or developed, for two reasons. First of all, we felt that we could use the techniques to concentrate the protein. Secondly, we were concerned that perhaps the cleaved fragments were being preferentially lost during membrane isolation. Photolysis of Npg-containing proteins captured on beads would allow us to both irradiate a large number of proteins in a very small area and also to analyze beads and supernatant directly after irradiation, to minimize any possibility of protein loss. As with the isolation of cell-surface proteins, we found that we were able to immunoprecipitate suppressed nAChR, but this isolation did not allow us to detect any effect of photolysis. (Figure 3.19)

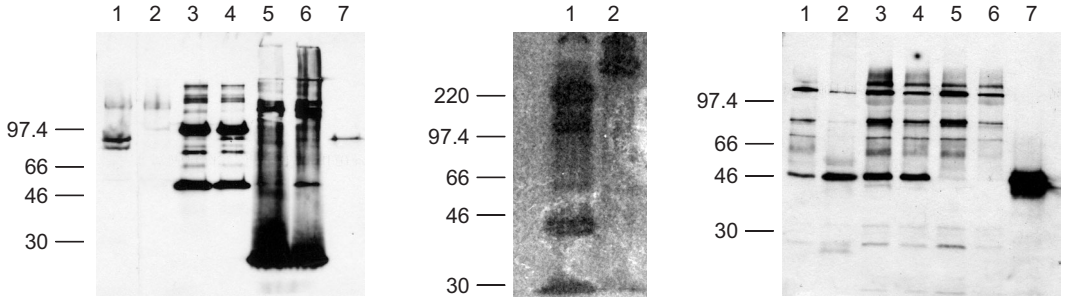

Figure 3.19 Immunoprecipitation protocols. Left panel: Immunoprecipitation from oocyte homogenate with Mab210 and HA.11 affinity matrix, followed by Western blot with HA.11. *Lane 1:* αHA, IP protocol without antibody. *Lane 2:* Uninjected oocytes, IP protocol without antibody. *Lane 3:* Uninjected, Mab210 IP. *Lane 4:* αHA, Mab210 IP. *Lane 5:* Uninjected, IP with HA affinity matrix. *Lane 6:* αHA, IP with HA affinity matrix. *Lane 7:* αHA standard. Protein was eluted from the affinity matrix with HA peptide. Note the very small amounts of recovered αHA relative to antibody. Middle panel: Metabolic labeling with ^{35}S-Met followed by immunoprecipitation with HA.11. *Lane 1:* αHA, IP with HA.11. *Lane 2:* αHA, dissected membranes. Right panel: IP with HA.11 followed by Western with biotinylated HA.11 and streptavidin-HRP. Also, testing the effect of SDS on membrane dissection. *Lane 1:* αβγδHA, dissected membranes. *Lane 2:* αβγδHA, IP with HA.11. *Lane 3:* αHA, dissected membranes (using SDS). *Lane 4:* αHA, dissected membranes (without SDS). *Lane 5:* αHA subunit injected alone, dissected membranes (with SDS). *Lane 6:* αHA subunit injected alone, dissected membranes (without SDS).

3.2.4.9 In vitro photolysis experiments

Ultimately, protein containing Npg was generated from *in vitro* translation and irradiated under non-physiological conditions. The results from oocytes gave us confidence that we could detect suppressed protein by Western blotting. Even if we were unable to recover cleaved protein from oocytes, we felt we should be able to make the protein, irradiate it, and see that it gave rise to two bands on the gel. Even this elementary experiment failed, however. The primary technical difficulty was a general loss of protein upon photolysis. Even recovery of wild-type protein was significantly and adversely affected by photolysis in the arc lamp. Pre-coating of the Eppendorf tubes in which irradiation was taking place failed to ameliorate this problem. Both BSA and coatings such as silicone and polylysine were tested, with negative results. In spite of the reduction of protein levels, it was obvious nonetheless that a band corresponding to cleaved protein was not appearing in the photolyzed samples. It was hypothesized that the alpha-keto acid formed as a photoproduct from the C-terminal cleavage fragment was perhaps susceptible to attack and thus cross-linking by nucleophilic residues on the N-terminal fragment. Photolysis in the presence of nucleophilic scavengers such as semicarbazide was attempted, again with negative results.

3.2.4.10 Cross-linking as a positive control for detecting chemical modification

The final kind of experiment that was attempted was a positive control to demonstrate that some chemical modification of any kind could be observed with suppressed proteins. A brief and unsuccessful attempt was made to treat oocytes with trypsin, to provide evidence that cleaved proteins could be isolated and detected from oocytes. More thorough experiments were performed, using chemical cross-linking as the positive

control for detectable chemical modification. In these experiments, the results of Schmalzing *et al*. on nickel bead-captured 7His-containing nAChR were used as a model.[53,54] Constructs were generated containing the C-terminal 7His tag and the HA epitope in the M3-M4 loop. Subsequent to capture on nickel-NTA agarose beads, protein was treated with DMS, the cross-linking reagent employed by Schmalzing.[53] This experiment gave decidedly mixed results. Higher-molecular weight density was observable in the treated lanes, but under no circumstances were we able to reproduce the discrete bands seen in the reported work.[53] (Figure 3.20)

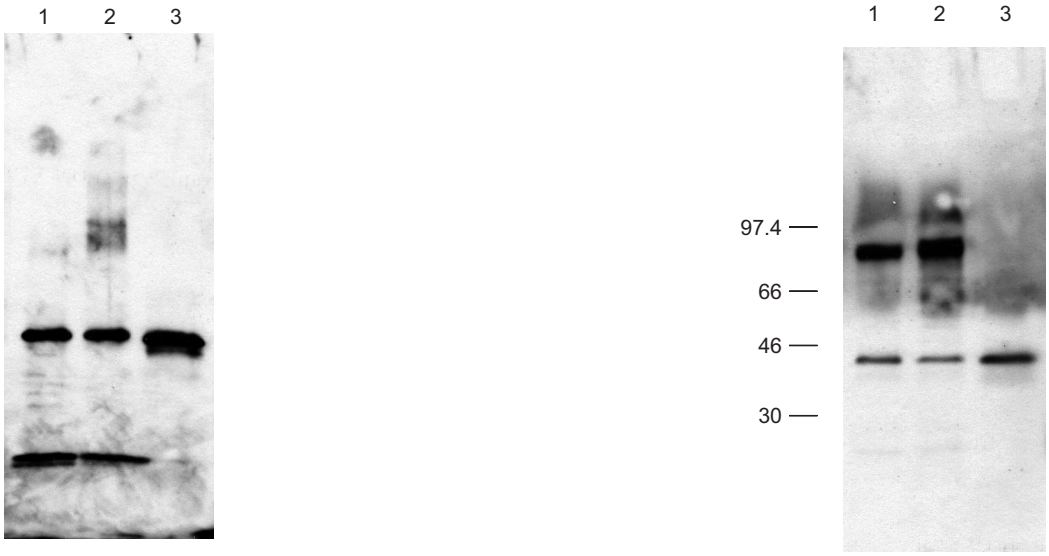

Figure 3.20 Results from treatment of oocytes and nAChR captured on Ni-NTA with the cross-linking reagent DMS. Left panel: Treatment of nAChR captured on beads with DMS, as in the procedure of Schmalzing.[53] *Lane 1:* αHA untreated. *Lane 2:* αHA treated with DMS. *Lane 3:* αHA standard. Right panel: Western blot showing the lack of higher-MW bands from membranes dissected from DMS-treated oocytes. *Lane 1:* αHA untreated. *Lane 2:* αHA treated with DMS. *Lane 3:* αHA standard.

The only substantive difference we could identify between the two experimental protocols was the fact that we were using immunological detection, whereas their protocol called for metabolic labeling with ^{35}S. Oocytes were accordingly labeled, with more or less identical results to our Western blots. Higher molecular-weight density

could be again discerned but not as discrete bands. Another report whose results we were unable to replicate was Hucho's treatment of oocytes with DMS.[55,56] In their experiment, they observed a reduction in whole-cell current upon treatment of oocytes with DMS.[56] In our initial experiments, the treatment had no effect at all, either electrophysiologically or by SDS-PAGE. (Figure 3.20)

A number of different cross-linkers and conditions were used during the course of these experiments. Many of them gave encouraging results, but it was also observed that artifactual aggregation which persisted during standard reducing SDS–PAGE conditions could arise from certain purification steps. (Figure 3.21)

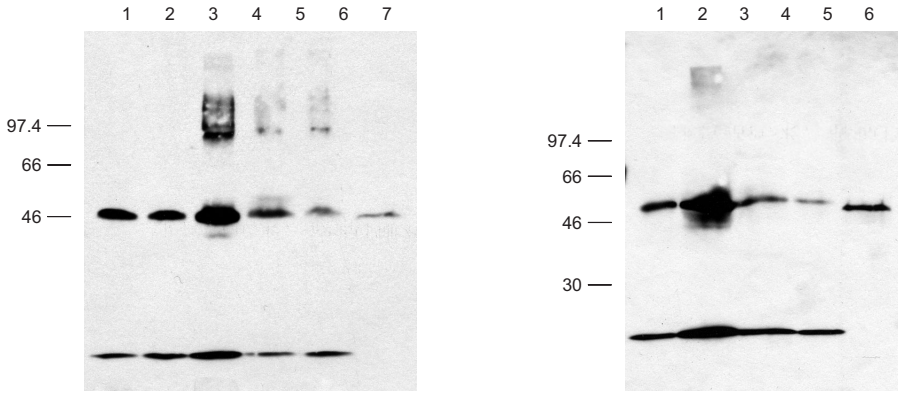

Figure 3.21 Apparent cross-linking is shown to be artifactual by heating gel samples prior to loading. Left panel: Investigation of Ni-NTA recovery protocol and treatment of captured protein with photo-crosslinking reagents. Oocytes were injected with 500 pg total mRNA containing alpha subunits that have both HA and 7His tags. *Lane 1:* Usual Ni-NTA protocol. *Lane 2:* Second imidazole elution from beads in usual protocol. *Lane 3:* Washing and elution of beads using a spin column. *Lane 4:* Treatment of captured protein with DASD. *Lane 5:* Treatment of captured protein with SANPAH in DMSO. *Lane 6:* αHA standard. Right panel: Same samples as left panel, except treated by heating to 100 °C for 10 min.

Collecting and washing Ni-NTA beads by low-speed centrifugation in fritted Eppendorf tubes is a very convenient procedure which results in high yields of protein. However, it appeared to induce aggregation, which could be alleviated by heating samples prior to loading. Apparent cross-linking with covalent reagents was thus also

revealed to be artifactual. As this effort to achieve cross-linking was somewhat peripheral to our interests, it was not pursued further.

3.2.4.11 Ni-NTA purification as a general technique

However, the ability to isolate pentameric nAChR by nickel-mediated capture of receptors containing a C-terminal 7His tag is potentially useful for a variety of biophysical studies. An experiment was performed to determine where receptors isolated from both oocyte homogenate and dissected membranes in the presence of the detergent β-dodecylmaltoside (DDM) maintain their inter-subunit contacts.[13] Oocytes were injected with a mixture of alphaHA and alpha7His subunits. The capture protocol should pull down only those receptors with a 7His tag, whereas the Western blotting detection protocol should only detect those with the HA tag. If the alpha subunit may de detected in a Western blot, the implication is that the two alpha subunits are captured as a non-covalent complex.

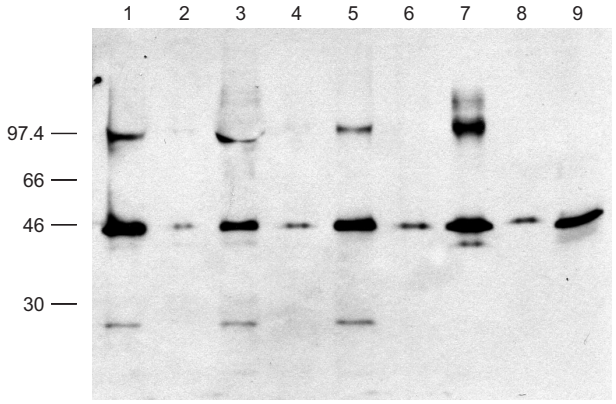

Figure 3.22 Determination whether dissection and Ni-NTA capture protocols with a variety of detergents maintain nAChR in its pentameric form. *Lane 1:* αHA:α7H – dissected membranes, no detergent. *Lane2:* αHA:α7H –Ni-NTA, no detergent. *Lane 3:* αHA:α7H – dissected membranes, with DDM. *Lane 4:* αHA:α7H – N-NTA, with DDM. *Lane 5:* αHA:α7H – dissected membranes, with SDS. *Lane 6:* αHA:α7H – Ni-NTA, with SDS. *Lane 7:* αHA:α7H – oocyte homogenate, Ni-NTA, DDM. *Lane 8:* αHA/7H – positive control, where alpha subunits contain both HA and 7His tags, Ni-NTA, SDS. *Lane 9:* αHA standard.

The results of this experiment imply that the pentamers remain intact in the presence of DDM, consistent with other studies on multi-subunit integral membrane proteins.[13] (Figure 3.22) In our work, SDS also appeared to maintain the intact receptor. The Ni-NTA isolation protocol was performed on dissected membranes, except in one case where it was carried out homogenized oocytes (Lane 7). In all cases, Ni-NTA results in a more pure sample, but one where the signal is correspondingly diminished. The negative control, where non-His tagged subunits are used, generally results in very little background, but there is also frequent variation between batches of oocytes, and such a control in this experiment is probably necessary to support the conclusion that the nAChR remains intact during isolation. However, the results are encouraging. In addition, techniques which only require the labeled subunit to be isolated have been carried out with these constructs in the work of John Leite.[57] Whether or not Ni-NTA purification will provide a means of purifying suppressed receptors remains to be seen.

3.2.5 Conclusions from non-alpha Npg cleavage

In summary, cleavage of proteins containing Npg was never able to be directly observed by PAGE. However, the whole-cell current of oocytes expressing nAChR with Npg in non-alpha Cys loops was reproducibly reduced to the level of dCA current. In the absence of biochemical evidence on cleavage, we were unable to determine whether this effect corresponds to 90% cleavage of Npg-containing receptors, with nAChR arising from read-through accounting for the residual current; or 50% cleavage of Npg-receptors, with un-cleaved receptors accounting for the remainder of the current.

One experiment which may shed light on this question was the determination of the dose-response pre- and post-photolysis. A change in the EC_{50} of the receptor may imply

that receptors have been affected by photolysis, as we had already shown that the read-through currents had the same EC_{50} as wild-type receptors. In fact, the EC_{50} values of receptors containing Npg in non-alpha Cys loops is identical before and after photolysis, even in cells where a 50% reduction in whole-cell current was observed. (Figure 3.23)

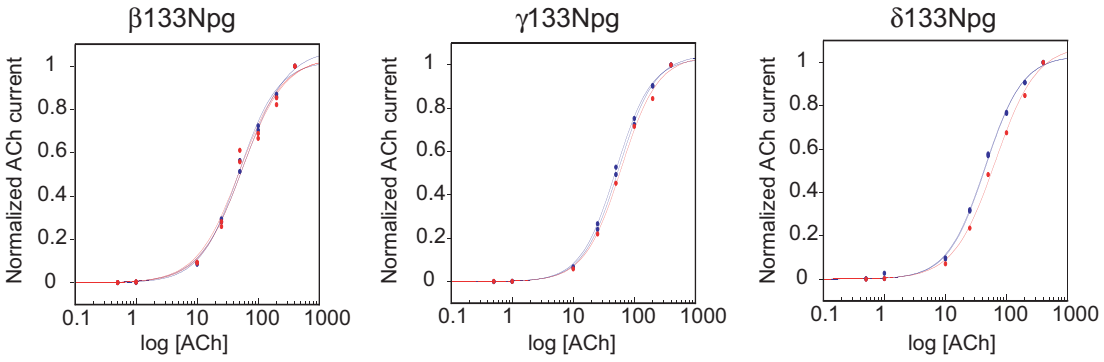

Figure 3.23 Dose-response relations for oocytes expressing nAChR suppressed with Npg in the indicated position, fit to the Hill equation. Photolyzed oocytes are indicated in red and un-photolyzed cells by blue.

Thus, interpretation of the results obtained by the photolysis of receptors containing Npg in non-alpha Cys loops remains difficult. A number of useful biochemical techniques were developed during the course of the study, including the use of epitope tags, methods for isolation of suppressed receptors from oocytes, detection of suppressed receptors in Western blots, immunoprecipitation in oocytes, *in vitro* translation of suppressed proteins using wheat germ extract, cell-surface labeling of oocytes, and purification of suppressed proteins by Ni-NTA.

3.3 Site-specific photocrosslinking with Bpa

3.3.1 Introduction to site-specific crosslinking

Both the difficulties in structurally characterizing membrane proteins and the large number of stoichiometries available to neuroreceptors have been mentioned above. In

addition, a great deal of active research is directed toward understanding the modulation of ion channel activity by protein-protein interactions, the targeting of ion channels to the cell surface by cytoskeletal interactions, and the localization of channels to membrane rafts and the proteins associated with them.[58-60] A general technique to identify the interaction partners of ion channel subunits would be of great utility. In addition, the ability to identify regions of a particular protein or subunit which constitute an interaction domain or protein-protein interface would be valuable for relating the primary sequence of a protein to the structure-function relationships inherent in its domain organization.

A number of photoactive functional groups have been employed in the design of photo-crosslinking reagents. The most common types, aryl azides, diazirines, and benzophenone-based molecules have been reviewed.[61] The various chemistries have advantages and disadvantages and are appropriate for different contexts. Experiments using diazirines introduced by nonsense suppression played an important part in establishing the role of the translocon in membrane protein synthesis.[62,63] However, some work performed here and elsewhere suggested that benzophenone-based residues may incorporate more efficiently under the conditions used in our laboratory.[2,64] In collaboration with Justin Gallivan, who had previously prepared dCA-Bpa, the work described here was carried out using 4-benzoylphenylalanine (Bpa).[64] (Figure 3.24)

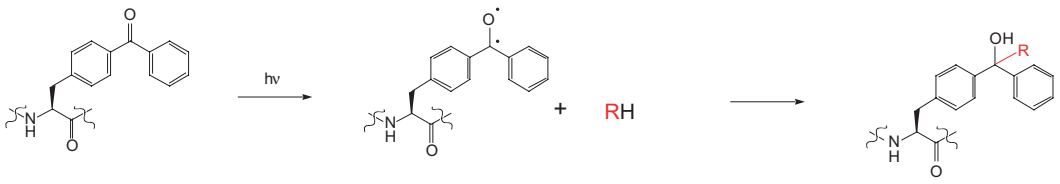

Figure 3.24 Schematic of the cross-linking chemistry of benzoylphenylalanine (Bpa). Irradiation of the residue leads to a biradical, which abstracts hydrogen from a neighboring side chain. The resulting covalent linkage may be an intrasubunit crosslink, or if the residue is interfacial, an intersubunit linkage.

Suppression was attempted with the photoactive residue in every position in the Cys loop of the gamma subunit of the nAChR. As indicated earlier, the belief at that time was that the Cys loop constituted a portion of the intersubunit interface. The position of gamma between the two alpha subunits was seen as desirable, in that cross-linking to alpha seemed probable. In addition to the fact that the stoichiometry of the receptor makes labeling both alpha subunits with the HA epitope tag trivially easy, it is also the case that the sensitivity of alphaHA in Western blots is higher than that of other subunits.

After introduction of the Bpa residue, the oocytes were tested for expression in the standard two-electrode voltage clamp configuration. Suppression was achieved at a number of sites, although several never gave appreciable current over background levels. (Figure 3.25) Additional data on the suppression efficiency is available.[64]

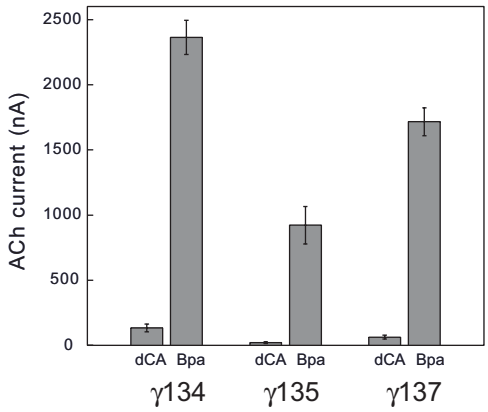

Figure 3.25 Suppression of Bpa at selected sites which gave good expression in the nAChR gamma Cys loop. Mean whole-cell currents (±SEM) are indicated.

Oocytes giving measurable whole-cell currents were then photolyzed in batches for four hours, using the same conditions as employed for Npg cleavage. After photolysis, the oocytes were recorded from. In addition, the membranes were dissected away and analyzed for high-molecular weight products arising from cross-linking between the alpha and gamma subunits. Both of these studies were in all cases negative. No

electrophysiological effects were ever observed to arise from photolysis. Nor were higher-molecular weight bands ever observed in Western blotting. (Figure 3.26)

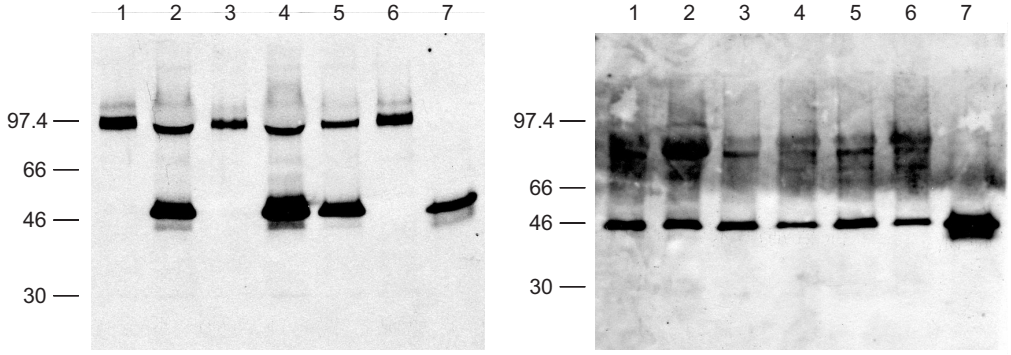

Figure 3.26 Western blotting from irradiated oocytes containing Bpa at a variety of sites in the gamma Cys loop, showing the lack of detectable cross-linking. Left panel: Irradiation of oocytes containing nAChR γ129Bpa followed by dissection of plasma membranes. *Lane 1:* Uninjected oocytes. *Lane 2:* γ129 Bpa. *Lane 3:* Uninjected, photolyzed 4 hr. *Lane 4:* γ129 Bpa, photolyzed 4 hr. *Lane 5:* γ129 Bpa, photolyzed in arc lamp. *Lane 6:* Uninjected, photolyzed in arc lamp. *Lane 7:* αHA standard. Right panel: Irradiation of oocytes containing nAChR γ134-137Bpa followed by dissection of plasma membranes. *Lane 1:* γ134 Bpa. *Lane 2:* γ134 Bpa, 4 hr hν. *Lane 3:* γ135 Bpa. *Lane 4:* γ135 Bpa, 4 hr hν. *Lane 5:* γ137 Bpa. *Lane 6:* γ137 Bpa, 4 hr hν. *Lane 7:* αHA standard.

Thus, although site-specific cross-linking remains an attractive use of unnatural amino acid mutagenesis, Bpa incorporation in the Cys loop of gamma appears in hindsight to have had little chance of success. The crystal structure of AChBP shows the Cys loop to be rather ill-positioned for intersubunit crosslinking.[65] (Figure 3.27) However, the sequence of this loop is very different from the highly conserved Cys loop sequence found in the family of ligand-gated ion channels, so it is possible that the AChBP is not a reliable indicator of the position of the Cys loop in the full receptor.

Figure 3.27 Two views of the AChBP crystal structure, showing the location of the Cys loop, in red.[65] Left panel: View from what would be the intracellular side of the receptor, if the AChBP contained transmembrane domains. Right panel: View from the side of the protein, where the Cys loops would contact the membrane in a true receptor. One subunit is rendered in dark gray to emphasize the subunit interface.

It may be the case also that the project suffers from a fundamental difficulty, namely, that introducing unnatural amino acids into interfacial regions of proteins is intrinsically destabilizing. This problem could potentially be surmounted by making a longer linker between the peptide backbone and photoactive functional groups in the side chain. Alternatively, serial incorporation of the unnatural amino acid into a contiguous sequence may be able to identify those sites where substitution of the natural side chain for the large hydrophobic Bpa residue is tolerated. Now that a crystal structure exists for the highly homologous AChBP, it may be possible to rapidly determine whether or not inter-subunit cross-linking may be realized with Bpa. In addition, the advent of mass spectrometry from ion channels expressed in oocytes raises the possibility that a more sensitive assay than Western blots may be employed.[57] Success of these proof-of-principle experiments could then justify a more intensive attempt to identify interfacial regions in less well-characterized channels using site-specific photocrosslinking. Thus, the efforts reported here should only be considered as the pioneering stage of a the project and were carried out using what may prove to be highly inaccurate structural assumptions.

3.4 Using hydroxy acids to determine Cys-Cys connectivity of the $P2X_2$ receptor

3.4.1 Experimental design

The unnatural amino acid Npg allows the protein backbone to be site-specifically cleaved in a functioning protein. Compared to this, it may appear that the ability to site-specifically cleave a polypeptide subsequent to isolation of the protein is a rather paltry achievement. However, site-specific cleavage of isolated proteins is a useful technique for solving a particular topological problem. The three-dimensional connectivity of a protein backbone is complicated by the existence of side chain-mediated contacts, namely the disulfide bonds between cysteines. In the absence of three-dimensional structural data, there is no way of knowing which cysteine in a primary sequence may be bonded to another. However, a technique developed by Pam England in this laboratory provides a means whereby site-specific cleavage may be used to determine this connecticity.[4] In this methodology, incorporation of hydroxy acids is used to introduce a specific site between selected cysteine residues where the backbone is base-labile.[3,4] (Figure 3.28)

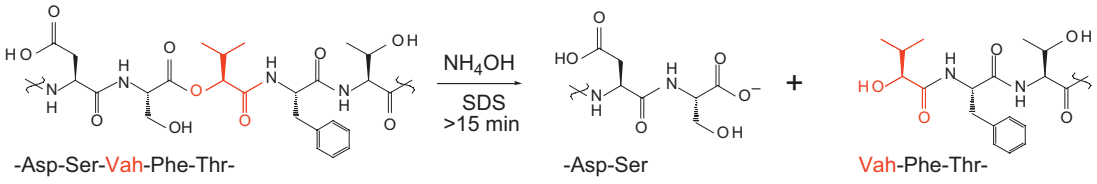

Figure 3.28 Schematic showing how introduction of a hydroxy acid (red) into the protein backbone creates a base-labile linkage.

In general, when a cleavable residue is placed between two disulfides and the protein is cleaved, two outcomes are possible. If the cysteines do not form a disulfide, the protein will be cut in two. If the side chains are connected by a disulfide bond, however, the backbone will be cleaved but the two halves of the protein will remain attached by the

covalent bond between side chains. This difference is easily observable by PAGE. Additional information may be obtained by treatment with reducing agents during electrophoresis. If disulfide-reducing agents are present, the disulfide-bonded halves will separate into two fragments, confirming that backbone cleavage has occurred. (Figure 3.29)

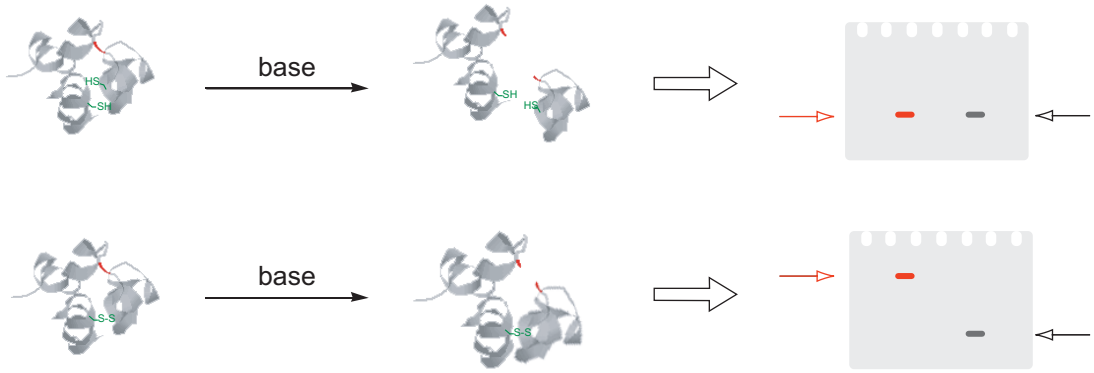

Figure 3.29 Schematic showing how site-specific backbone cleavage may be used to determine the disulfide connectivity of a protein.[4] Targeted inter-cysteine backbone cleavage is followed by comparison of SDS-PAGE mobility in the presence and absence of disulfide reducing agents . The gel mobility of the cleaved protein reveals whether or not the cysteines on either side of the cleavage site are in a disulfide. Red arrows indicate treatment with both base and reducing agent. Black arrows indicate treatment with base alone in the absence of reducing agent.

It has been relatively recently appreciated that disulfides provide small proteins the opportunity to create highly stable scaffolds. A number of disulfide knot toxins have recently been discovered, such as the snail-derived conotoxins.[66,67] These small peptides are able to form a relatively rigid binding domain with excellent complementarity to the extracellular domains of ion channels. The paralytic ability of conotoxins arises because of this binding, which inhibits the nicotinic receptors that motoneurons rely upon to turn synaptic signals into muscle movement. However, toxins are not the only proteins to rely upon disulfides to scaffold binding domains. The primary structure of P2X channels has

recently been determined and has shown these receptors to be extremely cysteine-rich.[68] (Figure 3.30)

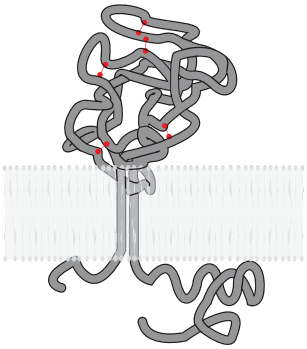

MVRRLARGCWSAFWDYETPKVIVVRNRRLGFVHRMVQLLILLY
FVWYVFIVQKSYQDSETGPESSIITKVKGITMSEDKVWDVEEY
VKPPEGGSVVSIITRIEVTPSQTLGTCPESMRVHSSTCHSDDD
CIAGQLDMQGNGIRTGHCVPYYHGDSKTCEVSAWCPVEDGTSD
NHFLGKMAPNFTILIKNSIHYPKFKFSKGNIASQKSDYLKHCT
FDQDSDPYCPIFRLGFIVEKAGENFTELAHKGGVIGVIINWNC
DLDLSESECNPKYSFRRLDPKYDPASSGYNFRFAKYYKINGTT
TTRTLIKAYGIRIDVIVHGQAGKFSLIPTIINLATALTSIGVG
SFLCDWILLTFMNKNKLYSHKKFDKVRTPKHPSSRWPVTLALV
LGQIPPPPSHYSQDQPPSPPSGEGPTLGEGAELPLAVQSPRPC
SISALTEQVVDTLGQHMGQRPPVPEPSQQDSTSTDPKGLAQL

Figure 3.30 Presumed structure and primary sequence of the ATP-binding receptor $P2X_2$. Extracellular cysteine residues are boxed in red. Sites of stop codon introduction discussed below are indicated with red text.

The predicted 283 aa ATP-binding extracellular region of these channels contains ten cysteine residues. Interestingly, the ATP-binding domain of the P2X receptors has no apparent sequence homology to known ATP-binding folds such as the Walker or Rossman motif.[69-71] So, structural information on the connectivity of the cysteines in the extracellular region of the $P2X_2$ receptor may be a valuable in guide in designing experiments to try to identify where ATP binds.

These experiments were carried out in collaboration with Baljit Khakh, who provided the initial $P2X_2$ constructs. A FLAG epitope was introduced into the receptor at the extreme C-terminus. In these two-transmembrane domain receptors, both termini are intracellular. In addition, he introduced stop codons between all ten cysteine residues. The sites of mutation were chosen based on rules established in the work of England *et al*. for optimal cleavage of hydroxy acids.[3,4] She found that there were sequence context effects on the efficiency of hydrolytic cleavage of hydroxy acids introduced into proteins. The sites chosen in the $P2X_2$ receptor were selected for favorable cleavage. Based on the

work of England, hydroxy acids of valine and alanine were employed for suppression experiments.

Protein isolated from oocytes subsequent to electrophysiological recording was thought to have the best chance of reflecting the native structure of the receptor, an important consideration for an *ex vivo* structural technique. However, it had also been found in the earlier studies of England that protein produced by *in vitro* translation could be valuable for establishing cleavage conditions.[3,4] Whether or not the receptor is being folded correctly in wheat germ extracts may even be determined by comparison to its cleavage behavior relative to that of isolated functional protein.

3.4.2 Results

Initial work in this receptor indicated that the specificity of the FLAG epitope in Western blotting was dramatically inferior to that of the HA antibody. In addition, the overall level expression of the channel was rather low in suppression experiments with hydroxy acids. In order to correct both of these problems, the $P2X_2$ gene was cloned into pAMV and an HA tag inserted at the extreme C-terminus. These changes resulted in increased expression and much better staining in Western blots. (Figure 3.31)

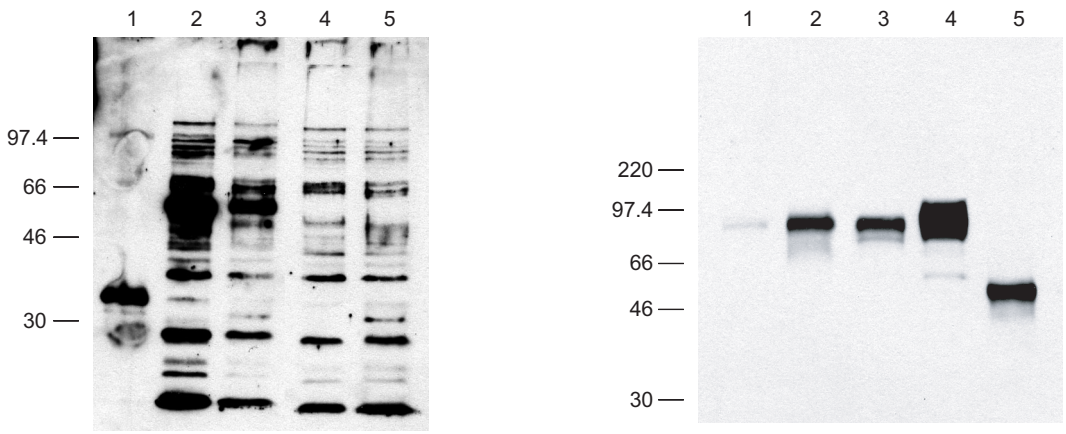

Figure 3.31 Western blot analysis of $P2X_2$ receptors showing the relative efficacy of C-terminal FLAG and HA epitope tags. Additionally, effects of PNGaseF on the receptor are examined, along with potential dominant-negative effects from truncated $P2X_2$ 142TAG. Left panel: Western blot of C-terminally FLAG-tagged $P2X_2$. *Lane 1:* Uninjected, dissected membranes. *Lane 2:* $P2X_2$, wheat germ extract. *Lane 3:* $P2X_2$, wheat germ extract, treated with PNGaseF. *Lane 4:* nAChR αHA/FLAG, wheat germ extract. *Lane 5:* nAChR αHA/FLAG, wheat germ extract, treated with PNGaseF. Right panel: Dissected membranes from oocytes expressing Vah-suppressed $P2X_2$ V142TAG with C-terminal HA tag. *Lane 1:* $P2X_2$ 142TAG, 74mer. *Lane 2:* $P2X_2$ 142TAG, Vah. *Lane 3:* $P2X_2$ 142TAG, mixed with WT $P2X_2$. *Lane 4:* $P2X_2$ wild-type receptor with C-terminal HA. *Lane 5:* αHA standard.

However, two rather knotty problems arose. First of all, wild-type $P2X_2$-HA showed a rather significant mobility shift upon treatment with ammonium hydroxide. (Figure 3.32) This may arise as a result of base-catalyzed hydrolysis of sugars post-translationally added to the receptor. Treatment of isolated wild-type $P2X_2$ with PNGase F, an enzyme which removes *N*-linked glycosylation showed little effect, though, so it may be that *O*-linked sugars or some other base-catalyzed chemistry was responsible for this mobility shift. (Figure 3.31)

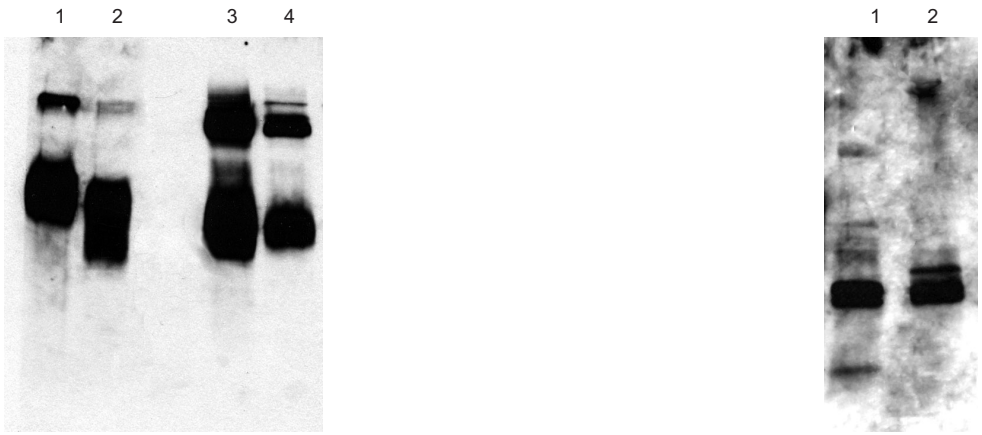

Figure 3.32 Western blot of base-treated $P2X_2$ containing Vah and wild-type residues, and nAChR positive control for ester cleavage. Left panel: Effects of treating Vah-suppressed and wild-type $P2X_2$ with base. *Lane 1:* WT $P2X_2$, treated with NH_4OH and β-ME. *Lane 2:* $P2X_2$ 142Vah, treated with NH_4OH and β-ME. *Lane 3:* WT $P2X_2$, treated with NH_4OH but not β-ME. *Lane 4:* $P2X_2$ 142Vah, treated with NH_4OH but not β-ME. Right panel: Positive control for NH_4OH cleavage and identification of disulfide formation with β-ME, showing cleavage only in the presence of disulfide reducing agent. *Lane 1:* nAChR α131Ser132Vah, treated with NH_4OH and β-ME. *Lane 2:* nAChR α131Ser132Vah, treated with NH_4OH but not with β-ME.

Secondly, incorporation of hydroxy acids worked at very few of the eight inter-Cys positions. (Figure 3.33) This was a surprising result in view of the fact that the amide-to-ester mutation is a rather slight perturbation, that it seemed unlikely that so many of the sites chosen would have represented critical residues to protein function, and that the work of England suggested rather great tolerance to hydroxy acids in the nAChR.[3,4]

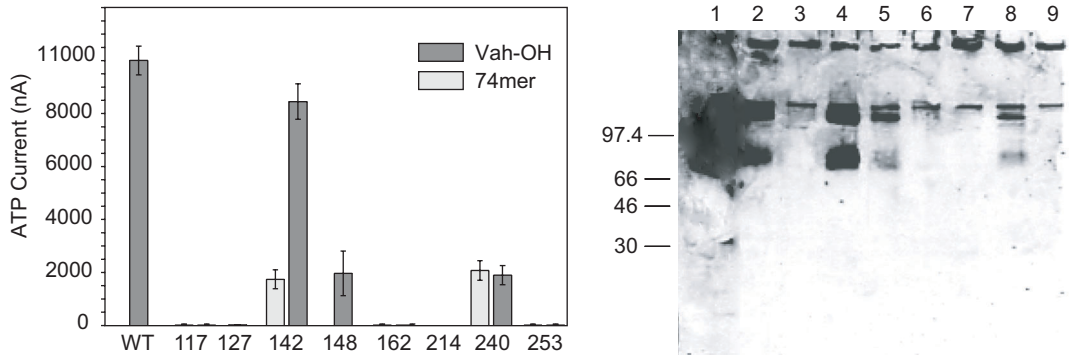

Figure 3.33 Electrophysiological and Western blot analysis showing the relatively low tolerance of $P2X_2$ receptor to incorporation of Vah. Left: Mean whole-cell current (±SEM) for oocytes suppressed with Vah at the indicated inter-Cys position. Right: Western blot of membranes dissected from the Vah-suppressed oocytes shown in left panel. *Lane 1:* WT. *Lane 2:* 117Vah. *Lane 3:* 127Vah. *Lane 4:* 142Vah. *Lane 5:* 148Vah. *Lane 6:* 162Vah. *Lane 7:* 117Vah. *Lane 8:* 240Vah. *Lane 9:* 253Vah.

When compared directly to the wild-type residue, receptors arising from suppression at 142 had somewhat different PAGE mobility. (Figure 3.32) Although the sequencing data from these constructs suggested that the region around the introduced mutation was consistent with the expected sequence, the constructs may well have been faulty. Even if this were the case, however, electrophysiology and Western results confirm that significantly greater current and staining intensity were observed upon supplying the cells with hydroxy acid-charged tRNA. Thus, by all standards currently employed, the hydroxy acid was present in these receptors. In no case was base-induced cleavage observed, however, although altered gel mobility in the presence of base was seen for 142 as well as the wild-type construct. Given the apparent lack of cleavage, a position which gave good cleavage in the nAChR in the earlier work of England was selected for use as a positive control.[3,4] Indeed, cleavage was observed as anticipated. (Figure 3.32)

3.4.3 Future directions

Because of the intractability of the $P2X_2$ system, with both gel mobility of wild-type protein induced by base treatment and no evidence of cleavage in hydroxy acid-containing protein, this line of experimentation was abandoned. Suggestions for the future involve treatment of the receptor with the glycosidase EndoH, which removes both *N*- and *O*-linked sugars, to attempt to resolve the mobility of WT receptor upon base and β-mercaptoethanol treatment. Additional sites of mutation could also be chosen, to determine whether better suppression efficiency might be achievable elsewhere in the receptor.

3.5 Use of photo-labile side chains to induce dynamic conformational change

3.5.1 Experimental design

In the case of Bpa, a photoactive side chain was incorporated for the purposes of cross-linking. Side chains with photo-cleavable protecting groups may also be introduced for the purposes of providing steric bulk which may then be removed by irradiation.[72,73] In this way, a conformational change may be induced experimentally. Typically, this conformational change is rather small, and a sensitive region of the protein is the best site for use of protected side chains for this purpose. Such a region is the gate of an ion channel. As indicated above, a conformational change resulting from binding of a ligand-gated ion channel's agonist is communicated to the gate in the transmembrane regions, resulting in channel opening. In the nAChR, this gate is thought to be near the L9' position.[28,29,31]

In work conducted in collaboration with Ken Philipson, tyrosine and cysteine with the alcohol and thiol, respectively, protected by a nitrobenzyl group, were introduced at the 9' position.[6] (Figure 3.34)

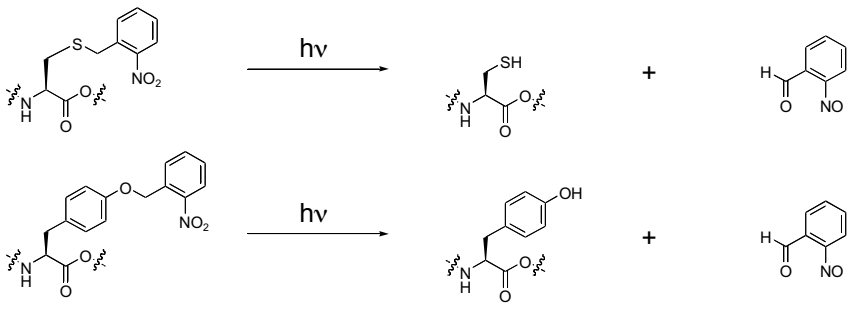

Figure 3.34 Schematic showing photolytic de-caging of Cys(ONb) and Tyr(ONb).

In these experiments, the removal of the protecting group was examined as a possible means of very rapidly controlling channel gating and gaining insight into the temporal mechanics of the gating process.

3.5.2 Results

Suppression in the alpha subunit proved rather inefficient, although better results were obtained in both beta and gamma subunits. Gamma suppression is exclusively considered below. The first observation from application of this technique was that very striking effects of photolysis were immediately evident. (Figure 3.35)

Figure 3.35 Light-induced decaging of Cys and Tyr analogs in the transmembrane region of nAChR γ. Left panel: Light-induced decaging of Cys(ONb). Current was first activated by the application of ACh (20 mM) to an oocyte expressing the ACh receptor. The oocyte had been injected with cRNA coding for wild-type α, β, and δ subunits and for the γ subunit with a Leu260TAG (γ9'TAG) mutation. Suppressor tRNA charged with Cys(ONb) was co-injected. Methanethiosulfonate ethylammonium (MTSEA; 0.35 mM) was included in the bathing medium as indicated. Three pulses of ultraviolet light of 3 s duration each are indicated by arrows. Spikes in current traces are artifacts due to switching of the bathing medium. Right panel: De-caging of Tyr(ONb). Current was activated by the application of ACh (20 μM) to oocytes expressing the ACh receptor. A Leu260TAG mutation was present in the γ-subunit (γ9' position of M2). The stop codon was suppressed by the co-injection of suppressor tRNA charged with Tyr(ONb). Two pulses of UV light of 3 s duration each are indicated by arrows. The current transient induced by the second flash is artifactual, as similar transients were sometimes also seen with the wild-type channel.

With both tyrosine and cysteine, irradiation caused an immediate increase in current. Continued 1 ms pulses of light reveal more and more current, with each flash activating approximately 5% of the available receptors. Detailed kinetic analysis showed that the response to cysteine de-caging was more rapid than could be measured by the apparatus

used. Receptor response to tyrosine de-caging was rather slower, an effect perhaps explained by greater steric perturbation resulting from the larger nitrobenzyl tyrosine residue. Apparently, conformational rearrangement must occur before the channel can respond properly to ligand binding. An alternative explanation might be that the photochemistry is slower for nitrobenzyl tyrosine than nitrobenzyl cysteine, although the efficiency of tyrosine photolysis appears greater than for cysteine.

An additional effect which was observed with tyrosine was that the presence of this residue at the 9'position appeared to greatly enhance ACh open-channel block. A cation-π effect was considered to explain this effect, with the residue being replaced sequentially by Trp and F_4-Trp. In both cases, robust channel block was observed. Substitution of the tyrosine with 4-methyl-tyrosine appeared to abrogate block, however, suggesting that the tyrosyl hydroxyl may have an important role in this effect.

3.5.3 Future directions

The applicability of caged amino acids to transmembrane domains was demonstrated. In order to know whether high-resolution kinetic information could be obtained with these residues, it will probably be necessary to employ rapid electrophysiological techniques, such as single-channel recording. If nonsense suppression is able to be achieved in mammalian cells, it is conceivable that that this technique might be used in situations where ultra-fast control over ion channels is required. Signaling processes associated with conductance could be examined in this way, for example.

As will be seen in the following chapter, caged amino acid side chains may also be used to control certain post-translational modifications. Tyrosine will be considered in depth in this regard in Chapter 4. Numerous processes rely on the modification of

cysteine side chains, such as protein lipidation, and they may be able to be subjected to control by caged cysteine. Thus, the demonstration that this residue is compatible with nonsense suppression is in itself an important precursor to such experiments.

3.6 References

1. England, P. M., Lester, H. A., Davidson, N. and Dougherty, D. A. Site-specific, photochemical proteolysis applied to ion channels *in vivo*. *PNAS* **94**, 11025-11030 (1997).
2. Kanamori, T., Nishikawa, S. I., Shin, I., Schultz, P. G. and Endo, T. Probing the environment along the protein import pathways in yeast mitochondria by site-specific photocrosslinking. *PNAS* **94**, 485-490 (1997).
3. England, P. M., Lester, H. A. and Dougherty, D. A. Incorporation of esters into proteins: Improved synthesis of hydroxyacyl tRNAs. *Tet. Lett.* **40**, 6189-6192 (1999).
4. England, P. M., Lester, H. A. and Dougherty, D. A. Mapping disulfide connectivity using backbone ester hydrolysis. *Biochemistry* **38**, 14409-14415 (1999).
5. Koh, J. T., Cornish, V. W. and Schultz, P. G. An experimental approach to evaluating the role of backbone interactions in proteins using unnatural amino acid mutagenesis. *Biochemistry* **36**, 11314-11322 (1997).
6. Philipson, K. D., Gallivan, J. P., Brandt, G. S., Dougherty, D. A. and Lester, H. A. Incorporation of caged cysteine and caged tyrosine into a transmembrane segment of the nicotinic ACh receptor. *Am. J. Phys. Cell Phys* **281**, C195-C206 (2001).
7. Lopez-Otin, C. and Overall, C. M. Protease degradomics: A new challenge for proteomics. *Nat. Rev. Mol. Cell Biol.* **3**, 509-519 (2002).
8. Ripka, W. C. New thrombin inhibitors in cardiovascular disease. *Curr. Op. Chem. Biol.* **1**, 242-253 (1997).
9. Condra, J. H., Miller, M. D., Hazuda, D. J. and Emini, E. A. Potential new therapies for the treatment of HIV-1 infection. *Ann. Rev. Med.* **53**, 541-555 (2002).
10. Steiner, D. F. The proprotein convertases. *Curr. Op. Chem. Biol.* **2**, 31-39 (1998).
11. Thorsett, E. D. and Latimer, L. H. Therapeutic approaches to Alzheimer's disease. *Curr. Op. Chem. Biol.* **4**, 377-382 (2000).
12. Macfarlane, S. R., Seatter, M. J., Kanke, T., Hunter, G. D. and Plevin, R. Proteinase-activated receptors. *Pharm. Rev.* **53**, 245-282 (2001).
13. Chang, G., Spencer, R. H., Lee, A. T., Barclay, M. T. and Rees, D. C. Structure of the MscL homolog from *Mycobacterium tuberculosis*: a gated mechanosensitive ion channel. *Science* **282**, 2220-2226 (1998).
14. Dervan, P. B. Molecular recognition of DNA by small molecules. *Bioorg. Med. Chem.* **9**, 2215-2235 (2001).
15. Sakurai, T., Wong, E., Drescher, U., Tanaka, H. and Jay, D. G. Ephrin-A5 restricts topographically specific arborization in the chick retinotectal projection in vivo. *PNAS* **99**, 10795-10800 (2002).
16. Jay, D. G. and Sakurai, T. Chromophore-assisted laser inactivation (CALI) to elucidate cellular mechanisms of cancer. *Biochim. Biophys. Acta* **1424**, M39-M48 (1999).
17. Kumar, C. V. and Buranaprapuk, A. Site-specific photocleavage of proteins. *Angew. Chem. Int. Ed. Eng.* **36**, 2085-2087 (1997).
18. Kumar, C. V. et al. Photochemical protease: Site-specific photocleavage of hen egg lysozyme and bovine serum albumin. *PNAS* **95**, 10361-10366 (1998).
19. Kumar, C. V., Buranaprapuk, A., Sze, H. C., Jockusch, S. and Turro, N. J. Chiral protein scissors: High enantiomeric selectivity for binding and its effect on protein photocleavage efficiency and specificity. *PNAS* **99**, 5810-5815 (2002).
20. Baird, T., Wang, B. X., Lodder, M., Hecht, S. M. and Craik, C. S. Generation of active trypsin by chemical cleavage. *Tetrahedron* **56**, 9477-9485 (2000).

21. Wang, B. X., Brown, K. C., Lodder, M., Craik, C. S. and Hecht, S. M. Chemically mediated site-specific proteolysis. Alteration of protein-protein interaction. *Biochemistry* **41**, 2805-2813 (2002).
22. Wang, B. X. et al. Chemically mediated site-specific cleavage of proteins. *J. Am. Chem. Soc.* **122**, 7402-7403 (2000).
23. Ortells, M. O. and Lunt, G. G. Evolutionary history of the ligand-gated ion-channel superfamily of receptors. *Trends Neurosci.* **18**, 121-127 (1995).
24. Fu, D. X. and Sine, S. M. Asymmetric contribution of the conserved disulfide loop to subunit oligomerization and assembly of the nicotinic acetylcholine receptor. *J. Biol. Chem.* **271**, 31479-31484 (1996).
25. Rickert, K. W. and Imperiali, B. Analysis of the conserved glycosylation site in the nicotinic acetylcholine-receptor - potential roles in complex assembly. *Chem. Biol.* **2**, 751-759 (1995).
26. Criado, M., Sarin, V., Fox, J. L. and Lindstrom, J. Evidence that the acetylcholine binding-site is not formed by the sequence alpha-127-143 of the acetylcholine-receptor. *Biochemistry* **25**, 2839-2846 (1986).
27. Green, W. N. and Wanamaker, C. P. The role of the cystine loop in acetylcholine receptor assembly. *J. Biol. Chem.* **272**, 20945-20953 (1997).
28. Labarca, C. et al. Channel gating governed symmetrically by conserved leucine residues in the M2 domain of nicotinic receptors. *Nature* **376**, 514-6 (1995).
29. Sansom, M. S. P. Ion-channel gating - twist to open. *Curr. Biol.* **5**, 373-375 (1995).
30. Kearney, P. C., Zhang, H. Y., Zhong, W., Dougherty, D. A. and Lester, H. A. Determinants of nicotinic receptor gating in natural and unnatural side chain structures at the M2 9' position. *Neuron* **17**, 1221-1229 (1996).
31. Kearney, P. C. et al. Interactions of leucine residues at the 9' position of the M2 domain of the AChR probed using unnatural amino acid mutagenesis. *Biophys. J.* **70**, Tuam5-Tuam5 (1996).
32. Charnet, P., Labarca, C. and Lester, H. A. Structure of the gamma-less nicotinic acetylcholine-receptor - learning from omission. *Mol. Pharm.* **41**, 708-717 (1992).
33. Anand, R. et al. Reporter epitopes - a novel-approach to examine transmembrane topology of integral membrane-proteins applied to the alpha-1 subunit of the nicotinic acetylcholine-receptor. *Biochemistry* **32**, 9975-9984 (1993).
34. Knappik, A. and Pluckthun, A. An improved affinity tag based on the flag(r) peptide for the detection and purification of recombinant antibody fragments. *Biotechniques* **17**, 754-761 (1994).
35. Sato, M. H. and Wada, Y. Universal template plasmid for introduction of the triple-HA epitope sequence into cloned genes. *Biotechniques* **23**, 254-256 (1997).
36. Canfield, V. A., Norbeck, L. and Levenson, R. Localization of cytoplasmic and extracellular domains of Na,K-ATPase by epitope tag insertion. *Biochemistry* **35**, 14165-14172 (1996).
37. Bretzel, G. et al. Isolation of plasma membranes from *Xenopus* embryos. *Roux Arch. Dev. Biol.* **195**, 117-122 (1986).
38. Quick, M. W., Corey, J. L., Davidson, N. and Lester, H. A. Second messengers, trafficking-related proteins, and amino acid residues that contribute to the functional regulation of the rat brain GABA transporter GAT1. *J. Neurosci.* **17**, 2967-2979 (1997).
39. Corey, J. L. and Stallcup, M. R. The effect of glucocorticoid on the subcellular-localization, oligomerization, and processing of mouse mammary-tumor virus envelope protein precursor-Pr74. *Mol. Endocrinol.* **6**, 450-458 (1992).
40. Corey, J. L., Davidson, N., Lester, H. A., Brecha, N. and Quick, M. W. Protein-kinase-C modulates the activity of a cloned gamma-aminobutyric-acid transporter expressed in *Xenopus* oocytes via regulated subcellular redistribution of the transporter. *J. Biol. Chem.* **269**, 14759-14767 (1994).
41. Ivanina, T. et al. Phosphorylation by protein-kinase-A of RCK1 K^+ channels expressed in *Xenopus* oocytes. *Biochemistry* **33**, 8786-8792 (1994).
42. Dumont, J. N. Oogenesis in *Xenopus laevis* (Daudin).1. Stages of oocyte development in laboratory maintained animals. *J. Morphol.* **136**, 153-and (1972).
43. Keady, B., Attfield, K. and Hake, L. Identification and characterization of a CCA adding tRNA nucleotidyl transferase in Xenopus. *FASEB J.* **16**, A164-A164 (2002).
44. Hansske, F. and Cramer, F. Studies on structure of periodate oxidated ribonucleosides and ribonucleotides. *Carb. Res.* **54**, 75-84 (1977).

45. Sampson, J. R. and Saks, M. E. Selection of aminoacylated tRNAs front RNA libraries having randomized acceptor stem sequences: Using old dogs to perform new tricks. *Combi. Chem.* **267**, 384-410 (1996).
46. Thiry, M. Immunodetection of RNA on ultra-thin sections incubated with polyadenylate nucleotidyl transferase. *J. Histochem. Cytochem.* **41**, 657-665 (1993).
47. Petersson, E. J., Shahgholi, M., Lester, H. A. and Dougherty, D. A. MALDI-TOF mass spectrometry methods for evaluation of in vitro aminoacyl tRNA production. *RNA* **8**, 542-547 (2002).
48. Li, Z. J., Sun, Y. and Thurlow, D. L. RNA minihelices as model substrates for ATP/CTP:TRNA nucleotidyltransferase. *Biochem. J.* **327**, 847-851 (1997).
49. Green, W. N. Perspective - Ion channel assembly: Creating structures that function. *J. Gen. Phys.* **113**, 163-169 (1999).
50. Green, W. N. and Wanamaker, C. P. Formation of the nicotinic acetylcholine receptor binding sites. *J. Neurosci.* **18**, 5555-5564 (1998).
51. Palacin, M., Fernandez, E., Chillaron, J. and Zorzano, A. The amino acid transport system b(o,+) and cystinuria. *Mol. Memb. Biol.* **18**, 21-26 (2001).
52. Kellenberger, S. et al. Subunit stoichiometry of oligomeric membrane proteins: GABA(A) receptors isolated by selective immunoprecipitation from the cell surface. *Neuropharmacology* **35**, 1403-1411 (1996).
53. Nicke, A. et al. P2X(1) and P2X(3) receptors form stable trimers: a novel structural motif of ligand-gated ion channels. *EMBO J.* **17**, 3016-3028 (1998).
54. Nicke, A., Rettinger, J., Mutschler, E. and Schmalzing, G. Blue native page as a useful method for the analysis of the assembly of distinct combinations of nicotinic acetylcholine receptor subunits. *J. Rec. Sig. Trans. Res.* **19**, 493-507 (1999).
55. Hucho, F., Methfessel, C. and Watty, A. The role of subunit interfaces for the nicotinic acetylcholine receptor's allosterism. *J. Physiol. Paris* **92**, 85-88 (1998).
56. Watty, A., Weise, C., Dreger, M., Franke, P. and Hucho, F. The accessible surface of the nicotinic acetylcholine receptor - Identification by chemical modification and cross-linking with C-14-dimethyl suberimidate. *Eur. J. Biochem.* **252**, 222-228 (1998).
57. Leite, J. F., Blanton, M. P., Dougherty, D. A. and Lester, H. A. Identification of gating-dependent changes in photochemical labeling of the nicotinic acetylcholine receptor. *Biophys. J.* **82**, 181a-182a (2002).
58. Holmes, T. C., Fadool, D. A., Ren, R. B. and Levitan, I. B. Association of Src tyrosine kinase with a human potassium channel mediated by SH3 domain. *Science* **274**, 2089-2091 (1996).
59. Colledge, M. and Froehner, S. C. Signals mediating ion channel clustering at the neuromuscular junction. *Curr. Op. Neurobiol.* **8**, 357-363 (1998).
60. Sheng, M. and Kim, E. Ion channel associated proteins. *Curr. Op. Neurobiol.* **6**, 602-608 (1996).
61. Weber, P. J. A. and Beck-Sickinger, A. G. Comparison of the photochemical behavior of four different photoactivatable probes. *J. Pept. Res.* **49**, 375-383 (1997).
62. Mothes, W. et al. Molecular mechanism of membrane protein integration into the endoplasmic reticulum. *Cell* **89**, 523-533 (1997).
63. High, S. et al. Site-specific photocross-linking reveals that Sec61p and Tram contact different regions of a membrane-inserted signal sequence. *J. Biol. Chem.* **268**, 26745-26751 (1993).
64. Gallivan, J. P. *Ph.D. thesis* (California Institute of Technology, Pasadena, CA, 2000).
65. Brejc, K. et al. Crystal structure of an ACh-binding protein reveals the ligand-binding domain of nicotinic receptors. *Nature* **411**, 269-276 (2001).
66. Walker, C. S. et al. The T-superfamily of conotoxins. *J. Biol. Chem.* **274**, 30664-30671 (1999).
67. Kaerner, A. and Rabenstein, D. L. Stability and structure-forming properties of the two disulfide bonds of alpha-conotoxin GI. *Biochemistry* **38**, 5459-5470 (1999).
68. Brake, A. J., Wagenbach, M. J. and Julius, D. New structural motif for ligand-gated ion channels defined by an ionotropic ATP receptor. *Nature* **371**, 519-523 (1994).
69. North, R. A. P2X receptors: A third family of ligand-gated ion channels. *Br. J. Pharm.* **122**, U151-U151 (1997).
70. Newbolt, A. et al. Membrane topology of an ATP-gated ion channel (P2X receptor). *J. Biol. Chem.* **273**, 15177-15182 (1998).

71. North, R. A. and Surprenant, A. Pharmacology of cloned P2X receptors. *Ann. Rev. Pharm.* **40**, 563-580 (2000).
72. Curley, K. and Lawrence, D. S. Light-activated proteins. *Curr Opin. Chem. Biol.* **3**, 84-88 (1999).
73. Marriott, G. and Walker, J. W. Caged peptides and proteins: new probes to study polypeptide function in complex biological systems. *Trends Plant Sci.* **4**, 330-334 (1999).

Chapter 4. Unnatural amino acids with caged side chains

4.1 Introduction

4.1.1 Caged compounds

The use of masks is practically universal, from the Halloween celebrations of Europe, to Malian *chiwara* dancers, the *nō* theater of Japan, and the False Face societies of the Iroquois. In the Americas, some of the most dramatic masks were carved by the people of the Northwest Coast. A particular specialty of the Kwakiutl is the intricately worked transformation mask, which is worn over the head of a dancer. At the climactic moment of a dance, the mask is flung open along concealed hinges, effecting a startling transformation of Raven into Sisuitl, a spirit represented by the face of a warrior flanked by coiling serpents. (Figure 4.1)

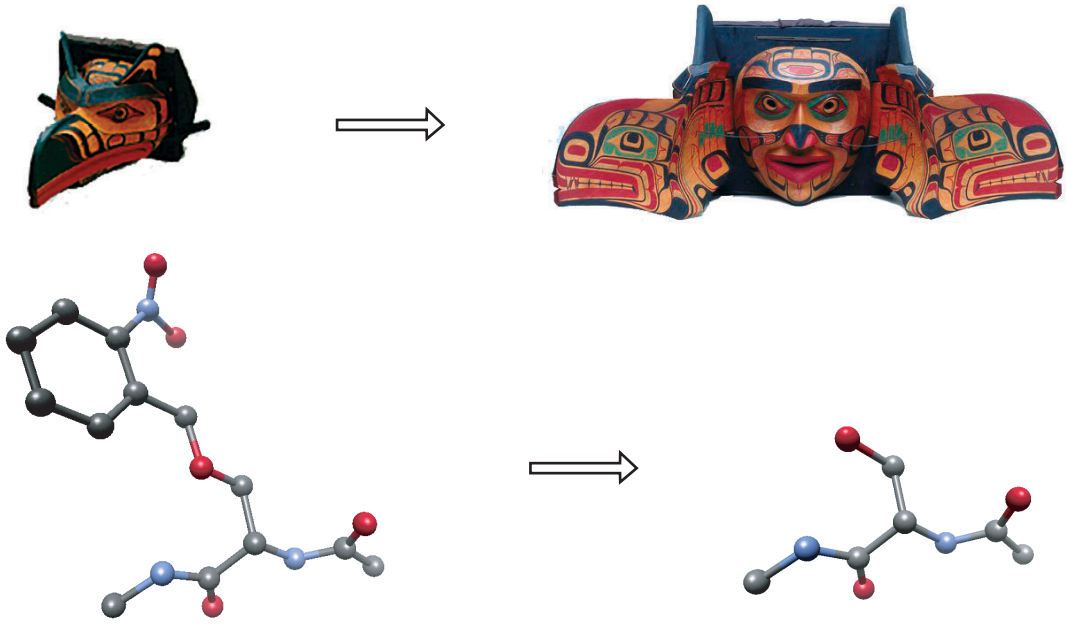

Figure 4.1 Kwakiutl transformation mask, which transforms Raven (left) into Sisuitl (right), compared to the photochemical transformation of an unnatural aromatic amino acid side chain (left) into serine (right).[1]

The instantaneous transformation of one material into another is likewise the most dramatic demonstration of chemical change. No popular chemistry demonstration concludes without a bang, a color change, a puff of smoke, a flash of light, a sudden phase transition. Instigating such a transformation with light for more serious purposes has a rather long history in chemical biology. Biologically active compounds may be protected with photo-removable protecting groups, altering important functionality in the molecule so as to block its biological efficacy. The protected compound is often thus referred to as being 'caged' or 'masked.' Irradiation of the system ('de-caging') removes the protecting groups and restores the intrinsic efficacy of the molecule.

This nomenclature disturbs some chemists, as the term is reserved in chemistry to describe solvation effects on reactivity, leading to the proposal that these compounds be referred to as 'phototriggered' rather than 'caged.'[2] However, the term 'caged' is superior grammatically and has found favor among biologists. The term will be used throughout this work, along with 'masked' and occasionally 'phototriggered.'

Classically, caged compounds have been used in biology for rapidly initiating processes which depend on small molecules.[3-6] High-resolution kinetic information may sometimes be obtained this way. Caged compounds can also be used because of their ability to bring small molecule-mediated processes under experimental control. A system dependent on a small molecule is primed by the diffusion of caged compounds into the proximity of the active site. Since the caged compounds lack the efficacy of the natural substrate, the process under consideration is held up until experimentally initiated. It is mostly in this latter sense that the compounds described below will be utilized.

4.1.2 Caged amino acids, particularly tyrosine

Caging drugs and bioactive small molecules has led naturally to the idea of caging peptides, many of which have important regulatory roles. Additionally, peptides offer a number of possibilities for caging. Both amines, such as the N-terminus of a peptide, and carboxylates (C-terminus) may be masked by photoactive protecting groups. Amino acid side chains also offer a number of easily caged functional groups. Caged serine, threonine, and tyrosine have all been reported.[7-9] Cysteine, methionine, aspartate, glutamate, and lysine have also been caged.[10-19] Given the wide range of possibilities for introducing a photo-labile protecting group and the large number of systems where peptide binding has an important role, it is not surprising that large numbers of caged peptides and amino acids have been reported.

Caged tyrosine, in particular, has been employed in a number of studies. Its earliest reported synthesis was in 1996, where the suitability of nitrobenzyl-protected tyrosine for solid-phase peptide synthesis was demonstrated. In this work, caged neuropeptide Y and caged angiotensin II peptides were synthesized. In the case of neuropeptide Y, the presence of a single caged tyrosine residue severely compromised binding to cells expressing the NK2 receptor, whereas no effect was seen for caged angiotensin II relative to the wild-type peptide.[9] More recent work by the laboratory of Jeffery Walker has used caged tyrosine in solid-phase synthesis to generate caged peptides which interact with calmodulin and the myosin light-chain kinase (MLCK). Photolysis of the caged inhibitory peptides in eosinophils caused contraction of these cells, implying an important role for calmodulin and MLCK in the motility of these immune cells.[20]

4.1.3 Caged proteins

The advent of techniques to alter the amino acids of proteins has permitted the consideration of 'caged proteins,' in which particular residues in a protein are provided with photo-removable protecting groups. A number of recent reviews have presented a survey of this literature.[21-23] Interesting experiments have been done with such caged proteins, including a number of caged kinases whose activity is dependent on de-caging.[23,24] In addition, protein-protein interactions essential to actin polymerization have been disrupted by caging a lysine on F-actin.[15] The laboratory of Hagan Bayley has a long-standing interest in caged proteins and has recently introduced a caged hemolysin which only conducts ions subsequent to photolysis.[25] A caged antibody which only binds upon irradiation has been developed.[26] Both enzymes, such as galactosidase, and proteins involved in signal transduction, such as $p21^{Ras}$, have been caged.[27,28]

The necessity in these experiments for forming the caged protein *in vitro* has meant that investigation of real cellular processes has been difficult. Additionally, of course, techniques relying on modification of reactive side chains in the protein suffer from limited specificity of caging, as differential reactivity of multiple nucleophilic residues can be difficult to guarantee. To solve the problem of specificity, proteins containing caged amino acids may be synthesized through either solid-phase methods, or by semi-synthesis followed by ligation of the unnatural amino acid-containing portion to the remainder of the protein. Still, experiments with these proteins may be performed *in situ* only insofar as modified proteins can be introduced into the cell. Although such techniques are being continually improved, this limitation provides clear incentive for this work to be done using unnatural amino acid mutagenesis, where the protein is

synthesized inside the cell itself. [29] In addition, caging integral membrane proteins remains a particularly challenging case for conventional methods, whereas unnatural amino acid mutagenesis is increasingly well-established for membrane proteins.

4.2 Using nonsense suppression to introduce caged amino acids into proteins

4.2.1 Expression systems

The first requirement for introducing an unnatural amino acid into a receptor is a viable expression system for that receptor. The majority of experiments employing nonsense suppression as a means of incorporating unnatural amino acids into proteins have relied on bacterial extracts to produce the proteins of interest. More recent efforts have employed bacterial extracts modified to increase suppression efficiency or extracts from eukaryotic systems.[30,31] *In vitro* systems such as wheat germ and rabbit reticulocyte extracts have been utilized for nonsense suppression of functional soluble proteins.[32-34] In our lab, wheat germ extracts are routinely used to generate full-length membrane proteins for PAGE analysis.[35,36] In principle, receptors containing unnatural amino acids could be reconstituted into bilayers using such a system supplemented with microsomes [37]. However, there is no precedent for unnatural amino acid mutagenesis of an integral membrane protein using a cellular extract. Expression in *Xenopus* oocytes is the only method to date that has been shown to be effective for incorporating unnatural amino acids into functional receptors.[38-42]

4.2.2 Caging groups

The choice of caged side chain depends, of course, on the exact nature of the information to be gained from the experiment. The literature contains precedents for

caged side chain hydroxyls (Tyr[43-45]and Ser[46]) thiols (Cys[44]), acids (Asp[47]), amines (β-aminoalanine[48]) and amides (Npg[49] in which backbone cleavage can be seen as photolytic "decaging" of the peptide bond). As mentioned above, the suppression efficiency of an unnatural amino acid is related to the nature of its side chain, but in a complex fashion. Most investigators have employed relatively small caging groups, because the charged tRNA must pass through the ribosome in order for the amino acid to be incorporated into the receptor. As will be discussed further, it is difficult to predict whether one will encounter problems in incorporating a particular amino acid. Workers in the field have generally reported that steric and especially charge conservation of the native side chain help promote efficient expression. In practice, there is no substitute for simply attempting the suppression at the desired position with the desired unnatural amino acid.

The only caging groups precedented for unnatural amino acid suppression thus far are nitrobenzyl (Nb)[43-50] and nitroveratryl.[50] Other photoactive protecting groups have very attractive photochemical properties, but it remains to be seen whether or not these groups can be incorporated by nonsense suppression. There are several considerations in choosing a caging group: 1) synthetic characteristics: the degree to which it is synthetically accessible and compatible with coupling to pdCpA; 2) photochemical characteristics: its action spectrum, quantum yield for photolysis, and speed of the dark reactions that complete photolysis; and 3) reactivity in the system of interest: its stability in water, and the possible reactivity of its photoproducts.

4.2.3 Side chain uncaging

Various types of photolysis apparatus have been employed for side chain decaging. Experiments involving photoreactive unnatural amino acids such as diazirine, aryl azides,

and benzophenone[32,51-55] are also relevant here, as are experiments with caged small molecules in *Xenopus* oocytes.[56,57] In general, methods of photolysis can be divided into those performed on single oocytes and those performed on batches of oocytes.

An apparatus for real-time decaging in single oocytes (Figure 4.2) was designed for the particular needs of these unusually large cells (~ 1 mm diameter).[43-45,58] In most cases, inexpensive arc lamps (either continuous irradiation or pulsed) are preferred over the much more costly lasers if one wishes to illuminate the entire oocyte.[57]

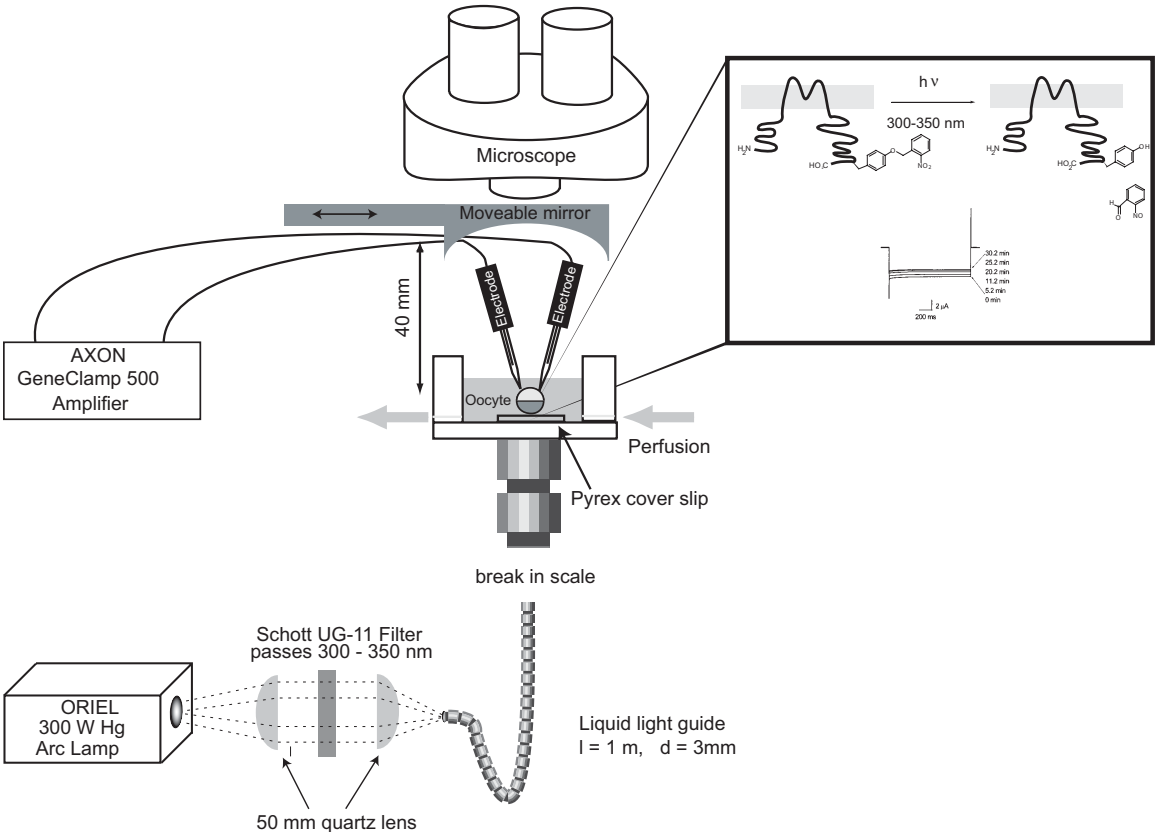

Figure 4.2 Protein decaging with real-time electrophysiological monitoring. Apparatus for simultaneous irradiation and electrophysiological recording from *Xenopus* oocytes. The output of the Oriel Hg arc lamp is passed through a 300 - 350 nm bandpass filter and focused onto a fiber optic liquid light guide. The light guide directs the beam onto the oocyte, which is clamped in a standard two-electrode configuration. A concave mirror can be moved into position above the bath, reflecting some of the beam that has passed around the oocyte back to the shadowed upper surface. The mirror increases the overall flash intensity by ~50%. The inset depicts the photolytic de-caging of a caged amino acid incorporated into a channel with attendant response. This example indicates incorporation of Tyr(ONb) into an extracellular domain of the protein, where removal of the caging group results in an increased number of active channels.

Methods for decaging proteins expressed in many oocytes at once are rather simpler.[49] In the particular case of Npg decaging, oocytes were irradiated for 4 hours at 4 °C in Pyrex vials with a 288 W Hg lamp equipped with a 360 nm band pass filter at a distance of 15-30 cm.

4.2.4 Choice of receptor

Suppression has been demonstrated in the major classes of neuroreceptors and ion channels. Unnatural amino acids have been incorporated into a number of ligand-gated channels, such as the nAChR (numerous subunits) and 5-HT_3 receptors, a G-protein-coupled receptor (NK1), GIRKs, and several potassium channels including Kir2.1 and Shaker.[38,39,42,43,45,49,59-61] In unpublished work from our lab, we have incorporated unnatural amino acids into CFTR, a P2X receptor, and a neurotransmitter transporter. Among these are monomeric and multimeric receptors, both homomeric and heteromeric versions of the latter. We emphasize that heterologous expression of any novel protein is by no means guaranteed, since it is uncertain whether the protein will be folded, assembled, or transported properly. However, our experience suggests that any protein that can be expressed effectively in *Xenopus* oocytes will be amenable to incorporation of unnatural amino acids by nonsense suppression.

4.2.5 Assay

Finally, a fundamental methodological requirement for unnatural amino acid mutagenesis is an assay capable of detecting the effects of photolyzing a caged side chain. In fact, one of the reasons that receptors are such an attractive target for studies of this nature is that electrophysiology may be employed for this purpose.

Electrophysiology is exquisitely sensitive and therefore capable of detecting the very small amounts of protein generated by nonsense suppression. To date, only two-electrode voltage clamp recordings have been made with receptors containing caged amino acids; but single-channel recordings are in principle possible. In addition, electrophysiology has been successfully coupled with irradiation in a number of experiments.[56,57]

Other methods may be employed to detect downstream effects of side-chain decaging. There is ample precedent for most biochemical methods on receptors expressed in oocytes.[62] However, given that small amounts of protein are produced in nonsense suppression experiments, these methods often require some adaptation for use. The literature is not terribly extensive, but there are examples on non-electrophysiological techniques that have been successful in the analysis of the effects of single side chain decaging, some of which are presented below.

4.2.6 Precedents for using nonsense suppression to introduce caged amino acids

Unnatural amino acid mutagenesis is an attractive technique for generating caged proteins, because of its absolute site-specificity. The Schultz group was the first to employ the technique for this purpose, caging a critical active-site serine in T4 lysozyme, bringing the activity of the enzyme under photocontrol.[47] Caged aspartate was also used by this laboratory to control protein-protein interactions important to the signaling protein $p21^{Ras}$.[28] A final example from the Schultz laboratory is the use of caged serine to control the intein splicing of a DNA polymerase.[46] *In vitro* nonsense suppression has been used to cage aspartate residues in an attempt to bring the dimerization of HIV protease under experimental control.[50] Again, these experiments are somewhat limited in scope by the

fact that the caged protein would have to be introduced into a cell to truly examine a biologically relevant interaction.

In vivo unnatural amino acid mutagenesis provides a means to solve both the problem of specificity and biological context of the caged protein. Experiments on nitrobenzyl-protected tyrosine residues have been carried out in this laboratory on the nAChR.[43] Particular tyrosine residues shown to be important in agonist binding were introduced into the receptor by unnatural amino acid mutagenesis in *Xenopus* oocytes. The presence of the caging groups was shown to impair the response of the receptor to acetylcholine. Upon removal of the protecting groups by irradiation of the oocyte, wild-type reactivity was restored. Using this system, important kinetic and optical parameters of caged tyrosine in oocytes were able to be determined, although it should be noted that these caged tyrosine residues were incorporated in an extracellular region of the protein. The experiments reported in Chapter 3 with incorporation of caged cysteine and tyrosine into the M2 transmembrane domain of the nAChR are an example of caged amino acids incorporated into membrane-resident protein domains.

The effectiveness of caged tyrosine in both of these contexts led to a consideration of the use of caged tyrosine to control the accessibility of this particular residue in a functioning ion channel.

4.2.7 Application of caged tyrosine to ion channels

Ion channels represent the first-line class of signal-transducing molecules. They are resident in the plasma membrane and are thus in intimate contact with the extracellular environment. In addition, of course, functioning ion channels are an imperative of earthly life, as any non-viral organism must maintain an ion gradient to power its

metabolic processes. As a result of these critical functions, ion channels are tightly regulated. All of a cell's regulatory mechanisms are probably brought to bear upon ion channels, including transcriptional control; translational control; RNA editing; post-translational modification of all varieties; dynamic insertion into and removal from the membrane; functional modulation by ligand binding, pressure, light, heat, interaction with other proteins, changes in membrane voltage, proteolysis, etc.

Phosphorylation is a modification that is presumed to be central to ion channel regulation. Surprisingly, however, there is remarkably little evidence that a specific residue in an ion channel under a particular circumstance at a given time has been phosphorylated. The technical barriers inherent in obtaining this information are steep. Any assay to determine whether or not a single residue has been phosphorylated must be extremely sensitive. Since the phosphate linkage is biologically labile (due to enzyme activity, if not metal-promoted hydrolysis), the analyte itself is delicate. Ion channels are integral membrane proteins, and isolating them for analysis is difficult, particularly under the required conditions of sensitivity and gentleness. Finally, the temporal sensitivity to determine whether a functional effect is caused by phosphorylation of a single residue is simply unattainable, although the following chapter will present a technique for perhaps achieving it.

Despite all of this, there are numerous reports of the direct detection of ion channel phosphorylation.[63-68] There are a few which show serine or threonine phosphorylation, but the bulk involve tyrosine phosphorylation. Partly, this could be because tyrosine phosphorylation may have unique importance in mediating protein-protein interactions. But it also reflects the existence of antibodies against phosphotyrosine which do not exist

for phosphoserine and phosphothreonine. In the work presented in this chapter, tyrosine phosphorylation will be the sole focus.

4.3 Incorporation of caged tyrosine into the potassium channel Kir2.1

4.3.1 Introduction

There is ample evidence to suggest that the activity of ion channels is modulated by the same regulatory mechanisms which operate on other signal transduction pathways. Generally speaking, modulation may be accomplished by modification of the channel itself or through the interaction of other proteins with the channel. Phosphorylation has been mentioned, where a charged phosphoryl group is transferred to a serine, threonine, or tyrosine side chain. An example of the latter mechanism is endocytosis. Through endocytosis, channel activity may be regulated by removal of channels from the cell surface, a process mediated through non-covalent interactions with proteins of the endocytotic pathway. These two fundamental kinds of mechanisms are by no means exclusive.[69-71] Covalent modification by phosphorylation induces conformational changes, which may directly affect the conducting pathway. Alternatively, phosphorylation may regulate the binding of modulatory proteins to ion channels, as it does with G-protein coupled receptors.[72,73]

As an example of the complications which arise from interaction among regulatory pathways, endocytosis is an interesting case. The rules whereby membrane proteins are targeted for endocytosis are not yet completely understood. One targeting motif for which there is a significant body of biochemical evidence is the tyrosine-based endocytosis motif, YXXΦ, where X may be any amino acid and Φ is a hydrophobic

amino acid, typically L, F, or M.[74] Tyrosine, however, is a residue which may be phosphorylated by tyrosine kinases. It is likely the case that the phosphorylation state of a channel governs whether or not it is able to be targeted for endocytosis. Furthermore, both phosphorylation and endocytosis are precedented in the literature as mechanisms of ion channel modulation. It would appear, then, that the pathways regulating ion channel modulation are likely to be tightly coupled. In order to determine the molecular-level details of ion channel modulation, it is essential to be able to distinguish the contributions of the various regulatory pathways. We introduce here an experimental technique which allows for making these distinctions. A caged form of tyrosine, a residue which plays a special role in recognition events leading to both phosphorylation and endocytosis, was incorporated into a potassium channel known to be sensitive to tyrosine phosphorylation. (Figure 4.3)

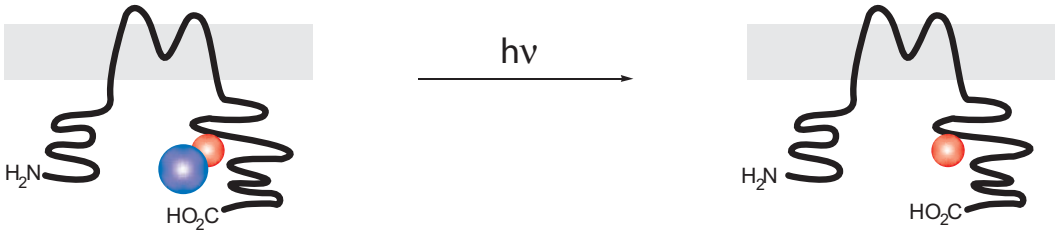

Figure 4.3 General schematic depicting the caging of an intracellular tyrosine residue in the potassium channel Kir2.1. The tyrosine residue of interest is indicated in red, and the caging group in blue.

Ion channels which have been found to respond to modification by tyrosine kinases include the potassium channel Kir2.1, a member of the family of inwardly rectifying K^+ channels with the important biological function of maintaining membrane potential.[75,76] As the name implies, these channels pass potassium only in the inward direction. They are, in fact, always open and have no apparent gating mechanism, other than the voltage-dependence of their rectification. Their physiological role is often described by analogy

to the latch on a drawer. These channels do permit some outward K^+ flow within several mV of E_K, which allow the cell's membrane potential to approach E_K. However, once V_m becomes more negative than E_K, these channels no longer pass K^+. The latch having been released, the cell's V_m is free to change, with inward rectifiers' ability to allow K^+ into the cell under hyperpolarizing conditions contributing to the return to resting V_m. Kir2.1 is a particular isoform of inward rectifier found in a variety of tissues in the periphery and CNS.[75] Kir2.1 currents have been found to be strongly inhibited by tyrosine phosphorylation. Mutation of a single tyrosine residue to phenylalanine abolishes this inhibition.[76] Interestingly, this intracellular C-terminal tyrosine (Y242) is also part of a YXXΦ tyrosine-based endocytosis motif. Such a motif has been demonstrated to regulate the expression of the ENaC sodium channel in oocytes.[77]

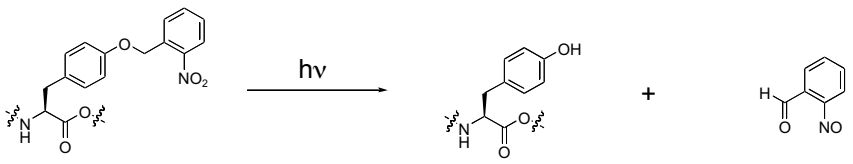

Figure 4.4 Schematic showing the chemistry whereby wild-type tyrosine is revealed by photolysis of Tyr(ONb).

By the nonsense codon suppression method, we have introduced the caged tyrosine analog *O*-nitrobenzyl tyrosine, Tyr(ONb), into Kir2.1 at the critical Y242 position. As introduced, the protected tyrosyl oxygen is incapable of acting as a tyrosine kinase substrate. Nor, based on crystallographic evidence, would it appear that tyrosine protected in this way would permit binding by components of the clathrin-mediated endocytotic pathway.[78] However, UV irradiation of the protein releases the nitrobenzyl protecting group, revealing the wild-type tyrosine residue. (Figure 4.4) Restoration of the native side chain, of course, permits both phosphorylation and/or recognition by the

endocytotic machinery. This technique thus brings the initiation of phosphorylation and endocytosis under some degree of experimental control. The experiments reported herein distinguish the contribution of phosphorylation from that of endocytosis, revealing important details about an interaction which may be fundamental to the regulation of ion channels *in vivo*.

4.3.2 Results

4.3.2.1 Kir2.1 currents are decreased by tyrosine kinase

Initially, we verified that the inwardly rectifying potassium channel Kir2.1 from *Mus musculus* is modulated by tyrosine phosphorylation under the present experimental conditions.[76] *Xenopus* oocytes expressing Kir2.1 were voltage clamped at 0 mV in a recording solution containing 96 mM KCl. Potassium currents elicited by a voltage step to a test potential of –80 mV were recorded. Table 4.1 shows that oocytes expressing Kir2.1 gave robust 13.3 ± 1.2 μA whole-cell potassium currents after 24 hours. Oocytes treated with the tyrosine phosphatase inhibitor phenylarsine oxide (PAO)[79] showed no reduction of current, giving whole-cell potassium currents of 13.1 ± 1.4 μA. However, oocytes co-injected with v-Src gave an average current of 7.8 ± 0.3 μA, a 57% current reduction relative to those injected with Kir2.1 alone. This effect was enhanced by treatment with PAO; oocytes co-injected with v-Src and treated with PAO gave average currents of only 5.7 ± 0.6 μA. Indeed, co-injection with v-Src alone did not always yield significant current reduction. This is consistent with results from other laboratories.[80] Although there appeared to be no strict requirement for the presence of phosphatase

inhibitors, the phosphatase inhibitor PAO was always added for consistency between experiments.

Treatment	**Mean current (μA±SEM)**	n
-	13.3±1.2	5
PAO	13.1±1.4	5
v-Src	7.8±0.3	5
v-Src + PAO	5.7±0.6	5
PYK-2	12.8±0.5	5
PYK-2 + PAO	6.9±0.8	5

Table 4.1 Averaged whole-cell currents for Kir2.1.

The proline-rich tyrosine kinase PyK2 gave results similar to v-Src. 48% current reduction was measured upon PAO treatment of oocytes co-injected with PyK2 (Table 4.1). In this case, co-injection of the kinase without phosphatase inhibitor was not sufficient to cause current reduction: oocytes co-expressing the channel with PyK2 gave 12.8 ± 0.5 μA.

Table 4.2 confirms that Y242 is critical for the effect of tyrosine kinases. The tyrosine residue at position 242 was changed to phenylalanine by site-directed mutagenesis. Oocytes expressing the Kir2.1-Y242F construct were unaffected by treatment with the tyrosine phosphatase inhibitor PAO and/or tyrosine kinases. For instance, untreated oocytes expressing the Y242F construct gave average whole-cell K^+ currents of 31.4 ± 2.7 μA.; oocytes co-expressing v-Src and treated with PAO gave currents of 31.2 ± 0.9 μA. The overall expression for the experiment depicted in Table 4.2 was higher than that for the WT Kir2.1, which represents imprecision in mRNA quantitation or batch-dependent expression differences among oocytes. There were no consistent differences in expression level between the WT (WT) and Y242F constructs. In other experiments on Y242F at expression levels comparable to those of Table 4.1, we

confirmed that no combination of v-Src expression and PAO gave significant decreases for this mutant.

Treatment	**Mean current (μA±SEM)**	n
-	31.4±2.7	6
PAO	34.0±2.0	5
v-Src	30.3±1.8	5
v-Src + PAO	31.2±0.9	4
PYK-2	34.3±2.1	4
PYK-2 + PAO	32.9±3.1	4

Table 4.2 Averaged whole-cell currents for Kir2.1 Y242F.

For both constructs, similar but less extensive results on the inhibition of K^+ currents were obtained with the tyrosine phosphatase inhibitor pervanadate substituting for PAO. Similar data were also obtained when the v-Src cRNA injection was omitted but oocytes were injected with TrkB, a receptor tyrosine kinase, and exposed to BDNF. These data suggest that several different activators of tyrosine phosphorylation can inhibit the function of Kir2.1.

4.3.2.2 Photolytic decaging of tyrosine-242 leads to a decrease in current

In order to gain temporal control over the state of the tyrosine side chain at position 242, the unnatural amino acid Tyr(ONb) was incorporated into Kir2.1 at position 242. The nonsense codon TAG was introduced using site-directed mutagenesis. mRNA encoding the Kir2.1-Y242TAG construct was generated by *in vitro* transcription. This message was co-injected into *Xenopus* oocytes along with the nonsense suppressor tRNA which had been chemically charged with the synthetic amino acid Tyr(ONb). In order to verify that functional protein was produced by this procedure and to assess the effect of decaging the caged tyrosine residue, oocytes were studied as in the experiments of Table 4.3. As in most unnatural amino-acid experiments to date, current measurements show that expression levels are rather lower—in this case by a factor of 5 to 10—than the

levels for WT channel or for conventional site-directed mutagenesis (compare the expression levels in Table 4.1 and Table 4.2 above). UV light was delivered to oocytes for 3 s.[43] Figure 4.5 presents normalized current values averaged over several oocytes.

v-Src	hν	Percent decrease±SEM
-	+	5.0±1.5
+	-	1.5±0.9
+	+	32±0.9

Table 4.3 Normalized average whole-cell current decrease of oocytes expressing Kir2.1 Y242TAG suppressed with Tyr(ONb) thirty minutes after initiation of experiment (n=5).

Control oocytes were injected with Kir2.1-Y242TAG mRNA and tRNA-Tyr(ONb) but not with v-Src mRNA. Current from these oocytes decreased by only 5.0 ± 1.5% over the 30 min interval, showing that irradiation itself had only a small effect on Kir2.1 currents. In a second control, whole-cell currents were measured in non-irradiated oocytes co-expressing Kir2.1 containing Tyr(ONb) and v-Src. After 30 min, the average current decrease was only 1.5 ± 0.9%. This is consistent with the supposition that while the nitrobenzyl protecting group remains, the residue at 242 is unavailable as a substrate for interaction with other proteins—either tyrosine kinases or adaptor proteins. Importantly, oocytes co-expressing Kir2.1 and v-Src, treated with PAO, and irradiated showed an average current decrease of 32.0 ± 0.9% 30 min after irradiation. This shows that the decaging of Kir2.1-Y242 under conditions favoring tyrosine phosphorylation leads to a large decrease in current.

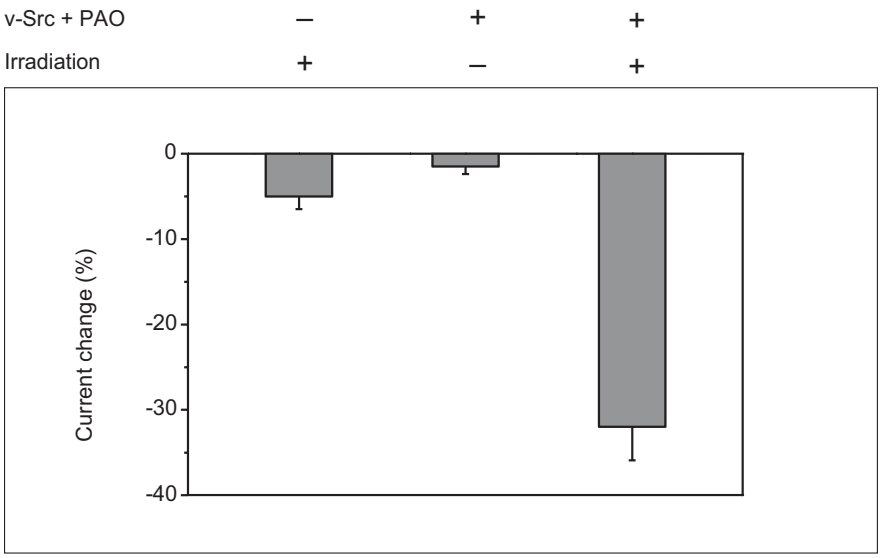

Figure 4.5 Inhibition of current in oocytes expressing Kir2.1-Y242TAG suppressed with Tyr(ONb). Averaged normalized data from batches of oocytes recorded at t = 30 min Average values (and ranges) for 100% current were 8.7 (5.5 to 13), 6.5 (4.5 to 10.4), and 6.6 (1.6 to 15.5) μA for the three groups (left to right). Error bars indicate SEM, n = 4 to 6 oocytes.

Although these data qualitatively agree with the data for the WT and Y242F construct, present limitations of the nonsense suppression technique prevent direct quantitative comparisons. First, suppression is incomplete, leading to a substantial proportion of Kir2.1 subunits truncated at the 242 position. To control for this effect, we expressed the Y242TAG construct alone; there were no currents. When we co-expressed Y242TAG and WT channels, we saw currents whose modulation properties were like those depicted in the experiment of Table 4.1. Therefore, dominant negative effects due to truncated subunits probably play no role in our experiments. Second, read-through may occur, so that natural residues would be incorporated at position 242. It is therefore possible that some channels would contain one or more Kir2.1 subunits with natural residues. Although we know that a channel with four Y242F subunits does not respond to v-Src and PAO (Table 4.2), we do not know how modulation would proceed for channels with varying numbers of subunits containing one or more of the other 18 natural

amino acid residues. In the unlikely event that read-through produces a channel with tyrosine at position 242 in one or more subunits, the modification has presumably occurred during the PAO incubation period (> 30 min). We assume that the general effect of read-through would be to decrease the modulatory effect of irradiation.

4.3.2.3 Decaging tyrosine-242 also causes a capacitance decrease

Importantly, Table 4.4 shows that the current decrease observed in oocytes expressing v-Src and Kir2.1-Y242-Tyr(ONb) was accompanied by a significant capacitance decrease. The change in capacitance is a direct measure of net endocytotic activity of a cell (i.e. exocytosis minus endocytosis). In both control cases where irradiation of oocytes caused no current inhibition, the capacitance remained essentially constant over the length of the experiment. Thus, the correlation between current and capacitance decrease is clear. (Figure 4.6)

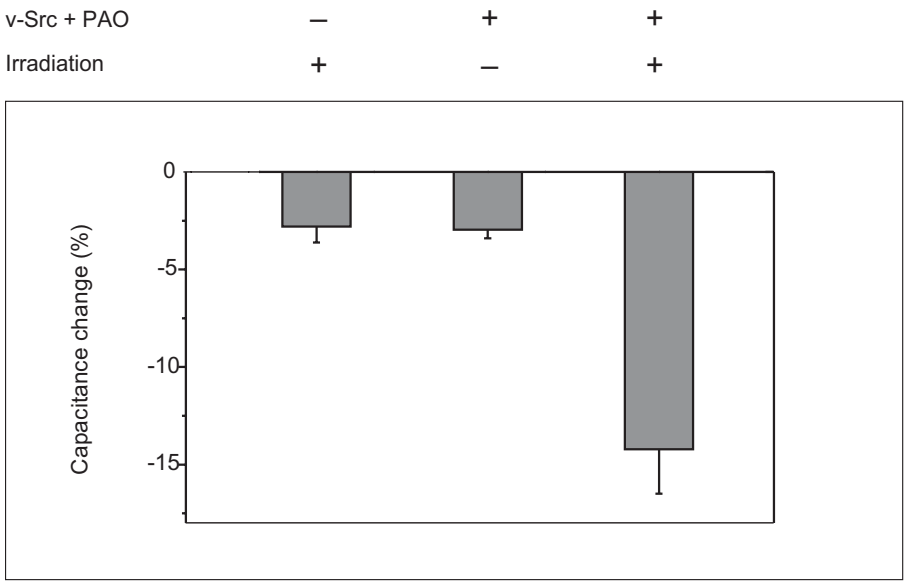

Figure 4.6 Decrease of capacitance in oocytes expressing Kir2.1-Y242TAG suppressed with Tyr(ONb). Average values (and ranges) for 100% capacitance were 190 (159 to 227), 187 (167 to 202), and 194 (132 to 234) nF for the three groups (left to right). Error bars indicate SEM, n = 4 to 6 oocytes.

Control oocytes that were irradiated without v-Src co-expression showed an overall capacitance decrease of only 2.8 ± 0.8% 30 min after irradiation. The second control, in which oocytes co-expressing Kir2.1 with caged tyrosine and v-Src were studied without irradiation, also showed little capacitance decrease (3.0 ± 0.4%) over the time course of recording. In contrast, oocytes expressing v-Src and Kir2.1 in which the Tyr(ONb) residue at 242 is uncaged by irradiation, showed an overall decrease in membrane capacitance of 14.1 ± 1.9% over 30 min. This decrease suggests that the membrane surface area has decreased as a result of increased endocytotic activity.

v-Src	**hν**	**Percent decrease±SEM**
-	+	2.8±0.8
+	-	3.0±0.4
+	+	14.1±1.9

Table 4.4 Normalized average whole-cell capacitance decrease of oocytes expressing Kir2.1Y242TAG suppressed with Tyr(ONB) thirty minutes after initiation of experiment (n=5).

In additional controls, we found no decrease in capacitance when oocytes were injected with v-Src cRNA, treated with PAO, and then irradiated. Therefore the capacitance change does not arise from possible photosensitive processes involving v-Src. In additional controls, oocytes were injected with tRNA-Tyr(ONb) and v-Src, and then treated with PAO. Again, irradiation produced no capacitance change, ruling out possible suppression of stop codons in endogenous proteins as the source of the photosensitivity. Furthermore, there were no changes in capacitance associated with decaging of tyrosine in our previous study of caged tyrosine at the nicotinic acetylcholine receptor. Therefore tyrosine decaging in general does not lead to membrane endocytosis.

Irradiated oocytes co-expressing wild-type Kir2.1 and v-Src showed no decrease over the time course of the experiment. Presumably, the wild-type channel is capable of phosphorylation by v-Src and would perhaps be expected to show a current decrease

upon application of PAO. Under certain conditions, current reduction with wild-type Kir2.1 could, in fact, be seen in response to PAO treatment. Oocytes recorded from shortly after addition of the phosphatase inhibitor showed significantly lower maximal currents than those which were untreated. This observation is consistent with the existence of a dynamic equilibrium between kinase and phosphatase activity. Under typical conditions, no special effort was taken to record immediately after phosphatase addition. Consequently, equilibrium was established prior to recording, and oocytes showed an apparent steady-state current. With suppressed proteins, the caged tyrosine provides a controllable switch to initiate a process which occurs on the native protein.

We compared the time course of the current decrease and the capacitance decrease by normalizing to the decrease at 30 min, then interpolating the approximate time to half-completion for this decrease. The average values were quite comparable: 11.8 min for current and 11.1 min for capacitance. These data indicate that the capacitance change and the current decrease followed similar time courses. Nonetheless some of our measurements suggest that the capacitance decrease begins after a delay of several minutes. This possible initial delay has not been investigated systematically.

4.3.2.4 Dominant negative dynamin eliminates capacitance decrease and partially eliminates current decrease

Capacitance measurements may reflect the contribution of various mechanisms of endocytosis. In order to test specifically whether clathrin-mediated pathways were involved, experiments were performed with a dominant negative dynamin isoform. If Kir2.1 inhibition resulted from clathrin-mediated endocytosis, co-injection of oocytes with dominant negative dynamin (dynamin-K44A) [81,82] at levels capable of blocking

endogenous dynamin activity would eliminate both the current change and the capacitance change. Table 4.5 and Table 4.6 present data that distinguish between these two events.

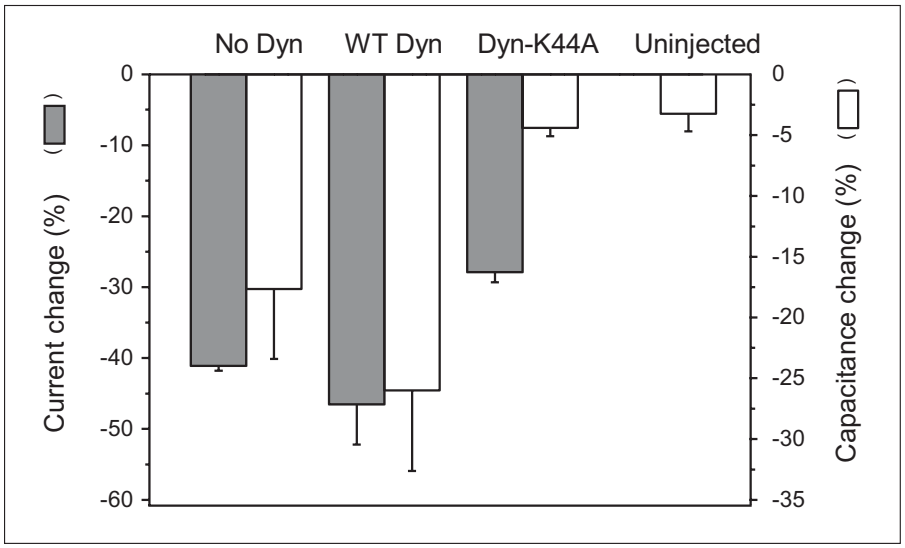

Figure 4.7 Data for current and capacitance for oocytes recorded 30 min after irradiation (mean ± SEM, n=5). Left-hand y-axis and full bars represent normalized current decrease. Average values (and ranges) for 100% were 4.1 (3.15 to 4.8), 3.1 (2.8 to 3.7), and 4.1 (3.0 to 5.7) μA for the three groups (left to right). Right-hand axis corresponds to hollow bars, representing normalized capacitance decrease. The rightmost column shows capacitance change of uninjected control oocytes. Average values (and ranges) for 100% capacitance were 197 (191 to 205), 225 (191 to 248), 189 (174 to 199), and 197 (190 to 209) nF for the four groups (left to right). Error bars represent SEM.

Figure 4.7 shows averaged current and capacitance data for three to eight oocytes and also the capacitance change of uninjected control oocytes over the course of the experiment. Current change is indicated by filled bars and the left-hand y-axis. When no dynamin mRNA was co-injected, the average current decrease 30 min after irradiation was 41.1 ± 0.7%, which is reasonably consistent with the value of 32% obtained in the experiment of Table 4.3 and Figure 4.5. Co-expression with a WT dynamin isoform had an insignificant effect on the current decrease: the average decrease was 46.5 ± 5.7%. Dominant negative dynamin affected the current decrease somewhat, but it remained relatively large at 27.9 ± 1.5%. The hollow bars and right-hand axis of Figure 4.7

represent the normalized capacitance decrease. Without added dynamin, the average capacitance change associated with decaging tyrosine on Kir2.1 in the presence of v-Src was 17.7 ± 5.8%, consistent with the average value of 14.1% reported in Table 4.4. Injection of WT dynamin gave rise to an average capacitance decrease of 26.0 ± 6.6%, not significantly larger than that of oocytes containing only endogenous dynamin. The effect of the dominant negative K44A dynamin isoform, however, was dramatic. Oocytes expressing dominant negative dynamin displayed an average capacitance change of 4.4 ± 0.7% over 30 min. This degree of change is not significantly different from the baseline capacitance change for uninjected oocytes (3.3 ± 1.4%).

Channel	**Dynamin**	**% decrease±SEM**	**n**
Kir2.1	-	41.1±0.7	3
Kir2.1	WT	46.5±5.7	5
Kir2.1	K44A	27.9±1.5	8

Table 4.5 Normalized average whole-cell current decrease of oocytes expressing Kir2.1Y242TAG suppressed with Tyr(ONb) treated with the indicated dynamin thirty minutes after initiation of experiment.

Channel	**Dynamin**	**% decrease±SEM**	**n**
Kir2.1	-	17.7±5.8	3
Kir2.1	WT	26.0±6.6	5
Kir2.1	K44A	4.4±0.7	8
-	-	3.3±1.4	5

Table 4.6 Normalized average whole-cell capacitance decrease of oocytes expressing Kir2.1Y242TAG suppressed with Tyr(ONb) treated with the indicated dynamin thirty minutes after initiation of experiment.

By combining current and capacitance measurements with the expression of dominant negative dynamin, we have shown that significant current decrease occurs in the absence of appreciable capacitance change. The 26% current reduction in the absence of clathrin-mediated endocytosis is smaller than the 41% or 32% reductions seen in cells where the endocytotic machinery has not been perturbed. Thus, clathrin-mediated endocytosis may account for a portion of the whole-cell current reduction. In addition, however, a non-endocytotic mechanism reduces current after the decaging of Tyr242.

4.3.2.5 Fluorescent labeling corroborates dynamin-mediated endocytosis

In order to directly observe loss of plasma membrane, and to complement the electrophysiological data on current and capacitance change, we labeled and measured surface proteins on the oocyte. Oocytes expressing Kir2.1 were exposed to the impermeant thiol-reactive fluorophore tetramethylrhodamine-5-maleimide. Since the reagent is not specific for Kir2.1, uninjected oocytes were also labeled as a control. Oocytes treated in this manner displayed fluorescence at the cell surface. Oocytes expressing the channel displayed 65% greater fluorescence intensity than uninjected oocytes, suggesting that one or both of the two putative extracellular cysteines of Kir2.1 are labeled by the maleimide. After 3 s of irradiation, fluorescence was measured at the animal pole at 2- or 2.5 min intervals over a 30-min period.[83] (Figure 4.8)

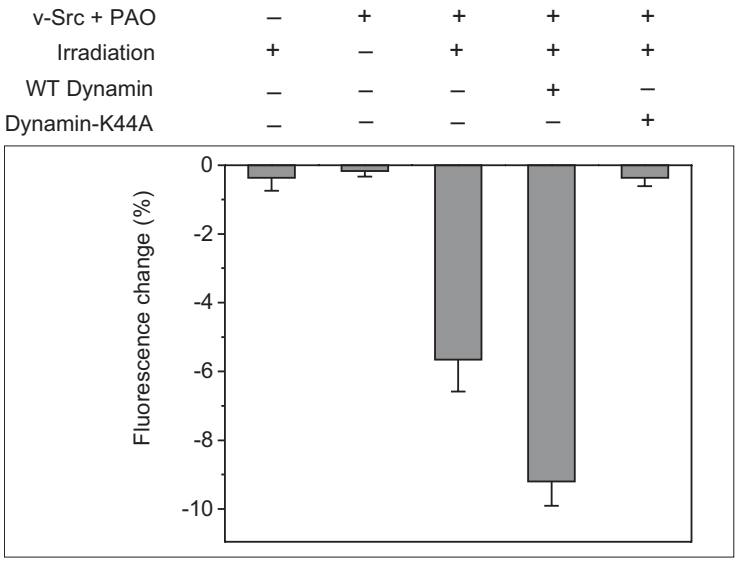

Figure 4.8 Normalized, average fluorescence change at t = 30 min for oocytes expressing Kir2.1-Y242TAG suppressed with Tyr(ONb) and treated with PAO, then labeled with tetramethylrhodamine maleimide. The first column represents a control in which oocytes were not co-injected with v-Src. In all other columns, oocytes expressed the Kir2.1-Y242Tyr(ONB) along with v-Src. The second column represents a control in which oocytes were not irradiated. In the third column, no exogenous dynamin was added. The fourth column shows oocytes co-expressing WT dynamin. The fifth column represents oocytes co-expressing dynamin-K44A. Each bar represents 6 or 7 oocytes. The average values (and ranges) for 100% fluorescence were 5.76 (3 to 9.5), 5.74 (3.5 to 7.2), 6.45 (3.7 to 9.5), 5.60 (3.93 to 6.92), and 5.62 (1 to 9.7) V.

Averaged data from six or seven oocytes are collected in Table 4.7. In oocytes expressing Kir2.1 with Tyr(ONb) at Y242 but not v-Src, the fluorescence change at 30 min was similar to that of non-irradiated cells expressing v-Src, $0.4 \pm 0.4\%$ and $0.2 \pm 0.2\%$, respectively. Cells that expressed both channel and kinase without added dynamin showed an average fluorescence change of $5.7 \pm 0.9\%$ 30 min after irradiation. The co-injection of WT dynamin increased endocytosis markedly: there was a $9.2 \pm 0.7\%$ change over 30 min. As before, dominant negative dynamin suppressed membrane turnover to the level of uninjected oocytes. Oocytes co-injected with dynamin-K44A showed only a $0.4 \pm 0.2\%$ fluorescence change 30 min after tyrosine decaging. Net membrane internalization is revealed by decreased fluorescence, possibly because the exciting and/or emitted light is partially shielded by intracellular pigment granules and other structures. Corroborating the capacitance measurements, irradiation leads to internalization only in oocytes co-expressing v-Src, caged Kir2.1, and endogenous or added WT dynamin under conditions favoring tyrosine phosphorylation. Thus, both capacitance and fluorescence measurements imply that dynamin is required for decaging-induced endocytotic activity in the cell.

v-Src	**hν**	**WT dynamin**	**K44A dynamin**	**% decrease±SEM**
-	+	-	-	0.4±0.4
+	-	-	-	0.2±0.2
+	+	-	-	5.7±0.9
+	+	+	-	9.2±0.7
+	+	-	+	0.4±0.2

Table 4.7 Normalized average surface fluorescence decrease of oocytes expressing Kir2.1 Y242TAG suppressed with Tyr(ONb) thirty minutes after initiation of experiment.

4.3.2.6 Tyrosine phosphorylation decreases Kir2.1 conductance and decreases total open channels per patch

In single-channel experiments on WT Kir2.1 at –80 mV and –100 mV, we found that co-expression of v-Src and treatment with PAO had two major effects on channel openings. First, conditions favoring tyrosine phosphorylation decrease the conductance of Kir2.1. For instance, Figure 4.9 presents tracings and all-points histograms for oocytes injected either with Kir2.1 alone, untreated with PAO, or with Kir and v-Src and treated with PAO. The single-channel conductances for control and Src and/or PAO oocytes were 17.5 $\pm$ 0.4 pS and 12.3 $\pm$ 0.2 pS (mean $\pm$ SEM, n = 8 and 5, respectively), amounting to a 30% decrease in single-channel conductance. We found no additional substates, suggesting that the conductance decrease is not graded with the number of affected subunits in a channel. Thus at least part of the phosphorylation-induced decrease in macroscopic currents derives from a decreased single-channel current.

Second, v-Src/PAO patches consistently displayed fewer active channels. In a series of recordings with tightly controlled pipette tip diameter, three of five untreated patches occasionally displayed two simultaneous openings, and the other two displayed only a single opening. Therefore the average peak was 1.6 simultaneous openings. On the other hand, none of five Src/PAO patches displayed more than one simultaneous opening; and two of these patches displayed no openings. Therefore the average number of peak simultaneous openings was 0.6. These data show that v-Src/PAO decreases either the number of active channels per patch or the open probability P_{open}. We noted that P_{open} was near 0.5 for both untreated and v-Src/PAO patches with only a single channel; therefore

the probable basis of the difference is that v-Src/PAO patches contained fewer active channels.

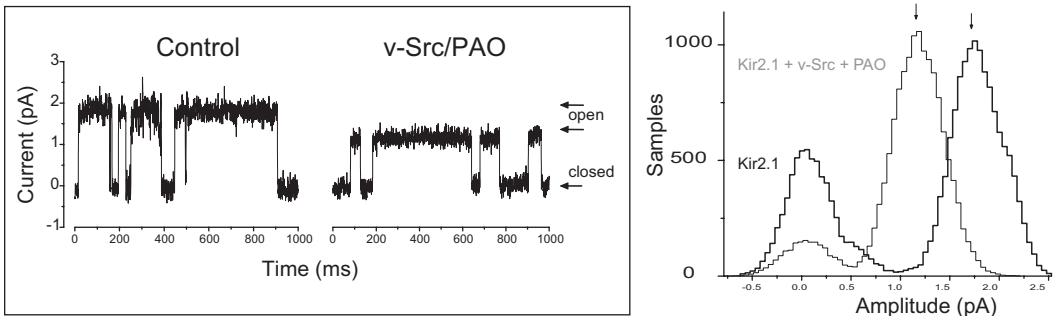

Figure 4.9 Conditions favoring tyrosine phosphorylation decrease single-channel conductance of WT Kir2.1. Left panel: Traces showing exemplar single-channel currents from cell-attached patches at –100 mV. The arrows point to the closed states and to the open states for control oocytes (left) and for oocytes co-injected with v-Src and treated with PAO (right). Right panel: Normalized all-points amplitude histograms for exemplar patches. Data from an oocyte injected with Kir2.1 alone are shown as heavy lines, and data from an oocyte injected with Kir2.1 + v-Src and exposed to PAO are shown as light lines. The arrows show open-channel amplitudes from Gaussian fits to the data, 1.69 and 1.15 pA for the control and v-Src/PAO patches, respectively.

4.3.2.7 There Is No Direct Evidence for Tyrosine Phosphorylation of Kir2.1

Active tyrosine kinases decrease the activity of WT Kir2.1 (Table 4.1), are required for the decreases in both current and membrane area after tyrosine decaging (Table 4.3 and Table 4.4), and produce decreases in active channel density per patch (Figure 4.9). None of these effects is observed for the Y242F mutant channel. The most direct interpretation of these data is that covalent modification of Y242 causes these effects, as proposed in earlier work on this system. It is also possible that this tyrosine residue is the interaction partner of proteins that must themselves be tyrosine phosphorylated for full activity, as is the case for many of the proteins in the clathrin-mediated endocytotic pathway.

Therefore, we sought evidence that Kir2.1 is phosphorylated at position 242 in the presence of kinases and phosphatase inhibitors. The primary strategy used to detect phosphorylation of Y242 was Western blotting with anti-phosphotyrosine antibodies. For

the purposes of immunoprecipitation and immunostaining of the channel, a Kir2.1 construct with the hemagglutinin (HA) epitope at the carboxyl terminus was generated. We verified in electrophysiological experiments that functional expression and inhibition by v-Src/PAO of Kir2.1-HA were similar to WT Kir2.1. In addition, a Y242F-HA construct was made and shown to behave like the Y242F channel.

Also, a panel of anti-phosphotyrosine antibodies was examined to optimize sensitivity under the present experimental conditions, with the result that 4G10 gave the highest sensitivity, followed closely by PY72. (Figure 4.10)

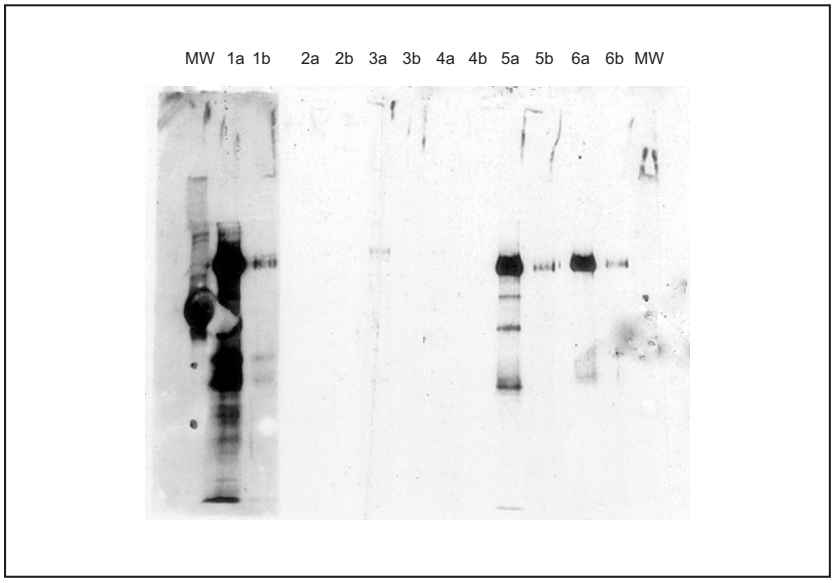

Figure 4.10 Comparison of anti-phosphotyrosine antibody affinities in a Western blot of positive control extract from EGF-stimulated cells (a = 2 μg, b = 0.2 μg total protein). Lane 1: Upstate Biotech 4G10. Lane 2: Covance 2G8-D6. Lane 3: Covance 6G9. Lane 4: Covance 1G2. Lane 5: Covance PY72. Lane 6: Covance PY20.

To establish whether Western blotting with anti-PY antibodies was sufficiently sensitive to detect tyrosine phosphorylation of integral membrane proteins expressed in oocytes, control experiments were performed using the receptor tyrosine kinase TrkB. This kinase undergoes auto-phosphorylation on tyrosine in response to the binding of its ligand, BDNF. Plasma membranes from BDNF-stimulated oocytes expressing TrkB were

isolated by physical dissection. Western blotting with an anti-TrkB antibody (Santa Cruz C14) shows readily observable staining at the expected molecular mass (Figure 4.11). As expected, uninjected oocytes show no anti-TrkB staining. Blotting with an anti-phosphotyrosine antibody (4G10) detects numerous phosphoproteins in the oocyte membrane, which is consistent with the effects of treating the oocytes with a tyrosine phosphatase inhibitor. Oocytes expressing TrkB contain a tyrosine-phosphorylated protein that co-localizes with TrkB and that is not present in uninjected oocytes. Densitometry showed that the phosphorylated TrkB band is roughly as intense as the nearby bands corresponding to endogenous phosphorylated proteins.

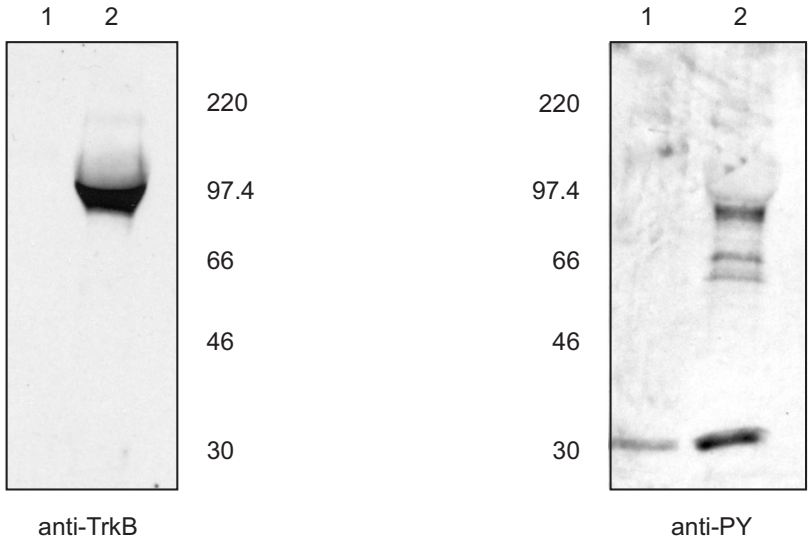

Figure 4.11 Detection of phosphorylated TrkB serves as a positive control for the detection of phosphorylated integral membrane protein from dissected oocyte plasma membranes. Western blot of membranes from BDNF-stimulated oocytes expressing TrkB shows positive staining with both anti-TrkB and anti-PY antibodies. The left panel was stained with Santa Cruz C14 anti-TrkB antibody. Lane 1: Uninjected oocytes. Lane 2: TrkB-expressing oocytes. The right panel was stained with Upstate Biotech 4G10 anti-phosphotyrosine antibody. Lane 1: Uninjected oocytes. Lane 2: TrkB-expressing oocytes.

Comparable experiments were carried out with Kir2.1-HA constructs (Figure 4.12). Kir2.1 constructs are clearly detectable by the anti-HA antibody (HA.11) at the appropriate molecular mass. A protein produced by *in vitro* translation of Kir2.1-HA

mRNA from wheat germ extract confirms the assignment of monomeric Kir2.1 subunits. The stained upper molecular mass bands presumably represent oligomers that are not denatured, even under SDS-PAGE conditions. In contrast, staining Western blots with the anti-phosphotyrosine antibody gives no convincing signal corresponding to Kir2.1 monomer or oligomer. Phosphoproteins are clearly present at a variety of other molecular masses, which is consistent with the TrkB results and corroborates that the assay does detect membrane phosphoproteins. That these phosphoproteins are also present in uninjected oocytes treated with PAO confirms that they do not arise from Kir2.1. Any staining in the region corresponding to monomeric Kir2.1 is <10% as intense as that for nearby endogenous phosphorylated proteins.

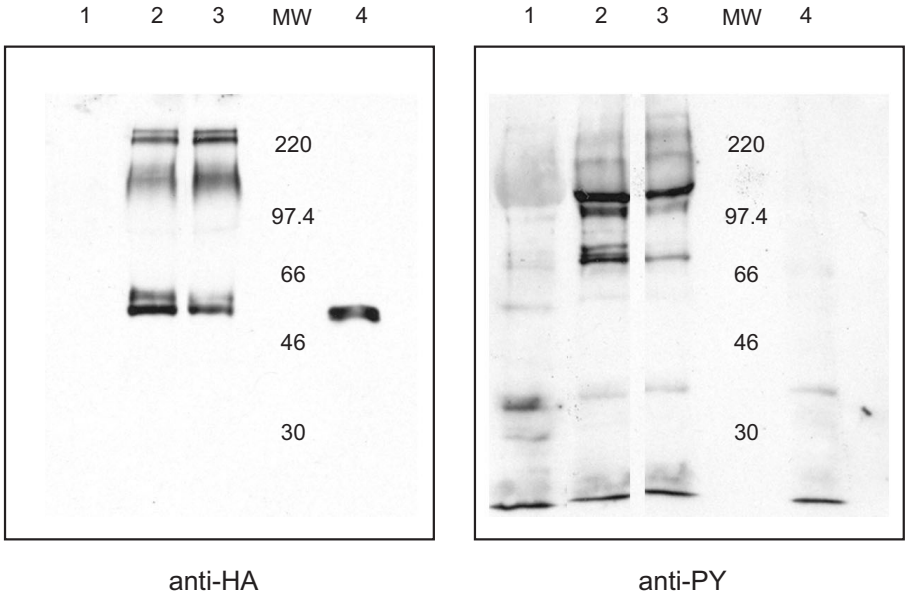

Figure 4.12 Failure to detect Kir2.1 phosphorylation in membranes dissected from oocytes expressing the channel. Western blot of membranes from oocytes expressing epitope-tagged Kir2.1 shows positive staining with anti-HA antibody, but not with the anti-phosphotyrosine antibody 4G10. The left panel is stained with Covance HA.11. Lane 1: Uninjected oocytes. Lane 2: Kir2.1-HA. Lane 3: Kir2.1Y242F-HA. Lane 4: Kir2.1-HA prepared by *in vitro* translation from wheat germ extract. Lanes 1-3 contain protein from membranes dissected from 21-23 oocytes.

In addition to these experiments, a number of other immunoprecipitation and immunodetection schemes were examined. Immunoprecipitation of phosphoproteins from oocyte homogenates with anti-PY antibodies followed by detection with anti-HA antibodies was undertaken, as well as the reverse. A completely different assay was also attempted, namely, autoradiography. Even though this technique is often considered to be more sensitive than Western blotting, it has the disadvantage of not distinguishing between phosphorylation on tyrosine, serine, or threonine without phosphopeptide mapping. Oocytes were supplied with ^{32}P either by co-injection with mRNA encoding the channel, or by incubation in γ-[^{32}P]ATP. HA-tagged channels were immunoprecipitated from whole-cell membrane preparations and from physically dissected membranes by both anti-HA and anti-PY antibodies and subjected to SDS PAGE. No differences between the Kir2.1-HA and Kir2.1-Y242F-HA channels were ever observed in ^{32}P autoradiography, and further mapping was not attempted. That we did not detect tyrosine phosphorylation of Kir2.1 is not conclusive, but it leads us to the explanation that other protein(s) may be phosphorylated. Interactions among these proteins, or between these proteins and Kir2.1, may lead to downregulation of K^+ current and endocytosis after Y242 is de-caged.

4.3.3 Discussion

4.3.3.1 Caged tyrosine allows study of ion channel modulation

Evidence for the regulation of ion channels by phosphorylation has become increasingly difficult to ignore in recent years.[84,85] In most cases, it has been impossible to establish the molecular basis for this regulation. In principle, phosphorylation could

directly influence channel properties by inducing conformational changes in ion channel proteins themselves. Alternatively, phosphorylation may promote, inhibit, or alter protein-protein interactions between the channel and other potential modulators of channel function. In the latter case, information about the kinetics of these events may be useful preliminary knowledge in helping to identify what kinds of processes may lie downstream of phosphoryl transfer. The use of caged compounds for determining the kinetics of cellular events is well-precedented.[4-6] Through the use of nonsense suppression to introduce unnatural amino acids, functional groups on the ion channel itself may be caged. The photolytic decaging of protected tyrosine has been demonstrated in the nicotinic acetylcholine receptor, but for the study of ion channel phosphorylation, caged tyrosine represents a new tool.[43] A particular tyrosine is rendered unsuitable as a substrate for phosphorylation until the moment it is released by UV irradiation provided by the experimenter.

Here, Kir2.1 was chosen as an experimental system, because there is a clearly detectable current reduction dependent upon a single tyrosine in the C-terminal intracellular tail of the receptor, Y242. Mutation of this residue to phenylalanine abolishes the effects of tyrosine kinases on whole-cell channel conductance.[76] (Figure 4.13)

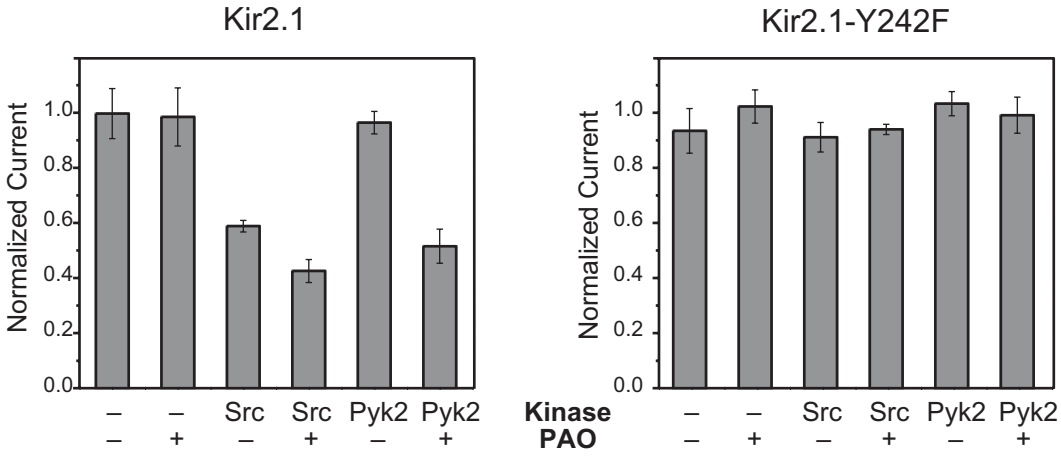

Figure 4.13 Whole-cell current from oocytes expressing Kir2.1 (left panel) and Kir2.1-Y242F (right panel). Data columns represent normalized currents (mean ± SEM, 4-5 oocytes). Where indicated, oocytes were co-injected with cRNA for tyrosine kinases v-Src or Pyk2 and incubated with 10 μM PAO for at least 30 min prior to recording. 100% corresponds to 13.3 μA for WT and 31.4 μA for Y242F.

When this tyrosine is replaced with Tyr(ONb), the channel becomes insensitive to the activity of v-Src, in the same way that the Y242F mutant fails to respond to tyrosine kinases. However, irradiation reveals the wild-type residue, rendering the channel sensitive to tyrosine kinase-mediated current modulation. Over the course of the next thirty minutes or so, the whole-cell current decreases by about 50%. (Figure 4.14)

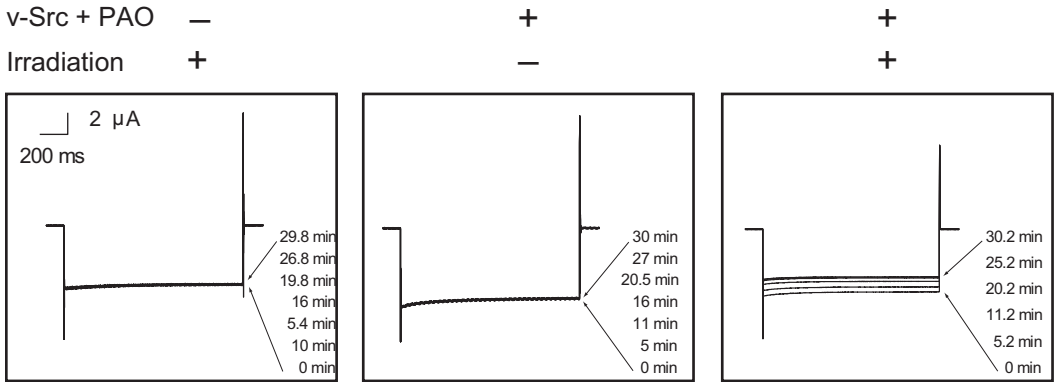

Figure 4.14 Inhibition of current in oocytes expressing Kir2.1-Y242TAG suppressed with Tyr(ONb), shown by typical current traces from individual oocytes. Left panel: The effect of irradiating an oocyte (3 s) that is neither co-expressing v-Src nor exposed to PAO. Center panel: Effect of co-expression of v-Src and exposure to PAO, but no irradiation of the oocyte. Right panel: Traces from an oocyte co-expressing v-Src, exposed to PAO, and irradiated. Oocytes were clamped at 0 mV and stepped to -80 mV to elicit inward current. Bath solutions contained 96 mM KCl. Time after irradiation is indicated.

This time course seems slow for a conformational change resulting in altered channel properties. It is possible that current reduction results from protein-protein interactions arising as a result of phosphorylation-induced conformational changes, however. In order to understand the nature of these interactions, it is necessary to consider the various pathways which could account for the phenomenon.

As in any mutagenesis experiment on an integral membrane protein, it is difficult to be certain that the conformation of the mutant protein is identical to that of the wild-type protein. The nitrobenzyl group adds steric bulk to the tyrosine side chain and prohibits the tyrosyl hydroxyl from engaging in hydrogen bonding. It could be the case that photolysis simply allows the protein to adopt the wild-type conformation, perhaps permitting the binding of another protein which is blocked by Tyr(ONb). The caged Kir2.1 behaves identically to the wild-type channel by most measures, and the necessity for both a tyrosine kinase and a phosphatase inhibitor to induce current inhibition point to a role for phosphorylation. However, we cannot rule out the possibility that a phosphoprotein which would normally bind to the C-terminal region of Kir2.1 and decrease its current is able to do so after removal of the protecting group.

4.3.3.2 Kir2.1 current decrease could result from endocytosis

Another possibility to account for the current reduction we observe upon liberating the tyrosine residue is that the tyrosine itself is an necessary component of some protein-protein interaction motif. In fact, the sequence in which Y242 occurs, YIPLD, is a consensus sequence for clathrin-mediated endocytosis. The motif YXXΦ, where X is any amino acid and Φ is a hydrophobic residue, has been proposed as the recognition signal for AP-2, an adapter protein which targets polypeptides to clathrin-coated vesicles.

Crystallographic evidence confirms that the AP-2 μ subunit is able to bind peptides containing the YXXΦ motif.[74,86] A study of the ENaC channel in *Xenopus* oocytes has demonstrated that a tyrosine residue in such a motif is functionally important in targeting an ion channel for removal from the plasma membrane.[77]

An obvious explanation for the phenomenon we observed with Kir2.1 would be that caged tyrosine protects Kir2.1 from incorporation into clathrin-coated vesicles. Once photolysis liberates the wild-type residue in a tyrosine-based endocytotic motif, however, the channel is removed from the plasma membrane by a clathrin-mediated pathway. This would neatly account for the observed loss in current. In addition, an endocytotic mechanism could easily be regulated by the phosphorylation state of tyrosine. For example, negative regulation of endocytosis by tyrosine kinases could occur if phosphorylation of the tyrosine in this motif precludes binding, as suggested by the crystal structure of a YXXΦ-containing peptide bound to AP-2 and a number of functional studies.[78,87-89] Alternatively, endocytosis could be positively regulated by a kinase if components of the endocytotic machinery required tyrosine phosphorylation for full activity.

4.3.3.3 Current decrease is not due solely to endocytosis

In order to establish the relative contribution of endocytotic and alternative phosphorylation-based mechanisms, experiments were performed to address the issue of receptor turnover. If Kir2.1 were being removed from the plasma membrane, this should be detectable in a number of ways. The two which we chose to examine are changes in whole-cell membrane capacitance, which is related to cellular surface area, and changes in surface fluorescence of thiol-labeled Kir2.1. First of all, there is a decrease in

membrane capacitance associated with current inhibition, as shown in Figure 4.15. Oocytes which are expressing receptors for which there is no current reduction upon irradiation also show no capacitance change. Conversely, oocytes expressing Kir2.1 suppressed with Tyr(ONb) at position 242 show capacitance decrease if and only if they are co-injected with tyrosine kinase, treated with a tyrosine phosphatase inhibitor, and are irradiated to remove the nitrobenzyl protecting group.

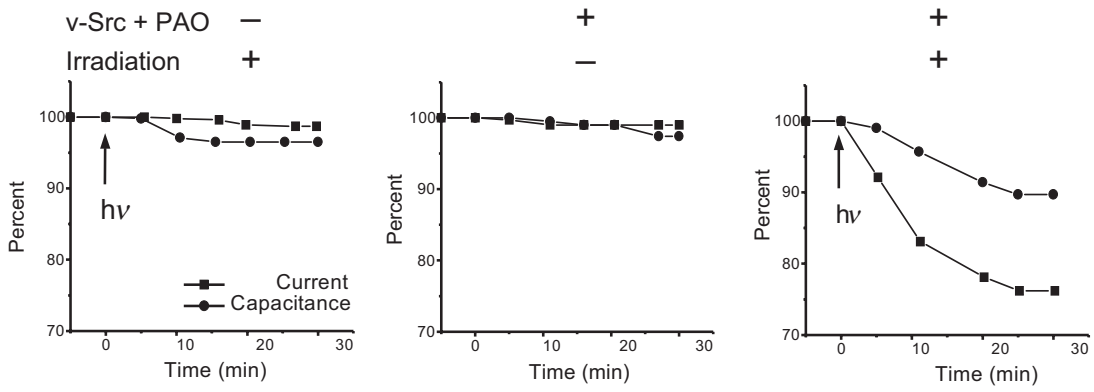

Figure 4.15 Inhibition of current and decrease of capacitance in oocytes expressing Kir2.1-Y242TAG suppressed with Tyr(ONb). Typical current traces from individual oocytes are shown. Left panel: The effect of irradiating an oocyte (3 s at arrow) that is neither co-expressing v-Src nor exposed to PAO. Center panel: Effect of co-expression of v-Src and exposure to PAO, but no irradiation of the oocyte. Right panel: Traces from an oocyte co-expressing v-Src, exposed to PAO, and irradiated. Oocytes were clamped at 0 mV and stepped to -80 mV to elicit inward current. Bath solutions contained 96 mM KCl.

The second experiment corroborates this. In this case, the oocyte surface was labeled with a membrane-impermeant thiol-reactive fluorescent compound (Figure 4.16). By viewing the fluorescence decrease over time, a similar trend to that seen by capacitance measurements was observed. Although the time course of the capacitance change and the extent are slower and not as great as those of the whole-cell current change, it appears that endocytosis is stimulated by kinase-mediated events subsequent to uncaging a tyrosine at position 242.

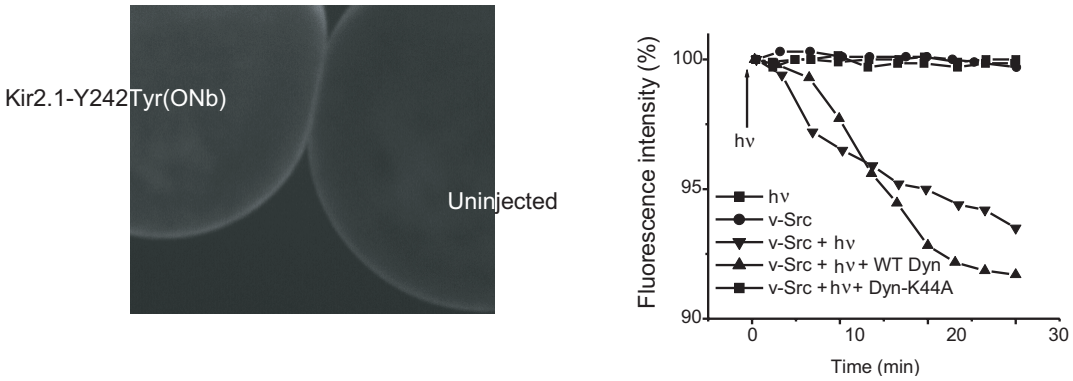

Figure 4.16 Fluorescence analysis of membrane retrieval. Left panel: Confocal image of two oocytes labeled with 10 μM tetramethylrhodamine-5-maleimide, a membrane-impermeant thiol-reactive fluorophore. The oocyte at left was injected with v-Src and Kir2.1-Y242TAG suppressed with Tyr(ONb). Oocyte on the right was not injected. Right panel: Fluorescence measurements for individual oocytes co-expressing v-Src and Kir2.1 Y242Tyr(ONb) and exposed to PAO. Oocytes were labeled with 10 μM tetramethylrhodamine maleimide for 30 min prior to recording. Fluorescence is measured as PMT output voltage. As indicated, controls included omission of co-injected v-Src and omission of irradiation.

Both of these experiments measured changes which would arise from any endocytotic mechanism. However, since the caged tyrosine makes up part of a tyrosine-based clathrin-mediated endocytosis motif, experiments to further delineate the role of specific endocytotic mechanisms are possible. The assembly of clathrin-coated vesicles is driven by the small GTPase dynamin. Previous work in other labs has shown that a K44A mutation in dynamin renders it unable to hydrolyze GTP.[81,82] More importantly, for the purposes of the experiments described here, this K44A dynamin is capable of exerting a dominant negative effect over wild-type dynamin. Indeed, dominant-negative dynamin has been used in *Xenopus* oocytes to suppress the activity of endogenous dynamin and largely shut down the clathrin-mediated endocytotic pathway.[77] Co-injection of dominant negative dynamin should render the tyrosine-based endocytosis motif of Kir2.1 ineffectual in removing channels from the plasma membrane. If this is the primary mechanism by which current is inhibited subsequent to the de-caging of Tyr(ONb) at position 242, dominant negative dynamin should remove the observed current reduction.

What was observed instead is that dominant negative dynamin diminishes the degree of current inhibition, but does not abolish it. (Figure 4.17)

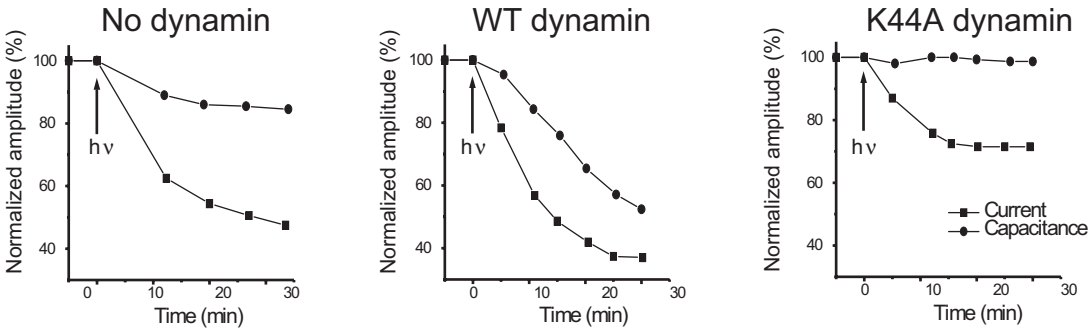

Figure 4.17 Dynamin expression distinguishes inhibition of the channel from endocytosis. Current and capacitance data from representative oocytes co-expressing v-Src and Kir2.1-Y242TAG suppressed with Tyr(ONb) and treated with PAO. Data were recorded 48 h after injection. Left panel: An oocyte without co-injected dynamin cRNA. Center panel: An oocyte co-injected with 10 ng WT dynamin cRNA. The capacitance decrease for this cell was unusually large. Right panel: An oocyte co-injected with 10 ng dominant negative dynamin-K44A.

In these experiments, the mean current reduction with the clathrin-dependent pathway intact was 41%. When the pathway is shut down (as evidenced by the 4% capacitance change, relative to 3% for uninjected oocytes), the current reduction was 28%. (Table 4.5 and Table 4.6) Thus, the current decrease appears to be partially dependent on endocytosis. Oocytes which are defective in their ability to remove membrane proteins from the cell surface do not undergo the full extent of current reduction. However, some current reduction is seen, in spite of the fact that plasma membrane retrieval has been practically eliminated by dominant negative dynamin. The conclusion from this set of experiments is that clathrin-mediated endocytosis is operative in reducing whole-cell K^+ currents, but that it is not responsible for all of the current inhibition observed after de-caging Y242. A non-clathrin pathway has been reported for ligand-gated ion channel endocytosis that operates even in the presence of dominant-negative dynamin.[90]

Alternatively, pathways acting directly on the channel may operate along with clathrin-mediated endocytosis.

In fact, endocytosis and phosphorylation are not completely independent phenomena in these experiments. Figure 4.15 shows that endocytosis appears to be stimulated by phosphorylation in an interesting way. Simply revealing the native YXXΦ endocytotic motif by photolysis does not cause the whole-cell capacitance change associated with endocytotic activity. Apparently, the clathrin-mediated pathway is unable by itself to cause endocytosis with its attendant change in membrane capacitance. Only when the tyrosine is revealed and tyrosine kinase is present is there an observable capacitance change. At present, it is difficult to know with certainty why native Kir2.1 and v-Src are required for whole-cell capacitance decrease. As indicated above, the crystal structure of AP-2 μ co-crystallized with YXXΦ peptide suggests that phosphotyrosine would be unable to make the requisite binding contacts.[78] Thus, it would be expected that v-Src might inhibit endocytosis. There are a number of reasons which might explain why our observation is at variance with this. First of all, there is presumably some regulation of AP-2 binding to tyrosine-based endocytosis motifs, which quite commonly occur multiple times in a single protein.[91] Kir2.1 contains two more C-terminal YXXΦ sequences, YEPV from 326-329 and YSRF, comprising residues 340-344 as well as a potential dileucine motif at 231-232. (Figure 4.18)

MGSVRTNRYSIVSSEEDGMKLATMAVANGFGNGKSKVHTRQQCR
SRFVKKDGHCNVQFINVGEKGQRYLADIFTTCVDIRWRWMLVIF
CLAFVLSWLFFGCVFWLIALLHGDLDTSKVSKACVSEVNSFTAA
FLFSIETQTTIGYGFRCVTDECPIAVFMVVFQSIVGCIIDAFII
GAVMAKMAKPKKRNETLVFSHNAVIAMRDGKLCLMWRVGNLRKS
HLVEAHVRAQLLKSRITSEGEYIPLDQIDINVGFDSGIDRIFLV
SPITIVHEIDEDSPLYDLSKQDIDNADFEIVVILEGMVEATAMT
TQCRSSYLANEILWGHRYEPVLFEEKHYYKVDYSRFHKTYEVPN
TPLCSARDLAEKKYILSNANSFCYENEVALTSKEEEEDSENGVP
ESTSTDSPPGIDLHNQASVPLEPRPLRRESEI

Figure 4.18 Primary sequence of Kir2.1 showing the presence of numerous endocytosis motifs. The motif including Y242 is indicated in red, the others in blue.

It may be that phosphorylation of Y242 positively regulates binding to the more N-terminal endocytotic motifs. Second, the method presented here relies on functional interactions between a multiple-subunit, multiple transmembrane-domain integral membrane protein in a living cell. It could be that the evidence collected thus far for downregulation of endocytosis via tyrosine phosphorylation represents only one of a number of important interactions for regulating endocytosis via tyrosine-based motifs.

4.3.3.4 Phosphorylation is implicated in Kir2.1 modulation

In addition, phosphorylation state may well regulate endocytosis at the level of the cycling of endocytotic vesicles. Just as there is an equilibrium between kinases and phosphatases, there must be an equilibrium between endocytosis and exocytosis. The signals by which integral membrane proteins are targeted to endocytotic vesicles are just beginning to be discovered, and even less is known about the signals for retrieval.[74,86] Progress in this area is likely to come from the study of G-protein coupled receptors, where the role of internalization and recycling in causing agonist-dependent desensitization is rapidly being elucidated.[92] Based on this work, it seems possible, even probable, that phosphorylation of ion channels determines whether they are recycled to

the plasma membrane or targeted for degradation. Since vesicle internalization and re-fusion modulate whole-cell capacitance changes, the mediation of their targeting by the phosphorylation state of their membrane protein contents could explain the apparent requirement for Kir2.1 to be phosphorylated at Y242.

4.3.3.5 Attempts to detect phosphorylation

Since the available evidence points strongly toward a role for tyrosine phosphorylation in the observed current reduction of Kir2.1, it would be valuable to know whether or not the channel is phosphorylated directly. Both anti-phosphotyrosine antibodies and ^{32}P were employed in an effort to detect the presence of a phosphoryl group on wild-type and de-caged Kir2.1. These experiments failed to detect such phosphorylation. The oocyte system has been reported to be difficult to work with in this way, so it is unwarranted to conclude that failure to detect phosphorylation implies that the protein is not phosphorylated. Experiments are ongoing to attempt to detect a role for phosphorylation of Y242 in *Xenopus* oocytes. Given the difficulty of biochemically detecting phosphorylation, the alternative technique of introducing non-hydrolyzable phosphotyrosine analogs at position 242 is being considered. Progress toward this goal will be discussed further in Chapter 5.

As noted earlier, a variety of tyrosine kinases are able to induce the current inhibition we observed. Since Y242 is unlikely to be a consensus phosphorylation site for all of these kinases, the implication is that a downstream kinase is ultimately responsible for the effect. Identification of this kinase represents a long-term goal for studies on the molecular detail of phosphorylation-mediated ion channel regulation. Introduction of a mechanism-based inhibitor as an amino acid side chain is a potentially useful method for

trapping the kinase responsible for phosphorylation. Alternatively, antisense mRNA to a series of tyrosine kinases may reveal that the diminished activity of a particular kinase ameliorates the current inhibition resulting from phosphorylation.

4.3.4 Summary

Active tyrosine kinases decrease the activity of WT Kir2.1, are required for the decreases in both current and membrane area following tyrosine decaging, and produce decreases in active channel density per patch. None of these effects is observed for the Y242F mutant channel. Usually, these data would be interpreted to suggest that phosphorylation of Y242 causes these effects, as proposed in earlier work on this system. However, the involvement of tyrosine 242 in an endocytosis motif suggests an alternative explanation. All of these observations are consistent with tyrosine-based endocytosis of the channel. The requirement for tyrosine kinases could reflect the need for components of the endocytotic machinery to be activated by tyrosine phosphorylation. The requirement for a native tyrosine at position 242 of Kir2.1 could be explained by the apparent involvement of this residue in binding of adapter proteins targeting the channel for endocytosis. Thus, the question arises of whether our observations result from phosphorylation of Y242 or from endocytosis of the channel subsequent to unmasking of a tyrosine-based sorting motif.

Biochemical evidence that Kir2.1 is phosphorylated at position 242 in cells which exhibit current decrease would permit a compelling claim that phosphorylation is the mechanism responsible for channel modulation subsequent to photolysis. We were unable to obtain such evidence. (Figure 4.12) Unfortunately, failure to detect phosphorylation is itself somewhat difficult to interpret. As a positive control for

tyrosine phosphorylation, the auto-phosphorylated receptor tyrosine kinase TrkB was expressed in oocytes. As expected, both the 4G10 anti-PY and the C14 anti-TrkB antibodies show easily observable staining and co-localization under standard Western blotting conditions. (Figure 4.11) It is evident that the technique is capable of directly detecting tyrosine phosphorylation of integral membrane proteins expressed in *Xenopus* oocytes. However, there are complications in extending this result to the detection of phosphorylated Kir2.1. The level of expression of the two proteins, the extent of tyrosine phosphorylation, the duration of protein phosphorylation, and the sensitivity of particular phosphotyrosine residues to de-phosphorylation may well differ. As a result, the inference that Kir2.1 is not phosphorylated is not conclusive.

Any proposed mechanism to account for the decrease in whole-cell current and capacitance subsequent to photolysis must take into account the following observations. First, both a free tyrosine side chain at position 242 and tyrosine kinases are required. (Figure 4.14) Second, the presence of kinases and Y242 brings about decreases in whole-cell current, membrane capacitance, and surface fluorescence. (Figure 4.14, Figure 4.15, Figure 4.16) Third, dominant-negative dynamin blocks the changes in capacitance and fluorescence and causes a partial block of current decrease. (Figure 4.17) Fourth, the presence of v-Src and PAO decreases the number of channels per patch without affecting the single-channel properties of individual channels. (Figure 4.9) Experiments by other laboratories have suggested also that phosphotyrosine is not competent for recognition by adapter proteins responsible for targeting membrane proteins for endocytosis.[78,87-89]

All of these observations (and our inability to detect phosphotyrosine) fit neatly with a model in which the role of Y242 is in targeting Kir2.1 for endocytosis, with one

exception. This exception is that a significant component of current decrease is insensitive to dominant-negative dynamin. It is clear that dominant-negative dynamin suppresses changes in membrane capacitance. (Figure 4.7) If current decrease were solely a result of channel endocytosis, the predicted result of halting membrane internalization would be to eliminate current decrease. Since this is not the observed result, it is tempting to speculate that multiple mechanisms of channel modulation may be involved. Cells almost certainly regulate channels through both phosphorylation and endocytotic targeting. However, both of these effects would have to be in the same direction, have the same time course, and result in no alteration of single-channel properties. We therefore prefer a model in which interaction with the endocytotic machinery is the sole regulatory mechanism acting on Y242, which is consistent with the similarity of the observed kinetics in the presence and absence of dominant-negative dynamin.

In this model, a protein-protein interaction which is responsible for targeting of the channel to endocytotic vesicles occurs, even though the downstream pinching off of clathrin vesicles may be prohibited by dominant-negative dynamin. Channels in these invaginations are unable to contribute to the whole-cell current, possibly as a result of restricted flow of the external high-potassium recording solution through the dynamin collar which constricts the neck of the vesicle. As a result, the whole-cell current decreases even though the cell's surface area and capacitance remain the same. The extent of current decrease may be less than before because the arresting of vesicles may down-regulate the assembly of dynamin collars, or perhaps because some of the vesicle-bound channels remain active. As indicated above, it is difficult to exclude the

possibility that Y242 may be phosphorylated. In the absence of direct evidence, though, we feel the most parsimonious explanation of the data is that presented above.

Undoubtedly, further details will be forthcoming on the modulation of ion channels by both phosphorylation and endocytosis. At the currently achievable level of molecular detail, this study represents a delineation of the roles of these two processes in modulating Kir2.1 current through the common intermediate of a C-terminal tyrosine residue. Because of the complexity of multiple regulatory processes involving a single residue, we introduce in the next chapter a technique involving caged phosphoamino acids. Through the use of this methodology, we hope to control directly, for the first time, the phosphorylation state of a particular residue in a functioning channel inside a living cell.

4.3.5 Experimental methods

4.3.5.1 Chemical synthesis

The 4PO-protected amino acid Tyr(ONb) was prepared as reported.[61] Briefly, L-tyrosine was complexed with copper(II) to protect the amino and carboxyl termini. To this complex was added nitrobenzyl chloride under basic conditions, yielding Try(ONb). Addition of 4-pentenoic anhydride gave the N-protected 4-PO-Tyr(ONb). The amino acid was coupled to the dinucleotide dCA by established procedures.[93] In summary, the carboxyl terminus was converted to the cyanomethyl ester by treatment with chloroacetonitrile. The active ester was condensed with dCA under basic conditions to give the aminoacylated dinucleotide, which was enzymatically ligated to a 74-base tRNA precursor with T4 RNA ligase.

4.3.5.2 DNA / RNA constructs

tRNA THG73 was modified from eukaryotic *Tetrahymena thermophila* tRNAGln(CUA) as described and inserted into pUC19 giving the plasmid pTHG73.[93] pTHG73 was linearized by *Fok* I and transcribed *in vitro* using the MegaShortscript kit (Ambion).

The tyrosine codon at position 242 of the mouse Kir2.1 cDNA in pcDNA I was mutated to phenylalanine or to the nonsense codon TAG, giving two mutants called Kir2.1(Y242F) and Kir2.1(Y242TAG), respectively. Mutagenesis was carried out using the QuikChange kit (Stratagene). Mutations were verified by sequencing of both strands through the affected regions. The hemagglutinin antigenic sequence YPYDVPDYA was added to the C-terminus of Kir2.1 using PCR amplification, giving Kir2.1-HA. The Kir2.1 plasmids were linearized by *Not* I.

The cDNA for v-Src kinase (a gift of Dr. I. B. Levitan), PyK2 (a gift of Dr. J. Schlessinger), human WT dynamin I and dynamin-I-K44A (gifts of Dr. Alex van der Bliek and Dr. Thomas Moss), and rat TrkB (gift of G. Yancoupolis) were linearized by *XbaI*, *Ssp*I, *SalI* and *SalI* , and *XbaI* or *NotI*, respectively. All mRNAs were transcribed *in vitro* using the SP6 or T7 mMessage mMachine kit (Ambion) as appropriate.

4.3.5.3 Suppression of Kir2.1-Y242TAG with Tyr(ONB) in Xenopus oocytes

The 4PO-Tyr(ONb)-tRNA in 1 mM NaOAc, pH 4.5, was de-protected just prior to injection by mixing with equal volume of a saturated aqueous solution of iodine (1.2 mM) for 10 min at ambient temperature. 10–15 ng of Kir2.1(Y242TAG) mRNA and 20-25 ng of tRNA-Tyr(ONb) in a total volume of 32.2 nL per oocyte were co-injected into stage V and VI oocytes by a Drummond automatic injector. The cRNA for WT Kir2.1 cRNA, the conventional mutant Kir2.1-Y242F, or Kir2.1-HA were injected at 1

ng/oocyte. Oocytes were incubated in 50% L-15 medium supplemented with 7.5 mM HEPES, 0.8 mM of glutamine and 10 μg/ml of gentamycin sulfate, pH 7.5, at 18-20^{0}C. After incubation for 24-48 h, functional measurements were made.

4.3.5.4 Electrophysiology

For macroscopic recordings, oocytes were voltage clamped at 0 mV in a high K^+ solution (96 mM KCl, 2 mM NaCl, 1 mM $MgCl_2$, 1.5 mM $CaCl_2$ and 5 mM HEPES, pH 7.5) with two electrodes (filled with 3 M KCl, resistance 0.5-3 MΩ) and then stepped to a test potential of -80 mV using a GeneClamp 500 (Axon Instruments). Membrane capacitance was measured on oocytes clamped at 0 mV in response to a train of 10 mV pulses delivered at 2.9 Hz with 50% duty cycle. Voltage command signals were generated, and membrane capacitance measured, by the algorithms in pCLAMP 8.0 software (Axon Instruments). In preliminary experiments, capacitance measurements were verified manually by integrating the response to 10 mV test pulses.

For cell-attached single-channel recordings, the pipette solution and the bath contained the same high K^+ solution. The patch channel of the GeneClamp 500 was employed, with 2 kHz filtering. The signals were recorded and analyzed using FETCHEX, FETCHAN, and pSTAT in the pCLAMP 6 suite.

4.3.5.5 Decaging optics

The apparatus for Tyr(ONb) decaging was reported previously.[43] Light from a 300 W Hg arc lamp was filtered through a Schott UG11 filter to provide 300-350 nm light and was focused through a 50 mm quartz lens (Oriel) onto a liquid light guide (Oriel, 1 m long and 3 mm in diameter) connected to the recording chamber. At the chamber, the end of

the liquid light guide contacted a Pyrex cover slip placed at the bottom surface of the chamber, upon which the oocyte rested. Miller *et al.* reported that 3 s irradiation was sufficient for photolysis of over 90% of caged tyrosine on the oocyte surface.[43]

4.3.5.6 Fluorescence labeling and measurements

For non-specific labeling of the cell surface, oocytes were incubated in ND96 solution (96 mM NaCl, 2 mM KCl, 1 mM $MgCl_2$, 1.5 mM $CaCl_2$ and 5 mM HEPES, pH 7.5) containing 10 μM tetramethylrhodamine-5-maleimide for 30 min at 20-22 °C. The labeled oocytes were then washed five times with ND96 solution to remove unbound fluorescent dye. The labeling intensity was examined at the animal pole. Confocal images were taken with a Bio-Rad MRC 600 microscope with a 10x objective lens, with 10 average scans.

Surface fluorescence from labeled oocytes was measured using an Olympus IX-70-FLA inverted reflected-light fluorescence microscope.[83] Exciting light was delivered from a stabilized 100 W Hg lamp. We used a 40X, NA1.3 objective lens. A photomultiplier tube (PMT) attached at the side port recorded the fluorescence. To avoid bleaching, a shutter in the excitation pathway was opened and the fluorescence was measured for only 10 to 20 sec at intervals of 2 to 2.5 min. The emitted signal, as voltage from the PMT output, was appropriately amplified and filtered, then sent to an Axon Digidata interface for collecting data by pCLAMP 7 (Axon Instruments, Foster city, CA).

4.3.5.7 Immunochemical detection

Oocytes were injected with Kir2.1-HA. Plasma membranes were isolated by physical dissection. The hypotonic solution used to prepare the oocytes for dissection was

modified to contain 5 mM PAO and 1 mM sodium orthovanadate, one EDTA-free Boehringer Complete tablet per 40 ml, and 0.08% SDS (which expedites dissection). PAO was dissolved in DMSO and stored at -80 °C. Yolk and pigment granules were removed by a 2 min 14,000 rpm spin at 4 °C and the supernatant dissolved in 15 ml 2x SDS gel loading buffer. Samples were boiled for 5 min or heated to 55 °C for 10 min prior to loading. SDS PAGE was performed using 10% polyacrylamide (40T:1C) gels or 10% Tris-Cl ReadyGels (BioRad, Hercules CA).

Proteins were transferred to nitrocellulose overnight at 30 V. Blots were blocked for 1 hr in 1x TPBS [PBS containing 0.1% (v/v) Tween-20] and 5% (w/v) non-fat dried milk (Carnation, Columbus OH). Blots were exposed to primary antibody for one h in TPBS with 5% milk, washed three times 10 min each in TPBS, then incubated one h in TPBS containing 5% milk and secondary antibody. Detection employed ECL reagents from Amersham.

Primary antibodies included monoclonal HA.11 ascites fluid; monoclonal anti-phosphotyrosine antibodies 2G8-D6, 6G9, 1G2, PY20, PY72 (Covance, Berkeley CA), and 4G10 (Upstate Biotechnology, Lake Placid NY); and anti-TrkB antibody C14 (Santa Cruz Biotechnology, Santa Cruz CA). All Covance antibodies and 4G10 were diluted 1:1000 for Western blotting; C14 was diluted 1:200. Of the phosphotyrosine antibodies, 4G10 had the highest affinity under our conditions. PY72 also performed well. HRP-conjugated secondary antibodies included goat anti-mouse (Jackson Immunologicals) and donkey anti-rabbit (Amersham), diluted 1:5000 and 1:200, respectively.

4.3.5.8 Data analysis

The experimental data were analyzed using ORIGIN (Microcal Software, Inc.) and CLAMPFIT 8 software (Axon Instruments, Foster City, CA).

4.3.5.9 Reagents

BDNF was kindly provided by Dr. Andy Welcher (Amgen, Inc., Thousand Oaks CA).

4.4 References

1. Hunt, R. (Minneapolis Institute of Arts, Minneapolis, 1993).
2. Givens, R. S., Weber, J. F., Jung, A. H. and Park, C. H. New photoprotecting groups: desyl and p-hydroxyphenacyl phosphate and carboxylate esters. *Meth. Enz.* **291**, 1-29 (1998).
3. Marriott, G. (ed.) *Caged Compounds* (Academic Press, San Diego, CA, 1998).
4. Adams, S. R. and Tsien, R. Y. Controlling cell chemistry with caged compounds. *Ann. Rev. Physiol.* **55**, 755-84 (1993).
5. Lester, H. A. and Nerbonne, J. M. Physiological and pharmacological manipulations with light-flashes. *Ann. Rev. Biophys.* **11**, 151-175 (1982).
6. McCray, J. A. and Trentham, D. R. Properties and uses of photoreactive caged compounds. *Ann. Rev. Biophys.* **18**, 239-70 (1989).
7. Pirrung, M. C. and Nunn, D. S. Synthesis of photodeprotectable serine derivatives - caged serine. *Bioorg. Med. Chem. Lett.* **2**, 1489-1492 (1992).
8. Gallivan, J. P. *Ph.D. Thesis* (California Institute of Technology, Pasadena, CA, 2000).
9. Tatsu, Y., Shigeri, Y., Sogabe, S., Yumoto, N. and Yoshikawa, S. Solid-phase synthesis of caged peptides using tyrosine modified with a photocleavable protecting group: Application to the synthesis of caged neuropeptide. *Biochem. Biophys. Res. Comm.* **227**, 688-693 (1996).
10. Cheng, Q., Steinmetz, M. G. and Jayaraman, V. Photolysis of gamma-(alpha-carboxy-2-nitrobenzyl)-L-glutamic acid investigated in the microsecond time scale by time-resolved FTIR. *J. Am. Chem. Soc.* **124**, 7676-7677 (2002).
11. Gee, K. R., Niu, L., Schaper, K. and Hess, G. P. Caged bioactive carboxylates - synthesis, photolysis studies, and biological characterization of a new caged N-methyl-D-aspartic acid. *J. Org. Chem.* **60**, 4260-4263 (1995).
12. Okuno, T., Hirota, S. and Yamauchi, O. Folding character of cytochrome c studied by o-nitrobenzyl modification of methionine 65 and subsequent ultraviolet light irradiation. *Biochemistry* **39**, 7538-7545 (2000).
13. Gee, K. R., Niu, L., Schaper, K., Jayaraman, V. and Hess, G. P. Synthesis and photochemistry of a photolabile precursor of N-methyl-D- aspartate (NMDA) that is photolyzed in the microsecond time region and is suitable for chemical kinetic investigations of the NMDA receptor. *Biochemistry* **38**, 3140-3147 (1999).
14. Gee, K. R., Carpenter, B. K. and Hess, G. P. Synthesis, photochemistry, and biological characterization of photolabile protecting groups for carboxylic acids and neurotransmitters. *Meth. Enz.* **291**, 30-50 (1998).
15. Marriott, G. Caged protein conjugates and light-directed generation of protein activity: preparation, photoactivation, and spectroscopic characterization of caged G-actin conjugates. *Biochemistry* **33**, 9092-9097 (1994).
16. Messenger, J. B., Katayama, Y., Ogden, D. C., Corrie, J. E. T. and Trentham, D. R. Photolytic Release of Glutamate from Caged Glutamate Expands Squid Chromatophores. *J. Physiol.* **438**, P293-P293 (1991).

17. Tatsu, Y. et al. Synthesis of caged peptides using caged lysine: Application to the synthesis of caged AIP, a highly specific inhibitor of calmodulin-dependent protein kinase II. *Bioorg. Med. Chem. Lett.* **9**, 1093-1096 (1999).
18. Watai, Y., Sase, I., Shiono, H. and Nakano, Y. Regulation of nuclear import by light-induced activation of caged nuclear localization signal in living cells. *FEBS Lett.* **488**, 39-44 (2001).
19. Wieboldt, R. et al. Photolabile precursors of glutamate - synthesis, photochemical properties, and activation of glutamate receptors on a microsecond time-scale. *PNAS* **91**, 8752-8756 (1994).
20. Walker, J. W. et al. Signaling pathways underlying eosinophil cell motility revealed by using caged peptides. *PNAS* **95**, 1568-1573 (1998).
21. Curley, K. and Lawrence, D. S. Light-activated proteins. *Curr. Op. Chem. Biol.* **3**, 84-88 (1999).
22. Marriott, G. and Walker, J. W. Caged peptides and proteins: new probes to study polypeptide function in complex biological systems. *Trends Plant. Sci.* **4**, 330-334 (1999).
23. Curley, K. and Lawrence, D. S. Photoactivation of a signal transduction pathway in living cells. *J. Am. Chem. Soc.* **120**, 8573-8574 (1998).
24. Chang, C., Fernandez, T., Panchal, R. and Bayley, H. Caged catalytic subunit of cAMP-dependent protein kinase. *J. Am. Chem. Soc.* **120**, 7661-7662 (1998).
25. Chang, C., Niblack, B., Walker, B. and Bayley, H. A photogenerated pore-forming protein. *Chem. Biol.* **2**, 391-400 (1995).
26. Self, C. H. and Thompson, S. Light activatable antibodies: Models for remotely activatable proteins. *Nat. Med.* **2**, 817-820 (1996).
27. Golan, R., Zehavi, U., Naim, M., Patchornick, A. and Smirnoff, P. Inhibition of *Escherichia coli* β-galactosidase by 2-nitro-1-(4,5-dimethoxy-2-nitrophenyl)ethyl, a photoreversible thiol label. *Biochm. Biophys. Acta* **1293**, 238-242 (1996).
28. Pollitt, S. K. and Schultz, P. G. A photochemical switch for controlling protein-protein interactions. *Angew. Chem. Int. Ed. Eng.* **37**, 2104-2107 (1998).
29. Petersson, E. J., Brandt, G. S., Zacharias, N. M., Dougherty, D. A. and Lester, H. A. Caging proteins through unnatural amino acid mutagenesis. *Meth. Enz.* in press (2002).
30. Karginov, A. V., Lodder, M. and Hecht, S. M. Facile characterization of translation initiation via nonsense codon suppression. *Nucl. Acids Res.* **27**, 3283-3290 (1999).
31. Gilmore, M. A., Steward, L. E. and Chamberlin, A. R. Incorporation of noncoded amino acids by *in vitro* protein biosynthesis. *Top. Curr. Chem.* **202**, 77-99 (1999).
32. Sisido, M. and Hohsaka, T. Extension of protein functions by the incorporation of nonnatural amino acids. *Bull. Chem. Soc. Japan* **72**, 1409-1425 (1999).
33. Karginov, V. A., Mamaev, S. V. and Hecht, S. M. *In vitro* suppression as a tool for the investigation of translation initiation. *Nucl. Acids Res.* **25**, 3912-3916 (1997).
34. Bain, J. D., Switzer, C., Chamberlin, A. R. and Benner, S. A. Ribosome-mediated incorporation of a non-standard amino acid into a peptide through expansion of the genetic code. *Nature* **356**, 537-539 (1992).
35. England, P. M., Lester, H. A. and Dougherty, D. A. Mapping disulfide connectivity using backbone ester hydrolysis. *Biochemistry* **38**, 14409-14415 (1999).
36. England, P. M., Lester, H. A. and Dougherty, D. A. Incorporation of esters into proteins: Improved synthesis of hydroxyacyl tRNAs. *Tet. Lett.* **40**, 6189-6192 (1999).
37. Lyford, L. K. and Rosenberg, R. L. Cell-free expression and functional reconstitution of homo-oligomeric alpha7 nicotinic acetylcholine receptors into planar lipid bilayers. *J. Biol. Chem.* **274**, 25675-25681 (1999).
38. Chollet, A. and Turcatti, G. Mapping the binding sites of peptide and non-peptide molecules to G protein-coupled receptors by fluorescence. *Lett. Pept. Sci.* **5**, 79-82 (1998).
39. Lu, T. et al. Probing ion permeation and gating in a K^+ channel with backbone mutations in the selectivity filter. *Nat. Neurosci.* **4**, 239-246 (2001).
40. Nowak, M. W. et al. Nicotinic receptor binding site probed with unnatural amino acid incorporation in intact cells. *Science* **268**, 439-442 (1995).
41. Turcatti, G. et al. Probing the structure and function of the tachykinin neurokinin-2 receptor through biosynthetic incorporation of fluorescent amino acids at specific sites. *J. Biol. Chem.* **271**, 19991-19998 (1996).

42. Turcatti, G. et al. Fluorescent labeling of NK2 receptor at specific sites in vivo and fluorescence energy transfer analysis of NK2 ligand-receptor complexes. *Receptors Channels* **5**, 201-207 (1997).
43. Miller, J. P., Silverman, S. K., England, P. M., Dougherty, D. A. and Lester, H. A. Flash decaging of tyrosine side chains in an ion channel. *Neuron* **20**, 619-624 (1998).
44. Phillipson, K. P., Gallivan, J. P., Brandt, G. S., Dougherty, D. A. and Lester, H. A. Incorporation of caged cysteine and caged tyrosine into a transmembrane segment of the nicotinic acetylcholine receptor. *Am. J. Phys. Cell Phys.* **281**, C195-C208 (2001).
45. Tong, Y. et al. Tyrosine decaging leads to substantial membrane trafficking during modulation of an inward rectifier potassium channel. *J. Gen. Phys.* **117**, 103-118 (2001).
46. Cook, S. N. et al. Photochemically initiated protein splicing. *Angew. Chem. Int. Ed. Eng.* 34, 1629-1630 (1995).
47. Mendel, D., Ellman, J. A. and Schultz, P. G. Construction of a light-activated protein by unnatural amino acid mutagenesis. *J. Am. Chem. Soc.* **113**, 2758-2760 (1991).
48. Cornish, V. W., Mendel, D. and Schultz, P. G. Probing protein structure and function with an expanded genetic code. *Angew. Chem. Int. Ed. Eng.* **34**, 621-633 (1995).
49. England, P. M., Lester, H. A., Davidson, N. and Dougherty, D. A. Site-specific, photochemical proteolysis applied to ion channels *in vivo*. *PNAS* **94**, 11025-11030 (1997).
50. Short, G. F., Lodder, M., Laikhter, A. L., Arslan, T. and Hecht, S. M. Caged HIV-1 protease: Dimerization is independent of the ionization state of the active site aspartates. *J. Am. Chem. Soc.* **121**, 478-479 (1999).
51. Hohsaka, T., Kajihara, D., Ashizuka, Y., Murakami, H. and Sisido, M. Efficient incorporation of nonnatural amino acids with large aromatic groups into steptavidin in *in vitro* protein synthesizing systems. *J. Am. Chem. Soc.* **121**, 34-40 (1999).
52. Kanamori, T., Nishikawa, S., Shin, I., Schultz, P. G. and Endo, T. Probing the environment along the protein import pathways in yeast mitochondria by site-specific photocrosslinking. *PNAS* **94**, 485-490 (1997).
53. Kanamori, T. et al. Uncoupling of transfer of the presequence and unfolding of the mature domain in precursor translocation across the mitochondrial outer membrane. *PNAS* **96**, 3634-3639 (1999).
54. Martoglio, B., Hofmann, M. W., Brunner, J. and Dobberstein, B. The protein-conducting channel in the membrane of the endoplasmic reticulum is open laterally toward the lipid bilayer. *Cell* **81**, 207-214 (1995).
55. Mothes, W. et al. Molecular mechanism of membrane protein integration into the endoplasmic reticulum. *Cell* **89**, 523-533 (1997).
56. Niu, L. et al. Rapid chemical kinetic techniques for investigations of neurotransmitter receptors expressed in *Xenopus* oocytes. *PNAS* **93**, 12964-12968 (1996).
57. Parker, I., Callamaras, N. and Wier, W. G. A high-resolution, confocal laser-scanning microscope and flash photolysis system for physiological studies. *Cell Calcium* **21**, 441-452 (1997).
58. Nargeot, J. et al. A photoisomerizable muscarinic antagonist. Studies of binding and of conductance relaxations in frog heart. *J. Gen. Phys.* **79**, 657-678 (1982).
59. Dang, H., England, P. M., Farivar, S. S., Dougherty, D. A. and Lester, H. A. Probing the role of a conserved M1 proline residue in 5- hydroxytryptamine(3) receptor gating. *Mol. Pharm.* **57**, 1114-1122 (2000).
60. Beene, D. L. et al. Cation-pi interactions in ligand recognition by serotonergic ($5\text{-}HT_{3A}$) and nicotinic acetylcholine receptors: theanomalous binding properties of nicotine. *Biochemistry* **41**, 10262-10269 (2002).
61. Silverman, S. K. *Ph.D. Thesis* (California Institute of Technology, Pasadena, CA, 1998).
62. Soreq, H. and Seidman, S. *Xenopus* oocyte microinjection: from gene to protein. *Meth. Enz.* **207**, 225-265 (1992).
63. Felsch, J. S., Cachero, T. G. and Peralta, E. G. Activation of protein tyrosine kinase PYK2 by the m1 muscarinic acetylcholine receptor. *PNAS* **95**, 5051-5056 (1998).
64. Holmes, T. C., Fadool, D. A., Ren, R. B. and Levitan, I. B. Association of Src tyrosine kinase with a human potassium channel mediated by SH3 domain. *Science* **274**, 2089-2091 (1996).
65. Holmes, T. C., Fadool, D. A. and Levitan, I. B. Tyrosine phosphorylation of the Kv1.3 potassium channel. *J. Neurosci.* **16**, 1581-1590 (1996).

66. Ling, S. Z., Woronuk, G., Sy, L., Lev, S. and Braun, A. P. Enhanced activity of a large conductance, calcium-sensitive K+ channel in the presence of Src tyrosine kinase. *J. Biol. Chem.* **275**, 30683-30689 (2000).
67. Rogalski, S. L., Appleyard, S. M., Pattillo, A., Terman, G. W. and Chavkin, C. TrkB activation by brain-derived neurotrophic factor inhibits the G protein-gated inward rectifier Kir3 by tyrosine phosphorylation of the channel. *J. Biol. Chem.* **275**, 25082-25088 (2000).
68. Yu, X. M., Askalan, R., Keil, G. J. and Salter, M. W. NMDA channel regulation by channel-associated protein tyrosine kinase Src. *Science* **275**, 674-678 (1997).
69. Glenney, J. R. et al. Ligand-induced endocytosis of the EGF receptor is blocked by mutational inactivation and by microinjection of anti-phosphotyrosine antibodies. *Cell* **52**, 675-684 (1988).
70. Schlessinger, J. and Ullrich, A. Growth factor signaling by receptor tyrosine kinases. *Neuron* **9**, 383-391 (1992).
71. van der Geer, P., Hunter, T. and Lindberg, R. A. Receptor protein-tyrosine kinases and their signal transduction pathways. *Ann. Rev. Cell Biol.* **10**, 251-337 (1994).
72. Chen, Y. H., Pouyssegur, J., Courtneidge, S. A. and Van Obberghen-Schilling, E. Activation of Src family kinase activity by the G protein-coupled thrombin receptor in growth-responsive fibroblasts. *J. Biol. Chem.* **269**, 27372-27377 (1994).
73. Dikic, I., Tokiwa, G., Lev, S., Courtneidge, S. A. and Schlessinger, J. A role for Pyk2 and Src in linking G-protein-coupled receptors with MAP kinase activation. *Nature* **383**, 547-550 (1996).
74. Kirchhausen, T., Bonifacino, J. S. and Riezman, H. Linking cargo to vesicle formation: receptor tail interactions with coat proteins. *Curr. Op. Cell Biol.* **9**, 488-495 (1997).
75. Kubo, Y., Baldwin, T. J., Jan, Y. N. and Jan, L. Y. Primary structure and functional expression of a mouse inward rectifier potassium channel. *Nature* **362**, 127-133 (1993).
76. Wischmeyer, E., Doring, F. and Karschin, A. Acute suppression of inwardly rectifying Kir2.1 channels by direct tyrosine kinase phosphorylation. *J. Biol. Chem.* **273**, 34063-34068 (1998).
77. Shimkets, R. A., Lifton, R. P. and Canessa, C. M. The activity of the epithelial sodium channel is regulated by clathrin- mediated endocytosis. *J. Biol. Chem.* **272**, 25537-25541 (1997).
78. Owen, D. J. and Evans, P. R. A structural explanation for the recognition of tyrosine-based endocytotic signals. *Science* **282**, 1327-1332 (1998).
79. Pafford, C. M., Simples, J. E. and Strong, J. A. Effects of the protein-tyrosine-phosphatase inhibitor phenylarsine oxide on excision-activated calcium channels in *Lymnaea* neurons. *Cell Calcium* **18**, 400-410 (1995).
80. Karschin, A. Personal communication – treatment with Src alone gives inconsistent results. (2000).
81. Damke, H., Baba, T., Warnock, D. E. and Schmid, S. L. Induction of mutant dynamin specifically blocks endocytic coated vesicle formation. *J. Cell. Biol.* **127**, 915-934 (1994).
82. van der Bliek, A. M. et al. Mutations in human dynamin block an intermediate stage in coated vesicle formation. *J. Cell. Biol.* **122**, 553-563 (1993).
83. Li, M., Farley, R. and Lester , H. A. An intermediate state of the GABA transporter GAT1 revealed by simultaneous voltage clamp and fluorescence. *J. Gen. Phys.* **115**, 491-508 (2000).
84. Jonas, E. and Kaczmarek, L. Regulation of potassium channels by protein kinases. *Curr. Op. Neurobiol.* **6**, 318-323 (1996).
85. Levitan, I. B. Modulation of ion channels by protein phosphorylation. How the brain works. *Adv. Second Messenger Phosphoprotein Res.* **33**, 3-22 (1999).
86. Ohno, H. et al. The medium subunits of adaptor complexes recognize distinct but overlapping sets of tyrosine-based sorting signals. *J. Biol. Chem.* **273**, 25915-25921 (1998).
87. Rapoport, I. et al. Regulatory interactions in the recognition of endocytic sorting signals by AP-2 complexes. *EMBO J.* **16**, 2240-2250 (1997).
88. Shiratori, T. et al. Tyrosine phosphorylation controls internalization of CTLA-4 by regulating its interaction with clathrin-associated adaptor complex AP- 2. *Immunity* **6**, 583-589 (1997).
89. Boll, W. et al. Sequence requirements for the recognition of tyrosine-based endocytic signals by clathrin AP-2 complexes. *EMBO J.* **15**, 5789-5795 (1996).
90. Cinar, H. and Barnes, E. M. Clathrin-independent endocytosis of GABA(A) receptors in HEK 293 cells. *Biochemistry* **40**, 14030-14036 (2001).
91. Haucke, V. and De Camilli, P. AP-2 recruitment to synaptotagmin stimulated by tyrosine-based endocytic motifs. *Science* **285**, 1268-1271 (1999).

92. Miller, W. E. and Lefkowitz, R. J. Expanding roles for beta-arrestins as scaffolds and adapters in GPCR signaling and trafficking. *Curr. Op. Cell. Biol.* **13**, 139-145 (2001).
93. Nowak, M. W. et al. *In vivo* incorporation of unnatural amino acids into ion channels in *Xenopus* oocyte expression system. *Meth. Enz.* **293**, 504-529 (1998).

Chapter 5. Caged phosphoamino acids

5.1 Introduction

One of the lessons of the work presented in the previous chapter is that the great complexity inside a cell requires chemical tools to be as precise as possible. Caged tyrosine allows some control over the phosphorylation state of a particular side chain, but the downstream activity of tyrosine kinases remains out of the hands of the experimenter. By introducing caged phosphoamino acids, an additional degree of control may be exerted. Here, the phosphoamino acid is masked as a large, neutral residue. Irradiation itself reveals the wild-type phosphoamino acid, thus placing the phosphorylation state of the protein under direct experimental control. Needless to say, this phosphorylation may be reversed through the activity of phosphatases once the wild-type phosphoamino acid has been revealed. This reversibility may prove to be a useful null control, in that reversion to the non-phosphorylated phenotype can act as an intrinsic confirmation that an observed effect is due to phosphorylation. Indeed, the synthesis of non-hydrolyzable mimics may provide important insight into the kinetics of phosphatases *in vivo*. The three unnatural amino acids discussed here, caged phosphorylatable residues, caged phosphoamino acids, and caged non-hydrolyzable phosphoamino acid mimics, constitute a complete set for analysis of phosphorylation of a particular side chain in a protein.

5.1.1 Design of caged phosphoamino acids

The most straightforward design for caged phosphoamino acids involves protecting the phosphate oxygens with photo-removable protecting groups. (Figure 5.1) This chemistry has a relatively long history, as ATP has been a common target for caging.[1-3]

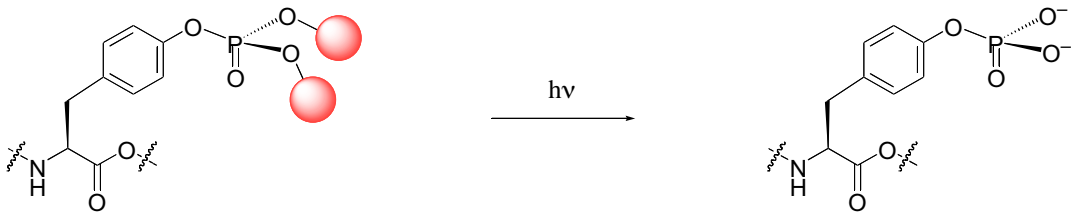

Figure 5.1 Schematic for the design of a phosphoamino acid where the side chain is caged. Photo-removable protecting groups are indicated as red spheres.

In addition to caged nucleotides, caged lipids have been widely reported, as has a caged phosphate-containing drug.[3-21] In addition to their synthetic relevance, a number of these studies provide important information on de-caging rates and conditions.[4,11,12,17-21] More recently, caged phosphoamino acid analogs have been developed and introduced into proteins and peptides.[22-25] Additionally, an interesting study has reported a caged mechanism-based inhibitor of tyrosine phosphatases, which is reversible only upon de-caging.[26] Solid-phase peptide synthesis using nitrophenethyl-caged phosphotyrosine, serine, and threonine has been accomplished very recently.[23] Although no application of these peptides has yet been reported, the de-caging efficiencies in water were determined. In the studies involving proteins, caging was performed by reaction of kinase-introduced thiophosphoryl groups with electrophilic reagents.[22,24,25] (Figure 5.2)

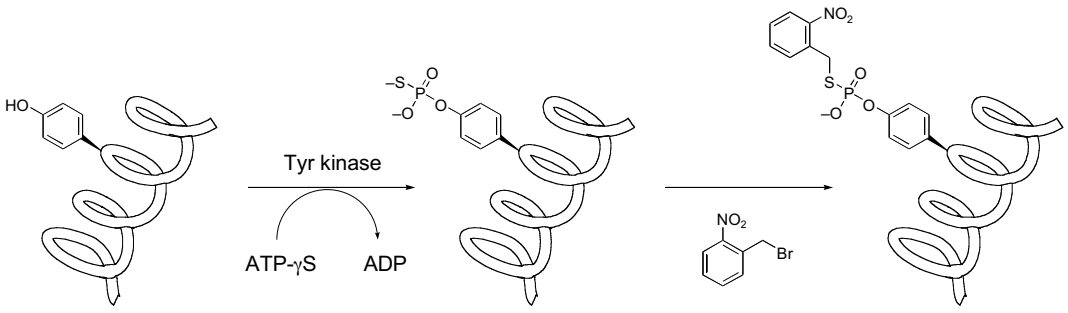

Figure 5.2 A strategy which has been reported for the incorporation of caged phosphoamino acids into proteins and synthetic peptides.[22,24,25]

Because of the requirement that the peptide or protein be modified with exogenously applied reagents, this technique is limited in both its specificity and *in vivo* application. Semi-synthetic peptides and proteins containing caged phosphoamino acids require transport into cells to be used to investigate signal transduction.

The introduction of caged phosphoamino acids by unnatural amino acid mutagenesis has the advantages of both site-specificity and compatibility with usage *in situ*. However, it has the potential drawback that steric bulk may be incompatible with ribosomal protein synthesis. It is encouraging that a number of very large residues have been incorporated via unnatural amino acid mutagenesis, notably the large hydrophobic residues introduced into streptavidin by the group of Sisido.[27] Nonetheless, caged phosphoamino acids are bulkier than any ribosomally incorporated amino acid. (Figure 5.3)

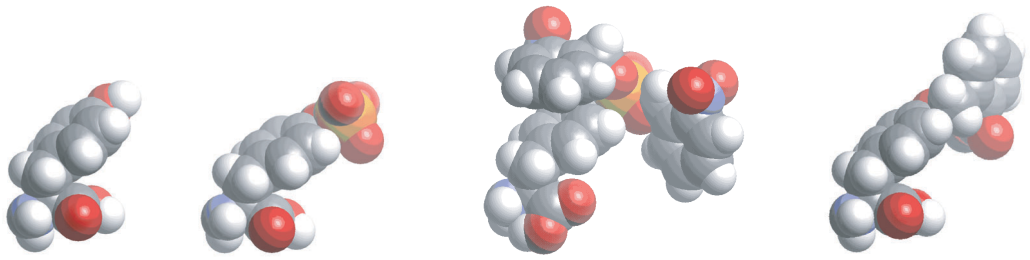

Figure 5.3 CPK models of tyrosine, phosphotyrosine, caged phosphotyrosine, and caged tyrosine, demonstrating the steric bulk of caged phosphotyrosine.

One potential solution to this problem of bulk would be to cage one, but not both of the phosphate oxygens. Indeed, in the studies cited above employed singly caged phosphoamino acids. However, the effects of phosphorylation are often successfully mimicked by replacing a potentially phosphorylated serine or threonine with a monoanionic residue, such as aspartate. Thus, a more certain means of ensuring that the caged residue is functionally equivalent to its non-phosphorylated form prior to photolysis is to utilize the neutral, doubly caged phosphodiester. By analogy to

isopropylidene or pivaloyl protection of vicinal diols, it might be possible to design a caged phosphate where both oxygens could be caged by a single photo-removable protecting group. Indeed, some compounds similar to this are known.[28] (Figure 5.4)

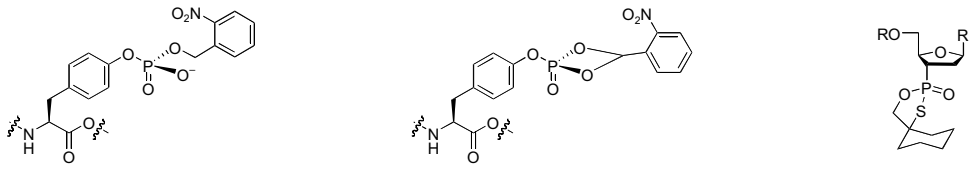

Figure 5.4 Possible solutions to the problem of caging group bulk. Two different mono-protected phosphoamino acid strategies are compared to the known oxathiaphosphalane ring system.[28]

However, for the initial experiments, the doubly caged phosphoamino acids represent a logical starting point. There is a large number of caging groups which may be utilized.[2,29-36] In fact, a flexible synthetic route which permits incorporation of a variety of these groups is desirable. The initial amino acid design relied on nitrobenzyl esters, which are well precedented, have optical properties which are appropriate for use in the oocyte system, and which are relatively sterically compact.

5.1.2 Non-hydrolyzable analogs

As indicated, another attribute which is desirable from a design perspective is stability to enzymatic removal. Phosphate groups are, of course, dynamically removed in a cell by phosphatases. Replacement of the O-P connectivity by a methylene unit is a common strategy for circumventing hydrolysis. The phosphonate which results from this replacement has rather different acidity than the parent phosphate. In order to more accurately mimic the natural phosphate group, difluoromethylene units are often utilized. (Figure 5.5)

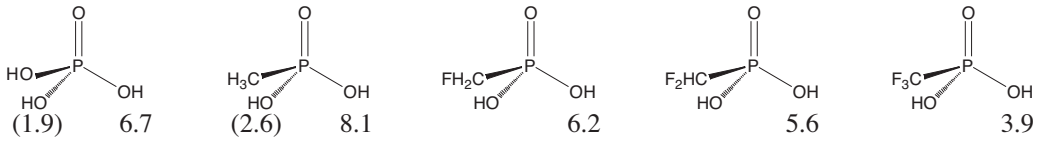

Figure 5.5 Values of phosphate pKa for phosphonate analogs containing fluorine.[37]

There is little question that the ionization state of difluorophosphonates more closely resemble that of phosphates, in that they are dianionic at physiological pH.[37-40] Whether or not phosphonates or difluorophosphonates are more effective analogs of phosphoamino acids, however, continues to be debated. A rather extensive literature on this subject suggests that context plays an important role. In some experiments, phosphonates have tighter binding, or are more effective than their difluorophosphonate congeners, while in others, the opposite trend is observed. (reviewed in Berkowitz)[41] No pattern has emerged such that an *a priori* evaluation may be made. Thus, the synthetic strategy for caged, non-hydrolyzable phosphoamino acid analogs should permit the synthesis of both phosphonate and difluorophosphonate analogs.

5.1.3 Mechanism-based phosphatase inhibitors

While difluorophosphonates act as non-hydrolyzable phosphate mimics, singly halogenated phosphonates have been shown to irreversibly inhibit phosphatases.[42,43] Covalent linkage of unnatural amino acid-containing proteins to phosphatases which act on them could provide a means for specifically identifying these phosphatases. While this methodology perhaps awaits the development of sensitive means for isolating and assaying the relevant phosphatases, the design of such molecules is straightforward and requires no great modification to the synthetic route to caged non-hydrolyzable phosphoamino acid analogs.

5.2 Synthesis of caged phosphoamino acids

The conversion of alcohols to phosphates has become a routine transformation, due to its central role in nucleic acid synthesis.[44] Phosphoramidites provide a mild, high-yielding methodology to accomplish the conversion, which has been applied to both phosphopeptides and to phosphate-containing prodrugs with labile phosphate modifications.[44-52] Bis(nitrobenzyl) phosphoramidite **1** is precedented, for the synthesis of a nitrobenzyl-protected phosphotyrosine and a caged phospholipid.[15,53] In both cases, nitrobenzyl alcohol is added to commercially available diisopropyl phosphoramidous dichloride. (Figure 5.6)

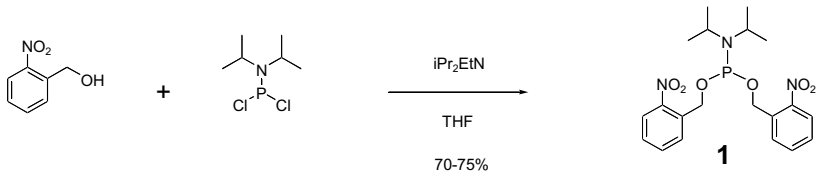

Figure 5.6 Synthesis of bis(nitrobenzyl) phosphoramidite **1**.[15,53]

The resulting phosphoramidite **1** may be conjugated to either aryl (tyrosine) or alkyl (serine or threonine) alcohols, catalyzed by 1*H*-tetrazole. The resulting trivalent intermediate is oxidized, to provide a mild, one-pot conversion of amino acid (e.g. **2**) to phosphoamino acid (e.g. **3**). (Figure 5.7)

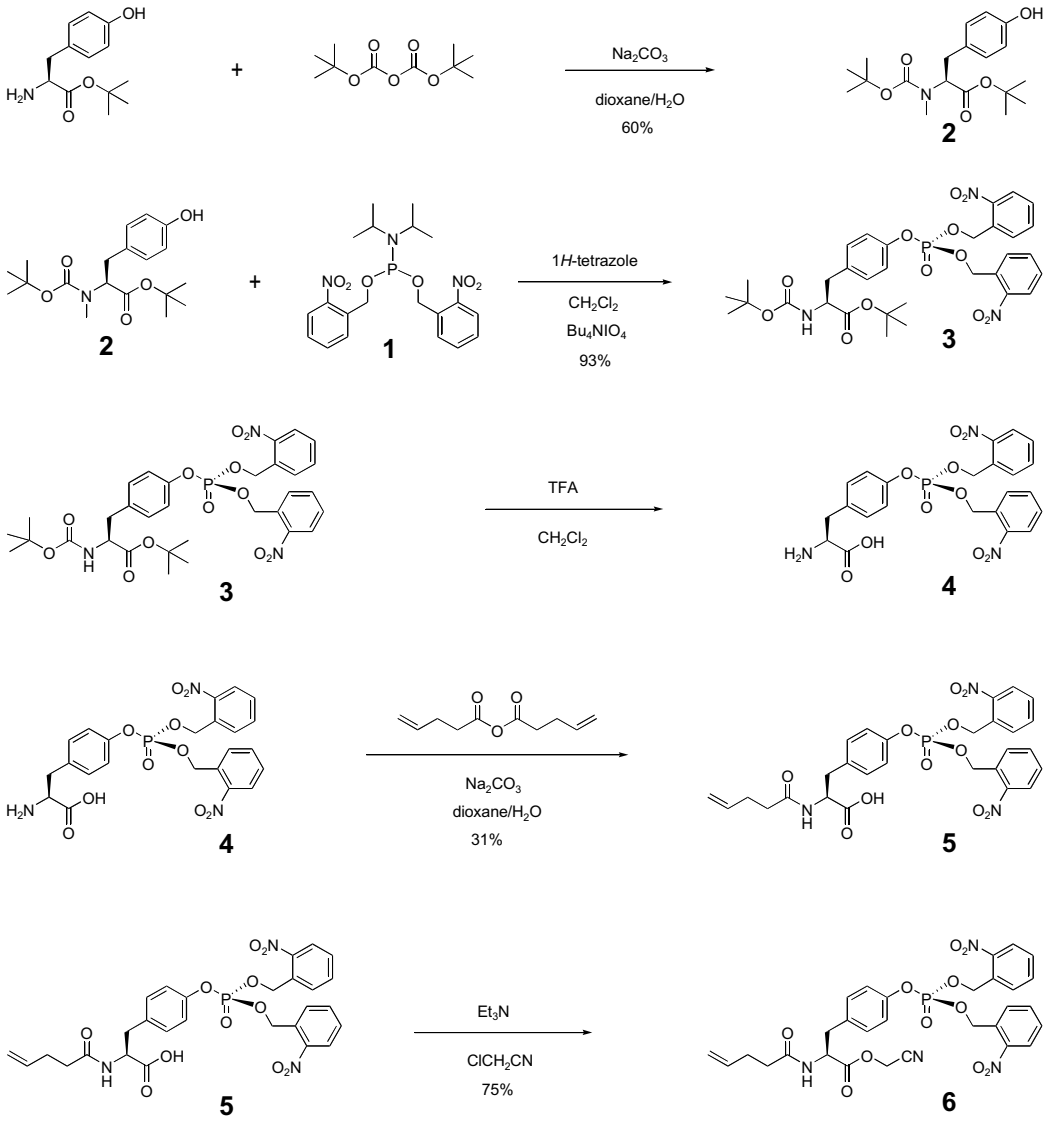

Figure 5.7 Synthesis of caged phosphotyrosine **6** from protected tyrosine **2** using bis(nitrobenzyl) phosphoramidite **1**.

Initially, it was feared that the 4-pentenoyl N-terminal protecting group would be unstable to the periodate oxidation involved in the final step of the phosphoramidite reaction. Thus, the amino acid was protected as the Boc t-butyl ester **3**, as shown in Figure 5.7. However, TLC experiments of 4PO-protected amino acids treated with tetrabutylammonium periodate at the appropriate conditions showed no apparent loss of

the protecting group. Thus, an even simpler route was subsequently used to generate caged phosphoserine **9** (Figure 5.8) and phosphothreonine **12** (Figure 5.9).

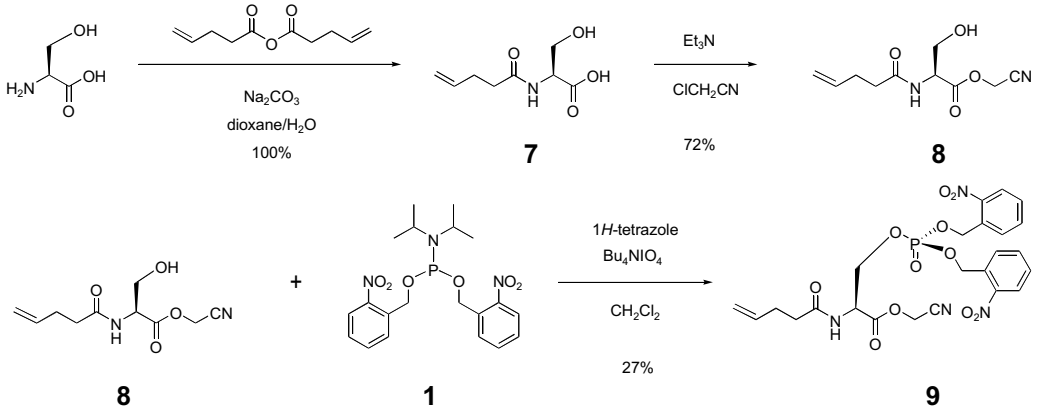

Figure 5.8 Synthesis of caged phosphoserine **9**.

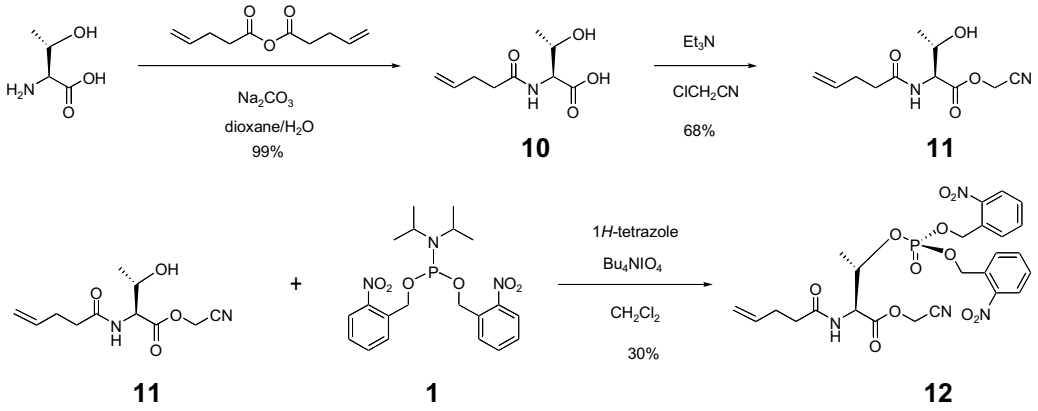

Figure 5.9 Synthesis of caged phosphothreonine **12**.

5.3 Synthesis of caged non-hydrolyzable phosphoamino acid analogs

The synthesis of non-hydrolyzable analogs is substantially more complicated than that of phosphoamino acid analogs. Phosphono and difluorophosphono analogs of tyrosine, serine, threonine, and histidine are all well precedented.[54-66] The initial synthetic routes to the fluorinated tyrosine compounds relied on fluorination using DAST.[58,60,67] In more modern routes, this methodology has been superceded by the milder, safer, more

specific metal-catalyzed cross-coupling developed independently by Shibuya and Burton.[68-70] (Figure 5.10)

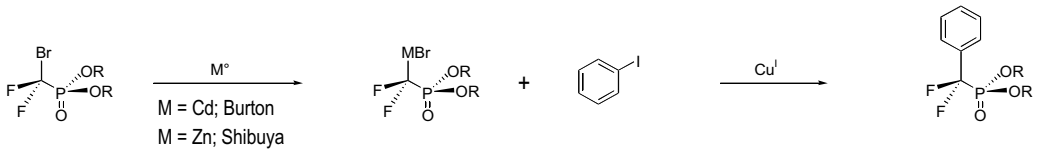

Figure 5.10 Methodology of Shibuya and Burton for the synthesis of difluorophosphonates from aryl iodides via copper(I)-catalyzed cross-coupling.[69,70]

For forming aliphatic carbon-phosphorus bonds, a number of methods exist.[67,71-81] Most of them are useful for generating phosphonates, although a number can be used to prepare difluorophosphonates.[67,71-81] The triflate displacement methodology employed by Berkowitz and others was selected for the synthesis of serine and threonine analogs.[41,61-65,82-90] (Figure 5.11)

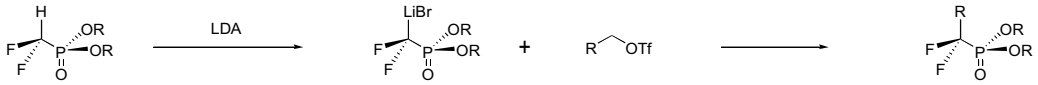

Figure 5.11 Berkowitz route to alkyl difluorophosphonates by direct nucleophilic displacement.[82]

In most cases, the phosphates are protected as the diethyl ester, although Berkowitz has reported benzyl- and alloc-protected difluorophosphonates.[41,83]

5.3.1 Difluorophosphonate intermediates

An important intermediate for the copper(I)-mediated crosslinking central to the routes of Shibuya and Burton is the dialkyl bromodifluorophosphonate. The diethyl version **15** is available from Aldrich, suggesting the possibility of coupling to suitably protected *p*-iodophenylalanine. The ethyl phosphodiester may be de-protected under the conditions of Rabinowitz, McKenna, and Jung (TMSI/TFA) to give the dianion.[55,56] Conditions analogous to those used in peptide coupling have been reported to generate

phosphodiesters.[91] Thus, coupling to nitrobenzyl alcohol may be possible, as indicated in Figure 5.12.

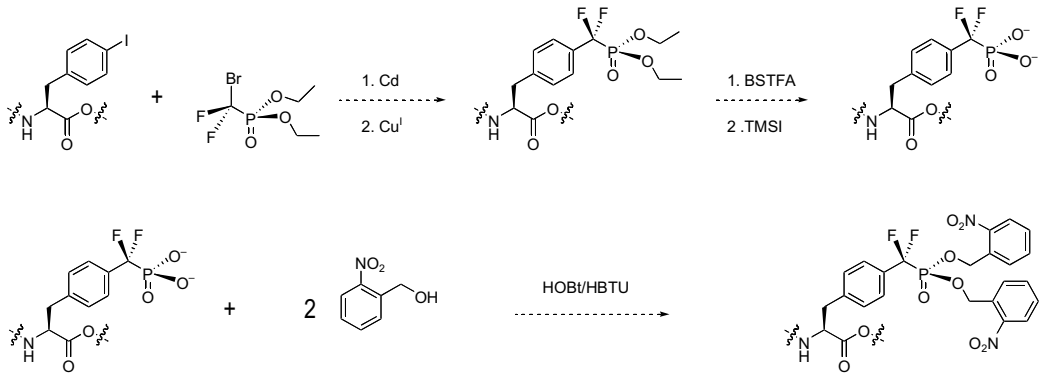

Figure 5.12 De-protection and re-protection scheme to replace ethyl esters of phosphate with nitrobenzyl esters.

Alternatively, the bis(nitrobenzyl) bromodifluorophosphonate **16** may be synthesized and utilized directly in the cross-coupling with protected *p*-iodophenylalanine. (Figure 5.13) The latter route, in fact, may be compatible with 4PO- (**13**) and cyanomethyl-protected iodophenylalanine **14**.

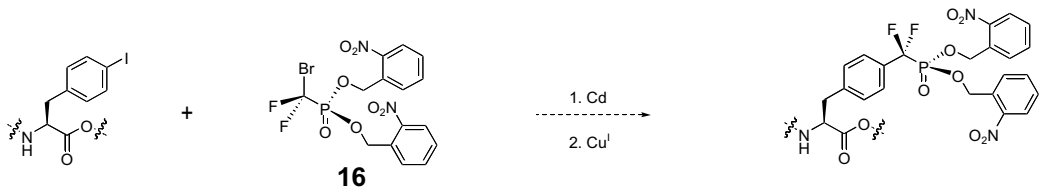

Figure 5.13 Installation of nitrobenzyl-protected phosphate.

A one-step synthesis of diethyl bromodifluorophosphonate from ethyl phosphite and CF_2Br_2 has been reported by the group of Savignac, following earlier syntheses of Burton.[81,92] Work by Mioskowski on the use of benzyl phosphites in the Arbuzov reaction suggests the necessity of *in vacuo* removal of the benzyl bromide product as it forms.[78] (Figure 5.14)

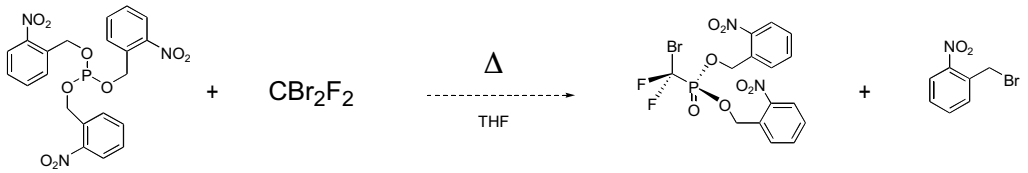

17 **16**

Figure 5.14 Proposed synthesis of bis(nitrobenzyl) bromodifluorophosphonate **16** following the route of Savignac to diethyl bromodifluorophosphonate.[81]

Nitrobenzyl phosphite **17** is easily available from the condensation of nitrobenzyl alcohol with PCl_3.[93] Pure material was re-crystallized from diethyl ether and fully characterized by NMR, although the compound proved unsuitable for electrospray mass spectrometry. However, nitrobenzyl phosphite appears to be significantly deactivated for Arbuzov chemistry relative to ethyl phosphite. The conditions of Savignac (60 °C, gently refluxing THF), gave no reaction. Heating the reaction to 100 °C overnight in a sealed tube also failed to give the desired product. The reactions were monitored by ^{31}P NMR. Because of fluorine-phosphorus coupling, the difluorophosphonate has a very distinctive triplet signal. (Figure 5.15)

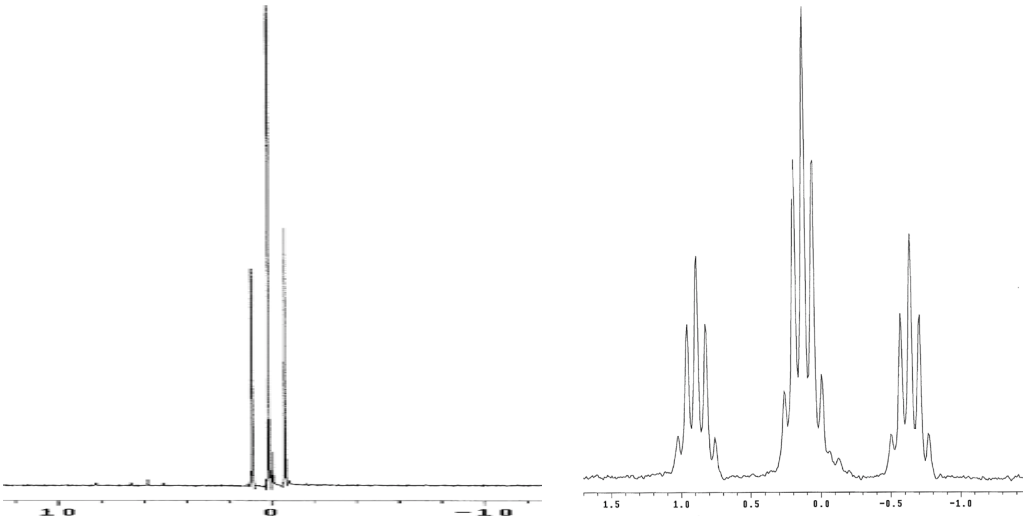

Figure 5.15 Characteristic triplet (J= 92 Hz) arising from $–CF_2$-P splitting (NMR of **15**).

The Aldrich diethyl bromodifluorophosphonate **15** provided an authentic sample in which this triplet was observed. Under the conditions of Savignac, the 134 ppm phosphite signal was still observed after overnight reaction, suggesting no formation of pentavalent phosphorus and, indeed, no reaction. After the sealed-tube reaction, pentavalent phosphorus signals were observed, although these could not be unequivocally assigned. The formation of nitrobenzyl phosphonate is a likely outcome of this reaction, although proton de-coupled phosphorus signals did not appear to correspond to the expected pattern from a methylene-phosphorus interaction.

An alternative route to dialkyl bromodifluorophosphonates was utilized by Berkowitz in a synthesis of bis(benzyl) bromodifluorophosphonoserine.[41] Here, a benzyl *H*-phosphonate is treated with sodium hydride or sodium HMDS and added to an electrophilic substrate. (Figure 5.16)

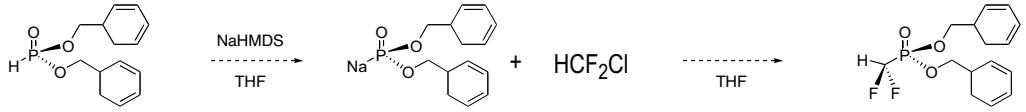

Figure 5.16 Alternative route to difluorophosphonates, involving benzyl *H*-phosphate.[41,74]

In the case of the Berkowitz reaction, $CHClF_2$ was used, and earlier reports show the addition of benzyl *H*-phosphonate to CH_2Cl_2.[41,74] To synthesize the bromodifluorophosphonate, addition to CBr_2F_2 would be required. As with nitrobenzyl phosphite **17**, nitrobenzyl *H*-phosphonate **18** was synthesized by simple modification of a preparation for the benzyl compound.[94] (Figure 5.17)

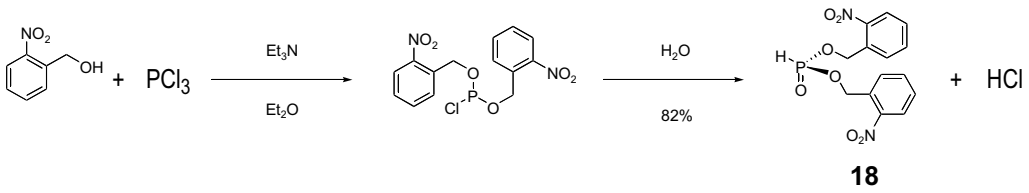

Figure 5.17 Route for preparation of nitrobenzyl *H*-phosphonate **18** from nitrobenzyl alcohol and phosphorus(III) chloride.[94]

The compound was re-crystallized from ethanol and characterized by carbon, proton, and phosphorus NMR. Again, it proved refractory to electrospray MS. The H-P interaction provides a very distinctive splitting pattern which was easily observed in proton-decoupled ^{31}P spectra. (Figure 5.18)

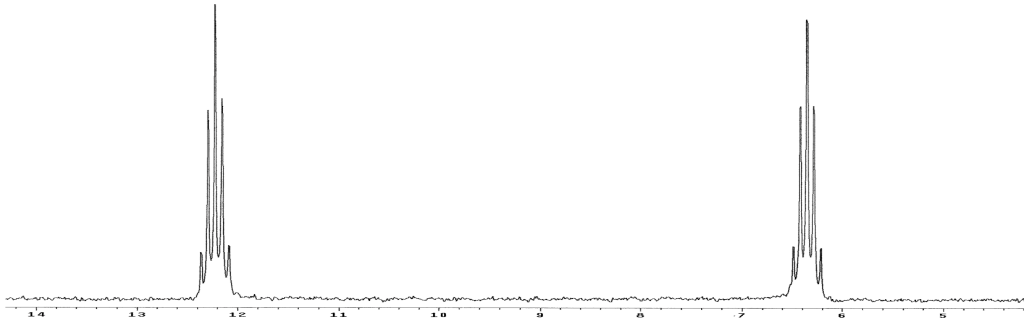

Figure 5.18 ^{31}P splitting pattern (J = 711 Hz) arising from H-P coupling in nitrobenzyl *H*-phosphonate **18**.

However, base-mediated condensation of compound **18** with neither CF_2Br_2 nor CH_2Br_2 was observed. Subsequent discussion with former group members confirmed the experience that nitrobenzyl compounds are not typically compatible with strong base, as an apparent result of increased acidity at the benzylic position relative to benzyl compounds which lack the nitro ring substitution.[95]

5.3.2 Future prospects

The routes thus far adopted to generate the important bromodifluorophosphonate intermediate **16** for direct installation of the caged phosphonate have proven

unsuccessful. Two strategies remain viable for further work in this area. First, the de-protection and re-protection strategy proposed above may be implemented to convert the commercially available ethyl phosphodiester to the desired nitrobenzyl compound **16**. (Figure 5.)

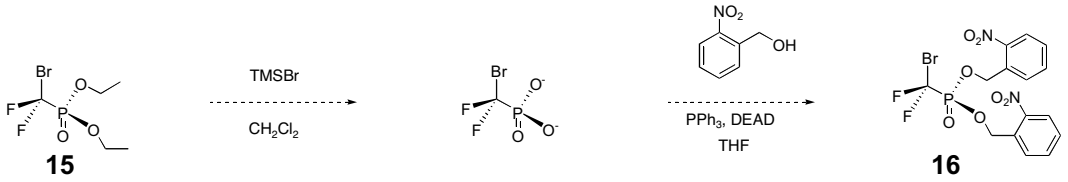

Figure 5.19 Generation of nitrobenzyl bromodifluorophosphonate **16** by de-protection of commercially available ethyl ester **15** followed by re-protection with nitrobenzyl alcohol.

As indicated previously, the conditions of Burton and Shibuya are expected to provide a mild and convenient synthesis of caged difluorophosphonotyrosine from this intermediate. (Figure 5.10) Given the difficulties encountered in using strong base in the presence of nitrobenzyl groups, the conditions of Berkowitz may prove incompatible with the direct installation of protected difluorophosphonate. One possible route is the use of metal-catalyzed addition to an α,β-unsaturated carboxylic acid, as in the report of Kawamoto *et al*.[96] (Figure 5.20)

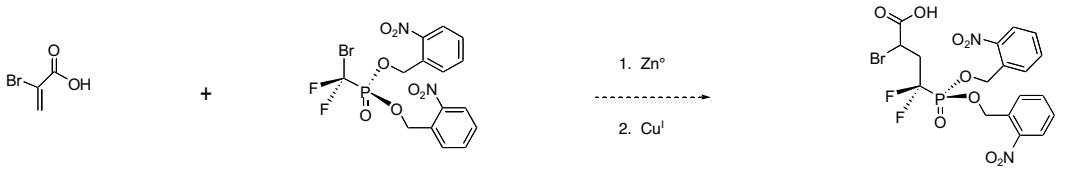

Figure 5.20 Proposal to employ Kawamoto's mild and selective metal-catalyzed bromodifluorophosphonate coupling on a vinyl halide substrate to provide an important intermediate for caged difluorphosphonoserine.[96]

In a second approach to synthesizing caged non-hydrolyzable phosphoamino acid analogs, the difluorophosphonate may be installed in its protected form. Subsequent de-protection of the difluorophosphonoamino acid may be accomplished and the desired

protecting group installed. Note that an unavoidable feature of this approach is the need for orthogonal protection of amine, carboxylate, and phosphate. Thus, a convenient means of simplifying this approach would be to synthesize a bromodifluorophosphonate with protecting groups orthogonal to those traditionally used for amino acid protection. An example is shown in Figure 5.21, where benzyl protection is utilized for formation of the caged non-hydrolyzable phosphoserine analog.

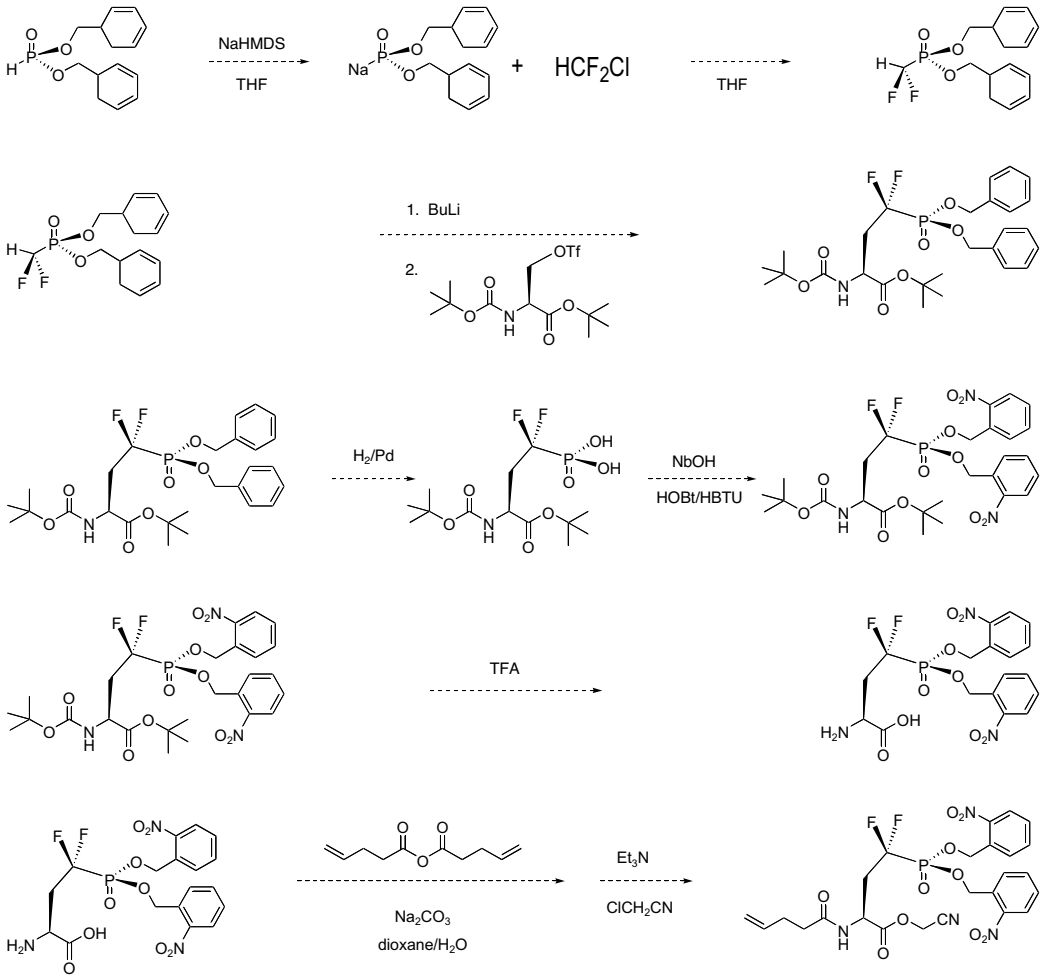

Figure 5.21 Proposed general scheme for synthesis of nitrobenzyl difluorophosphonoserine, involving installation of the protected difluorophosphonate followed by de-protection and re-protection with nitrobenzyl alcohol.

The 2-(trimethyl)silylethoxy (TSE) protecting group is also useful to consider, and is perhaps more desirable than benzyl because of its expected increased reactivity in Michaelis-Arbuzov chemistry.[97] This chemistry may be important in preparing phosphonate analogs. As indicated earlier, there is no good means of predicting whether difluorophosphonates or simple phosphonates will prove to be more effective phosphate mimics. Thus, the importance of developing synthetic schemes which permit phosphonate synthesis was cited. In general, there are two convenient routes for tyrosine analogs and one for serine or threonine analogs. In the case of tyrosine, the method of Shibuya and Burton could be used, employing a simple bromophosphonate. (Figure 5.22) Because the TSE phosphite is expected to be active in Michaelis-Arbuzov chemistry, the bromophosphonate may be generated via its condensation with dibromomethane, as in Figure 5.14. If desired, this compound could be de-protected and converted to a nitrobenzyl bromophosphonate by the Mitsonobu chemistry proposed above. (Figure 5.)

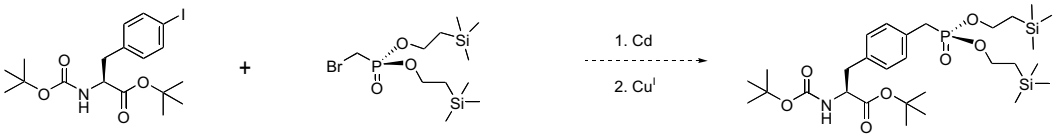

Figure 5.22 Proposed synthetic scheme for preparation of caged phosphonotyrosine, employing metal-mediated cross-coupling between an aryl iodide and bromophosphonate.

An alternative strategy for synthesis of tyrosine phosphonate would employ Arbuzov chemistry directly on a benzyl bromide analog of tyrosine.[53] (Figure 5.23)

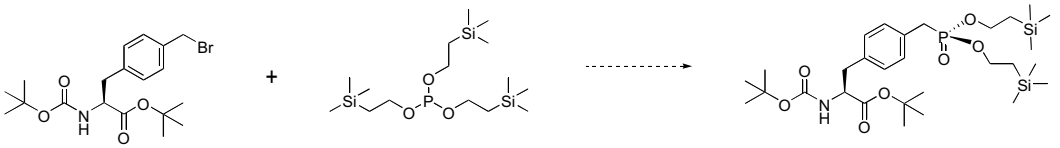

Figure 5.23 Proposed generalized Michaelis-Arbuzov scheme for synthesis of phosphonotyrosine.

A similar route is available for serine phosphonate analogs. (Figure 5.)

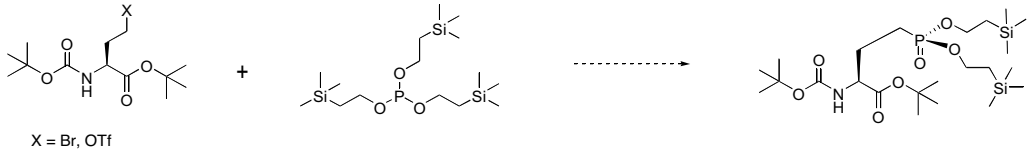

Figure 5.24 Proposed route to the synthesis of caged phosphonoserine.

A final strategy which would ameliorate problems associated with the nitrobenzyl group is to utilize different caging chemistry. Phenacyl groups, for instance, should behave more like benzyl substituents in both Arbuzov and dialkyl phosphate chemistry than do nitrobenzyl groups. (Figure 5.25)

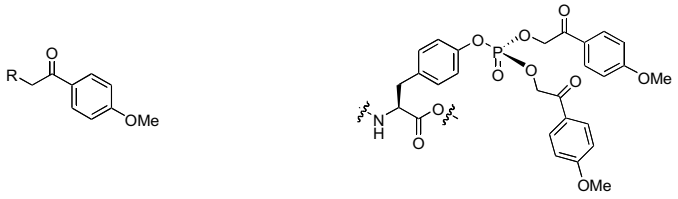

Figure 5.25 The *p*-methoxyphenacyl group, a synthetically tractable phototrigger for alcohols and carboxylic acids, and a phosphotyrosine analog showing the use of phenacyl as a phosphate caging group.[34,36]

To date, both phosphoserine and phosphothreonine have been synthesized as the active, protected amino acids **9** and **12**. However, coupling to dCA has yet to be performed. One possible difficulty which may be anticipated is β-elimination of the phosphate from the side chain.[98-100] Such elimination was observed by Fahmi *et al*. with a glycosylated serine derivative upon coupling to dCA, but the conditions of the coupling were able to be altered in such a way as to permit formation of the desired product.[98] Also, the solid-phase conditions for preparing peptides in the presence of singly caged phosphoamino acids involve piperidine in DMF, to which the linkage was apparently stable.[23] If elimination is a complicating factor in dCA coupling, the switch to acetonitrile from DMF reported by Fahmi will be employed in an effort to overcome the

problem.[98] If elimination persists, alternative coupling methodologies may need to be investigated.

Attempts to circumvent the synthetic problems outline above and prepare caged non-hydrolyzable phosphoamino acid analogs are ongoing.

5.4 Identification of appropriate biological systems for analysis by caged pAA

Both tyrosine and serine phosphorylation are highly important to the functional regulation of ion channels. Direct observation of phosphorylated side chains has been difficult, as noted in Chapter 4. The unequivocal introduction of a phosphorylated side chain by the method outlined here presents a unique opportunity to study the regulation of channels by serine, threonine, or tyrosine phosphorylation. The initial experiments to establish the proof of principle should target channels for which a very distinctive change occurs upon phosphorylation.

5.4.1 Tyrosine phosphorylation

The work on Kir2.1 described in Chapter 4 makes this ion channel a very attractive target for preliminary studies of tyrosine phosphorylation. Revealing the wild-type tyrosine residue at 242 results in current decrement with a time course of approximately 11 minutes. It would be very interesting to observe the effect of uncaging phosphotyrosine at this position. An immediate decrease in current would imply that the events taking place over minutes that are observed by uncaging tyrosine correspond to phosphorylation itself. If the kinetics of tyrosine kinases in a living cell could be observed in this fashion, it would represent a unique kind of information that may be obtained by this technique. Alternatively, if the de-caging of phosphotyrosine results in a

current decrease over a similarly long time course it may suggest that the kinetics of a protein-protein interaction are being observed, although it is possible that a very slow conformational change could be occurring. In either case, suppression of Kir2.1 with phosphotyrosine analogs provides a valuable test case for observing the effects of tyrosine phosphorylation on ion channel activity.

5.4.2 Serine phosphorylation

Recently, a striking change accompanying serine phosphorylation has been observed in the potassium channel KCNK2.[101] Phosphorylation of a single C-terminal serine residue causes the channel to acquire voltage dependence. (Figure 5.26) The presence of a such a dramatic phenotype makes this channel an excellent system for studying phosphoserine analogs.[102]

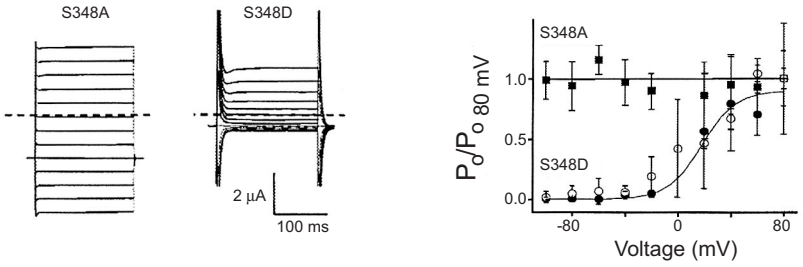

Figure 5.26 Voltage dependence of KCNK2 upon introduction of negative charge at Ser348 [adapted from Bockenhauer, *Nat. Neurosci.* **4**, 486 (2001)]. The effects of PKA were successfully mimicked by mutagenesis of Ser to Asp at position 348. The left panel illustrates the voltage dependence of the S348D but not S348A channels expressed in *Xenopus* oocytes, in response to voltage steps in 100 mM external K^+. The right panel shows the dependence of channel open probability on voltage for S348D (circles) relative to wild-type (squares) channels.[101]

5.5 Progress toward controlling phosphorylation with unnatural amino acids

5.5.1 Tyrosine phosphorylation

One important prerequisite for the use of phosphotyrosine analogs to control tyrosine phosphorylation is that they can be employed in suppression experiments. Encouraging results have been obtained in this regard in the nAChR. Mouse muscle receptors containing A122, I123, or F124TAG mutations in the alpha subunit were suppressed with pTyr(ONb)$_2$ and Tyr. As shown in Figure 5.27, significant currents were obtained, suggesting that the residue is competent for ribosomal translation. However, suppression efficiency of the caged phosphotyrosine was significantly diminished relative to the wild-type residue, which produced five to ten times the current of pTyr(ONb)$_2$ suppression at these sites.

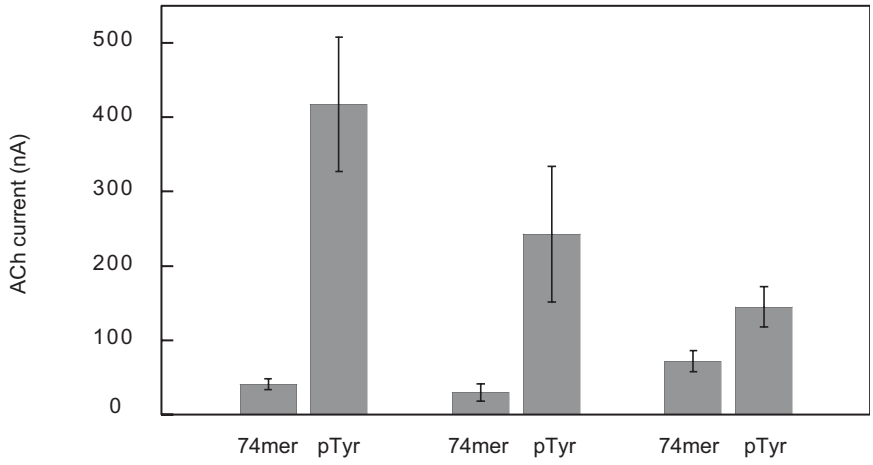

Figure 5.27 Suppression at nAChR αA123, αI123, and αF124 with 74mer and pTyr(ONb)$_2$. Currents elicited by 200 μM ACh were measured 36 hr after the injection of 2 ng total mRNA in the ratio of 10:1:1:1 α:β:γ:δ.

Early experiments in Kir2.1 provided little evidence for incorporation at Y242, even though Tyr(ONb) was successfully suppressed at this position. (Figure 5.28) However, it

may well be the case that this situation may be remediated by optimization of suppression conditions.

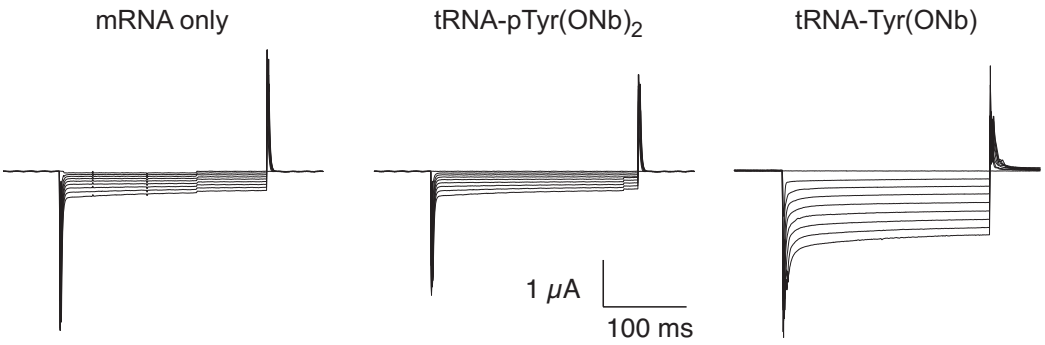

Figure 5.28 Attempted suppression at Kir2.1 Y242 with pTyr(ONb)$_2$. Currents were measured in High K^+ solution 48 hr after the injection of 12.5 ng total mRNA.

A final test that was performed with the phosphotyrosine analog involved recognition of the residue by anti-phosphotyrosine antibodies. A dot blot of 6 nmol of dCA-pTyr(ONb)$_2$ was performed. Development of the blot with BAbCo PY72 anti-phosphotyrosine antibody reveals that only irradiated dCA-amino acid is recognized by the antibody. (Figure 5.29)

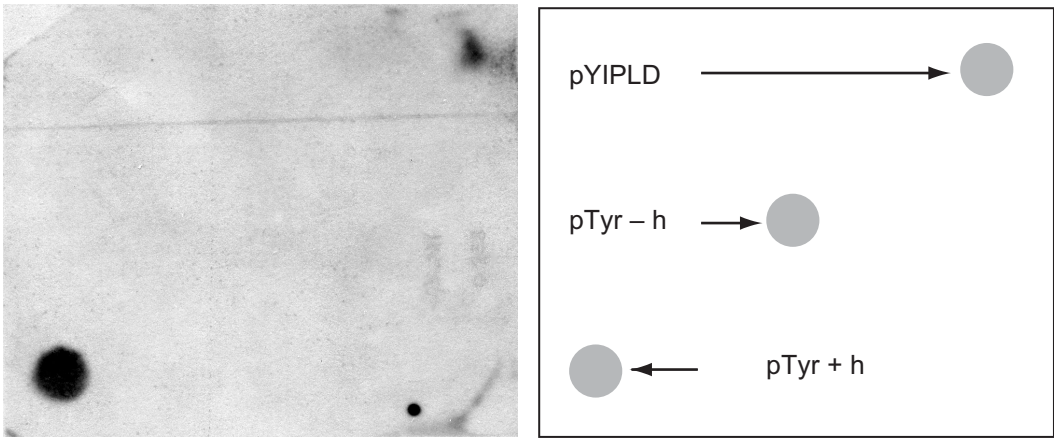

Figure 5.29 Dot blot of irradiated and non-irradiated dCA-pTyr(ONb)$_2$ **21** with the anti-phosphotyrosine antibody PY72. The right panel shows the pattern of spotting, where pYIPLD is a positive control peptide.

This experiment confirms that the residue, when caged, is inequivalent to phosphotyrosine, but that the irradiated residue reflects the properties of native pTyr.

5.6 Synthetic methods

5.6.1 General experimental procedures

All reactions were run under positive argon pressure, except where indicated. Anhydrous solvents were obtained from BakerDRY™ drums and were used without further purification. Amino acids and most commercially available reagents were obtained from Sigma-Aldrich. Thin-layer chromatography was performed using Whatman glass plates pre-coated with 60 Å silica gel. Nuclear magnetic resonance spectroscopy was performed on divisional Bruker spectrometers at the following frequencies: ^{1}H (300 MHz), ^{13}C (75 MHz) ^{31}P (121 MHz), ^{19}F (282 MHz). Mass spectrometry data were obtained from the divisional facility. Analytical and preparative HPLC was carried out using a Millipore system with fixed-wavelength and diode-array UV detection fitted with a C_{18} reverse-phase column.

5.6.2 Bis(nitrobenzyl) diisopropyl phosphoramidite 1

Diisopropyl phosphoramidous chloride (1 eq, 5 mmol) was thawed and dissolved in 4 mL anhydrous THF. In a flame-dried reaction vessel, nitrobenzyl alcohol (2 eq, 10 mmol) and dry diisopropylethylamine (3 eq, 15 mmol) were combined in 10 mL dry THF. The flask was fitted with an addition funnel and cooled to 0 °C in a water/ice bath. The addition funnel was charged with the phosphoramidous chloride solution, and it was added dropwise to the reaction flask. After 30 min reaction at 0 °C, the ice bath was removed and the reaction permitted to stir an additional 30 min at room temperature.

TLC (1:1 ethyl acetate:hexane, R_f = 0.8) confirmed reaction, although some starting nitrobenzyl alcohol remained. Filtration of the precipitate in a coarse fritted funnel, followed by washing with 25 mL ethyl acetate produced a clear, golden filtrate. The filtrate was washed with 25 mL saturated $NaHCO_3$ and 25 mL saturated brine. The organic layer was dried over $MgSO_4$ and concentrated to an amber solid by rotary evaporation. The residue was brought up in ether and purified by flash column chromatography (1:20 triethylamine:ether, R_f = 0.9) to give a pale yellow solid in 70-75% yield. ^{1}H NMR ($CDCl_3$) δ = 1.25 (d, *J* = 6.9 Hz, 12H), 3.75 (m, 2H), 5.17 (m, 2H), 7.44 (t, *J* = 9 Hz, 2H), 7.67 (t, *J* = 9 Hz, 2H), 8.10 (d, *J* = 8.1 Hz). ^{13}C NMR ($CDCl_3$) δ = 25.0, 25.1, 43.6, 43.7, 62.6, 62.9, 124.9, 128.0, 128.7, 134.0, 136.2, 136.3, 146.9. ^{31}P NMR ($CDCl_3$) δ = 151.7. MS (ESI) Calcd for $C_{20}H_{27}N_3O_6P$ $(M+H)^+$: 436.16. Found 458.2 $(M+Na^+)^+$, 474.2 $(M+K^+)^+$.

5.6.3 Boc-Tyrosine-OtBu 2

Commercially available Tyr-OtBu (1 eq, 3.46 mmol) was weighed into a flask and dissolved in 25 mL dioxane:water (5:1). Boc anhydride (1.2 eq, 4.16 mmol) was added, which dissolved readily. Triethlyamine (1.2 eq, 4.16 mmol) was added, without overt effervescence. After overnight stirring at room temperature, the reaction was monitored by TLC (1:1 ethyl acetate:hexane, R_f = 0.6) and shown to be complete. The reaction was quenched by the addition of 50 mL of 1 *M* $NaHSO_4$ and 50 mL CH_2Cl_2. The reaction mixture was then extracted thrice with CH_2Cl_2 (15 mL portions) and dried over Na_2SO_4. After rotary evaporation, the crude product was dissolved in a minimum volume of ethyl acetate:hexane (1:1). Flash column chromatography (1:1 ethyl acetate:hexane) gave the pure compound in approximately 60% yield. ^{1}H NMR (CD_3CN) δ = 1.43 (s, 18H), 2.93

(ABM, J = 25.2, 15, 7.8 Hz, 2H), 5.58 (d, J = 8.1 Hz, 1H), 6.78 (d, J = 6 Hz, 2H), 7.07 (d, J = 8.4 Hz, 2H). ^{13}C NMR (CD_3CN) δ = 27.5, 27.9, 28.3, 37.1, 56.2, 79.4, 81.6, 115.3, 115.5, 128.2, 130.5, 130.8, 155.7, 155.9, 171.4.

5.6.4 Boc-pTyr(ONb)$_2$-OtBu 3

N- and C-terminally protected Boc-tyrosine-OtBu **2** (1 eq, 0.78 mmol) was combined with freshly sublimed tetrazole (1.8 eq, 1.51 mmol) in a flame-dried flask fitted with a stirbar. Dry acetonitrile (10 mL) was added to solubilize the tetrazole, followed by 38 mL dry CH_2Cl_2. The reaction vessel was cooled to 0 °C in a water/ice bath. A solution of bis(nitrobenzyl) phosphoramidite **1** (1.5 eq, 1.15 mmol, in 2 mL dry CH_2Cl_2) was added dropwise via syringe. After 5 min mixing at 0 °C, the ice bath was removed and the reaction allowed to proceed 2.5 hr at room temperature. TLC (1:1 ethyl acetate:hexane, R_f = 0.7) revealed possible product formation. Oxidation was performed with tetrabutylammonium periodate (1.5 eq, 1.15 mmol) added in 5 mL dry THF. After 10 min reaction at room temperature, TLC (1:1 ethyl acetate:hexane, R_f = 0.4) indicated that the starting nitrobenzyl alcohol had been consumed. The reaction was quenched with 200 mL CH_2Cl_2 and washed twice (50 mL saturated $NaHCO_3$, 50 mL saturated NaCl). The organic layer was dried over Na_2SO_4 and concentrated to a thin yellow oil under reduced pressure. Flash column chromatography (1:1 ethyl acetate:hexane) gave the purified title compound in 93% yield. ^{1}H NMR ($CDCl_3$) δ = 1.36 (s, 18H), 3.05 (m, 2H), 4.42 (m, 1H), 5.1 (d, J = 12.9 Hz, 1H), 5.61 (d, J = 7.5 Hz, 4H), 7.17 (s, 4H), 7.52 (m, 2H), 7.7 (m, 4H), 8.13 (d, J= 8.1 Hz, 2H). ^{31}P NMR ($CDCl_3$) δ = -3.96.

5.6.5 pTyr(ONb)$_2$ 4

Deprotection of N- and C-protected caged pTyr **3** was performed with TFA. Boc-pTyr(ONb)$_2$-OtBu (1 eq, 0.5 mmol) and *p*-methoxybenzene (6 eq, 3 mmol) were added to a dry reaction vessel. Dry CH_2Cl_2 (5 mL) was added to produce a clear yellow solution. A 5 mL portion of trifluoroacetic acid was added. The reaction was stirred 60 min at room temperature, resulting in a solution of variable color, ranging from salmon to green. TLC (1:20 triethlyamine:ether, R_f = 0.1, and 1:20 acetic acid:ethyl acetate, R_f = 0.2, developed with ninhydrin) revealed the removal of both protecting groups. Volatiles were removed under high vacuum, after which 10 mL toluene were added and the flask returned to vacuum. The resulting compound was taken on to the subsequent steps without further purification or characterization.

5.6.6 4PO-pTyr(ONb)$_2$ 5

De-protected pTyr(ONb)$_2$ **4** was dissolved in 6 mL *p*-dioxane and 6 mL water. Na_2CO_3 (1.4 eq, 0.67 mmol) was added. Complete solubilization of reactants was achieved through *ad libitum* addition of dioxane (approximately 10 mL). 4PO-anhydride (1.4 eq, 0.67 mmol) was added in one portion and reaction allowed to proceed 4 hr at room temperature. Starting material appeared completely converted by TLC (1:20 acetic acid:ethyl acetate, R_f = 0.4). The reaction was quenched with 25 mL of 1 *M* $NaHSO_4$ and 25 mL CH_2Cl_2. Extraction with CH_2Cl_2 (3x, 10 mL each) was followed by drying over Na_2SO_4. After rotary evaporation, the thin yellow oil was brought up in 1:20 acetic acid:ethyl acetate and purified by flash column chromatography (1:20 acetic acid:ethyl acetate). Under the conditions used, a stiff gel formed in certain column fractions, resulting in some loss of product. Thus, the purified title compound was obtained in 31%

yield. ^{1}H NMR (CD_3CN) δ = 2.22 (m, 4H), 3.06 (ABM, *J* = 50.6, 14.1, 4.8 Hz, 2H), 4.64 (m, 1H), 4.94 (m, 2 H), 5.58 (d, *J* = 7.8 Hz, 4H), 5.75 (m, 1H), 6.87 (m, 2H), 7.25 (m, 4H), 7.58 (m, 2H), 8.09 (d, *J*= 7.5 Hz, 2H). ^{13}C NMR (CD_3CN) δ = 29.6, 35.1, 36.5, 67.0, 68.0, 114.9, 117.6, 119.8, 120.3, 124.8, 125.6, 126.4, 128.1, 128.7, 129.0, 130.0, 131.3, 133.4, 134.5, 135.0, 135.5, 147.2, 149.2, 149.3, 172.8, 172.9. ^{31}P NMR (CD_3CN) δ = -8.5. MS Calcd for $C_{28}H_{28}N_3O_{11}P$: 613.15 Found: (ESI$^+$) 614.4 $(M+H^+)^+$, 636.4 $(M+Na^+)^+$, 652.0 $(M+K^+)^+$. Found: (ESI$^-$) 612.0 $(M-H^+)^-$.

5.6.7 4PO-pTyr(ONb)$_2$ cyanomethyl ester 6

A dry flask was charged with 4PO-pTyr(ONb)$_2$ **5** (1 eq, 0.15 mmol), 1.5 mL dry DMF, and 1.5 mL chloroacetonitrile (160 eq, 24 mmol). Triethlyamine (3 eq, 0.45 mmol) was added and the reaction stirred 8.5 hr at room temperature. Progress was monitored by TLC (1:1 ethyl acetate:hexane, R_f = 0.1 and ethyl acetate, R_f = 0.7). The reaction was quenched with 50 mL ethyl acetate and washed twice (25 mL saturated $NaHCO_3$ and 25 mL saturated NaCl). The organic portion was dried over Na_2SO_4 and the solvent removed *in vacuo*. Flash column chromatography (1:1 ethyl acetate:hexane) gave the purified compound, typically in approximately 75% yield. ^{1}H NMR ($CDCl_3$) δ = 2.32 (m, 4H), 3.13 (d, *J* = 3.9 Hz, 2H), 4.75 (q, *J* = 35.7, 15.6 Hz, 2H), 5.01 (m, 2H), 5.63 (d, *J* = 6.0 Hz, 4H), 6.06 (d, *J* = 7.8 Hz, 1H), 7.18 (m, 2H), 7.53 (m, 2H), 7.66 (m, 4H), 8.14 (d, *J*= 7.8 Hz, 2H). ^{13}C NMR ($CDCl_3$) δ = 29.6, 35.6, 37.1, 49.3, 53.1, 67.1, 67.2, 116.1, 120.5, 120.6, 125.3, 128.7, 128.8, 129.4, 130.9, 132.7, 134.4, 136.8, 170.3, 172.3. ^{31}P NMR ($CDCl_3$) δ = -4.2. MS Calcd for $C_{30}H_{29}N_4O_{11}P$: 652.16. Found: (ESI$^+$) 653.2 $(M+H^+)^+$, 675.2 $(M+Na^+)^+$, 691.0 $(M+K^+)^+$. Found: (ESI$^-$) 516.0 $(M-Nb)^-$.

5.6.8 4PO-Serine 7

Serine (1 eq, 4.76 mmol) and Na_2CO_3 (1.4 eq, 6.66 mmol) were dissolved in 60 mL water, 30 mL hexane. A solution of 4-pentenoyl anhydride (1.4 eq, 6.66 mmol) in 15 mL dioxane was added in one portion. After 2 h at room temperature, TLC (10:10:1 ethyl acetate: hexanes: acetic acid, R_f = 0.7, developed with iodine and ninhydrin) revealed complete conversion of starting amino acid. Reaction was stopped by addition of 250 mL of 1 *M* $NaHSO_4$ and 250 mL CH_2Cl_2. After extraction with CH_2Cl_2 (3x, 100 mL each), the aqueous layer was treated with 350 mL saturated NaCl solution and extracted twice with 100 mL portions of THF. The organic layers were combined and dried over Na_2SO_4. Solvent was removed by rotary evaporation and the residue brought up in CH_2Cl_2. Flash column chromatography (CH_2Cl_2 followed by 1:1 CH_2Cl_2:ethyl acetate) was carried out, and the product isolated in nearly quantitative yield. ^{1}H NMR (CD_3CN) δ = 2.38 (m, 4H), 3.89 (ABM, *J* = 26.7, 11.4, 3.9 Hz, 2H), 4.56 (m, 1H), 5.03 (m, 2H), 5.83 (m, 1H), 7.51 (d, *J* = 7.8 Hz, 1H). ^{13}C NMR (CD_3CN) δ = 29.8, 35.2, 54.9, 62.1, 115.3, 137.2, 172.4, 174.8.

5.6.9 4PO-Serine cyanomethyl ester 8

4PO-Serine **7** (1 eq, 4.5 mmol) was dissolved in 25 mL dry DMF. To this solution were added 25 mL chloroacetonitrile (88 eq, 395 mmol) and triethylamine (3 eq, 13.5 mmol). Overnight stirring at room temperature gave complete reaction (TLC in ethyl acetate, R_f = 0.5). Volatiles were removed under vacuum and the residue was dissolved in ethyl acetate with a small amount of methanol. Flash column chromatography (ethyl acetate) gave the compound in 72% yield. ^{1}H NMR (CD_3CN) δ = 2.34 (m, 4H), 3.86 (dd, *J* = 23.4, 6 Hz, 2H), 4.56 (m, 1H), 4.84 (s, 2H), 5.05 (m, 2H), 5.86 (m, 1H), 7.25 (d, *J* = 7.8

Hz, 1H). ^{13}C NMR (CD_3CN) δ = 29.7, 35.2, 54.2, 61.9, 115.2, 117.9, 137.6, 169.9, 173.3.

5.6.10 4PO-pSer(ONb)$_2$ cyanomethyl ester 9

In a dry flask, 4PO-Ser cyanomethyl ester **8** (1 eq, 0.6 mmol) and tetrazole (1.8 eq, 1.08 mmol, used without purification) were combined. Dry acetonitrile (7 mL) and dry CH_2Cl_2 (30 mL) were added. After complete dissolution, the flask was cooled to 0 °C in a water/ice bath. A solution of bis(nitrobenzyl) phosphoramidite **1** (1.5 eq, 0.92 mmol, in 2 mL dry CH_2Cl_2) was added dropwise via syringe. The reaction was mixed for 5 min at 0 °C and then returned to room temperature. After 2.5 hrs at room temperature, TLC (1:1 ethyl acetate:hexane, R_f = 0.3) confirmed that the starting material had been completely converted. After an additional 2.5 hr, the oxidant mCPBA (1.1 eq, 0.66 mmol, in 5 ml dry CH_2Cl_2) was added and the reaction allowed to stir 15 min at room temperature. After TLC (1:1 ethyl acetate:hexane, R_f = 0.2), the reaction stirred another 15 min and was then quenched with 50 mL CH_2Cl_2 and washed twice (20 mL saturated $NaHCO_3$ and 20 mL brine). The aqueous phase was extracted with CH_2Cl_2 and the combined organic phases dried over Na_2SO_4. Rotary evaporation gave a yellow oil, which was purified by flash column chromatography (1:1 ethyl acetate:hexane, to ethyl acetate after fraction 12) in 27% yield. ^{1}H NMR ($CDCl_3$) δ = 2.35 (m, 4H), 3.99 (m, 2H), 4.47 (m, 1H), 4.81 (s, 2H), 5.51 (m, 4H), 5.79 (m, 1H), 7.06 (d, *J* = 7.5 Hz, 1H), 7.51 (m, 2H), 7.66 (m, 4H), 8.11 (d, *J* = 8,1 Hz, 2H). ^{13}C NMR ($CDCl_3$) δ = 29.5, 35.5, 67.1, 67.6, 67.7, 114.4, 115.9, 125.4, 129.0, 129.6, 129.9, 131.5, 134.4, 136.8, 147.0, 167.9, 172.9. ^{31}P NMR ($CDCl_3$) δ = -0.52.

5.6.11 4PO-Threonine 10

A reaction vessel was charged with threonine (1 eq, 4.20 mmol) and Na_2CO_3 (1.4 eq, 5.89 mmol) along with 60 mL water and 30 mL *p*-dioxane. A solution of 4-pentenoyl anhydride (1.4 eq, 5.89 mmol) was prepared in 15 mL dioxane and added to the reaction vessel in a single portion. TLC (10:10:1 ethyl acetate: hexanes: acetic acid, R_f = 0.7, developed with iodine and ninhydrin) subsequent to 2 h stirring at room temperature showed complete reaction. The reaction was quenched (250 mL of 1 *M* $NaHSO_4$ and 250 mL CH_2Cl_2) and extracted thrice with CH_2Cl_2 (100 mL portions). Considerable amounts of product remained in the aqueous layer, so it was treated with an equal volume of brine and extracted twice with THF (100 mL each time). The combined organic layers were dried over Na_2SO_4 and concentrated. A flash column was prepared in CH_2Cl_2 and the residue re-dissolved in CH_2Cl_2. Chromatography (CH_2Cl_2, followed by 1:1 CH_2Cl_2:ethyl acetate) produced purified 4PO-threonine in 99% yield. ^{1}H NMR (CD_3CN) δ = 1.17 (d, *J* = 6.3 Hz, 3H), 2.40 (m, 4H), 4.34 (d, *J* = 4.2 Hz, 1H), 4.51 (d, *J* = 6.3 Hz, 1H), 5.02 (m, 2H), 5.85 (m, 1H), 7.40 (d, *J* = 8.4 Hz, 1H). ^{13}C NMR (CD_3CN) δ = 19.7, 29.9, 35.2, 57.9, 67.7, 115.3, 137.3, 172.7, 174.6, 175.0.

5.6.12 4PO-Threonine cyanomethyl ester 11

To a flame-dried flask were added 4PO-threonine **10** (1 eq, 4.5 mmol), 25 mL dry DMF, and 25 mL chloroacetonitrile (88 eq, 395 mmol). After addition of triethylamine (3 eq, 13.5 mmol), the reaction was stirred overnight. TLC (ethyl acetate, R_f = 0.6) indicated complete reaction, and the solvent was removed under vacuum. The residual solids were brought up in a minimal volume of ethyl acetate with a few drops of methanol. Flash column chromatography (ethyl acetate) was performed and the compound isolated in

68% yield. ^{1}H NMR (CD_3CN) δ = 1.16 (d, *J* = 6.3 Hz, 3H), 2.36 (m, 4H), 4.29 (m, 2H), 4.52 (dd, *J* = 8.4, 3 Hz, 1H), 4.83 (s, 2H), 5.05 (m, 2H), 5.87 (m, 1H), 7.06 (d, *J* = 8.4 Hz, 1H). ^{13}C NMR (CD_3CN) δ = 20.4, 29.8, 35.4, 50.3, 57.4, 67.3, 115.4, 117.8, 170.1, 173.6.

5.6.13 4PO-pThr(ONb)$_2$ cyanomethyl ester 12

In a flame-dried flask, 4PO-Thr cyanomethyl ester **11** (1 eq, 0.77 mmol) was combined with sublimed tetrazole (1.8 eq, 1.38 mmol). By syringe, dry acetonitrile (10 mL) and dry CH_2Cl_2 (34 mL) were added. The flask was cooled to 0 °C in a water/ice bath after the solids had completely dissolved. A solution of bis(nitrobenzyl) phosphoramidite **1** (1.5 eq, 1.15 mmol, in 2 mL dry CH_2Cl_2) was slowly added. After 5 min at 0 °C, the reaction was allowed to warm to room temperature. After 2.5 hrs at room temperature, TLC (1:1 ethyl acetate:hexane, R_f = 0.3) suggested that reaction was complete. Tetrabutylammonium periodate (1.5 eq, 1.15 mmol, in 5 ml dry THF) was added and the reaction stirred 15 min at room temperature. TLC (1:1 ethyl acetate:hexane, R_f = 0.2) indicated complete conversion, and quenching with 60 mL CH_2Cl_2 was followed by washing the organic layer (40 mL saturated $NaHCO_3$ and 40 mL brine). The combined organic phases were dried over Na_2SO_4. White needles were observed upon standing. Rotary evaporation gave a yellow oil, which was purified by flash column chromatography (7:3 ethyl acetate:hexane) in 30% yield. ^{1}H NMR ($CDCl_3$) δ = 1.23 d, *J* = 6.3 Hz, 3H), 2.42 (m, 4H), 3.31 (m, 2H), 4.47 (m, 1H), 4.84 (s, 2H), 5.5 (m, 4H), 5.9 (m, 1H), 6.6 (d, *J* = 7.5 Hz, 1H), 7.6 (m, 2H), 7.8 (m, 4H), 8.2 (d, *J* = 8,1 Hz, 2H). ^{31}P NMR ($CDCl_3$) δ = -0.62. Found: (ESI$^+$) 590.8 $(M+H^+)^+$, 613.0 $(M+Na^+)^+$.

5.6.14 Nitrobenzyl phosphite 17

In a 500 mL RBF, 1 mL PCl_3 (1 eq, 11.4 mmol, Acros Organics) was added to 300 mL dry ether. The reaction was cooled to –78 °C and 4.95 mL triethylamine (3.1 eq, 35.5 mmol) were slowly added via syringe. A small amount of white vapor was produced during the addition. After approximately 5 min stirring, a solution of 5.26 g nitrobenzyl alcohol (3 eq, 34.3 mmol) in 60 mL dry ether were added over 10 min through an addition funnel. Reaction continued for 2 hr at –78 °C, after which the reaction was allowed to come to room temperature and stir overnight. The copious cream-colored precipitate was removed by filtration through a fine frit. The solid was washed with ether and the filtrate evaporated *in vacuo* to give 4.6 g yellowish solid with a single ^{31}P resonance (crude yield 82%). Crystallization from ether gave 2.1 g of pure nitrobenzyl phosphite as white crystals. Only one crop was collected, then the filtrate was rotovapped to recover the remaining crude product. ^{1}H NMR ($CDCl_3$) δ = 5.36 (d, J = 6.6 Hz, 6H),7.44 (t, J = 7.8 Hz, 3H), 7.63 (m, 3H), 7.77 (m, 3H), 8.06 (d, J = 8.4 Hz, 3H). ^{13}C NMR ($CDCl_3$) δ = 61.8, 124.5, 129.6, 133.2, 135.0, 146.8. ^{31}P NMR ($CDCl_3$) δ = 143.13. MS Calcd for $C_{21}H_{18}N_3O_9P$: 487.08. Found: (ESI$^+$) 488.2 $(M+H^+)^+$, 510.2 $(M+Na^+)^+$, 256.0 $(M+K^+)^+$.

5.6.15 Nitrobenzyl H-phosphonate 18

Similarly to the synthesis of nitrobenzyl phosphite **17**, 1 mL PCl_3 (1 eq, 11.4 mmol, Acros Organics) and 3.34 mL triethylamine (2.1 eq, 23.9 mmol) were combined in 300 mL dry ether at -78 °C. Nitrobenzyl alcohol was added (2 eq, 22.8 mmol, a solution of 3.50 g in 60 mL anhydrous ether) over 10 min via addition funnel. The reaction was stirred 2 hr at -78 °C and allowed to warm to room temperature overnight. After

approximately 12 hr total reaction time, 100 mL water were added and the reaction stirred 30 min at room temperature. The crystals were filtered out and washed with water. The filtrate was washed with 100 mL 5% K_2CO_3 and 100 mL water. After drying over Na_2SO_4, the ether was removed *in vacuo* to give 3.3 g orange solid (82% crude yield). Crystallization from ethanol gave 1.3 g pure nitrobenzyl *H*-phosphonate as off-white crystals. The remaining product was recovered from the mother liquor. ^{1}H NMR ($CDCl_3$) δ = 5.53 (sept, $J \approx 6.2$ Hz, 4H),7.14 (d, $J_{P\text{-}H} = 716.7$ Hz, 1H), 7.75 (m, 2H), 7.68 (m, 4H), 8.09 (d, $J = 7.2$ Hz 2H). ^{13}C NMR ($CDCl_3$) δ = 64.5, 126.0, 128.0, 128.6, 129.6, 130.1, 132.2, 135.3, 146.8. ^{31}P NMR ($CDCl_3$) δ = 9.8 (m). [H-coupled]: 9.3 (dquint, $J_{P\text{-}H}$ = 711 Hz, $J_{\text{-}CH\text{-}O\text{-}P} = 8.3$ Hz).

5.6.16 4PO-Tyrosine 19

Tyrosine (1 eq, 4.14 mmol) and sodium carbonate (1.4 eq, 5.7 mmol) were weighed into a 250 mL round-bottom flask equipped with a stirbar. A total of 60 mL water and 60 mL dioxane were added, until both solids were nearly completely dissolved. 4-Pentenoic anhydride (1.4 eq, 5.7 mmol) was added in a single portion and the reaction stirred at room temperature. Progress was monitored by TLC (1:20 acetic acid:ethyl acetate, R_f = 0.5, developed with iodine and ninhydrin). After 4 h, 10 mL of 1 *N* HCl were added (resulting in a pH of approximately 4.5) and the reaction stirred 15 min to hydrolyze any pentenoyl ester formed from side chain reactivity. The reaction was quenched with 100 mL of 1 *M* $NaHSO_4$ and 200 mL CH_2Cl_2. The organic layer was removed, and the aqueous layer was treated with 200 mL saturated NaCl and extracted thrice with 50 mL portions of THF. The combined organic layers were dried over Na_2SO_4 and solvent evaporated *in vacuo*. The crude mixture was re-dissolved in a minimal volume of ethyl

acetate with a small amount of methanol and loaded on a silica gel column. Flash column chromatography (1:20 acetic acid:ethyl acetate) gave purified product in 75% yield. ^{1}H NMR (CD_3CN) δ = 2.25 (m, 4H), 2.99 (ABM, *J* = 30.9, 14.1, 5.7 Hz, 2H), 4.62 (m, 1H), 4.96 (m, 2H), 5.7 (m, 1H), 6.75 (d, *J* = 6.6 Hz, 2H), 6.93 (d, *J* = 8.1 Hz, 1H), 7.06 (d, *J* = 4.5 Hz, 2H).

5.6.17 4PO-Tyrosine cyanomethyl ester 20

A solution of 4PO-tyrosine **19** (1 eq, 0.44 mmol) was prepared in 2 mL dry DMF and 2 mL chloroacetonitrile (107 eq, 31.6 mmol). Triethylamine (3 eq, 1.32 mmol) was added and the reaction stirred 6 h at room temperature. TLC (ethyl acetate, R_f = 0.5) showed the reaction to be complete. Solvent was removed under high vacuum and the residue dissolved in 10:1 CH_2Cl_2:ethyl acetate with a few drops of methanol. Flash column chromatography (ethyl acetate) produced the title compound in 56% yield. ^{1}H NMR (CD_3CN) δ = 2.24 (m, 4H), 2.99 (ABM, *J* = 30.9, 14.1, 5.7 Hz, 2H), 4.64 (m, 1H), 4.77 (s, 2H), 5.00 (m, 2H), 5.8 (m, 1H), 6.74 (d, *J* = 4.8 Hz, 2H), 6.85 (d, *J* = 7.5 Hz, 1H), 7.06 (d, *J* = 8.7 Hz, 2H). MS Calcd for $C_{16}H_{18}N_2O_4$: 302.13. Found (ESI$^-$): 301.2 $(M\text{-}H^+)^-$, 337.0 $(M+Cl)^-$.

5.6.18 dCA-4PO-pTyr(ONb)$_2$ 21

4PO-pTyr(ONb)$_2$ cyanomethyl ester **6** (1 eq, 0.05 mmol) was dissolved in 0.8 mL dry DMF in a flame-dried 5 mL conical flask fitted with a stirbar. The dinucleotide dCA (10 mg) was added in one portion, and the reaction was allowed to continue 3 h at room temperature. The reaction was monitored by analytical HPLC (gradient: 25 mM ammonium acetate, pH 4.5 to CH_3CN). The addition of tetrabutylammonium acetate was

necessary to promote reaction. Upon completion of the reaction, the pure compound was obtained by preparative HPLC (gradient: 25 mM ammonium acetate, pH 4.5 to CH_3CN). MS (ESI) Calcd for $C_{47}H_{52}N_{11}O_{23}P_{33}$: 1231.25. Found ($ESI^-$): 546.0 $(M\text{-}Nb)^{2-}$, 806.2 (M-Nb-pdC)$^-$. Found ($MALDI^-$): 1265.1 $(M+Cl^-)^-$. Found ($MALDI^+$): 1097.2 $(M\text{-}Nb)^+$, 962.2 $(M\text{-}2Nb)^+$.

5.7 References

1. Kaplan, J. H., Forbush, B. and Hoffman, J. F. Caged-ATP, a photolabile source of ATP. *Biophys. J* **21**, A72-A72 (1978).
2. Corrie, J. E. T., Reid, G. P., Trentham, D. R., Hursthouse, M. B. and Mazid, M. A. Synthesis and absolute stereochemistry of the 2 diastereoisomers of p3-1-(2-nitrophenyl)ethyl adenosine-triphosphate (caged ATP). *J. Chem. Soc. Perkin Trans. I*, 1015-1019 (1992).
3. Rubinstein, M., Amit, B. and Patchornik, A. Use of a light-sensitive phosphate protecting group for some mononucleotide syntheses. *Tet. Lett.*, 1445-1448 (1975).
4. Alvarez, K., Vasseur, J. J., Beltran, T. and Imbach, J. L. Photocleavable protecting groups as nucleobase protections allowed the solid-phase synthesis of base-sensitive SATE-prooligonucleotides. *J. Org. Chem.* **64**, 6319-6328 (1999).
5. Furuta, T., Torigai, H., Osawa, T. and Iwamura, M. Direct esterification of phosphates with various halides and its application to synthesis of cAMP alkyl triesters. *J. Chem. Soc. Perkin Trans. I,* 3139-3142 (1993).
6. Hausch, F. and Jaschke, A. Libraries of multifunctional RNA conjugates for the selection of new RNA catalysts. *Bioconj. Chem.* **8**, 885-890 (1997).
7. Hausch, F. and Jaschke, A. A novel carboxy-functionalized photocleavable dinucleotide analog for the selection of RNA catalysts. *Tet. Lett.* **39**, 6157-6158 (1998).
8. Meier, C. and Mauritz, R. Synthesis of protected 3',5'-di-2'-deoxythymidine-(alpha-hydroxy-2-nitrobenzyl)-phosphonate diesters as dimer building-blocks for oligonucleotides. *Nucleos. Nucleot.* **14**, 803-804 (1995).
9. Ohtsuka, E., Miyake, T. and Ikehara, M. Studies on transfer ribonucleic-acids and related compounds .25. synthesis of *Escherichia coli* tRNA-fMet 5'-terminal tetranucleotide C-G-C-Gp and its sequence analog U-G-C-Gp. *Chem. Pharm. Bull.* **27**, 341-345 (1979).
10. Olejnik, J., Krzymanska-Olejnik, E. and Rothschild, K. J. Photocleavable aminotag phosphoramidites for 5 '-termini DNA/RNA labeling. *Nucl. Acids Res.* **26**, 3572-3576 (1998).
11. Olejnik, J. et al. Photocleavable peptide-DNA conjugates: synthesis and applications to DNA analysis using MALDI-MS. *Nucl. Acids Res.* **27**, 4626-4631 (1999).
12. Ordoukhanian, P. and Taylor, J. S. Caged single and double strand breaks. *Bioconj. Chem.* **11**, 94-103 (2000).
13. Schwartz, M. E., Breaker, R. R., Asteriadis, G. T., Debear, J. S. and Gough, G. R. Rapid synthesis of oligoribonucleotides using 2'-o-(ortho-nitrobenzyloxymethyl)-protected monomers. *Bioorg. Med. Chem. Lett.* **2**, 1019-1024 (1992).
14. Zhang, K. J. and Taylor, J. S. A caged ligatable DNA strand break. *J. Am. Chem. Soc.* **121**, 11579-11580 (1999).
15. Chen, J. A. and Prestwich, G. D. Regioselective synthesis of photolabile P(1,2)- and P(4,5)-(o-nitrobenzyl) esters of myo-inositol 1,2,3,4,5,6-hexakisphosphate. *Tet. Lett.* **38**, 969-972 (1997).
16. Gu, Q. M. and Prestwich, G. D. Synthesis of phosphotriester analogues of the phosphoinositides PtdIns(4,5)P-2 and PtdIns(3,4,5)P-3. *J. Org. Chem.* **61**, 8642-8647 (1996).
17. Qiao, L. X., Kozikowski, A. P., Olivera, A. and Spiegel, S. Synthesis and evaluation of a photolyzable derivative of sphingosine 1-phosphate - caged SPP. *Bioorg. Med. Chem. Lett.* **8**, 711-714 (1998).

18. Williger, B. T., Reich, R., Neeman, M., Bercovici, T. and Liscovitch, M. Release of Gelatinase-a (Matrix Metalloproteinase-2) Induced by photolysis of caged phosphatidic-acid in Ht-1080 metastatic fibrosarcoma cells. *J. Biol. Chem.* **270**, 29656-29659 (1995).
19. Yamaguchi, K., Tsuda, E., Shimakage, T. A. and Kusumi, A. Syntheses of phospholipids containing 2-nitrobenzyl ester moieties at the terminals of alkyl chains and properties of photodegradable liposomes from the lipids. *Bull. Chem. Soc. Japan* **71**, 1923-1929 (1998).
20. Reinhard, R. and Schmidt, B. F. Nitrobenzyl-based photosensitive phosphoramide mustards: Synthesis and photochemical properties of potential prodrugs for cancer therapy *J. Org. Chem.* **63**, 3152-3152 (1998).
21. Reinhard, R. and Schmidt, B. F. Nitrobenzyl-based photosensitive phosphoramide mustards: Synthesis and photochemical properties of potential prodrugs for cancer therapy. *J. Org. Chem.* **63**, 2434-2441 (1998).
22. Pan, P. and Bayley, H. Caged cysteine and thiophosphoryl peptides. *FEBS Lett.* **405**, 81-85 (1997).
23. Rothman, D. D., Vázquez, M. E., Vogel, E. M. and Imperiali, B. General method for the synthesis of caged phosphopeptides: tools for the exploration of signal transduction pathways. *Org. Lett.* **4**, 2865-2868 (2002).
24. Zou, K. Y., Miller, W. T., Givens, R. S. and Bayley, H. Caged thiophosphotyrosine peptides. *Angew. Chem. Int. Ed. Eng.* **40**, 3049-3051 (2001).
25. Zou, K. Y., Cheley, S., Givens, R. S. and Bayley, H. Catalytic subunit of protein kinase A caged at the activating phosphothreonine. *J. Am. Chem. Soc.* **124**, 8220-8229 (2002).
26. Arabaci, G., Guo, X. C., Beebe, K. D., Coggeshall, K. M. and Pei, D. alpha-Haloacetophenone derivatives as photoreversible covalent inhibitors of protein tyrosine phosphatases. *J. Am. Chem. Soc.* **121**, 5085-5086 (1999).
27. Hohsaka, T., Kajihara, D., Ashizuka, Y., Murakami, H. and Sisido, M. Efficient incorporation of nonnatural amino acids with large aromatic groups into streptavidin in *in vitro* protein synthesizing systems. *J. Am. Chem. Soc.* **121**, 34-40 (1999).
28. Guga, P., Orkruszek, A. and Wojciech, J. S. in *New Aspects in Phosphorus Chemistry I* (ed. Majoral, J. P.) 169-200 (Springer, Berlin, 2002).
29. Baldwin, J. E., McConnaughie, A. W., Moloney, M. G., Pratt, A. J. and Shim, S. B. New photolabile phosphate protecting groups. *Tetrahedron* **46**, 6879-6884 (1990).
30. Cossy, J. and Rakotoarisoa, H. The N-(2-acetoxyethyl) group as a new photolabile protecting group. *Tet. Lett.* 41, 2097-2099 (2000).
31. Furuta, T. et al. Acyloxycoumarinylmethyl-caged cAMP, the photolabile and membrane-permeable derivative of cAMP that effectively stimulates pigment-dispersion response of melanophores. *Biochem. Biophys. Res. Comm.* **228**, 193-198 (1996).
32. Furuta, T. et al. Brominated 7-hydroxycoumarin-4-ylmethyls: Photolabile protecting groups with biologically useful cross-sections for two photon photolysis. *PNAS* **96**, 1193-1200 (1999).
33. Jayaraman, V., Thiran, S. and Madden, D. R. Fourier transform infrared spectroscopic characterization of a photolabile precursor of glutamate. *FEBS Letters* **475**, 278-282 (2000).
34. Park, C. H. and Givens, R. S. New photoactivated protecting groups.6. p-hydroxyphenacyl: A phototrigger for chemical and biochemical probes. *J. Am. Chem. Soc.* **119**, 2453-2463 (1997).
35. Rock, R. S. and Chan, S. I. Preparation of a water-soluble "cage" based on 3 ',5 '-dimethoxybenzoin. *J. Am. Chem. Soc.* **120**, 10766-10767 (1998).
36. Givens, R. S., Jung, A., Park, C. H., Weber, J. and Bartlett, W. New photoactivated protecting groups.7. p-Hydroxyphenacyl: A phototrigger for excitatory amino acids and peptides. *J. Am. Chem. Soc.* **119**, 8369-8370 (1997).
37. Schlosser, M. Parametrization of substituents: Effects of fluorine and other heteroatoms on OH, NH, and CH acidities. *Angew. Chem. Int. Ed. Eng.* **37**, 1497-1513 (1998).
38. Chen, L. et al. Why is phosphonodifluoromethyl phenylalanine a more potent inhibitory moiety than phosphonomethyl phenylalanine toward protein-tyrosine phosphatases. *Biochem. Biophys. Res. Comm.* **216**, 976-984 (1995).
39. Blackburn, G. M., Brown, D., Martin, S. J. and Parratt, M. J. Studies on selected transformations of some fluoromethanephosphonate esters. *J. Chem. Soc. Perkin Trans. I*, 181-186 (1987).
40. Nieschalk, J. and Ohagan, D. Monofluorophosphonates as phosphate mimics in bioorganic chemistry - a comparative-study of CH_2-phosphonate, CHF-phosphonate and CF_2-phosphonate analogs of sn-

glycerol-3-phosphate as substrates for sn-glycerol-3-phosphate dehydrogenase. *J. Chem. Soc. Chem. Comm.*, 719-720 (1995).

41. Berkowitz, D. B., Bhuniya, D. and Peris, G. Facile installation of the phosphonate and (alpha,alpha-difluoromethyl)phosphonate functionalities equipped with benzyl protection. *Tet. Lett.* **40**, 1869-1872 (1999).
42. Ripka, W. C. Protein tyrosine phosphatase inhibition. *Ann. Rep. Med. Chem.* **35**, 231-250 (2000).
43. Taylor, W. P., Zhang, Z. Y. and Widlanski, T. S. Quiescent affinity inactivators of protein tyrosine phosphatases. *Bioorg. Med. Chem.* **4**, 1515-1520 (1996).
44. Beaucage, S. L. and Iyer, R. P. The synthesis of specific ribonucleotides and unrelated phosphorylated biomolecules by the phosphoramidite method. *Tetrahedron* **49**, 10441-10488 (1993).
45. Bannwarth, W. and Trzeciak, A. A simple and effective chemical phosphorylation procedure for biomolecules. *Helv. Chim. Acta* **70**, 175-186 (1987).
46. McMurray, J. S., Coleman, D. R., Wang, W. and Campbell, M. L. The synthesis of phosphopeptides. *Biopolymers* **60**, 3-31 (2001).
47. Perich, J. W. Synthesis of phosphopeptides using modern chemical approaches. *Meth. Enz.* **289**, 245-266 (1997).
48. Hoffmann, R., Tholey, A., Hoffmann, T. and Kalbitzer, H. R. Solid-phase synthesis of H- and methylphosphonopeptides. *Int. J. Pept. Prot. Res.* **47**, 245-253 (1996).
49. Kupihar, Z., Varadi, G., Monostori, E. and Toth, G. K. Preparation of an asymmetrically protected phosphoramidite and its application in solid-phase synthesis of phosphopeptides. *Tet. Lett.* **41**, 4457-4461 (2000).
50. Shapiro, G. et al. Combined Fmoc-Alloc strategy for a general SPPS of phosphoserine peptides; Preparation of phosphorylation-dependent tau antisera. *Bioorg. Med. Chem.* **5**, 147-156 (1997).
51. Wakamiya, T., Saruta, K., Yasuoka, J. and Kusumoto, S. An efficient procedure for solid-phase synthesis of phosphopeptides by the Fmoc strategy. *Chem. Lett.* 1099-1102 (1994).
52. Mathe, C., Perigaud, C., Gosselin, G. and Imbach, J. L. Phosphopeptide prodrug bearing an S-acyl-2-thioethyl enzyme-labile phosphate protection. *J. Org. Chem.* **63**, 8547-8550 (1998).
53. Arslan, T., Mamaev, S. V., Mamaeva, N. V. and Hecht, S. M. Structurally modified firefly luciferase, effects of amino acid substitution at position 286. *J. Am. Chem. Soc.* **119**, 10877-10887 (1997).
54. Blades, K. et al. Synthesis of activated alkenes bearing the difluoromethylenephosphonate group: a range of building blocks for the synthesis of secondary difluorophosphonates. *J. Chem. Soc. Perkin Trans. I*, 3609-3614 (1999).
55. Park, S. B. and Standaert, R. F. alpha,alpha-difluorophosphonomethyl azobenzene derivatives as photo-regulated phosphoamino acid analogs. 1. Design and synthesis. *Tet. Lett.* **40**, 6557-6560 (1999).
56. Qabar, M. N., Urban, J. and Kahn, M. A facile solution and solid phase synthesis of phosphotyrosine mimetic L-4-[diethylphosphono(difluoromethyl)]-phenylalanine (F(2)Pmp(EtO)(2)) derivatives. *Tetrahedron* **53**, 11171-11178 (1997).
57. Shakespeare, W. C. et al. An efficient synthesis of a 4 '-phosphonodifluoromethyl-3 '-formyl-phenylalanine containing Src SH2 ligand. *Bioorg. Med. Chem. Lett.* **9**, 3109-3112 (1999).
58. Solas, D., Hale, R. L. and Patel, D. V. An efficient synthesis of N-alpha-Fmoc-4-(phosphonodifluoromethyl)-L-phenylalanine. *J. Org. Chem.* **61**, 1537-1539 (1996).
59. Yokomatsu, T., Yamagishi, T., Matsumoto, K. and Shibuya, S. Stereocontrolled synthesis of hydroxymethylene phosphonate analogues of phosphorylated tyrosine and their conversion to monofluoromethylene phosphonate analogues. *Tetrahedron* **52**, 11725-11738 (1996).
60. Burke, T. R. et al. Phosphotyrosyl-based motifs in the structure-based design of protein-tyrosine phosphatase inhibitors. *Abstr. Pap. Am. Chem. Soc.* **219**, U7-U7 (2000).
61. Chetyrkina, S., Estieu-Gionnet, K., Lain, G., Bayle, M. and Deleris, G. Synthesis of N-Fmoc-4-[(diethylphosphono)-2 ',2 '-difluoro-1 '-hydroxyethyl]phenylalanine, a novel phosphotyrosyl mimic for the preparation of signal transduction inhibitory peptides. *Tet. Lett.* **41**, 1923-1926 (2000).
62. Szardenings, A. K., Gordeev, M. F. and Patel, D. V. A general and convenient synthesis of novel phosphotyrosine mimetics. *Tet. Lett.* **37**, 3635-3638 (1996).
63. Berkowitz, D. B., Shen, Q. R. and Maeng, J. H. Synthesis of the (alpha,alpha-difluoroalkyl)phosphonate analog of phosphoserine. *Tet. Lett.* **35**, 6445-6448 (1994).
64. Berkowitz, D. B., Eggen, M., Shen, Q. R. and Shoemaker, R. K. Ready access to fluorinated phosphonate mimics of secondary phosphates. Synthesis of (alpha,alpha-

difluoromethylene)phosphonate analogues of L-phosphoallothreonine and L-phosphothreonine. *Abstr. Pap. Am. Chem. Soc.* **212**, 233-Orgn (1996).

65. Otaka, A., Mitsuyama, E., Kinoshita, T., Tamamura, H. and Fujii, N. Stereoselective synthesis of CF_2-substituted phosphothreonine mimetics and their incorporation into peptides using newly developed deprotection procedures. *J. Org. Chem.* **65**, 4888-4899 (2000).
66. Schenkels, C., Erni, B. and Reymond, J. L. Phosphofurylalanine, a stable analog of phosphohistidine. *Bioorg. Med. Chem. Lett.* **9**, 1443-1446 (1999).
67. Tozer, M. J. and Herpin, T. F. Methods for the synthesis of gem-difluoromethylene compounds. *Tetrahedron* **52**, 8619-8683 (1996).
68. Burton, D. J., Yang, Z. Y. and Qiu, W. M. Fluorinated ylides and related compounds. *Chem. Rev.* **96**, 1641-1715 (1996).
69. Qiu, W. M. and Burton, D. J. A facile and general preparation of alpha,alpha-difluoro benzylic phosphonates by the CuCl promoted coupling reaction of the (diethylphosphonyl)difluoromethylcadmium reagent with aryl iodides. *Tet. Lett.* **37**, 2745-2748 (1996).
70. Yokomatsu, T., Murano, T., Suemune, K. and Shibuya, S. Facile synthesis of aryl(difluoromethyl)phosphonates through CuBr-mediated cross coupling reactions of [(Diethoxyphosphinyl)difluoromethyl] zinc bromide with aryl iodides. *Tetrahedron* **53**, 815-822 (1997).
71. Benayoud, F. et al. Efficient syntheses of (alpha-fluoropropargyl)phosphonate esters. *J. Org. Chem.* **61**, 5159-5164 (1996).
72. Boetzel, R. and Hagele, G. C-Fluorinated Phosphate Analogs. *J. Fluor. Chem.* **68**, 11-13 (1994).
73. Fields, S. C. Synthesis of natural products containing a C-P bond. *Tetrahedron* **55**, 12237-12272 (1999).
74. Kamber, M. and Just, G. Gamma-phosphono-gamma-lactones - the use of allyl esters as easily removable phosphonate protecting groups. *Can. J. Chem.* **63**, 823-827 (1985).
75. Kobayashi, Y., William, A. D. and Tokoro, Y. Sharpless asymmetric dihydroxylation of trans-propenylphosphonate by using a modified AD-mix-alpha and the synthesis of fosfomycin. *J. Org. Chem.* **66**, 7903-7906 (2001).
76. Nair, H. K. and Burton, D. J. Facile synthesis of fluorinated phosphonates via photochemical and thermal reactions. *J. Am. Chem. Soc.* **119**, 9137-9143 (1997).
77. Piettre, S. R. Simple and efficient synthesis of 2,2-disubstituted-1,1-difluorophosphonates and phosphonothioates. *Tet. Lett.* **37**, 2233-2236 (1996).
78. Saady, M., Lebeau, L. and Mioskowski, C. First use of benzyl phosphites in the Michaelis-Arbuzov reaction - synthesis of monophosphate, diphosphate, and triphosphate analogs. *Helv. Chim. Acta* **78**, 670-678 (1995).
79. Sikora, D. and Gajda, T. A new synthesis of protected phosphonodipeptides with an N-terminal amino acid. *Tetrahedron* **56**, 3755-3761 (2000).
80. Vayron, P., Renard, P. Y., Valleix, A. and Mioskowski, C. Design and synthesis of an alpha,alpha-difluorophosphinate hapten for antibody-catalyzed hydrolysis of organophosphorus nerve agents. *Chem. Eur. J.* **6**, 1050-1063 (2000).
81. Waschbusch, R., Samadi, M. and Savignac, P. A useful magnesium reagent for the preparation of 1,1-difluoro-2-hydroxyphosphonates from diethyl bromodifluoromethylphosphonate via a metal-halogen exchange reaction. *J. Organomet. Chem.* **529**, 267-278 (1997).
82. Berkowitz, D. B., Eggen, M., Shen, Q. and Sloss, D. G. Synthesis of (alpha,alpha-difluoroalkyl)phosphonates by displacement of primary triflates. *J. Org. Chem.* **58**, 6174-6176 (1993).
83. Berkowitz, D. B. and Sloss, D. G. Diallyl (lithiodifluoromethyl)phosphonate - a new reagent for the introduction of the (difluoromethylene)phosphonate functionality. *J. Org. Chem.* **60**, 7047-7050 (1995).
84. Berkowitz, D. B., Bose, M., Pfannenstiel, T. J. and Doukov, T. alpha-fluorinated phosphonates as substrate mimics for glucose 6-phosphate dehydrogenase: the CHF stereochemistry matters. *J. Org. Chem.* **65**, 4498-4508 (2000).
85. Kim, C. U. et al. Acyclic purine phosphonate analogs as antiviral agents - synthesis and structure-activity-relationships. *J. Med. Chem.* **33**, 1207-1213 (1990).
86. Kondo, H. et al. Glycosyl phosphites as glycosylation reagents - scope and mechanism. *J. Org. Chem.* **59**, 864-877 (1994).

87. Obayashi, M., Ito, E., Matsui, K. and Kondo, K. (Diethylphosphinyl)difluoromethyllithium - preparation and synthetic application. *Tet. Lett.* **23**, 2323-2326 (1982).
88. Piettre, S. R., Girol, C. and Schelcher, C. G. A new strategy for the conversion of aldehydes into difluoromethyl ketones. *Tet. Lett.* **37**, 4711-4712 (1996).
89. Ruel, R., Bouvier, J. P. and Young, R. N. Single-step preparation of 1-hydroxybisphosphonates via addition of dialkyl phosphite potassium anions to acid-chlorides. *J. Org. Chem.* **60**, 5209-5213 (1995).
90. Valerio, R. M., Alewood, P. F. and Johns, R. B. Synthesis of optically-active 2-(tert-butyloxycarbonylamino)-4-dialkoxyphosphorylbutanoate protected isosteres of o-phosphonoserine for peptide-synthesis. *Synth.* 786-789 (1988).
91. Campagne, J. M., Coste, J. and Jouin, P. (1H-Benzotriazol-1-yloxy)tris(dimethylamino)phosphonium hexafluorophosphate-mediated and (1H-benzotriazol-1-yloxy)tripyrrolidinophosphonium hexafluorophosphate-mediated activation of monophosphonate esters - synthesis of mixed phosphonate diesters, the reactivity of the benzotriazolyl phosphonic esters *vs* the reactivity of the benzotriazolyl carboxylic Esters. *J. Org. Chem.* **60**, 5214-5223 (1995).
92. Burton, D. J. and Flynn, R. M. Michaelis-Arbuzov preparation of halo-F-methylphosphonates. *J. Fluor. Chem.* **10**, 329-332 (1977).
93. Houben-Weyl. in *Methoden der organsichen Chemie*. (ed. Houben-Weyl) 54-58 (Georg Thieme Verlag, Stuttgart, 1964).
94. Houben-Weyl. in *Methoden der organischen Chemie*. (ed. Houben-Weyl) 28 (Georg Thieme Verlag, Stuttgart, 1964).
95. Gallivan, J. (2002).
96. Kawamoto, A. M. and Campbell, M. M. A new method for the synthesis of a phosphonic acid analogue of phosphoserine via a novel 1,1-difluorophosphonate intermediate. *J. Fluor. Chem.* **81**, 181-186 (1997).
97. Greene, T. W. and Wuts, R. G. M. *Protective groups in organic synthesis* (Wiley-Interscience, New York, 1999).
98. Fahmi, N. E., Golovine, S., Wang, B. X. and Hecht, S. M. Studies toward the site specific incorporation of sugars into proteins: Synthesis of glycosylated aminoacyl-tRNAs. *Carb. Res.* **330**, 149-164 (2001).
99. Paquet, A. Preparation of Dehydroalanine Peptides from bis-(2,2,2-trichloroethyl) and diphenyl phosphonoserine derivatives. *Tet. Lett.* **31**, 5269-5272 (1990).
100. Paquet, A. and Johns, M. Synthesis of oligophosphoseryl sequences occurring in casein - identification of beta-elimination during phosphorylation. *Int. J. Pept. Prot. Res.* **36**, 97-103 (1990).
101. Bockenhauer, D., Zilberberg, N. and Goldstein, S. A. N. KCNK2: reversible conversion of a hippocampal potassium leak into a voltage-dependent channel. *Nat. Neurosci.* **4**, 486-491 (2001).
102. Maylie, J. and Adelman, J. P. Beam me up, Scottie! TREK channels swing both ways. *Nat. Neurosci.* **4**, 457-458 (2001).